COMPOSITE BOX GIRDERS LOADED TO COLLAPSE

A thesis submitted for the degree of
Doctor of Philosophy in the
Faculty of Engineering of
the University of London

by

Paul Andrew Warren B.Sc.(Eng), A.C.G.I.

Imperial College of Science and Technology,
London

July 1980

ABSTRACT

The work described here is concerned with the ultimate load behaviour of steel and composite steel and concrete hollow sections. Particular attention has been paid to the effects of material, rather than geometric, non-linearity.

Upper and lower bound solutions to the ultimate load of a steel rolled hollow section under combined bending, shear and torsion load are derived. A computer program, using the dynamic relaxation method, to solve the plane stress equations for four plates joined to form a steel hollow section, is described. Results obtained from this program are compared with the upper and lower bound solutions.

The dynamic relaxation program is extended to analyse both open and closed composite box girders. The program is then used to study the behaviour of composite box girders under various load combinations, and, in particular, the torsional rigidity of open composite boxes.

A series of six tests on small-scale composite steel and concrete box girders is described. Stresses measured in the elastic regions of these tests are compared with those predicted by the dynamic relaxation analysis and also, for one of the tests, with a finite element analysis. The ultimate loads measured in the experiments are compared with those predicted by the dynamic relaxation program. Good agreement has been found between theoretical and experimental ultimate loads for the closed box tests, and also for the open box under a bending load. For the open boxes subjected to a loading containing a torsion component the experimental ultimate loads were found to be seriously reduced by transverse bending of the slab. As a result of this the measured ultimate loads for these two sections were considerably lower than those predicted by the theory.

ACKNOWLEDGEMENTS

The author wishes to express his thanks to the following:

Professor P J Dowling, who supervised this work, for his advice and encouragement throughout the project.

Professor B G Neal, Head of the Civil Engineering Department, for accommodating the project and for his advice on the work in chapter 2 of this thesis.

The Department of Transport for sponsorship of this work.

The staff of the Engineering Structures Laboratory, in particular Messrs. J Neale, J Galvin and R Watson for their help with the experimental work.

Mrs S Wright for typing this thesis, Mrs H Guile for preparation of the drawings and Miss J Gurr for the photographs.

CONTENTS

CHAPTER 1

INTRODUCTION & LITERATURE REVIEW

1.1 INTRODUCTION

In recent years a great deal of money has been spent on bridges, and two forms of construction have become increasingly popular; they are box girder construction and composite steel-concrete construction. Box girders have a number of advantages over other types of beam used in bridge construction; the most important of these is the high torsional rigidity associated with closed box sections. This high torsional rigidity ensures good distribution across the width of the bridge of any eccentric forces which may be caused by superimposed loading or eccentric positioning of the support reactions.

Many bridges with main beams of steel have a concrete deck slab to give continuity between the steel beams, and to provide a wearing surface. Over the last twenty or thirty years designers have become more aware of the increase in strength which may be gained by providing a shear connection between the steel beams and the concrete slab.

The modern trend has been to combine the advantages of both of these types of construction and to use composite box girders. There are two ways in which this may be done: one is to attach shear connectors to the top flange of a normal closed steel box girder and to cast a concrete slab on top of the steel box, resulting in a 'closed' composite box, (fig 1.1). The second method is to remove the central portion of the top flange of the steel box, and to use the concrete slab to provide the fourth side of the box, shear connectors being provided only in the area close to the webs; this type is called an 'open' composite box (fig 1.2).

In the last ten years the codes of practice relating to various forms of bridge construction have been under review with the intention of providing a unified bridge code. It is intended that this code will be based on the principle of limit state design. One of these limit states is the collapse limit state,

and here the designer is required to calculate the ultimate load of the structure and check this against a set of factored loads and material strengths. A considerable amount of work has been done on the ultimate load behaviour of steel box girders and composite T-beams, but little is known about the ultimate load behaviour of composite box girders, and in particular their behaviour under torsion loads. The use of the open type of composite box poses considerable problems, particularly when it is subject to torsion loading. Here the flexibility of the shear connection and the possibility of cracking of the concrete slab lead to some doubts as to the torsional rigidity and load capacity of the section.

The United States Steel Design Handbook (36) gives a method of calculating the lateral distribution of load in a composite twin box bridge. This is an elastic analysis and full interaction between the steel and concrete is assumed for the purposes of calculating the section properties.

The research presented in this thesis is concerned with both theoretical and experimental aspects of the behaviour of composite box girders, concentrating particularly on the hogging moment region.

1.2 LITERATURE REVIEW

Very little work has been published giving the results of tests or theoretical analyses of composite box girders, but a considerable amount of information is available on the subjects of composite action (particularly related to T-beams), and steel box girders. A few papers are also available describing practical examples of the use of composite box girders. This literature review is divided into four sections:

(1) Examples of the use of composite boxes.
(2) Composite action.
(3) Behaviour of steel box girders
(4) Behaviour of composite box girders

1.2.1 Examples of the use of composite box girders

The design and construction of the Tay Road Bridge is described by Fairhurst and Beveridge (1). The main components of the bridge are a concrete deck slab acting compositely with two closed steel box girders. Fig 1.1 shows a very simplified cross-section of one box and the associated slab. The bridge was designed and constructed in the years 1959 to 1965 and design stresses are in accordance with BS.153; shear connection is provided by 19mm diameter by 100mm long headed studs, the safe loads for the studs being as recommended by Viest, et al. (2), using a safety factor of 3. Hogging moment regions were designed on the assumption that composite action can be relied on only if the concrete slab is pre-stressed sufficiently to avoid cracking.

As part of the design of this bridge a 1:4 scale model of one span of the bridge was tested (3); the following conclusions were drawn from this test:

(1) Simple bending theory applied and no shear lag was evident.

(2) In the elastic range the concrete carried 90 per cent of the load calculated for full interaction and no permanent slip was noted.

(3) Collapse took place by buckling of a web-stiffener assembly.

In addition to the above it was noted that a concentrated load applied over one web produced distortion of the section equivalent to a 70 per cent reduction in torsional rigidity. The problem of distortion of box sections has been discussed by Billington (4).

The Birkenhead-Mersey Tunnel approach viaducts are described by Gray, Clark and Gent (5). The structure consists of an open-topped steel box acting compositely with a reinforced concrete deck slab. The scheme was designed and constructed in the years 1966 to 1969 and designed in accordance with BS.153, CP.114 and CP.117, part 2. Tests were conducted on a 1:4 scale model of part of the bridge. One test on the torsional stiffness of the model led to the following conclusion:

"In general it appears that the torsional rigidity of a stiff composite box cannot be treated as a constant. The effect of interface slip should be considered in assessing the worst forces in an indeterminate structure."

A number of papers (6, 7, 8) concerning the construction of composite bridges were presented at the Conference on Steel Bridges in 1968. The White Cart Viaduct (6) was opened in 1968 and consisted of twin mild steel trapezoidal girders acting compositely with an eight inch reinforced concrete deck slab. The following features are worthy of note:

(1) Shear connectors are headed studs welded to the top flange immediately over the line of the stiffening angles. In this way there is no fear of flange plate buckling due to stud loading.

(2) In the shops the boxes were tested for torsional rigidity by jacking up one corner, and it was found that a 16.75m long unit was more flexible than anticipated by calculation. This was due to the ability of the short box to warp. whereas a similar test on a 67m portion showed torsional deflection to be negligible.

Five examples of the use, in Germany and Holland, of open composite box girders, are given in ref. 36. Comparison of two of these examples shows the great variation in the dimensions of bridge for which this type of structure may be suitable. Fig 1.3 shows the cross-section of a viaduct constructed in Hanover, Germany; it consists of a 2m x 0.8m steel section acting compositely with a 5m wide deck slab. The span of the bridge (20m) is comparatively small, but part of the structure is built on a horizontal curve, and hence the structure had to be designed to resist comparatively large torsional loads. In order to obtain good composite action the steel section was connected to the pre-cast concrete slab by high strength bolts passing through the slab, thus composite action was achieved by friction between the steel and concrete as well as by shearing of the connectors.

The Schloss Bridge at Mulheim On Ruhr, again in Germany, (fig 1.4) is an example of a much larger open composite box girder. This is a continuous bridge with spans of 42m, 45m and 42m; here two open steel boxes 4.5m x 2.2m act compositely with a 24.5m wide concrete deck slab. In order to prevent cracking of the concrete the deck is prestressed both laterally and longitudinally.

Two papers on the stress analysis of composite box girders have been presented in Japan (9, 10). In ref. 9 the theoretical and measured stresses in a composite, single box bridge are compared; ref. 10, available only in Japanese, gives the derivation of the equations used to calculate the stresses in ref. 9.

1.2.2 Composite Action

There are numerous references to composite action (e.g. 11-17) but the majority of these are concerned with tests on shear connectors and the strength of simply-supported T-beams loaded with compression in the concrete. These references give a large amount of information about the load-slip characteristics of shear connectors and the effect of interface slip on the deflections and ultimate loads of simply supported beams loaded in bending. When attempting to apply results of tests on composite T-beams to composite box girders it should be remembered that there are important differences between the geometries of these two types of section. A typical composite T-beam is made up from a 1.5m x 150mm slab on a 305mm x 165mm x 54kg BSB (ref 12), giving a neutral axis close to the steel-concrete interface; a typical composite box girder (fig 1.1) has a neutral axis between one third and half way down the steel section. This different neutral axis position results in different types of loading on the concrete slab.

Barnard (11) describes a series of tests on simply-supported T-beams loaded with a symmetrical two-point load such that the interface slip was zero in the area of maximum moment. Conclusions drawn from this work include the following:

(1) The use of the stress-strain properties of the steel and concrete and the assumption of linear continuous strain distribution throughout the depth of the section leads to an accurate prediction of the ultimate strength.

(2) Because of residual stresses, the moment-curvature curve will cease to be linear elastic at a lower moment than predicted from the stress-strain relations.

Chapman (12) and Chapman and Balakrishnan (13) describe tests on various types of shear connection and on sixteen simply supported composite T-beams. Recommendations for the method of design of shear connections in T-beams are given.

Johnson, Greenwood and Van Dalen (14) give the results of pushout tests on small (8mm diameter) studs set in cracked reinforced concrete slabs. Recommendations for the design of stud shear connections in hogging moment regions are given.

Johnson, Van Dalen and Kemp (15) describe four series of tests designed to investigate the strength of continuous composite beams for buildings; in particular the ultimate load behaviour in the hogging moment region was considered. As a result of these tests the authors say that there is no doubt that full composite action can occur in hogging moment regions and stud shear connectors can transfer shear in regions where the concrete slab is badly cracked due to longitudinal tension.

1.2.3 Behaviour of Steel Box Girders

A great deal of literature has been published on various aspects of the analysis and design of box girders. The most powerful method of analysis available is the finite element method (16), with this method problems such as shear lag and the presence of stiffeners and diaphragms can all be accounted for. The development of new types of element designed specifically for box girder analysis (17) has resulted in a reduction in the number of elements required to describe the structure accurately and has hence reduced both the computer costs and amount of data

preparation required. Even so the high computer costs involved with the use of the finite element method has greatly restricted its use.

A second method of analysis results from the fact that a point load over one web of a box girder may be split into three components, causing bending, twisting and distortion of the section. For elastic analysis of sections of practical dimensions these components may be considered independently (18).

The bending component may be treated by simple bending theory.

The torsion component produces shears which twist the box and, in all but a few special cases, also produces longitudinal warping stresses. These stresses may be calculated by simple torsion theory.

The distortion component produces transverse bending in the box and, if the amount of distortion varies along the length of the box, longitudinal warping stresses will result. The evaluation of these stresses has been discussed by Billington (4).

Lamas (19) has used the dynamic relaxation method to investigate the behaviour of the compression flanges of a box girder. Extension of this method to analyse a complete box is possible, but presents the same problems with computer time as the finite element method.

A more detailed review of the various methods of analysis and design of steel plate and box girders is given by Dowling (37). This paper includes an outline of the various approaches to the inelastic analysis of the components making up a steel plate or box girder, and also discusses the application of results obtained from these analyses to formulation of design rules.

1.2.4 Behaviour of Composite Box Girders

Any of the above methods of analysis may be adapted for use with composite box girders. The simplest method of doing this is to replace the concrete slab with an equivalent area

of steel and then analyse the beam as before. The use of this method assumes a completely rigid shear connection between the steel and the concrete, which can only be ensured by having an excessive number of shear connectors.

The problem of incomplete interaction has been solved for elastic, simply supported composite T-beams under a central point load (20). This method could be adapted for use with composite box girders provided that the dimensions of the beams are such that shear lag may be neglected. Moffatt (21) has developed a finite element program which can take account of partial interaction in composite box sections; this has been used to investigate the longitudinal bending behaviour of such sections and, in particular, the influence of shear lag on the stresses, deflections and shear connector forces.

Mattock and Johnston (38) have conducted a theoretical and experimental investigation into the lateral distribution of load in composite box girder bridges. For the theoretical work the stiffness method of analysis was used, and all plates were assumed to be linear elastic and isotropic. The theoretical results were compared with experimental results obtained from one quarter scale models of two bridges, one consisting of three open boxes and the other of two open boxes, both sets of boxes acting compositely with a reinforced concrete deck slab. Influence lines were plotted for the strains in the bottom flanges and for the overall deflections of the models, for a concentrated load moving across the midspan of the bridge. Good general agreement was obtained between the theoretical and experimental results, but the models proved to have a slightly higher torsional rigidity than predicted by the theory.

No previous investigators have considered the effect of interface slip on the torsional properties of composite boxes. As mentioned previously (section 1.1) the flexibility of the shear connection is particularly important in the design of open composite boxes under torsion loading, but it is also of significance when calculating stud loadings in closed composite boxes.

A second problem associated with composite boxes is that of cracking of the concrete slab; this problem is particularly important in the area around the supports of a continuous beam, where there will be a hogging moment, putting the slab into tension. Any cracking of the concrete in this region may affect two important properties of the Section:

(1) The ability of the shear connection to transmit shear force from the steel flange to the reinforcement in the concrete.

(2) The torsional rigidity of the section.

The second of these problems is of particular importance in open composite box sections where the cracking of the concrete could result in the loss of some of the advantageous properties of a closed section in resisting any torsional component of loading.

Another problem which has not yet been adequately studied is that of shear lag in the hogging moment region. Moffatt's finite element program (see above) has been used to study the problem theoretically but there are no experimental results with which to compare this theoretical work.

Associated with the problems of shear lag and of partial interaction is that of distribution of forces in the shear connection, and hence the required distribution of the shear connectors. Current design methods involve distribution of the connectors uniformly across the section; this method has been proved to be perfectly adequate for composite T-beams where, because of the narrow steel flange, the shear lag effect in the steel section is small. In composite box construction the steel flange is much wider, hence shear lag is of greater significance; this leads to strains in the central portion of the flange being much smaller than those in the outer portions. As a result of this the shear force transmitted from the steel flange to the concrete slab will vary across the width of the flange, and hence the method of distributing the connectors uniformly across the flange must be questioned. This problem

has been partially tackled in recent design codes, where the number of shear connectors required to resist the shear force must be placed inside the effective breadth of the section, and extra connectors must be placed outside this width to give uniform spacing across the whole section. It seems likely that this method will result in an excessive number of connectors in the central region of the flange, and work by Moffatt has indicated that connectors in the regions near the webs may be overloaded.

1.3 OBJECTS OF THIS THESIS

The work described in this thesis was intended to provide theoretical and experimental results concerning the behaviour up to ultimate load of open and closed composite box girders under various combinations of bending, shear and torsion loading.

A large amount of theoretical and experimental data on the effect of geometric non-linearity on steel box girders is already available (36). The object of the work described here was to investigate the effects of material non-linearity and partial interaction on the behaviour of composite box girders. Because of the complexity of the problem of interaction of material and geometric non-linearity it was decided that all the models should be designed such that plate buckling would not occur, and in all theoretical work it was assumed that the plates forming the box girders were stiffened sufficiently to avoid buckling.

Whilst doing the preliminary reading for this project it was found that there was no adequate method available for calculating the ultimate load of a steel hollow section under bending, shear and torsion load; hence chapter 2 of this thesis contains proposed upper and lower bound solutions to this problem. Following other work at Imperial College (e.g. Lamas (19)) it was decided that for the main theoretical work the dynamic relaxation method would be used to solve the finite difference equations for a set of plates joined to form a box girder. The application of this method to the analysis of a steel section is described in chapter 3 and results obtained are

compared with the upper and lower bound solutions. In chapter 4 this method of analysis is extended to both open and closed composite box girders.

The experimental work described (chapter 5) consisted of a series of tests on small (approx. $^1/_8$) scale composite box girders under various combinations of load. The object of this series of tests was to identify some of the problems associated, in particular, with the hogging moment region of composite box girders.

ULTIMATE LOAD BEHAVIOUR OF STEEL HOLLOW SECTIONS

2.1 REVIEW OF PREVIOUS WORK

Several investigations into the ultimate load behaviour of non-buckling steel hollow sections under various combinations of bending and torsion loading have been reported.

Hill and Siebel (22) consider the behaviour of thin, hollow circular sections under bending moment and torsion. Solutions are based on the Von Mises yield criterion and the following relation between increments of stress and strain for a plastic region of the section:

$$\frac{d\gamma - d\tau/G}{dE - d\sigma/E} = \frac{3\tau}{\sigma}$$

where τ = shear stress, $d\tau$ = shear stress increment
σ = direct stress, $d\sigma$ = direct stress increment
$d\gamma$ = shear strain increment, dE = direct strain increment
G = shear modulus, E = Young's modulus

Using the above yield criterion and flow rule the authors are able to plot moment-curvature and torque-twist relations for various combinations of moment and torque. They are also able to give limiting values of moment and torque, which are shown to fall on the curve $m^2 + t^2 = 1$

where $m = M/M_p$, $t = T/T_p$
M_p = Plastic moment under pure bending
T_p = Plastic torque under pure torsion
M = Ultimate moment in presence of torque T.

Siebel (23) reports results of tests on hollow cylinders which show good agreement with the above theory.

Gaydon and Nuttall (24) give upper and lower bounds to the relation between bending moment and torsion load at yield for various sections. For the lower bound solution, distributions of shear and direct stress are assumed to be a constant fraction of those for plastic bending and plastic torsion applied separately; it is then assumed that the Von Mises yield criterion must not be violated at any point. These assumptions lead to the interaction formula $m^2 + t^2 = 1$, as derived by Hill and Siebel, but in this case it has been derived as a lower bound for a general cross-section, whereas in Ref 2.1 it was shown to be an upper bound for a thin, hollow circular section.

The upper bound solution presented in ref. 24 is based on an assumed velocity distribution representing a combination of bending and twisting (including the associated warping displacements). From this assumed velocity distribution, by the use of Hill's inequality (26) they are able to produce upper bounds to the ultimate load of solid and hollow rectangular sections. As shown in fig. 4 of this reference this upper bound solution is very high in cases where the ratio of torsion load to bending load is high.

Komatsu and Sakimoto (25) present a solution to the problem of the elasto-plastic behaviour of hollow sections under bi-axial bending, torsion and axial compression. The Von Mises yield criterion and Prandtl-Reuss stress-strain relationship are assumed and the cross-sectional shape is assumed to be such that warping torsion may be neglected. The presençe of residual stresses is also considered. Test and theoretical results are given for square and circular hollow sections under axial load and torsion, results plotted show the relation between torsion load and twist angle for a constant axial load. Theoretical results are given for both the flow and deformation theories of plasticity and it is shown that, while the ultimate load predictions of the two theories both agree closely with the test results, the flow theory gives much better agreement with the test results for the shape of the torque-twist curve.

In the discussion so far no consideration has been given to the effect of bending shear forces. A discussion of various methods of analysis of solid rectangular sections and I-sections under bending moment and shear force is given by Neal (27). For an I-section which, under bending and shear loading behaves very similarly to a rectangular hollow section, Neal concludes that, for practical purposes, an empirical relation suggested by Heyman and Dutton gives good results. This relation is given by:

$$M_F = M_p \left\{1-\left[\frac{A_W}{2A_F + A_W}\right]\left[1-(1-f^2)^{\frac{1}{2}}\right]\right\} \quad f \leqslant 1$$

where A_w = Area of web A_F = Total area of flanges

M_p = Plastic moment with no shear force

M_F = Plastic moment in presence of shear force F

F_p = Fully plastic shear force assuming shear force is carried solely by the web i.e. $F_p = A_w\sigma_o/\sqrt{3}$

$f = F/F_p$

Neal also warns against analysis of the effect of shear on ultimate load behaviour by consideration of stress distributions or plastic deformations at the critical section only, with no attention being paid to conditions in the remainder of the cantilever. By consideration of a single cross-section neither a true upper nor lower bound may be obtained. Both the upper and lower bound approaches outlined in the next section consider only the critical cross-section, the justification for this is that they give satisfactory agreement with Heyman and Dutton's empirical result (see above) and with the finite difference analysis presented in the next chapter.

The methods proposed in the next section give upper and lower bounds to the ultimate load of a hollow rectangular section subject to bending, shear and torsion load. Only uniaxial bending and shear is considered but extension to consider biaxial bending and shear and also axial tension or compression is possible.

2.2 UPPER BOUND SOLUTION

Consider a rectangular hollow section with dimensions 2B x 2D and thickness t.

The following assumptions are made:

(1) t is small compared with B and D.

(2) σ and τ are the only non-zero stress components where σ is the axial stress along the length of the hollow section and τ is the shear stress around the section.

(3) A plastic hinge is formed with the following displacement components:

(a) Bending rotation α corresponding to the applied moment M.

(b) Twisting rotation β corresponding to the applied torque T.

(c) Shear strain d/ℓ corresponding to the applied shear force F where ℓ is the length of the plastic hinge.

(4) Warping of the section due to torsion is negligable.

Fig 2·1(a)

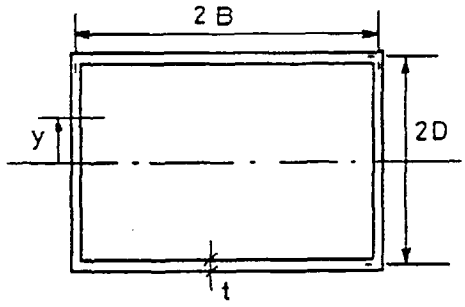

For the webs: shear strain = $\frac{\beta B}{\ell} \pm \frac{d}{\ell} = \gamma_w$

axial strain = $\frac{\alpha y}{\ell} = \varepsilon_w$

For the flanges: shear strain = $\frac{\beta D}{\ell} = \gamma_F$

axial strain = $\frac{\alpha D}{\ell} = \varepsilon_F$

Hence for the flanges $\frac{\varepsilon_F}{\gamma_F} = \frac{\alpha}{\beta}$

webs $\frac{\varepsilon_w}{\gamma_w} = \frac{\alpha y}{\beta B \pm d}$ ——————(1)

For the solution of these equations it is necessary to find the stress distribution in the section caused by these strains and integrate the stresses around the section to find the corresponding applied loads. For calculation of the stress distribution a rigid-plastic stress-strain relation and the Von Mises yield criterion and associated flow rule are assumed. (These assumptions are appropriate provided the strains are large compared with the elastic strains).

Von Mises yield criterion: $\sigma^2 + 3\tau^2 = \sigma_o^2$ ——————(2)

where σ_o is the yield stress is tension.

Von Mises flow rule $\frac{\sigma}{\tau} = \frac{3\varepsilon}{\gamma}$ ——————(3)

Substituting (2) and (3) in (1) gives:

For flanges: $\sigma_F = \frac{\lambda\sigma_o}{\sqrt{1+\lambda^2}}$ $\qquad \tau_F = \frac{\sigma_o}{\sqrt{3}\sqrt{1+\lambda^2}}$

For webs: $\sigma_w = \frac{\lambda\sigma_o y/B}{\left[(1\pm\nu)^2+(\lambda y/B)^2\right]^{\frac{1}{2}}}$ $\qquad \tau_w = \frac{\sigma_o(1\pm\nu)}{\sqrt{3}\left[(1\pm\nu)^2+(\lambda y/B)^2\right]^{\frac{1}{2}}}$ ——(4)

where $\lambda = \frac{\sqrt{3}\alpha}{\beta}$ $\qquad \nu = \frac{d}{B\beta}$

The significance of the $(1\pm\nu)$ terms should be noted here. The + sign applies in the web where the bending and torsion shear strains are in the same direction, the - sign in the web where they are in opposite directions.

If $\nu<1$ the shear strain due to bending is less than that due to torsion, if $\nu>1$ the shear strain due to bending is greater than that due to torsion.

Integrating equations (4) around the section gives:

$$\text{Moment } M = \left\{\frac{\lambda\sigma o}{\sqrt{1+\lambda^2}}\right\} 4Bt + 2\int_o^D \sigma_{w1}\, ty\,dy + 2\int_o^D \sigma_{w2}\, ty\,dy \qquad \text{——(5A)}$$

$$\text{where } \sigma_{w1} = \frac{\sigma o\lambda y/B}{\left[(1+\nu)^2 + (\lambda y/B)^2\right]^{\frac{1}{2}}} \qquad \sigma_{w2} = \frac{\sigma o\lambda y/B}{\left[(1-\nu)^2 + (\lambda y/B)^2\right]^{\frac{1}{2}}}$$

$$\text{Torque } T = \left\{\frac{\sigma o}{\sqrt{3}\sqrt{1+\lambda^2}}\right\} 4BDt + 2\int_o^D B\tau_{w1}\, t\,dy + 2\int_o^D B\tau_{w2}\, t\,dy \qquad \text{——(5B)}$$

$$\text{where } \tau_{w1} = \frac{\sigma o(1+\nu)}{\sqrt{3}\left[(1+\nu)^2 + (\lambda y/B)^2\right]^{\frac{1}{2}}} \qquad \tau_{w2} = \frac{\sigma o(1-\nu)}{\sqrt{3}\left[(1-\nu)^2 + (\lambda y/B)^2\right]^{\frac{1}{2}}}$$

$$\text{Shear force } F = 2\int_o^D \tau_{w1}\, t\,dy - 2\int_o^D \tau_{w2}\, t\,dy \qquad \text{————————(5C)}$$

Re-writing equation 5A

$$M = \frac{\lambda\sigma o}{\sqrt{1+\lambda^2}} 4BDt + I_1 + I_2 \qquad \text{————————(6)}$$

Evaluation of I_1

Put $K = \frac{\lambda t\sigma o}{B}$; $a = (1+\nu)$; $b = \frac{\lambda}{B}$

$$\therefore\ I_1 = 2k\int_o^D \frac{y^2 dy}{\left[a^2+b^2y^2\right]^{\frac{1}{2}}}$$

$$\therefore\ I_1 = \frac{2k}{b^2}\int_o^D \left[b\sqrt{y^2+a^2/b^2} - \frac{a^2}{b\sqrt{y^2+a^2/b^2}}\right] dy$$

$$\therefore \quad I_1 = \frac{2k}{b^2}\left[\frac{by}{2}\sqrt{y^2+a^2/b^2} + \frac{b}{2}\frac{a^2}{b^2}\ln\left(y+\sqrt{y^2+a^2/b^2}\right) - \frac{a^2}{b}\left\{\ln\left(y+\sqrt{y^2+a^2/b^2}\right) - \ln a/b\right\}\right]_0^D$$

substituting back values for a, b and k

$$\text{gives} \quad I_1 = \frac{2B^2 t\sigma_o}{\lambda^2}\left[\frac{\lambda D}{2B}\sqrt{\frac{\lambda^2 D^2}{B^2}+(1+\nu)^2} - \frac{(1+\nu)^2}{2}\ln\left\{\frac{\frac{\lambda D}{B}+\sqrt{\frac{\lambda^2 D^2}{B^2}+(1+\nu)^2}}{(1+\nu)}\right\}\right]$$

Similar evaluation of I_2 and substitution into equation 5A leads to:

$$M = Bt\sigma_o\left\{\frac{4D\lambda}{\sqrt{1+\lambda^2}} + \frac{D}{\lambda}\left[\sqrt{\frac{\lambda^2 D^2}{B^2}+(1+\nu)^2} + \sqrt{\frac{\lambda^2 D^2}{B^2}+(1-\nu)^2}\right] - \frac{B}{\lambda^2}\left[(1+\nu)^2 A_1 + (1-\nu)^2 A_2\right]\right\}$$

Similarly equations 5B & 5C reduce to

$$T = \frac{Bt\sigma_o}{\sqrt{3}}\left\{\frac{4D}{\sqrt{1+\lambda^2}} + \frac{2B}{\lambda}\left[(1+\nu)A_1 + (1-\nu)A_2\right]\right\} \qquad (7)$$

$$F = \frac{2Bt\sigma_o}{\sqrt{3}\,\lambda}\left\{(1+\nu)A_1 - (1-\nu)A_2\right\} \qquad (8)$$

where $A_1 = \ln\left\{\frac{\lambda D/B+\sqrt{(\lambda D/B)^2+(1+\nu)^2}}{(1+\nu)}\right\}$

$$A_2 = \ln\left\{\frac{\lambda D/B+\sqrt{(\lambda D/B)^2+(1-\nu)^2}}{|(1-\nu)|}\right\}$$

The solution of these equations will be discussed after derivation of the lower bound solution.

2.3 LOWER BOUND SOLUTION

The basic requirement for a lower bound solution is that a stress distribution in equilibrium with the applied loads must be found. One possible state of stress which satisfies this condition is given by assuming that: (1) shear and torsion loads are resisted by shear forces distributed as given by elastic theory; (2) bending stresses are distributed such that the section becomes fully plastic.

As before consider a section 2B x 2D of thickness t and assume that it is subject to bending, shear and torsion loading.

Assume the following bending and torsion shear stress distributions:

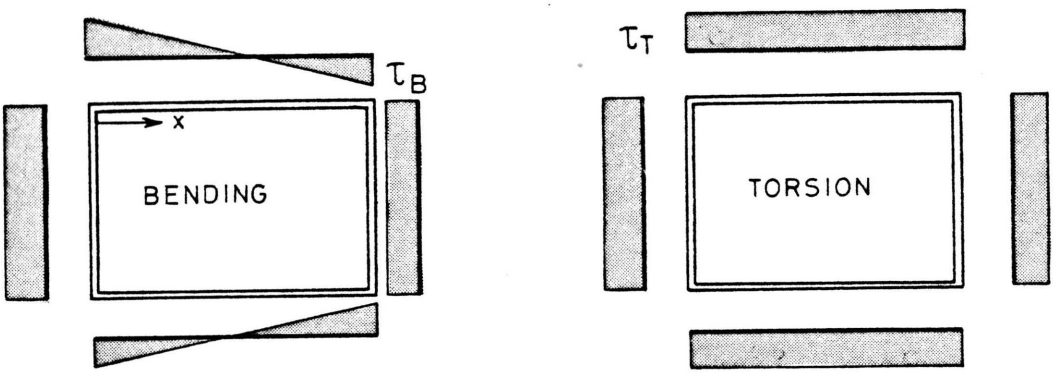

For the flanges total shear stress = $\tau_T + \tau_B(1 - \frac{x}{B}) = \tau_F$

For the left hand web shear stress = $\tau_T + \tau_B = \tau_{WL}$

For the right hand web shear stress = $\tau_T - \tau_B = \tau_{WR}$

Hence, in order to yield the whole section, using Von Mises yield criterion:

In the flanges direct stress = $\sqrt{\sigma o^2 - 3[\tau_T - \tau_B(1-\frac{x}{B})]^2} = \sigma_F$

In the L.H. web direct stress = $\sqrt{\sigma o^2 - 3[\tau_T + \tau_B]^2} = \sigma_{WL}$

In the R.H. web direct stress = $\sqrt{\sigma o^2 - 3[\tau_T - \tau_B]^2} = \sigma_{WR}$

Integrating around the section gives:

Moment $M = D^2 t\,(\sigma_{WL} + \sigma_{WR}) + 2\int_0^{2B} \sigma_F D t dx$ ——————(9)

Torque $T = 8BDt\tau_T$ ——————(10)

Shear force $F = 4Dt\tau_B$ ——————(11)

Length of beam = $\frac{M}{F}$

Evaluation of the integral in equation (9) gives:

$$M = D^2 t(\sigma_{WL} + \sigma_{WR}) + \frac{BDt\sigma_o^2}{\sqrt{3}\tau_B}\left\{\text{Sin}^{-1}\frac{\sqrt{3}(\tau_T+\tau_B)}{\sigma o} - \text{Sin}^{-1}\frac{\sqrt{3}(\tau_T-\tau_B)}{\sigma o} - \frac{\sqrt{3}(\tau_T-\tau_B)\sigma_{WR}}{\sigma o^2} + \frac{\sqrt{3}(\tau_T+\tau_B)\sigma_{WL}}{\sigma o^2}\right\} \quad (12)$$

In addition to the lower bound condition discussed above consideration must also be given to the possibility that the heavily loaded web, (where the shear stresses due to torsion and those due to the shear load are of the same sign), will fail in shear before overall failure of the beam occurs. In order to allow for this possibility a second lower bound must be considered, this condition being that the section fails when $\tau_T + \tau_B = \sigma o/\sqrt{3}$. In practice this is likely to be a rather pessimistic lower bound as frame action and the presence of any diaphragms will lead to redistribution of stresses and an increase in the load which the beam can support. In all following work the lower bound solution is considered to be the lower of the two conditions discussed above.

2.4 SOLUTION OF UPPER AND LOWER BOUND EQUATIONS

2.4.1 Upper Bound Equations

Re-writing equations (6) - (8)

$$\left.\begin{aligned} M &= \phi(\lambda,\nu) \\ T &= \psi(\lambda,\nu) \\ F &= \theta(\lambda,\nu) \end{aligned}\right\} \quad (12)$$

In order to solve the equations for a given length of beam (L) and a given load combination it would be desirable to solve the above equations (12) subject to the additional conditions:

$$\left.\begin{aligned} L &= M/F \\ R &= F/T \end{aligned}\right\} \quad (13)$$

where L and R are specified.

Equations (12) and (13) may be re-written as

$$\left.\begin{aligned} E_1 &= \phi(\lambda,\nu) - L \times \theta(\lambda,\nu) \\ E_2 &= \psi(\lambda,\nu) - \theta(\lambda,\nu)/R \end{aligned}\right\} \quad (14)$$

The desired solution is obtained when values of λ and ν are found which give $E_1 = E_2 = 0$. In order to obtain the required values of ν and λ the Newton-Raphson method for simultaneous equations (Ref 28) may be used. From initial guesses of values for ν and λ (νn and λn) new approximations are found from the equations

$$\nu_{n+1} = \nu_n + \frac{E_2 \frac{\partial E_1}{\partial \lambda} - E_1 \frac{\partial E_2}{\partial \lambda}}{\frac{\partial E_1}{\partial \lambda}\frac{\partial E_2}{\partial \nu} - \frac{\partial E_1}{\partial \nu}\frac{\partial E_2}{\partial \lambda}}$$

$$\lambda_{n+1} = \lambda_n + \frac{E_1 \frac{\partial E_2}{\partial \nu} - E_2 \frac{\partial E_1}{\partial \nu}}{\frac{\partial E_1}{\partial \lambda}\frac{\partial E_2}{\partial \nu} - \frac{\partial E_1}{\partial \nu}\frac{\partial E_2}{\partial \lambda}}$$

In order to obtain reasonable initial guesses for ν and λ a family of curves of L against λ for various values of ν may be plotted.

2.4.2 Lower Bound Equations

These equations may be solved in a similar manner to that described above for the upper bound equations.

2.5 RESULTS OBTAINED FROM UPPER & LOWER BOUND SOLUTIONS

2.5.1 Sections under bending and shear only.

Fig 2.1 shows a comparison between results obtained from the proposed upper and lower bound solutions and those obtained from the Heyman-Dutton empirical relation; the beam considered is a rectangular hollow section 200 mm x 300 mm of uniform thickness. It can be seen that for L>500 mm the empirical relation lies between the upper and lower bound solutions, but for very short beams (L<500 mm) the empirical relation indicates a strength even higher than the upper bound solution. For these very short beams the gradients of stress and strain along the beam are very high, and hence the errors introduced by considering a single cross-section of the beam are likely to be more significant than for the longer beams. In addition the strength of a very short beam is likely to depend greatly on the conditions at the point of application of the load and at the support; hence it is probably not possible to give an accurate general formula for the strength of such a beam. It can also be seen from fig.2.1 that the reduction in ultimate moment due to the presence of shear is very small for beams with D/L<0.25 (where 2D = depth of section, L = cantilever length), at D/L = 0.25 the reduction in ultimate moment is between 3½% (upper bound solution) and 7% (lower bound solution).

2.5.2 Sections under Bending, Shear and Torsion Load

Figs 2.2 and 2.3 show interaction curves for a hollow section of uniform thickness and dimensions 300 mms x 200 mms. Fig 2.2 is for bending about the major axis, Fig 2.3 for bending about the minor axis, cantilevers of length 300 mms, 600mms and 1200 mms are considered. These interaction curves show that in the high torque regions the lower bound solution is governed by the local web failure, but in the high moment regions the overall failure mode becomes the significant lower bound. The point at which the change in lower bound failure mode takes place depends on the length of the beam, for the longer beams the overall failure governs for torque ratios (T/T_p) up to about 0.9, whereas for the short, shallow beam the local failure mode becomes significant at a torque ratio of about 0.15. It can also be seen that for the longer beams the difference between the upper and lower bound solutions is quite small (<5%), and hence a reasonably accurate prediction of the ultimate load may be made. For the shorter beams, particularly in regions where $M/M_p \approx T/T_p$, the difference between the upper and lower bound solutions is much greater. The difference between the two solutions is particularly large where the web failure governs the lower bound; as already discussed (Section 3) these lower bounds are likely to be rather pessimistic. It is interesting to note that, particularly for short beams, the effect of a small bending moment and associated shear force on the ultimate torque is much greater than the effect of a small torque on the ultimate moment (provided that the effect of the bending shear on the ultimate moment has been allowed for).

2.6 EXTENSION TO INCLUDE OTHER LOADING CONDITIONS

Extension of the upper and lower bound solutions to include biaxial bending and the presence of axial tension of compression may be effected by including corresponding extra strains (upper bound solution) or stresses (lower bound solution). Inclusion of these extra components will lead to much more complex integrals in equations 5 and 9 and the solution by the Newton-Raphson method will have to be extended to include three or more variables.

FINITE DIFFERENCE ANALYSIS OF STEEL HOLLOW SECTIONS

3.1 INTRODUCTION

The object of this section of the work was to use the finite difference method to analyse the behaviour of closed steel hollow sections under various combinations of bending, shear and torsion loading. The results obtained by this method are compared with the upper and lower bound solutions described in chapter 2.

Experience of other investigators (19) has shown that a full analysis of the behaviour of a box girder under only bending and shear loading poses considerable problems in defining and satisfying the boundary conditons at the plate junctions; addition of the torsion component of loading would add considerably to these problems because the symmetry present in the bending case would be lost. The emphasis in all work described here was on non-linear material behaviour rather than non-linear geometric behaviour and hence throughout the analysis it has been assumed that no buckling of the plates forming the hollow section will occur. Having decided not to consider plate buckling problems only small extra approximations are involved in assuming that each of the four plates is in a state of plane stress. These extra approximations are discussed here.

3.2 THE PLANE STRESS ASSUMPTION

If it can be proved that the plane stress assumption is valid for a box under bending and shear load and for a box under torsion load it may be assumed that it is also valid for a box under bending, shear and torsion load. Both the bending and torsion cases are discussed with reference to a square box of uniform thickness, but may be extended to include other cases.

3.2.1 Action of a square uniform thickness box under torsion loading.

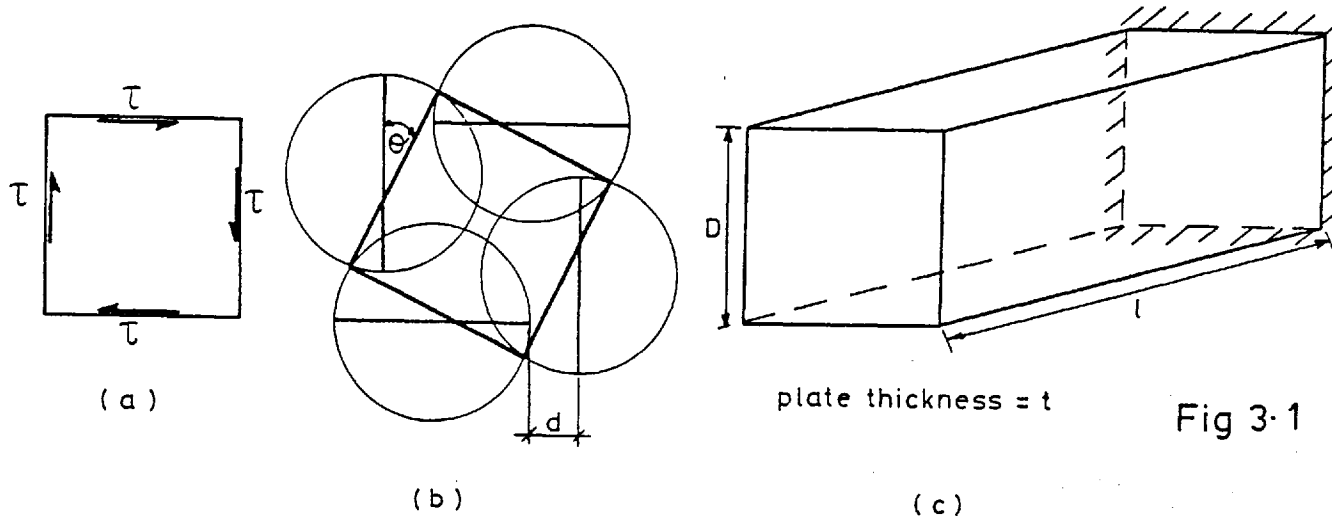

Fig 3·1

Assume that the torsion load is applied by a uniform shear stress around the end of the section (fig 3.1a). The shear stress in each plate causes it to displace a distance d in its own plane. This displacement alone would cause a discontinuity at the plate junctions; this discontinuity is closed by the plates twisting out of their plane by an angle θ (fig 3.1b).

Consider a cantilever beam with dimensions as in fig 3.1c.

In-plane displacement of each plate = $d = \frac{\tau \ell}{G}$

Rotation of each plate $\theta = \frac{2d}{D} = \frac{2\tau\ell}{DG}$

let τ_T be the maximum shear stress in the plate caused by this twisting

$$\tau_T = \frac{tG\theta}{\ell} = \frac{2\tau\ell}{DG} \times \frac{Gt}{\ell}$$

$$\tau_T = \frac{2\tau t}{D}$$

Hence, provided D>>t the maximum stress due to the plate twisting is negligable compared with the in-plane shear stress.

3.2.2. Action under bending load.

In this case the most important error in the plane stress assumption is present in the top and bottom flanges, where the direct stress is greater on the outer faces than on the inner faces of the plates. For a box as in fig 3.1 let

σo = direct stress on outside of flanges

σI = direct stress on inside of flanges

$$\frac{\sigma o}{\sigma I} = \frac{D+t}{D-t}$$

Hence it can be seen that for D>>t it can be assumed that $\sigma o = \sigma I$, and hence the plane stress assumption is valid.

3.3 THE PLANE STRESS THEORETICAL MODEL

In the previous section it has been demonstrated that a steel hollow section may be represented by four steel plates joined to form a box. For this analysis a cantilever box loaded at its free end is considered.

3.3.1 Plane stress plate equations

The plane stress equilibrium equations for a plate are as follows:

$$\left.\begin{aligned} \text{x-direction equilibrium } & \frac{\partial Nx}{\partial x} + \frac{\partial Nxy}{\partial y} = 0 \\ \text{y-direction equilibrium } & \frac{\partial Ny}{\partial y} + \frac{\partial Nxy}{\partial x} = 0 \end{aligned}\right\} \quad 3.1$$

Increments of the stress resultants (ΔNx, ΔNy, ΔNxy) are related to increments of the strains in the plate ($\Delta\varepsilon x$, $\Delta\varepsilon y$, $\Delta\gamma xy$) by a rigidity matrix $\underline{C}$

$$\begin{bmatrix} \Delta Nx \\ \Delta Ny \\ \Delta Nxy \end{bmatrix} = \begin{bmatrix} C11 & C12 & C13 \\ C21 & C22 & C23 \\ C31 & C32 & C33 \end{bmatrix} \begin{bmatrix} \Delta\varepsilon x \\ \Delta\varepsilon y \\ \Delta\gamma xy \end{bmatrix}$$

where $\varepsilon x = \partial u/\partial x$; $\varepsilon y = \partial v/\partial y$; $\gamma xy = \partial u/\partial y + \partial v/\partial x$

The method of evaluating the rigidity matrix is discussed in section 3.4. In order to obtain a solution to the problem under investigation equations 3.1 must be solved, subject to a suitable set of boundary conditions, for four plates joined to form a box.

3.4 EVALUATION OF RIGIDITY MATRIX (Ref 30)

The Ilyushin yield criterion for a plane stress condition may be expressed as

$$f = (Nx^2 + Ny^2 - NxNy + 3Nxy^2)/No^2 < 1 \qquad 3.2$$

where $No = \sigma ot$

After yielding, for plastic flow to take place, the stress resultants must remain on the yield surface, hence

$$\delta f = 0 \qquad 3.3$$

and hence $\underset{\sim}{fn}^T \Delta\underset{\sim}{N} = 0 \qquad 3.4$

where $\underset{\sim}{fn} = \begin{Bmatrix} \frac{\partial f}{\partial Nx} \\ \frac{\partial f}{\partial Ny} \\ \frac{\partial f}{\partial Nxy} \end{Bmatrix}$ $\qquad \underset{\sim}{\Delta N} = \begin{Bmatrix} \Delta Nx \\ \Delta Ny \\ \Delta Nxy \end{Bmatrix}$

The plastic flow law may be expressed as

$$\Delta\underset{\sim}{\varepsilon}p = \lambda f\underset{\sim}{n} \qquad 3.5$$

where $\Delta\underset{\sim}{\varepsilon}p$ represents the plastic components of $\Delta\underset{\sim}{\varepsilon}$ and λ is a positive scaler.

The elastic incremental stress-strain relations may be written as

$$\Delta\underset{\sim}{N} = \underset{\sim}{CE}(\Delta\underset{\sim}{\varepsilon}-\Delta\underset{\sim}{\varepsilon}p) \qquad 3.6$$

From 3.4, 3.5 and 3.6 we get

$$\lambda = \frac{f\underset{\sim}{n}^T \underset{\sim}{CE}\ \Delta\underset{\sim}{\varepsilon}}{f\underset{\sim}{n}^T \underset{\sim}{CE}\ f\underset{\sim}{n}} \qquad 3.7$$

Substituting 3.7 into 3.5 gives

$$\Delta\varepsilon p = \frac{f\underset{\sim}{n}^T \underset{\sim}{CE}\ \Delta\underset{\sim}{\varepsilon}}{n}\ f\underset{\sim}{n}$$

where $n = f\underset{\sim}{n}^T \underset{\sim}{CE}\ f\underset{\sim}{n}$

and hence from equation 3.6 we get

$$\Delta\underset{\sim}{N} = \underset{\sim}{CE}\left[\Delta\underset{\sim}{\varepsilon} - \frac{f\underset{\sim}{n}^T \underset{\sim}{CE}\ \Delta\underset{\sim}{\varepsilon}}{n}\ f\underset{\sim}{n}\right]$$

this may be written as

$$\Delta\underset{\sim}{N} = \underset{\sim}{CE}\left[\underset{\sim}{I} - \frac{f\underset{\sim}{n}f\underset{\sim}{n}^T \underset{\sim}{CE}}{n}\right]\Delta\varepsilon$$

where $\underset{\sim}{CE}$ is the elastic stiffness matrix

$$\underset{\sim}{CE} = \left(\frac{Et}{1-\nu^2}\right)\begin{bmatrix} 1 & \nu & 0 \\ \nu & 1 & 0 \\ 0 & 0 & \frac{1-\nu}{2} \end{bmatrix}$$

$$f\underset{\sim}{n} = \begin{Bmatrix} 2Nx - Ny \\ 2Ny - Nx \\ 6Nxy \end{Bmatrix}$$

In most applications of these equations the possibility of unloading must be considered, but because of the plane stress and proportional loading nature of this problem, it was considered safe to assume that, once a node had yielded, no unloading would occur.

3.5 BOUNDARY CONDITIONS

For a plane stress problem two degrees of freedom are considered for each plate, these being the displacements along the plate (x-direction) and across the plate (y-direction). Hence two boundary conditions are required at each edge.

3.5.1 Plate junctions

(a) The direct stress at the plate edge, normal to the plate edge is zero. This condition comes from the plane stress assumption that the out of plane stiffness of the plates is zero, and hence the edges of the plates are free to pull in and make the normal stress (Ny) zero at the plate edges.

(b) The displacement along the box (x-displacement) at the edge of any plate is equal to the x-displacement of the adjacent edge of the next plate.

(c) Equilibrium of the corner of the box requires that the shear flow (Nxy) at the edge of any plate is equal to the shear flow at the adjacent edge of the next plate.

At each plate junction conditions (a) and (b) are applied to one plate and conditions (a) and (c) to the other plate.

3.5.2 At supported ends

Again two conditions are required to define these ends of the plate:

(a) The longitudinal (x) displacement at the supported end is zero. Since an interlacing finite difference mesh is used (see section 3.6), and the longitudinal displacements are not defined on the ends of the plates, this condition is applied by putting the external fictitious displacement (u(1,j,k)) equal to

minus the corresponding internal displacement (u(2,j,k)). Application of this condition means that any warping introduced by the torsion loading is totally restrained at the support, and hence for some sections high warping stresses are introduced. A possible modification to allow for a free warping condition is discussed later in this section.

(b) The second condition must be obtained by defining the external fictitious shear stress (Nxy(1,j,k)) at the support. In defining this stress a conflict occurs between the correct representation of the bending and torsion behaviour. For a beam under torsion loading the shear stress remains constant along the beam, and hence the external shear stress (Nxy(1,j,k)) should be equal to the internal shear stress (Nxy(2,j,k)). For a beam subjected to bending shear there is a change of sign of shear stress at the central support (represented in this analysis by the cantilever support), and hence the external shear stress should be made equal to minus the internal shear stress. In practice, for a beam under combined load, it is difficult to separate the bending shear from the torsion shear, and hence both conditions cannot be satisfied. Application of the bending condition will result in high stress gradients and the exact distribution of these stresses will be greatly influenced by details such as the welding and diaphragms at the support. As a result of this, it was thought to be more satisfactory to apply the torsion condition (Nxy(1,j,k) = Nxy (2,j,k)).

(c) In addition to these two conditions, in order to prevent rigid body motion, one transverse (y) displacement at the support on each plate must be defined as zero.

3.5.3 Possible improvement to supported end conditions.

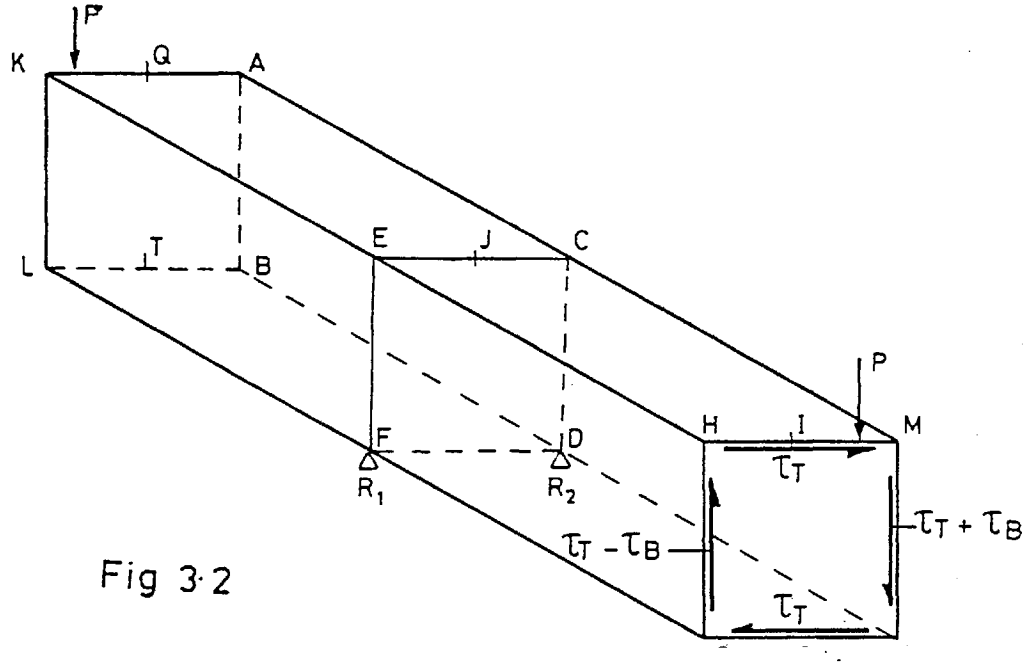

Fig 3·2

Consider a simply supported beam A-K-L-B-N-M-H-G represented in the theoretical analysis by a cantilever C-E-F-D-N-M-H-G. Assume that the beam is symmetrical about a vertical plane Q-I-S-T and is loaded by 2 eccentric point loads P, balanced by support reactions R_1 and R_2. The applied loads are represented in the analysis by applied shear forces TT and TB representing respectively the torsion and bending components of P. The symmetry of the section and loading indicate that the stresses and displacements in the web A-C-D-B are the same as those in the web H-E-F-G; similarly, in the half of the flange A-Q-J-C they will be the same as in H-I-J-E. It appears that it should be possible to make use of this symmetry when defining the values of the shear stress and longitudinal displacement at the external nodes. A considerable amount of time was spent in trying to apply these conditions but it was found to be very difficult to obtain good convergence of the dynamic relaxation solution. For all results given here the end boundary conditions described in section 3.5.2 were used.

3.5.4 Loaded end boundary conditions

In most previous applications of the dynamic relaxation method the structure has been loaded by applying specified displacements rather than loads. Application of displacements has the great advantage that it leads to a higher frequency of oscillation, and hence more rapid convergence, than is obtained when loads are applied. In the case being discussed here, it was required that the ratio of applied bending moment to applied torque should remain constant, and in order to achieve this it is essential that the loading be applied as stresses rather than displacements. Hence the boundary conditions at the loaded end are that the direct stress along the box (Nx) and the shear stress (Nxy) should take specified values. In general the direct stress was taken to be zero, but in the analysis of long, slender boxes it is advantageous to be able to analyse only the support region; in order to do this an elastic analysis can give the distribution of Nx and Nxy at a convenient point along the box and these distributions may then be applied as boundary conditions for the analysis of the smaller critical region up to ultimate load.

3.5.5 End diaphragm condition

In all practical situations there will be some resistance of the cross-section to distortion. In most cases this will be provided by a diaphragm, but some contribution may also come from the frame action of the cross-section. In the theoretical analysis presented here it has been assumed that any diaphragm provided is sufficiently strong to prevent any departure from linear elastic behaviour. The diaphragm is represented by a single plate element, and it is assumed to apply a uniform shear stress to each of the four beam plates such that compatibility at the loaded end is maintained. The distortion of the diaphragm, and hence the shear stress applied to the beam, is calculated from the transverse displacements at the longitudinal centreline of the loaded ends of the four plates. The calculated diaphragm shear is added to or subtracted from the applied shear load as appropriate.

3.6 INTRODUCTION TO THE DYNAMIC RELAXATION METHOD

The application of finite differences and dynamic relaxation (DR) to the analysis of isolated plates and plate assemblages is now well-established. (19, 31, 32). The method involves the addition of acceleration and viscous damping terms to the equilibrium equations (equns. 3.1) to form equations 3.8 and solution of these equations in step-by-step increments of time.

$$\left.\begin{aligned} \rho u \left\{\frac{\partial^2 u}{\partial t^2} + ku \frac{\partial u}{\partial t}\right\} &= \frac{\partial Nx}{\partial x} + \frac{\partial Nxy}{\partial y} \\ \rho v \left\{\frac{\partial^2 v}{\partial t^2} + kv \frac{\partial v}{\partial t}\right\} &= \frac{\partial Ny}{\partial y} + \frac{\partial Nxy}{\partial x} \end{aligned}\right\} \quad 3.8$$

For any state of stress $\underset{\sim}{N}$ corresponding to a set of displacements $\underset{\sim}{\delta}$ equations 3.8 may be used to calculate velocities, and hence, for a specified time increment, new displacements. In order to do this values have to be assigned to three parameters; the densities (ρu and ρv), the time increment (Δt) and the damping factors (ku and kv). Following the method described by Cassell (33) a unit time increment is chosen and fictitious densities are calculated. In most previous applications it has been found satisfactory, even after the onset of plasticity, to calculate

the densities using the elastic stiffnesses. In this case considerable problems were encountered with the slow rate of convergence, particularly when a considerable amount of the structure had become plastic, and some advantage was found in calculating new densities for each load increment, based, where appropriate, on the plastic stiffnesses.

A summary of the DR technique is given in the flow chart, fig. 3.3.

3.7 THE FINITE DIFFERENCE METHOD

In order to describe the displacement and stress distribution in the plates equations 3.8 may be re-written in finite difference form, with values taken at various points on a mesh covering the plates. There is no necessity for the mesh associated with each component to coincide, and because the strains and stresses are calculated from the differentials of the displacements considerable advantages in accuracy have been found to result from the use of interlacing meshes. The mesh arrangements, coordinate system and node numbering system used in this investigation are shown in fig 3.4. In addition to the nodes marked in fig. 3.4 it is useful, in the definition of boundary conditions, to consider external fictitious values of v at the plate junctions, u at the plate ends, and Nxy at the plate junctions and ends.

3.8 LOAD INCREMENTATION

In all investigations of non-linear behaviour attention must be given to the size of load increment applied. For this application displacements are linear, and hence, provided that the material properties within any load increment are linear, the overall behaviour within that increment will be linear. For the structure in a state of stress such that n nodes have yielded, provided that the strains required at the n plastic nodes to yield the (n+1)th node are not large, the stiffness of the structure may be considered constant until the (n+1)th node yields. The reason for the restriction on the amount of straining at the yielded nodes is that the plastic rigidities are calculated such that the

flow of stress is tangential to the yield surface; because of the curved nature of the yield surface the consideration of large strains, without modification of the stiffnesses, will result in perforation of the yield surface.

3.8.1 Calculation of increment size

The linear nature of the behaviour of the structure between the yielding of two successive nodes may be used in the design of a method of calculating suitable load increment sizes.

Consider a box with N nodes unyielded, assume a load increment α is placed on the box. Initially the state of stress at node n may be represented by the stress resultants N_{xn}, N_{yn}, N_{xyn}; application of the load increment α causes changes ΔN_{xn}, ΔN_{yn}, ΔN_{xyn}, in the stress resultants. For any node n the factor (γ) by which α must be multiplied to cause that node to yield may be calculated from

$$\gamma = \frac{\sqrt{1} - \sqrt{F_1}}{\sqrt{F} - \sqrt{F_1}} \qquad \text{——————(3.9)}$$

where F_1 and F are the values of the yield function before and after application of α

$$\text{i.e.} \quad F_1 = \frac{N^2_{xn} + N^2_{yn} - N_{xn}N_{yn} + 3N_{xyn}^2}{N_o^2}$$

$$F = \frac{(N_{xn} + \Delta N_{xn})^2 + (N_{yn} + \Delta N_{yn})^2 - (N_{xn} + \Delta N_{xn})(N_{yn} + \Delta N_{yn}) + 3(N_{xyn} + \Delta N_{xyn})^2}{N_o^2}$$

The value γ is calculated at all nodes and multiplication of the load increment size α by the smallest positive value of γ obtained gives the size of the load increment required just to yield the next node. In practice it was found useful to replace the value $\sqrt{1}$ in equation 3.9 by $\sqrt{1.003}$, i.e. to allow a very small (0.3%) penetration of the yield surface. The purpose of this was to prevent a situation where a very small rounding error caused one node to remain elastic when a symmetric node had become plastic.

In order to make use of this factor γ the D.R. cycle is applied until equilibrium is obtained under an arbitrary load increment α, and hence stress and displacement increments $\Delta\underset{\sim}{N}$ and $\Delta\underset{\sim}{U}$ corresponding to α are known. The value of γ is then calculated as described above all stress and displacement increments $\Delta\underset{\sim}{N}$ and $\Delta\underset{\sim}{U}$ are multiplied by γ before addition to the previous total stresses and displacements. It should be noted that, regardless of whether load increment α causes any nodes to yield the stiffnesses calculated at the start of the increment are used. The great advantage of this method of calculating the size of the load increment is that penetration of the yield surface does not occur.

3.9 MESH SIZE REQUIREMENTS

When using methods such as finite differences a compromise must be reached between the use of a fine mesh, giving very accurate results at a high cost in computer time and storage, and a coarse mesh giving less accurate results at a lower cost. The problem of finding a suitable mesh size is of particular importance in regions where the variation of stresses around or along the box is non-linear. For boxes with the dimensions and loadings considered here the most severely non-linear stresses are the direct stresses in the box flanges, which, due to the shear lag effect, have a parabolic variation across the plate. Generally it is found that the mesh size is more critical in elastic than in ultimate load analyses. This is because yielding of the steel tends to even out the peaks and troughs of stress.

In order to examine the mesh size requirements of the program described in this chapter the beam shown in fig. 3.5 was considered. The reason for the choice of a section with a very high flange width to length ratio is that, in this type of section, shear lag effects are very large (see fig 3.6), and hence it was thought that this section would be comparatively sensitive to the mesh size.

If the flanges have N nodes across them and M nodes along them the following mesh arrangements N x M were considered: (1) 13 x 7, (2) 11 x 7, (3) 9 x 7, (4) 7 x 7, (5) 6 x 7, (6) 9 x 11. Fig. 2.5 shows the elastic distribution of direct stress obtained at the support for the mesh arrangements (1), (5) and (6), the box being loaded with a bending shear force applied at the free end. Fig 3.7 shows the load-deflection curve up to ultimate load for this section and loading. Both of these sets of results show that the coarse mesh gives good agreement with the finer meshes, and suggest that little advantage is likely to be gained by the use of a fine mesh; hence it was thought that a mesh with 7 nodes across and 7 nodes along the flanges should give results which are sufficiently accurate for all practical purposes.

3.10 RESULTS OBTAINED FROM D.R. PROGRAM

In order to compare the results given by the D.R. method with those obtained from the upper and lower bound solutions a beam with the cross-section shown in fig 2.3 was used. Cantilever lengths of 300 mms (model 1) and 600 mms (model 2) were used. Following the mesh size study described in the previous section the meshes shown in fig 3.8 were used. Three load cases were considered for each section: for model 1 ratios of bending moment at support to torque (M/T) of ∞, 6 and 1.5, and for model 2 ratios of ∞, 3 and 1.2.

In figs 3.9 and 3.10 graphs of applied load against end displacement are shown. The applied load is plotted in terms of M/M_p where M is the bending moment at the supported end of the beam and M_p is the plastic moment of the beam calculated by simple plastic bending theory. The displacement plotted is the average of the displacements of the loaded ends of the two webs. Upper and lower bound predictions of the ultimate load, calculated by the methods described in chapter 2 are also plotted. Figs 3.11 and 3.12 show a comparison of the ultimate load stress distributions at the supported end, given by the three methods. Where the lower bound has been governed by the failure of one web it is not possible to plot this stress distribution.

It appears from figs 3.9 and 3.10 that, for some load cases, there is still quite a significant amount of stiffness remaining in the beam when the final point from the D.R. solution has been plotted, and hence the ultimate load may be considerably above the maximum point plotted. In most of these cases an attempt was made to apply another load increment, but this resulted in divergence of the D.R. solution, indicating that the stiffness of the section had become very small or zero.

For section (1) (the short beam) loaded under moment-torque ratios of ∞ and 6 the D.R. solution gives an ultimate load considerably below the lower bound result. The stress distributions at failure for these loadings (see fig 3.11) indicate that, according to the D.R. solution the webs will fail before the section has become fully plastic (hence the unyielded area in the middle of the flanges), whereas the lower bound solution indicated that full plasticity of the cross-section would be reached. The reason for the failure of the lower bound web check to predict this mode of failure is that it is only a check against failure under shear stresses alone, whereas in practice the failure is caused by the combined effects of shear and direct stresses. For the short section with an M/T ratio of 1.5 the D.R. solution shows very good agreement with the lower bound solution. In this case the ratio of shear strains to axial strains in the web which fails is large enough for the shear stresses in this web given by the D.R. solution to be very close to the fully plastic shear values.

It has already been shown (figs 2.2 and 2.3) that for longer sections, where the influence of bending shear is small, the upper and lower bound solutions are much closer together than for the shorter sections. This is again demonstrated in figs. 3.9 and 3.10. Fig 3.10 shows that for the longer section (section 2) with an M/T ratio of ∞ the D.R. solution comes between the upper and lower bounds, which are themselves only about 5% apart. For the other 2 load cases (M/T = 3 and 1.2) the D.R. solution again comes below the lower bound; as with the shorter beam this is caused by interaction of the shear and direct stresses causing a failure of the heavily loaded web earlier than is predicted by the lower bound solution.

3.11 CONCLUSIONS

(1) Upper and lower bound solutions may be calculated for a section under combined bending, shear and torsion load, but the lower bound depends on the failure being due to either:

(a) full plasticity of the cross-section being reached

or (b) one web reaching its full shear capacity.

(2) The lower bound web failure check described in section 2.3 is not a completely satisfactory check against (b) occurring, as a web failure will be influenced by the presence of direct stresses in the web.

(3) An experimental investigation is required to establish the significance of the web failure mode, as it is probable that, for many sections, there will be a considerable capacity for redistribution of the stresses to the unyielded areas, leading to the ultimate load being higher than predicted by these theories.

CHAPTER 4

APPLICATION OF THE D.R. METHOD TO COMPOSITE BOX GIRDERS

4.1 INTRODUCTION AND MODIFICATION OF STEEL PLATE EQUATIONS

A typical closed composite box may be considered as a steel hollow section, similar to that discussed in chapter 3, and a concrete plate, joined by a flexible shear connection. Generally the concrete flange will be wider than the steel flange, and only the part of the flange in contact with the steel will be directly affected by the shear connection; for the purposes of this analysis it is convenient to represent the concrete by three joined plates (see fig 4.1). The plane stress assumption discussed in section 3.2 is again used here; owing to the greater thickness of the concrete plates a greater approximation is involved in applying this assumption but, for composite beams of practical dimensions it was still thought to be reasonable.

The plane stress equilibrium equations for plates 1,2,3,5 and 7 (fig 4.1) are the same as for the steel section (equations 3.1) but for plates 4 and 6 an additional term must be included to allow for the interaction between the plates.

4.1.1 Equilibrium equations for plates 4 & 6

Considering a small element of plate 4 as shown in fig 4.2 where:

$P_x = \gamma_x K \, dxdy$

$P_y = \gamma_y K \, dxdy$

K = slip stiffness

$\gamma_x = U_{st} - U_{conc}$

$\gamma_y = V_{st} - V_{conc}$

U_{st}, U_{conc}, V_{st} & V_{conc} are the x and y displacements in the steel and concrete

Resolving in the x and y directions gives:

$$t\left\{\frac{d\sigma_x}{dx} + \frac{d\tau_{xy}}{dy}\right\} - \gamma_x K = 0$$

$$t\left\{\frac{d\sigma_y}{dy} + \frac{d\tau_{xy}}{dx}\right\} - \gamma_y K = 0 \qquad \text{4.1}$$

For plate 6 the signs on the slip terms will be reversed giving:

$$t\left\{\frac{d\sigma_x}{dx} + \frac{d\tau_{xy}}{dy}\right\} + \gamma_x K = 0$$

$$t\left\{\frac{d\sigma_y}{dy} + \frac{d\tau_{xy}}{dx}\right\} + \gamma_y K = 0 \qquad \text{4.2}$$

4.2 CONCRETE RIGIDITY MATRIX

In order to investigate the ultimate load behaviour of the hogging moment region of a composite beam it is necessary to establish a relationship between the stresses and strains in a reinforced concrete slab. As already discussed, (section 4.1), the slab is assumed to be in a state of plane stress; because of the type of loading being considered it was assumed that the concrete would never be sufficiently heavily loaded in compression for the crushing strength to be reached. Having made this assumption the possibility of an element of the slab being in any one of three states must be considered: (1) Element uncracked; (2) Element with cracks in one direction; (3) Element with cracks in two directions. Also the strength of the reinforcement in the slab must be allowed for. In the following work it has been assumed that the reinforcing bars run parallel to the x (x reinforcement) any y (y reinforcement) coordinate axes.

4.2.1. Uncracked slab element

Until the first crack is formed the slab is assumed to be homogenous and isotropic, the stress-strain relationship being given by:

$$\begin{bmatrix} N_x \\ N_y \\ N_{xy} \end{bmatrix} = \frac{E_c T_c}{1-\nu_c^2} \begin{bmatrix} 1 & \nu_c & 0 \\ \nu_c & 1 & 0 \\ 0 & 0 & \frac{1-\nu_c}{2} \end{bmatrix} \begin{bmatrix} \varepsilon_x \\ \varepsilon_x \\ \gamma_{xy} \end{bmatrix} \text{———} 4.3$$

The contribution of the reinforcement is given by:

$$\begin{bmatrix} N_x \\ N_y \\ N_{xy} \end{bmatrix} = E_R \left[T_{sx} \begin{bmatrix} 1 & 0 & 0 \\ 0 & 0 & 0 \\ 0 & 0 & 0 \end{bmatrix} + T_{sy} \begin{bmatrix} 0 & 0 & 0 \\ 0 & 1 & 0 \\ 0 & 0 & 0 \end{bmatrix} \right] \text{———} 4.4$$

where E_c = Young's modulus for concrete

ν_c = Poisson's ratio for concrete

T_c = Thickness of concrete slab

E_R = Young's modulus for reinforcement

T_{sx} = Ratio of cross-sectional area of x reinforcement to slab width

T_{sy} = Ratio of cross-sectional area of y reinforcement to slab width.

These rigidities may be used until the first crack appears in the slab, this will occur when the maximum tensile stress in the slab becomes equal to the tensile strength of the concrete. When this stress is reached a crack will be formed at 90^o to the direction of the maximum tensile stress.

4.2.2. One crack element

Once the concrete element has cracked a new rigidity matrix must be found. The concrete can transmit no tensile stresses across the crack, and hence Young's modulus for the concrete must be zero in the direction perpendicular to the crack. Aggregate interlock allows transmission of shear stresses across the crack, but the shear rigidity will be lower than for the uncracked element; this is allowed for by the introduction of an aggregate interlock factor (ξ). According to Arnaouti (34) the value of ξ has been found to vary between 0.33 and 0.5.

The stress-strain relationship for a concrete element with one crack is given by:

$$\begin{bmatrix} N_x \\ N_y \\ N_{xy} \end{bmatrix} = \underset{\sim}{T}\, E_c T_c \begin{bmatrix} 1 & 0 & 0 \\ 0 & 0 & 0 \\ 0 & 0 & \xi/2(1+\nu) \end{bmatrix} \underset{\sim}{T}^t \begin{bmatrix} \varepsilon_x \\ \varepsilon_y \\ \gamma_{xy} \end{bmatrix} \qquad 4.5$$

where $\underset{\sim}{T}$, the transformation matrix is given by:

$$\underset{\sim}{T} = \begin{bmatrix} C^2 & S^2 & -2SC \\ S^2 & C^2 & 2SC \\ SC & -SC & C^2-S^2 \end{bmatrix} \qquad 4.6$$

where $C = \cos\phi$

$S = \sin\phi$

ϕ = angle between x-axis and crack direction.

Once the concrete has cracked some shear stress will be transmitted across the crack by the dowell action of the reinforcement. The contribution of this to the shear stiffness is taken to be a factor (μ, the dowell factor) times the shear rigidity of the reinforcing bars; hence the contribution of the reinforcing bars to the overall stiffness is given by:

$$\begin{bmatrix} N_x \\ N_y \\ N_{xy} \end{bmatrix} = E_R \begin{bmatrix} T_{sx} & 0 & 0 \\ 0 & T_{sy} & 0 \\ 0 & 0 & \frac{\mu(T_{sx}+T_{sy})}{2(1+\nu_c)} \end{bmatrix} \begin{bmatrix} \varepsilon_x \\ \varepsilon_y \\ \gamma_{xy} \end{bmatrix} \qquad 4.7$$

The concrete rigidities given by equation 4.5 are applicable until the maximum tensile stress in the concrete again reaches the cracking stress. When this stress is reached a second crack will form at an angle of 90° to the direction of the maximum tensile stress. (For the beams and loadings considered in this thesis the ultimate load of the structure had generally been reached, or very nearly reached, before a second crack had been formed in any element, but the possibility of the second crack forming must still be considered.)

4.3.2. Two crack element

Following the formation of the second crack no tensile stresses can be carried across either crack, but shear stresses may be carried by aggregate interlock. In general it is found that the angle between the two cracks is of the order of 80 degrees and hence it may be assumed that an element with two cracks is unable to carry any tensile stress (34).

The new concrete stress-strain relationship is given by:

$$\begin{bmatrix} N_x \\ N_y \\ N_{xy} \end{bmatrix} = \underset{\sim}{T} E_c T_c \begin{bmatrix} 0 & 0 & 0 \\ 0 & 0 & 0 \\ 0 & 0 & \xi/2(1+\nu_c) \end{bmatrix} \underset{\sim}{T}^t \begin{bmatrix} \varepsilon_x \\ \varepsilon_y \\ \gamma_{xy} \end{bmatrix} \qquad 4.8$$

The transformation matrix T has been defined in equation 4.6 and for this case the angle ϕ is defined as the mean value of the angle between the two cracks and the x-axis. The contribution of the reinforcement in the two crack case remains as shown in equation 4.7.

4.3 APPLICATION OF THE DYNAMIC RELAXATION METHOD

Application of the D.R. method to the solution of the equations for seven plates joined to form a composite box girder presents a number of problems not encountered in the analysis of a steel section.

4.3.1. Load incrementation

The most important of these extra problems is caused by the differences between the stress-strain relationships for steel and those for concrete. For steel these are formulated in terms of increments of strain and stress, and hence each load increment must be treated separately, whereas for the concrete they are formulated in terms of total stresses and strains, and hence one increment may not be considered separately from previous increments.

The logical extension of the method of load incrementation described in chapter three would be to apply an arbitrary load increment, and then calculate the factor by which this increment must be reduced (or increased) for one steel element to yield or for one concrete element to crack. If this method was applied, for cases where the increment size was governed by a concrete element cracking there would then be the problem of dealing with the stresses released by the cracking of the concrete element. It would be possible to overcome this problem by applying a further set of relaxation cycles with loads applied at the newly-cracked nodes to balance the released stresses. The problem associated with this method is that before a composite section fails a large number of the concrete nodes will crack, and the computer time involved in applying one increment, (and hence two sets of D.R. cycles), for every node that cracks is prohibitive. The fact that the concrete stresses are dependent only on the total strains means that the problem of penetration of the cracking surface does not occur, and hence it is not important to recalculate the concrete stiffnesses as soon as the element cracks. As a result of this the method of load incrementation adopted for the composite box programs was as shown in the flowchart fig. 4.3. The initial increment size ((1)) is chosen such that, assuming no steel nodes yield, a reasonable number (say 5% of the total number) of concrete nodes will crack. In some cases it was found necessary to run a load case twice in order to find suitable increment sizes but, in general, the solutions were not found to be very sensitive to the exact size of increment chosen. At point (2) on the flowchart a number of concrete nodes may be loaded above the cracking stress, the next section of the program releases and redistributes these stresses. Having calculated these stresses and associated strains and displacements they are added to the existing total stresses, strains and displacements, new stiffnesses calculated and a new load increment applied.

4.3.2 Boundary conditions

Derivation of the boundary conditions for the composite box is basically the same as for the steel box, but at the top corners of the web account must be taken of the effect of the shear connection. In order to illustrate the method used to deal with this problem the boundary conditions at the junction of plates 1 and 4 are discussed here. The forces acting on a small section of this junction are shown in fig 4.4. As for the steel box girder (section 3.5.1) the first condition is that the direct stress at the plate edges, normal to the plate edge, are zero. Hence all four NY forces shown in fig 4.4 are zero. In addition the conditions of equilibrium in the x direction and compatibility between the two plates must be satisfied. To do this the equilibrium condition is used to calculate the x-direction velocity at the edge of plate 1 (eqn. 4.9) in the velocity routine (fig 3.3) and the compatibility condition is satisfied by making the x displacement at the edge of plate 4 equal to that at the corresponding edge of plate 1. The x-direction equilibrium equation for the section of the plate junction shown in fig 4.4 is given by:

$$0 = (NX(I+1, N-1, 4) - NX(I,N-1, 4)) \times DY(4)/2$$
$$+(NX(I+1, 2, 1) - NX(I,2,1)) \times DY(1)/2$$
$$+ (NXY(I,2,1) - NXY(I,N-2, 4)) \times DX - PX(I,N-1, 4)$$

where $$PX(I,N-1,4) = \frac{k \times DX \times DY(4)}{2} \times (U(I,N-1,4)-U(I,N-1,6))$$

k = shear connection stiffness ($N/mm/mm^2$)

Other plate junctions are treated in a similar manner to that described above.

The remaining boundary conditions are all very similar to those described in chapter 3 for the steel section.

4.4 EXTENSION TO OPEN COMPOSITE BOXES

In extending the program to the case of an open composite box girder it was found to be convenient to represent the beam by six plates joined as shown in fig 4.5. Representing the whole of the concrete by only one plate meant that it was necessary to add the extra shear connection force term to the equilibrium equations only at specified nodes on this plate; (i.e. those

in contact with plates 4 and 5). Appropriate modifications to the boundary conditions at the top of webs were also required. Apart from this the method of solution of the equations was as for the closed composite box.

CHAPTER 5

THE DESIGN AND TESTING OF A SERIES OF MODEL OPEN AND CLOSED COMPOSITE BOX GIRDERS

5.1 INTRODUCTION

This series of tests on model composite box girders was designed to give a general understanding of the behaviour of composite boxes under various combinations of bending, shear and torsion loading. The six tests were as follows:

(1) Action of a closed composite box under central point load (Model C1)

(2) Action of a closed composite box under eccentric point load (Model C2)

(3) Action of a closed composite box under torsion (Model C3).

The above three tests were then repeated on open composite boxes (Models 01-03 respectively). The main interest of this investigation was in the effect of material non-linearity rather than geometric non-linearity, and hence the models were designed with all the steel plates thick enough to ensure that none of them would buckle. Although this resulted in the model dimensions not being an accurate scale model of a practical beam,(the plate thicknesses were much too large), it was thought that such models would be of considerable help in understanding the effect of material non-linearity on the behaviour of practical composite boxes.

5.2 DESIGN OF MODELS

In order to reduce the costs of this series of tests it was intially proposed that, instead of fabricating the steel sections from flat plates, rolled hollow sections should be used, the required web and flange thicknesses being obtained by machining down the faces of the section. The most suitable available section was an 18" x 10" x 0.5" rolled hollow section. After consideration of other work done on web and flange stability it was decided that the top flange, (one 18" side of the r.h.s.), should be reduced to 4mms thick and the webs (the 10" sides) reduced to 6mms thick, the bottom flange was to be

left 12.7mms, (½ inch), thick. In practice it was found that the faces of large rolled hollow sections may be several millimetres out of flat, which made it almost impossible to machine them down to the required thicknesses. As a result of this problem it was decided that the steel sections of the models would have to be fabricated from flat plates.

Following various discussions it was decided that the cost of manufacturing the models would be considerably reduced if the webs and bottom flanges could be fabricated from a single plate bent to form a U section rather than from three plates welded together. It was desirable to avoid having a large number of stiffeners on the model and hence the cross-sectional dimensions shown in Figs 5.1 and 5.2 were chosen. In most practical situations the length of beam under hogging moment is quite small, hence the effect of shear forces is considerable, so a suitable length for the models was thought to be 1400 mms between end diaphragms.

The concrete top flange for the models was a 30mm thick reinforced micro-concrete slab. For the first model the mix was 1:$\frac{3}{4}$:2$\frac{1}{4}$ proportions of ordinary portland cement, 25 to 100 sieve fine aggregate and $\frac{3}{16}$" to 25 sieve coarse aggregate with a water-cement ratio of 0.56. The following test results were obtained with this mix.

(1) 4" cube strength at 28 days - 51 N/mm²

(2) 6" cylinder splitting strength at 28 days: 2.4 N/mm²

A major problem encountered with this mix was that drying shrinkage of the slab, restrained by the shear connection and slab reinforcement, caused a crack to form across the centre of the slab. The large amount of drying shrinkage present was caused by the high water-cement ratio required to enable the concrete to be compacted around the reinforcing mesh. For subsequent models the mix was redesigned as follows: the mix proportions were changed to 1:1:3 and the water-cement ratio

reduced to 0.5. In order to maintain the required workability with the reduced water-cement ratio it was necessary to use a water-reducing admixture, for this purpose a 2%, by weight of cement, addition of Sicament was used. The new mix gave the following test strengths:

(1) 4" cube strength at 28 days - 58 N/mm²

(2) 6" cylinder splitting strength at 28 days - 4.1 N/mm²

Top and bottom slab reinforcement was provided by a mesh of 16 ga (1.626 mm diameter) steel bars at half inch centres longitudinally and transversely. Concrete cover to the reinforcement was 3mms and the ultimate strength of the reinforcement was 510 N/mm². Shear connection between the steel and concrete was by ½" x $^{3}/_{16}$" inch headed studs at 2" centres.

5.3 PRELIMINARY TESTS

The stress-strain properties of the steel used in various parts of the model were measured in the usual way, and results are shown in Figs 5.3 to 5.6. An attempt was made to measure the stress-strain properties of a piece of reinforced concrete in tension using specimens as shown in Fig 5.7. Load was applied, using a tension testing machine, in 0.05 ton increments and strains were measured from the deflections of the jaws of the testing machine. Many inaccuracies are present in a test of this sort, the most important being :(1) bending stresses may be introduced into the slab by clamping it into the jaws of the testing machine; (2) the test specimen is very much narrower than the true slab and hence edge effects are more important. The results obtained from these tests indicate that the stress-strain behaviour of a concrete slab in tension may be approximately represented by two straight lines (Fig 5.8), the junction between the lines occurring when the concrete stress is approximately equal to the tensile strength given by a cylinder splitting test. In this and all other preliminary tests the concrete mix used was that described for the first test (section 5.2) and the specimens were tested 28 days after casting.

In order to measure the stress-strain properties of the concrete, a series of 2" x 2" x 6" prisms were instrumented with one 10mm gauge length strain gauge rosette on each face. These prisms were loaded in a compression testing machine with 0.5 ton (1.9 N/mm^2) increments; strain readings were taken 3 minutes after application of the load. As the load increased considerable creep was noted, where this creep was present an initial reading was taken 3 minutes after application of the load, and a second reading 7 minutes later. As a result of these tests an approximate compressive stress-strain curve for the concrete has been plotted (Fig 5.9).

The stiffness of the shear connection was measured with a scaled-down version of the standard push-out test. The outside faces of a 102 mm x 64 mm joist were machined down to give a flange thickness of 4 mms at ½ inch from the web-flange junction. Two ½" x $^3/_{16}$" headed studs were welded to each flange as shown in Fig 5.10. The outer faces of the flanges were lightly oiled to eliminate bond between the steel and the concrete, and the two concrete slabs, reinforced with the ½ inch wire mesh, were cast simultaneously, on edge, in wooden moulds. After hardening of the concrete the wooden moulds were removed and the specimens were tested in a compression testing machine as follows. A central axial load was applied to the joist, and slip measurements were taken from dial gauges attached to the steel joist and bearing against the steel plate on which the slabs rested. Load was applied in increments of 500 lbs up to 4500 lbs and then in increments of 100 lbs up to failure. Two slip readings were taken for each load increment, one immediately after application of the load, the other one minute later, the difference between the two readings gave an indication of the amount of creep present. The load-slip curves obtained from a series of four such push-out tests are shown in Fig 5.11. It can be seen that the results are rather inconsistent, this is probably caused by inadequate compaction of the concrete around the studs. The ultimate load carried by the studs varies from 5100 lbs to 6100 lbs (load on four studs),

the stiffness of the studs in the elastic region (taken as a load of 500 lbs to 3500 lbs) varied from 280 x 10^3 lbs/in to 400 x 10^3 lbs/in (stiffness for four studs).

5.4 CASTING OF SLAB

The main formwork for both the open and closed box models was made of timber (Figs 5.14 & 5.15), but for closing the gap between the two flanges in the open box models expanded polystyrene was used. The reason for the use of polystyrene was that, once the slab had been cast, it would have been impossible to remove the central section of formwork, and it was thought that the use of timber could add to the strength of the model.

To assist with the fixing of the reinforcement a number of concrete spacing blocks were cast. These were 10 x 10 x 18 mms (18 mms being the spacing required between the top and bottom transverse reinforcing bars to give the required 3 mms cover), with a hole through the length of the block to enable a wire to be passed through. By passing a thin wire around the top reinforcement, through one of these blocks and tying it off around the bottom reinforcement it was possible to obtain the required spacing between the two layers of reinforcement. A number of small holes were then drilled in the wooden formwork and the reinforcing meshes were tied to the formwork with wires passing through the holes and around the mesh; 3 mm thick nuts were placed between the formwork and the mesh at each of these points to give the correct cover to the reinforcement. Once the mesh had been tied in place these holes were sealed with wax, and prior to removal of the formwork, after casting and hardening of the slab, the wires through the formwork were cut. After casting the slabs were cured for 28 days under wet sacking.

5.5 DESIGN OF TEST RIGS

5.5.1 Bending and eccentric load tests

As already discussed, (section 5.1), a series of tests on six models was undertaken, and four of these involved loading the model under either an eccentric or central point load. For

all of these models the ultimate load test was to be under hogging moment, (i.e. with the slab in tension), but it was desirable that each model should initially be tested, within the elastic region, under a sagging moment. It was thought that a 10 ton end load would be well within this region, and that a 50 ton end load would be above the ultimate load for all the models; hence the central support was designed to carry 20 tons in tension and 100 tons in compression. A photograph of the central support is shown in fig. 5.16. For the elastic tests the load was applied at one end of the beam by a 10 ton jack standing on the floor and reaction at the other end by a two inch diameter by four inch long steel roller resting on a steel plate and concrete blocks.

For the ultimate load tests it was necessary to reverse the direction of loading so that the concrete slab was put into tension. A photograph showing the position of the loading jack and support column is shown in fig. 5.17. In the design of the end support for the ultimate load tests it was desirable that the same support should be suitable for all four tests. In order for this to be the case the support had to allow freedom of movement in the following directions: (1) Translation along the length of the beam, (2) Rotation about a horizontal axis in the plane of the end diaphragm, (3) Rotation about a horizontal axis along the length of the beam. The most suitable method of doing this was found to be by using a column pinned at both ends, as shown in fig. 5.17.

5.5.2 Torsion Tests

Three photographs of the rig for the torsion tests (models 03 and C3) are shown in figs. 5.18 to 5.20. The load was applied over one web with a 100 ton jack, reaction under the other web at this end was provided by a spherical plain thrust bearing. This arrangement allowed the loaded end to be free to rotate but the thrust bearing provided restraint against any horizontal movement. At the supported end of the beam reaction was provided top and bottom by load cells resting on rollers (fig. 5.20). The load

cells provided pin joints to allow rotation about a horizontal axis parallel to the diaphragm, (a small rotation about this axis will be caused by twisting of the box). The rollers allowed longitudinal movement so that the end of the beam was free from warping restraint.

5.6 INSTRUMENTATION OF MODELS

During the testing of all the models strains were measured at two cross-sections: (1) at one quarter-point of the model; (2) as near as possible to the central support. At each of these cross-sections strains were measured at various points around the steel section with 10mm gauge length electrical resistance strain gauge rosettes, and on the concrete slab strains were measured with two inch gauge length demec gauges. On the open boxes an additional longitudinal strain reading was taken at the outside edge of the flange at the central cross-section. Two of the demec gauges were checked with electrical resistance gauges. For the first model the strain gauges on the steel top flanges were covered with a layer of AK22 covering putty to protect them from damage by water during casting of the slab. Despite this some problems were encountered with these gauges during testing and, for subsequent models, the junction between the steel and the putty was additionally sealed with hot wax. Details of the strain gauge positions may be found in figs 5.12, 5.12A & 5.13.

Readings of the slip between the steel and the concrete were taken at various points along each side and end of the boxes. Across the ends of the boxes readings were taken with dial gauges with a resolution of 10^{-4} inches. Access to the steel-concrete junction at the sides of the boxes was rather restricted (particularly in the closed box models), as a result of this the slip here was measured with electrical transducers; subject to correct calibration and a stable power supply these can give readings accurate to 10^{-2}mms. Overall deflections were measured at various points around the models, for the models under torsion load dial gauges with a resolution of 10^{-4} i . were used, for the other models gauges with a resolution of 10^{-3}mms were used.

5.7 THE TESTING OF MODEL C1

The object of the tests on the first model was to investigate the behaviour of a closed composite box under bending load. In order to provide the bending load the jack was placed under the longitudinal centre-line at one end of the beam and the roller under the centre-line at the other end of the beam. A total of three tests were done on this beam - two elastic tests putting the slab into compression, followed by an ultimate load test with the slab in tension.

5.7.1 Results of elastic tests

For this test the jack load was increased from 0 to 10 tons in two ton increments, (thus the maximum load was equivalent to a 20 ton central point load), and then reduced to zero, again in two ton increments. Since, as expected, all results were very nearly linear and elastic, all results given for these tests are average readings for two tests for a 10 ton end load; also the ultimate load test (slab in tension) results for a 10 ton end load are shown. Two sets of theoretical results are given: (1) Results given by the finite element program described in ref. 21; (2) Results given by the dynamic relaxation program described in chapter 4 of this thesis. Both sets of theoretical results relate to the elastic tests.

Figs. 5.21 and 5.22 show the distributions of longitudinal stress at the two gauged cross-sections. For gauged section 1 it can be seen that the stresses in the steel top flange and the webs show very good agreement with the theoretical results given by both the finite element and dynamic relaxation methods. The bottom flange stresses measured at this section are consistently about 10% higher than the theoretical results. This is rather surprising, particularly in view of the presence of the stiffener in the tested model, which was not allowed for in the theoretical work.

For gauged section 2 the measured top flange longitudinal stresses are consistently about 10% below the theoretical values and the measured bottom flange longitudinal stresses are about 10% above the theoretical values. Disagreements of this size between the theoretical and experimental results were to be ex-

pected since the theoretical results are quite sensitive to the values taken for the slip stiffness and the concrete modulus of elasticity, and the accurate measurement of these values poses considerable problems. The sensitivity of the theoretical results to the values assumed for various material properties will be further discussed in chapter 6.

Shear stress distributions for the two gauged sections are shown in figs 5.23 and 5.24. The flange shear stresses at section 1 are greatly affected by the details of the welding of the flanges to the central diaphragm, and hence neither theoretical nor experimental results are given for these stresses. The finite element program assumes a uniform shear stress distribution down the webs, and hence these results are not shown. It can be seen that the agreement between the theoretical and practical results is quite good. In general the experimental results show slightly lower stresses than the theoretical results, this suggests that the load being applied by the jack may have been slightly over-estimated.

Fig 5.25 shows the distribution of longitudinal slip around the box. For the elastic tests the measured slips along the edges of the box are consistently below the theoretical results. This difference could be caused by either an under-estimate of the slip stiffness or an over-estimate of the Young's modulus for the concrete in the theoretical work. The distribution of slip across the ends of the box clearly demonstrates the importance of shear lag in this type of beam - the slips, and hence the shear connector forces, are very much higher over the webs than over the longitudinal centreline. Comparison of the two sets of theoretical results for this part of the beam demonstrates the importance of the choice of mesh size used in the theoretical work - the use of a greater number of nodes across the beam in the F.E. analysis (9 instead of 5) has enabled a more accorate prediction of the slip distribution across the beam to be made. Mesh size effects will be further discussed in chapter 6.

5.7.2. Results of ultimate load test

For the ultimate load test the direction of loading was reversed so that the slab was put into tension. The jack load was increased in two ton increments up to ultimate load, which was found to be 41.7 tons. Readings of strains, slips and deflections were taken for each load increment; also the slab was inspected for cracks, the position of each new crack being marked and the crack numbered to indicate the load at which it formed. The results of this test are presented in two forms:

(1) Comparison of the stresses and slips recorded for a ten ton load with those obtained in the elastic tests for a ten ton load (Figs 5.21 - 5.25).

(2) Plots of the strain distribution around the section at various load levels (Figs 5.26 - 5.32).

The load-deflection curve is shown in fig. 5.33 and a photograph of the cracked concrete slab in fig. 5.34.

Figs 5.21 and 5.22 show that, as expected, the longitudinal stresses in the steel flange are considerably greater for the test with tension in the concrete than for the test with compression in the concrete. The increase at the quarter-point (gauged section 2) is about 50%, compared with about 20% at the centre-line (gauged section 1). Comparison of the web and bottom flange stresses with those in the elastic test shows that, because of a downward movement of the neutral axis when the concrete cracks, the bottom flange steel stresses are slightly lower for the case where the slab has cracked.

Figs. 5.23 and 5.24 show that the distribution of shear stress in the steel is not significantly affected by the cracking of the slab in the ultimate load test. Fig 5.25 shows that there is considerably less slip between the steel and concrete (and hence lower shear connector forces) in the ultimate load test than in the elastic test. This is particularly evident at the end of the slab, but it is thought that, particularly in the ultimate load test, the end slip readings are likely to have been affected by the proximity of the gauges to the point of

application of the load. When considering the slip readings for the ultimate load test it must be remembered that, when the slab is cracked, there will be a considerable difference between the slip readings taken on different sides of the crack.

Figs. 5.26 to 5.29 show the distributions of longitudinal and shear strain around the section for various applied loads. It is interesting to note that, as the ultimate load is approached, the shear strains in the webs at the central cross-section become very much larger at the top of the web than at the bottom. Equilibrium of the web-flange junction requires that the shear flow in the flange should be equal to the shear flow in the web; since the flange is thinner than the web this equilibrium requirement suggests that the shear strains in the flange are likely to be even higher than those in the web. In beams with a high breadth to length ratio the shear capacity of the web-flange junction may govern the overall strength of the beam, and is particularly critical when a torsion component of loading is present.

Figs. 5.30 and 5.31 show the distribution of longitudinal strain in the slab at the gauged cross-sections. It would be expected that, due to cracking of the slab, the strains in the ultimate load test would be somewhat higher than for the corresponding load in the elastic test. Fig. 5.30 shows that the measured concrete strains at the slab centre-line in the ultimate load test are, in fact, considerably smaller than those in the elastic test; the unexpectedly high strains in the elastic test are almost certainly caused by the shrinkage cracking discussed in section 5.2. In fig. 5.31 it is noticeable that the longitudinal strains at the quarterpoint decrease very rapidly towards the edge of the slab; this is another indication of the importance of shear lag in this type of beam. It is possible that this shear lag effect is much more significant in simply supported beams, where the end of the slab is free, than in the more practical case of a continuous beam.

Fig 5.33 shows the theoretical and experimental load-deflection curves. In order to compare the two sets of results it was necessary to adjust the theoretical results to allow for the following:

(1) The theoretical results are for the deflection of a cantilever representing one half of a simply supported beam, whereas the deflections measured in the experiments were for the loaded end of a beam supported at the mid-point and at the other end.

(2) The deflections of the supports in the experiments.

Allowance for these two factors was made as follows:-

for (1) The theoretical deflections were doubled.
for (2) By comparison of the theoretical and experimental deflections in the elastic region it was found that the deflection of the rig gave rise to an increase in the measured end deflection of 0.143 x P mms (P = jack load in tons).

As a result of this it can be seen that the theoretical deflections (δp) plotted in fig. 5.33 are given by:-

$$\delta p = 2\delta c + 0.143\ P \qquad (5.1)$$

where δc = theoretical end deflection of cantilever (in mms)

P = applied load (in tons)

It can be seen from fig 5.33 that the theoretical and experimental load-deflection curves show good agreement. The ultimate load reached in the experiment was 41.7 tons compared with 38.2 tons given by the theoretical work. It appears from the gradient of the load-deflection curve that the ultimate load of the theoretical model may not have been reached; study of the state of stress around the section shows that only two unyielded nodes remained, and these were both located very close to the neutral axis, which suggests that very little further load could have been carried by the section. This problem of identification of the ultimate load has been discussed with respect to steel sections in section 3.10 of this thesis.

Fig 5.34 shows a photograph of the slab after testing; the lines on the slab indicate cracks in the concrete, and the number adjacent to each line indicates the load stage at which that section of crack was first observed. The cracks close to the midpoint of the slab are at almost exactly 90 degrees to the longitudinal axis of the beam, indicating that they are caused almost entirely by direct stress, further towards the ends of the beam the cracks are not at 90 degrees to the beam axis, indicating that they have been influenced by the shear stresses in the slab.

5.8 THE TESTING OF MODEL 01

The object of this test was to investigate the behaviour of an open composite box under bending load. The loading arrangement and testing procedure were as for the closed box tests described in section 5.7.

5.8.1 Results of elastic tests

The testing procedure was as described in section 5.7.1 for the closed box model. The results are also presented as for the previous model except that finite element theoretical results are not shown.

Comparison of figs. 5.35 and 5.36 with figs. 5.21 and 5.22 shows that the longitudinal stresses measured in the steel top flanges of the open box are considerably lower than those measured in the closed box tests. There are two possible causes of this:

(1) The shrinkage cracking of the concrete in model C1 (see section 5.2) would lead to an increase in the steel stresses because, until the cracks close up due to compression of the concrete, the only stiffness of the slab in compression would be that of the reinforcement, and hence the load carried by the slab would be quite small.

(2) The shear connectors in the model 01 are distributed much closer to the webs than those in model C1, this may well lead to a more efficient transfer of load into the concrete slab. Further discussion of the effects of the distribution of the shear connection may be found in ref. 34.

The distribution of longitudinal stress at the centreline, (fig 5.35), shows the importance of shear lag in the steel top flanges - the stresses midway between the webs and the edges of the flanges being 30 to 50 per cent lower than those directly over the webs. As expected there is very little evidence of shear lag at the quarter-point cross-section. Comparison of the bottom flange longitudinal stresses with those from the closed box test shows that the open box gives slightly lower stresses than the closed box; this difference is similar to the difference in the top flange stresses which has been discussed above.

Comparison of the theoretical and experimental longitudinal stresses shows that, for the bottom flange stresses, excellent agreement is obtained between the two sets of results. For the top flanges the theory predicts consistently higher stresses than those measured in the experiments. Problems associated with the evaluation of the concrete and shear connection stiffnesses have already been discussed, and after allowing for these problems the agreement between the theoretical and experimental results seems reasonably satisfactory.

Both the theoretical and experimental results for the shear stress distribution in the webs and bottom flange (figs. 5.37 and 5.38) show very close agreement with the results from the closed box test. (figs 5.23 and 5.24). The most significant difference between the open and closed box results occurs in the top flange where the maximum shear stress in the open box is very much lower than that in the closed box. This is caused by the fact that in the open box there are two paths for the shear flow to travel from the top flange into the web, compared with only one in the closed box. This difference is particularly significant when the flange plates are thinner than the web plates, as it makes yielding of the flange, along the web-flange junction, (as discussed in section 5.7.2), much less likely to occur in an open box.

Fig. 5.39 shows the distribution of longitudinal slip between the steel and the concrete, this having been measured along the outer edges and across the ends of the steel top flanges. Comparison of these results with those obtained in the closed box test (fig. 5.25) suggests that much smaller slips and hence much lower shear connector forces are present in the open box. One reason for this difference is that the slips along the sides of the open box model were measured on the edge of the flange, and hence at a considerable distance from the web; here the shear lag effect would result in the measured slip being below the average for the cross-section. This situation should be compared with that in the closed box where the slip was measured directly adjacent to the webs, and hence the measured slip would be above the average for the cross-section. Consideration of the slip distribution across the ends of the box (fig. 5.39) indicates that this argument is not correct - at the ends of the open box the maximum slip was found to be at the outer edges of the steel flanges. Theoretical work does not confirm this observation but gives maximum slips above the webs. It is thought likely that these experimental readings at the ends of the model have been influenced by local effects due to the loading.

Comparison of the measured slips with those predicted by the theoretical work again shows that the measured slips are much lower than expected. It is quite likely that the mesh used in the theoretical work was too coarse to give accurate predictions of the effect of shear lag on the slip, but it is most unlikely that this would account for all of the difference.

5.8.2 Results of ultimate load test

The rig and loading procedure for this test were as for the closed box test (model C1), the ultimate load was found to be 39 tons compared with 41.7 tons for the closed box. Readings taken and presentation of the results were as described in section 5.7.2.

Figs 5.35 and 5.36 show that the longitudinal stresses in the steel top flanges are between 80 and 150 per cent higher in the ultimate load test than in the elastic tests. This increase is considerably greater than that noted in the closed box test, the comparatively small increase in the closed box test probably being caused by the shrinkage crack already discussed. It is interesting to note that the shear lag in the top flange is much less noticeable in the ultimate load test than in the elastic tests (fig 5.35); this is probably caused by the reduction in the ratio of direct to shear stiffness of he concrete flange when cracking occurs (ref 35). As with the closed box model the downward movement of the neutral axis as the concrete slab cracked has resulted in the bottom flange stresses being very nearly the same in the ultimate load test as in the elastic test.

As in the previous test the shear stress distribution is not significantly affected by the cracking of the slab in the ultimate load test. Fig. 5.39 shows that the slip measured in the ultimate load test is very small.

Figs 5.40 and 5.41 show the distribution of longitudinal strain at various load levels. Comparison of these readings with the corresponding readings from the closed box test (figs 5.26 and 5.27) shows that for nearly all the gauges the agreement between the two tests is very close. In fig 5.40 it can be seen that the gauges on the outer edges of the flanges seem to have given very high readings at the higher loads; these two gauges were 2mm gauge length, linear gauges, whereas all the other gauges were 10 mm gauge length rosettes, and it is thought that this may have had some effect on the readings at these high strain levels. The very high readings given by one gauge at cross-section 1 are almost certainly caused by a faulty gauge. In this test there is much less evidence of the rapidly increasing shear strains at the web-flange junction which were present in the closed box test.

The longitudinal slab strains are shown in figs 5.44 and 5.45, comparison of these with the corresponding diagrams for the closed box (figs 5.30 and 5.31) show that for the elastic tests the results are very similar. For the ultimate load test on the open box there is no evidence of the fall in strain, towards the edge of the slab, which was noted in the closed box test (fig 5.31). Comparison of these two sets of results suggests that the differing distributions of shear connection lead to a more efficient transfer of load into the slab from the open box than from the closed box.

The theoretical and experimental load-deflection curves are shown in fig 3.47, the plotted theoretical displacements were again derived from the cantilever deflections using equation 5.1. The theoretical and experimental curves show good agreement, the ultimate load predicted by the theory is 41 tons compared with 39 tons obtained in the experiment.

The photograph of the concrete slab after testing (fig 5.48) shows the distribution of cracking in the slab. Comparison of this with the corresponding photograph for the closed box, (fig. 5.34), shows that the change from closed to open section leads to much greater cracking of the slab. It is possible that this increase in cracking is, at least partly, caused by the shrinkage crack in the closed box model leading to a release of the residual shrinkage stresses in the slab. It seems unlikely that this alone would lead to such a noticeable difference and another contributing factor is likely to be the different distribution of shear connection discussed above. There is very little indication of the influence of shear stresses on the cracking of the open box slab (all cracks are at about 90° to the longitudinal axis of the box).

5.9 THE TESTING OF MODEL C2

The object of this test was to investigate the behaviour of a closed composite box under bending, shear and torsion loading. The details of the loading arrangement were as for

model C1 except that the jack load and end support reaction were over diagonally opposite web-diaphragm junctions instead of over the centres of the end diaphragms. Hence, for any given jack load the bending and shear loads were as for model C1 but model C2 had an additional torsion component of Pb/2 where P is the jack load and b the distance between the webs of the box.

5.9.1 Results of elastic tests

The testing procedure and presentation of results were as described for the tests C1 and 01.

The distributions of longitudinal stress are shown in figs. 5.49 and 5.50. The theoretical results shown suggest that the torsion component of load should lead to quite significant warping stresses, particularly in the top flange. Study of the experimental results shows that they do not confirm this prediction, and show no evidence of the presence of warping stresses. The likely cause of this disagreement is that the warping restraint present in the experiments is less severe than that assumed in the theoretical work. A possible improvement to the supported end boundary conditions assumed in the theoretical work has been discussed, with respect to the analysis of steel hollow sections, in section 3.5.3. In the absence of warping stresses the longitudinal stresses in this test would be expected to be the same as those in test C1; comparison of these two sets of results shows that, for the webs and bottom flange, very good agreement is obtained. For the top flange the stresses in model C1 are generally slightly higher than those in model C2, this difference is almost certainly caused by the shrinkage crack already discussed.

The distributions of shear stress, (figs. 5.51 and 5.52), show clearly the influence of the torsion component of load - the shear stresses in the loaded web are two to three times larger than those in the unloaded web. The influence of the torsion loading on the shear connector forces is clearly visible in fig. 5.53, the connectors over the loaded webs being very much more

heavily loaded than those over the unloaded webs. Again the theoretical results give very much larger slips than were measured in practice; this problem has already been discussed in section 5.7.1. The influence of shear lag on the shear connector forces is again very evident in this test.

5.9.2 Results of ultimate load test

For this test the direction of the jack load was again reversed so that the slab was put into tension, the maximum jack load was found to be 37 tons. The testing procedure and readings taken were as for the previous two ultimate load tests.

Figs 5.49 and 5.50 show that the cracking of the slab again leads to the longitudinal stresses in the steel top flange being very much higher in the ultimate load test than at the corresponding load in the elastic tests. This increase (about 60 per cent at the centreline and about 90 per cent at the quarter-point) is considerably larger than in the previous two tests; this is almost certainly caused by the extra cracking in the slab caused by the torsion component of loading. In this test the change in neutral axis position due to the cracking of the slab is not sufficient to reduce the bottom flange stresses, and for the ultimate load test these are about 10 per cent higher than the elastic test values.

Fig. 5.53 shows that in this model the cracking of the slab leads to a noticeable increase in the shear stresses in the steel top flange - this indicates that the concrete plays a significant part in resisting any torsion loading on this type of section. The reduction in slip, and hence in the shear connector forces, caused by the cracking of the slab, is again demonstrated by fig. 5.53.

The strain distributions around the section (figs 5.54 to 5.57) show that failure has taken place by shearing of the loaded web. Following the discussion in section 5.7.2, concerning the strength of the web flange junction, it is interesting to note that the shear strain in the top flange adjacent to the heavily

loaded web is much smaller than in the corresponding web; this suggests that the shear failure along the edge of the flange, discussed earlier, has not occurred. Contrary to this evidence is that of the rapidly increasing longitudinal slip on the loaded side of the box (see fig 5.60); since this slip is measured between the top of the webs and the concrete slab just above the webs this rapidly increasing slip could be evidence of large shear strains at the edge of the flange. It is possible that these large strains are confined to the area between the web-flange junction and the first row of studs, (at this row of studs some load will be transferred into the concrete slab), and hence the strain gauges present on the top flange would not provide evidence of these strains.

The load deflection curves (fig 5.61) show that the torsional deflections, (given by the difference between the deflections of the two webs), are quite small, illustrating the high torsional rigidity of the closed section. Comparing fig 5.61 with fig. 5.33 it may be seen that, according to the theoretical work, the bending stiffness, (i.e. that given by the average deflection of the two webs) of model C2, should, for loads up to about 20 tons, be very nearly equal to that of model C1. The experimental results suggest that the bending stiffness of model C2 is a little lower than that of model C1; it seems most likely that this difference is caused by a difference in the support stiffnesses, but there is no direct evidence to support this suggestion. The ultimate load predicted by the theory was 33.8 tons, compared with 37 tons measured in the experiment. Hence, according to the experiments, the reduction in the ultimate strength caused by the presence of the torsion component of load in test C2 was 10.6 per cent. This should be compared with the 11.5 per cent reduction predicted by the theoretical work.

The photograph of the cracked slab (fig. 5.62) shows clearly two sets of cracks - the bending cracks, running at 90 degress to the longitudinal axis of the slab, and the cracks influenced by shear stresses, running at between 60 and 45 degrees to the

longitudinal axis. In general the bending cracks appeared at considerably lower loads than the shear cracks. The slab cracks in this test were much more numerous and distributed over a much larger area of the slab than in the bending test.

5.10 THE TESTING OF MODEL 02

The object of this test was to investigate the behaviour of an open composite box under bending, shear and torsion loading. The loading arrangement was as described in section 5.9.

5.10.1 Results of elastic tests

The testing procedure and presentation of the results was the same as for the previous three models. The theoretical predictions of the longitudinal stress distributions, (figs 5.63 and 5.64), suggest that the warping stresses for this model will be considerably greater than for the closed box. The stresses measured in the experiment again show very little evidence of the presence of warping stresses, the longitudinal stresses measured in this test being very similar to those measured in the bending test (model 01). These results again demonstrate that very little warping restraint was present in the tested models.

As in the closed box model the distributions of the shear stress (figs. 5.65 and 5.66) are clearly influenced by the torsion load. Both the theoretical and experimental results show that the web and bottom flange shear stresses are very similar in this test to those found in the closed box model. As in the bending tests it can be seen that the shear stresses in the top flanges are considerably smaller in the open box model than in the closed box model; again this is caused by the two shear paths from the top flanges into each web in the open box, compared with only one in the closed box, and again is of particular importance when the top flange is thinner than the web.

The influence of the torsion on the longitudinal slip distribution is demonstrated in fig. 5.67. The experimental results suggest that the torsion load causes a reduction in the slips over the unloaded web, making these slips very nearly zero, but show very little corresponding increase in the slips over the loaded web. This is very surprising, as it would be expected that any decrease in slips on one side of the box would be matched by an equal increase on the other side. No measurements of the transverse slip were taken in the experiments but the theoretical work suggests that for this model the maximum transverse slip may be as much as 50% of the maximum longitudinal slip. Since the maximum longitudinal and transverse slips both occur at the loaded end of the model these transverse slips will have a significant effect on the maximum loads that the shear connectors are required to carry.

5.10.2 Results of ultimate load test

For this test the direction of the jack load was again reversed so that the slab was put into tension; the maximum jack load was found to be 32 tons.

Figs 5.63 and 5.64 show that the top flange longitudinal stresses are very much higher in this test than in the elastic test. The magnitude of the increase of these stresses in this model (up to 250% at the quarter-point) is very much larger than in any of the previous models, the reason for this being the much more extensive cracking of the slab in this test than in the previous tests. This extra cracking is caused by the much higher shear stresses present in the slab in this test because of the absence of a steel plate closing the top of the box. In this model the change in neutral axis position results in very little difference between the bottom flange longitudinal stresses measured in the elastic tests and those measured in the ultimate load test. Fig. 5.66 shows that the cracking of the slab causes no significant change in the shear stress distribution.

The longitudinal slip distribution (fig 5.67) shows that the cracking of the slab in the ultimate load test leads to the torsional component of the slip increasing much more significantly than the bending component. (The slip distribution may be assumed to be made up of a bending component symmetrical about the longitudinal centreline and a torsion component anti-symmetrical about the longitudinal centreline). This increase in the torsional component of slip leads to the slip in the unloaded web being in the opposite direction to that in the loaded web.

Figs 5.68 and 5.69 show that as the load increases the strains in the top flange above the unloaded web increase more rapidly than those in the flange above the loaded web. This seems rather surprising since, in general, the warping stresses and bending stresses would be expected to be of the same sign in the loaded web and of opposite sign in the unloaded web. One possible explanation of the results obtained in the experiment is as follows:

Consider an open steel section as shown in fig 5.92

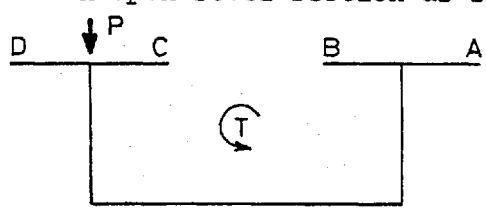

Fig 5.92

Assume that one end of the section is fully restrained against warping, and that the section is loaded with a torque T in the direction shown. Under this loading the warping stresses at the restrained end will result in flange AB going into compression and flange CD into tension. If the torsion load T is replaced by an eccentric bending load P on flange CD it can be seen that the direct stresses due to bending and those due to torsion will be of the same sign in CD and of different signs in AB. Hence the total direct stress in CD will be greater than that in AB.

Now consider a composite section as tested (fig. 5.93).

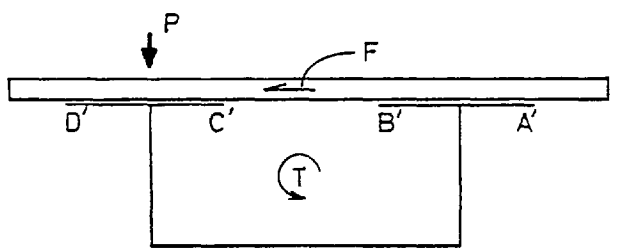

Fig 5.93

Again assume that one end is fully restrained against warping and that the section is loaded with a torque T. Again the warping of the section will result in flange A'B' going into compression and flange C'D' going into tension. The torsion load would also cause shear stresses in the concrete flange in the direction F. These shear forces would cause the slab above C'D' to go into compression and the slab above A'B' to go into tension; i.e. the warping stresses in the concrete flange are of opposite sign to those in the corresponding steel flange. If the torsion load T is then replaced by an eccentric point load P, again the direct stresses due to the bending and those due to the torsion are of the same sign in C'D' and of different sign in A'B', but in the concrete slab the two sets of stresses will be of the same sign above A'B' and of different sign above C'D'. As a result of this the slab is much more likely to crack in the area above A'B' than above C'D'. When the slab cracks the tensile forces in it must be released and carried by another part of the beam, and a large amount of the load released will be carried by the steel flange A'B', resulting in an increase in the tensile stresses in A'B'. If the extra tensile stress carried by A'B' due to the cracking of the concrete is more than twice the original warping stress in A'B' then this would result in the tensile stress in the flange above the unloaded web (flange A'B') being higher than that in the flange above the loaded web (flange C'D').

Fig 5.74 shows that, throughout the test, the slip between the steel and the concrete, and hence the shear connector forces, are highest in the area close to the longitudinal centreline of the model.

For this test the load-deflection curves (fig 5.75) are plotted as bending and torsion deflections against applied load. The reason for plotting in this manner rather than as done for the closed box is that, because of the likely weakness of this type of section in torsion, approaching failure of the section might be more clearly indicated by the torsion deflection than by the bending deflection. Both the theoretical and experimental

curves show that as the ultimate load approaches the loss of torsional stiffness is much faster than the loss of bending stiffness. Fig 5.75 shows that the theoretical and experimental ultimate loads show less good agreement than in previous tests; comparison of the reduction in ultimate load caused by moving the load from the centreline to the web shows that the reduction given by the theory is 12.5 per cent compared with 17.9 per cent obtained in the experiments. Failure of this model was caused by a crack along the longitudinal centreline of the slab (figs 5.76 and 5.76A). This crack was primarily caused by shear stresses in the plane of the slab, but the tested model shows some evidence of the presence of a transverse hogging bending moment in the slab which would help to lead to an earlier failure of the slab. With the plane stress assumption made in the theoretical work, any such bending moments are neglected, and hence an over-estimate of the strength may be given. An important difference between this model and the other three so far discussed is that the ultimate strength of this model is governed mainly by the strength of the concrete, whereas in the other three models the ultimate strength was controlled mainly by the strength of the steel section. This is important because the values of the strength and stress- strain properties of the steel can be measured more accurately than those of the concrete.

Fig.5.76a shows a photograph of the slab after testing and fig 5.76a shows a detail of a section of the central crack. The deformation of the reinforcing bars shown in fig. 5.76a (originally the longitudinal and transverse bars were orthogonal) shows that this crack was caused by shearing of the slab.

5.11 THE TESTING OF MODEL C3

The object of this test was to investigate the behaviour of a closed composite box under torsion load. Details of the test rig and loading arrangement are given in section 5.2.2. For the torsion tests the elastic and ultimate load tests were conducted with the same rig and loading arrangement. Again three tests were done, two elastic tests followed by the ultimate load test.

5.11.1 Results of elastic and ultimate load tests

For the elastic tests the jack load was increased from 0 to 10 tons in 2 ton increments, and then reduced to 0, again in 2 ton increments. For the ultimate load test a two ton load was applied to take up any slack in the supports, the load was then increased in 4 ton increments up to 38 tons, and then in 2 ton increments up to failure (46 tons).

For comparison of the theoretical and experimental work only one set of experimental results is given, this being the average of the two sets of elastic test readings and the ultimate load test readings, all for a 10 ton jack load. No direct stress distributions are plotted, the maximum longitudinal stress measured in the experiments for a 10 ton load was only about 3 N/mm^2, which was not thought to be significant. This lack of longitudinal stresses indicates that the tested section was effectively free from warping restraint.

The shear stress distributions (figs 5.77 and 5.78) show quite good agreement between the theoretical and experimental results. The fact that the experimental results were consistently a little below the theoretical results indicates that the jack load might have been slightly over-estimated. It is important to note that the shear stresses at the edge of the steel top flange are considerably higher than those at the midpoint of the flange. At the web-flange junction the shear flow in the flange must be equal to that in the web, but by the middle of the flange a significant amount of the shear load in the top flange will be carried by the concrete slab.

Fig. 5.79 (the longitudinal slip distribution) clearly demonstrates a difference between the built-in end assumed in the theoretical work and the situation present in the model. The built-in end assumption made in the theoretical work leads to a condition of zero slip at the centreline of the model, whereas in the tested model the slip was found to be nearly uniform along the length of the beam. Near the loaded end of the box the theoretical and experimental results for the slip

at the edge of the box agree quite closely. Across the end of the box virtually no slip was measured in the tests, whereas the theoretical work predicts a uniform change from the positive slip at one side of the box to the negative slip at the other side of the box. There are two possible causes of this disagreement between the theoretical and experimental work:

(1) The concentrated load applied at the end of the box may have affected the readings.

(2) In the tested model, in order to avoid premature failure of the end of the box, the slab was extended about 50 mms beyond the end diaphragm; this section of the slab is not loaded and may have resulted in reduced slip readings.

The plots of strain and slip distribution around the section for increasing load (figs 5.80 to 5.82) clearly demonstrate that the weakness of this type of section occurs in the steel top flange, close to the web-flange junction. In fig 5.80 it can be seen that this leads to rapidly increasing shear strains in this area. The longitudinal slip plotted in fig 5.82 has been measured between the top of the web and the bottom of the concrete slab immediately above the web. The first row of studs on the steel top flange are placed 24 mms from the web, and hence the very large slips shown in fig. 5.82 could be an indication of high shear strains in the area between the web and the first row of studs, rather than an indication of failure of the shear connection.

Fig.5.82a (the load-rotation curve) shows that in the elastic region the stiffness of the model measured in the experimental work is almost identical to that given by the theory. Unfortunately, owing to convergence problems discussed in chapter 6, it was not possible to continue the dynamic relaxation analysis up to the ultimate load. Using simple torsion theory the ultimate load measured in the experiment (46 tons) gives a shear stress of 183 N/mm^2 at the edge of the steel top flange. Taking the yield stress of steel in shear as $\sigma o/\sqrt{3}$, where σo is the yield stress in tension, the yield stress of the steel top

flange in the model is $280/\sqrt{3} = 162$ N/mm²; hence it seems that taking the ultimate load of the section as the load at which the thinnest plate yields in shear gives quite a reasonable estimate of the ultimate load of the section.

The photograph of the cracked slab (fig 5.83) shows that the cracks are quite widely spaced and confined to the area above the steel flange.

5.12 THE TESTING OF MODEL 03

The object of this test was to investigate the behaviour of an open composite box under torsion loading. Details of the test rig and loading arrangement are as discussed for model C3.

5.12.1 Results of elastic and ultimate load tests

Because of the likely torsional weakness of this model the maximum jack load for the elastic tests was restricted to 6 tons, hence the stress and slip distributions (figs 5.84 - 5.86) are plotted for a 6 ton load.

Comparison of the theoretical stress distributions shown in figs 5.84 and 5.85 shows that, particularly in the top flanges, the two stress distributions are different. This difference is caused by local effects due to the built-in end assumed at gauged section 1, and it could be argued that it would be more appropriate to compare both experimental stress distributions with the theoretical one at gauged section 2. Fig. 5.85 shows that very good agreement was obtained between the theoretical and experimental distributions at this section. It should be noted here that the problem of high shear stresses at the web-flange junction does not occur in the open box.

Again the longitudinal stresses are not plotted; in this test they were a little more significant than in the closed box test, averaging about 8 N/mm² in the top flange and about 4 N/mm² in the bottom flange, both being tensile stresses. The likely cause of these tensile stresses is the release, as the slab cracked, of the residual tensile stresses caused by the drying skrinkage of the concrete.

The longitudinal slip distribution (fig 5.86) shows that the theoretical work gives a good prediction of the slip distribution, but the magnitude of the slips measured in the experimental work was only 30 to 50 per cent of those predicted by the theoretical work. It can be seen that for this type of model and loading the most critical stud loadings occur along the inside edge of the steel flanges. Again the disagreement between the theoretical and experimental slips at the midpoint of the box is caused by the built-in condition assumed in the theoretical work.

The rapidly increasing slips along the inside edge of the unloaded flange (fig 5.89) indicate a possible weakness of the shear connection in this area, particularly since, with the twisting of this model, there is likely to be quite substantial transverse slip (the theoretical work indicates that the maximum transverse slip is about three-quarters of the maximum longitudinal slip).

The load-deflection curve (fig 5.90) shows that the cracking of the slab causes a considerable reduction in stiffness at a load of 8 tons, and from there on the stiffness gradually decreases until the ultimate load (19 tons) is reached. For this model the agreement between the theoretical and experimental results is poor - the ultimate load predicted by the theory is 54 tons. As for model 02 the reason for this disagreement is the inability of the theoretical work to take account of the transverse bending of the slab and the uplift of the shear connectors. Fig 5.90 also shows that the elastic stiffness of this model predicted by the theoretical work is slightly less than that measured in the experiments. This is the first model in which a significant difference has occurred between the theoretical and experimental stiffnesses, and is probably an indication of the sensitivity of this model to the values of shear connector stiffness and the Young's modulus for concrete used in the theoretical work.

Fig 5.91 shows a photograph of the cracked slab. Again the cracks are confined almost entirely to the area between the webs, but in this model there are considerably more cracks than in the closed box model under similar loading.

5.13 SUMMARY OF IMPORTANT RESULTS FROM EXPERIMENTS

(1) The series of tests has clearly demonstrated the weakness of the open type of composite box section when it is subjected to torsional loads. This weakness is of importance not only in terms of the ultimate strength of the structure, but also in terms of the extra cracking of the concrete slab in the open type of box.

(2) The applicability of the plane stress analysis to the closed section has been demonstrated, but for the open box section the out of plane deflections of the slab, caused by even quite small torsion loads, causes problems in the application of this type of analysis.

CHAPTER 6

APPLICATION OF COMPOSITE BOX PROGRAMS

6.1 MODELS USED IN THEORETICAL STUDY

The basic closed box model used in this study was adapted from models 3 and 4 in Moffatt's study (ref 21); details are given in fig 6.1. The shear connection stiffness used is that obtained by Moffatt using the working load criteria of CP117 part 2 1967; it is equivalent to the provision of 19mm x 100mm headed studs at 600mm centres longitudinally and transversely. The basic open box model is shown in fig 6.2. It can be seen that this is identical to the closed box model except that the top flange has been split along the longitudinal centreline and each half moved 915mms outwards.

6.2 MESH SIZE STUDY

In order to examine the effect of variation of the finite difference mesh size on the stress distributions and load-deflection curves, the open box model (01), loaded with a point load over one web, was used. Two mesh arrangements were considered; the coarse mesh is shown in fig 6.3 and the fine mesh in fig 6.4. It should be noted that the choice of mesh size is greatly restricted by the geometry of the beam.

For comparison of the elastic stresses obtained with the two different mesh sizes a load of 56 tons (a shear stress of 25 N/mm^2) applied over one web was considered. The direct and shear stresses at the cantilever support are shown in figs. 6.5 and 6.6 In general the agreement between the two sets of results is very good; the most significant difference is in the steel top flanges, where the fine mesh shows up the peaks of direct stress above the webs. Other investigators (Lamas (19)) have found that, because the onset of plasticity tends to even out the peaks and troughs of stress, mesh size effects are of greater significance in the elastic region than in the ultimate load region. In order to check the effect of mesh size on the ultimate load behaviour the load-deflection curves obtained with the two meshes are compared in fig 6.7. The general agreement between the two curves is quite good, the main difference being

the fact that the fine mesh evens out the changes in sitffness predicted by the coarse mesh (e.g. in the area around 130 tons load). The reason for these changes in stiffness is that cracking of the concrete leads to a release of stress, and with the coarse mesh the cracking of a small number of nodes can lead to a significant deflection due to the released stresses. Problems with convergence and the amount of computer time used meant that the fine mesh analysis was stopped at 260 tons load (80% of the ultimate load predicted by the coarse mesh analysis). An illustration of the effects of mesh size on computer time requirements is that in the fine mesh analysis of this model 8 load increments were applied and the cost was 11 computer units, in the coarse mesh analysis 19 load increments were applied and the cost was 5 computer units. Another point in favour of the coarse mesh was that, in order to obtain good convergence, it was most desirable that the program should be run from a telex terminal; convergence of each increment could then be judged by eye and, if required, further iterations could be applied to give better convergence; also, damping factors for each increment could be chosen according to the results of the previous increment. Because of memory space limitations it was not possible to run the fine mesh program in this way.

Additional verification that quite a coarse mesh is adequate for this type of analysis is given by the good agreement obtained between the theoretical and experimental results discussed in chapter 5.

As a result of the points discussed above it was thought that the mesh shown in fig 6.3 would provide sufficiently accurate results for this investigation.

6.3 BEHAVIOUR OF BOX 01 UNDER VARIOUS COMBINATIONS OF LOAD

Fig 6.8 shows the load-deflection curves for model 01 under various combinations of bending and torsion load. For load case 1 equal loads of P/2 were applied to each web. The loss of stiffness

at about 150 tons load indicates the onset of cracking of the slab but, after the temporary reduction due to the release of cracking stresses in the concrete, the overall stiffness is almost completely regained. After this there is no great reduction in stiffness until a load of about 320 tons, when the steel begins to yield, and failure follows quickly, the ultimate load reached being 335 tons. In practice, if a beam of these dimensions was tested, the sudden loss of stiffness due to cracking would probably not be observed, the cracking of the concrete being more gradual and spread over a larger range of loads.

For load case 4 a torsion load was applied to the free end of the model. Under this loading the first cracking of the concrete occurs at a load of about 350 T-m, and this cracking leads to a reduction in torsional stiffness of about 22%. Following this initial cracking the stiffness of the model remains reasonably constant until a load of 2200 T-m is reached, from here there is a rapid loss of stiffness and the ultimate load is 2280 T-m.

Load cases 2 and 3 involved application of a combination of bending and torsion. For load case 2 a shear load was applied to one web of the section, hence an applied load of P gives a torsion load of PB/2 where B is the distance between the webs of the section. For load case 3 a torsion load of PB was applied for a bending load of P. For both of these load cases the initial reduction in bending stiffness due to cracking of the slab occurs at a lower load than in load case 1 - for load case 2 this occurs at 130 tons and for load case 3 at 110 tons load. For load case 2, after this initial loss of stiffness, the load-bending deflection curve rejoins that for load case 1, and the curves remain very similar up to a load of 245 tons. Above this load the torsion component of load in load case 2 causes a more rapid reduction in bending stiffness than in load case 1, and the ultimate load reached is 325 tons, hence the eccentricity of the load causes about a 3 per cent reduction in the ultimate load.

For load case 3, after the initial loss of stiffness at 110 tons load the deflections are consistently higher than those for the corresponding bending loads in load case 1. The ultimate load reached is 275 tons - 18 per cent lower than for load case 1.

Comparing the torsion load-deflection curves it can be seen that in all three cases the cracking of the slab leads to a reduction in the torsional stiffness of the section. For load case 4 the reduction in stiffness was 22 per cent, for load case 3, 34 per cent and for load case 2, 37 per cent. Hence it can be seen that the higher the bending load relative to the torsion load, the greater the reduction in torsional stiffness due to the cracking of the slab. The differences are almost certainly caused by the different crack directions caused by the different load combinations.

6.4 BEHAVIOUR OF BOX C1 UNDER VARIOUS COMBINATIONS OF LOAD

The load combinations investigated for this model are the same as for model 01; the load-deflection curves are shown in fig 6.9.

Under the bending load (load case 1) the behaviour of this model is very similar to that of the open box model. Again, at about 150 tons load there is a reduction in stiffness due to cracking of the slab, but there is no serious permanent loss of stiffness until a load of about 315 tons is reached. Above this load the stiffness rapidly decreases and the ultimate load is about 328 tons. This ultimate load is very slightly (about 2 per cent) lower than that for the open box; the reason for this is the slightly greater influence of bending shear stresses on the steel top flange of a closed box than on an open box.

Under load case 4 the problem of stability of the dynamic relaxation solution, when applied to a closed box under torsion load, again occurred. This problem has already been mentioned in chapter 5 with respect to the analysis of the test specimens. For the beam considered here quite adequate convergence was obtained

up to a load of 2200 T-m, and also for the relaxation cycles of the next applied load increment. The problem occurred when an attempt was made to redistribute the cracking stresses in this increment, when the solution rapidly diverged to infinity. The most likely cause of divergence of the D.R. solution is that the structure has lost all stiffness and hence is unable to carry the load being applied. This is not the case here since, with the plane stress assumption made in this solution complete loss of stiffness will occur only at the very large deflections. Comparison of the load at which the instability occurs with the ultimate load calculated by simple torsion theory (assuming that the section fails when the shear stress in the thinnest steel plate reaches yield) shows that the ultimate load of the section has nearly been reached. The result of these convergence problems is that, for the closed box under load case 4, almost the full elastic torsional stiffness is maintained up to a load of 2200 T-m, and the ultimate load of the section is probably just under 2400 T-m. Comparing this with the results obtained from the open box model it can be seen that the ultimate load appears to be very similar, but, for a load of 2000 T-m the deflection of the open box is about 35% higher than that of the closed box.

For the closed box, under load cases 2 and 3, the bending load at which the initial slab cracking occurs is reduced to about 130 tons, compared with 150 tons for load case 1. This reduction, particularly for load case 3, is not as great as for the open box, indicating the smaller influence of the torsion load component on the cracking of the closed box slab. After this initial cracking the load-bending deflection curves for this model under load cases 1, 2 and 3 remain very similar up to a bending load of about 260 tons. At loads above 260 tons the model under load case 3 becomes noticeably less stiff than the other two and at loads above 290 tons the model under load case 2 shows higher deflections than for load case 1. Comparing the ultimate loads

reached by the closed box under these loads with those reached by the open box shows that, for load case 3, the ultimate load of the closed box is considerably, (about 15 per cent), higher than for the open box, but under load case 2 the ultimate loads are very nearly the same.

6.5 EFFECT OF VARIATION OF STEEL TOP FLANGE WIDTH

As discussed in section 6.1 the dimensions of model 01 were derived from those of model C1. In practice the steel top flanges are likely to be much narrower than those in model 01, and hence the effect of vatiation of the width of these flanges must be considered. In order to do this the behaviour of model 02 (fig 6.11) was considered. The top flanges of model 02 are half the width of those in model 01 but, in order to maintain the basic cross-sectional properties of model 01, are doubled in thickness. Since the area of contact between the steel and concrete is halved, in order to maintain similar total shear connection properties the stiffness of the shear connection is doubled. In order to represent this cross-section in terms of finite differences it is necessary to use a finer mesh across the flanges than for model 01; 17 nodes were taken across the concrete flange, 3 across each steel top flange, and 9 across the bottom flange. The longitudinal mesh size was reduced to 1830 mms.

For this model only load case 2 (load over one web) was considered.

Figs 6.12 to 6.15 show the direct and shear stress distributions at the cantilever support for models 01 and 02 under a load of 130 tons. In the steel sections the direct stresses for the two models are almost identical, as are the shear stresses in the webs and bottom flanges. In the steel top flanges the maximum shear stresses in model 01 are approximately double those in model 02. This is another illustration of the importance of the relative thicknesses of the steel plates, the top flanges in model 01, being

half the thickness of those in model 02, require double the shear stress to give the same shear flow as in model 02. Considering the stress distributions in the concrete the main difference between the two models is that, in model 02, one concrete node above the loaded web has cracked; apart from this the direct stress distributions are very similar. With the shear stress distribution the peak above the loaded web is caused by the cracking of the adjacent node.

Fig. 6.16 shows the load-deflection curves for the two models. Comparison of the bending load-deflection curves shows that they are very similar up to a load of 310 tons (95 per cent of the ultimate load of model 01). Comparison of the torsion load-rotation curves from the two models shows that the narrower top flange in model 02 leads to a small reduction in the torsional stiffness of the model. This reduction is about 4 per cent in the elastic region, but considerably more as the ultimate load is approached.

One of the problems associated with the use of a fine mesh size is illustrated here. When using the normal mesh it was possible to run the program from a telex terminal and the convergence of each increment could be watched by printing out, every ten cycles, the values of various displacements. As a result of this the decision as to whether a further load increment was required and if so, the damping factors to be used, could be made according to the results of the previous increment. For the finer mesh sizes restrictions on computer memory space available from a telex terminal meant that the program had to be run as a batch job. In order to do this the number and size of the load increments and the damping factor for each increment must be decided in advance. An example of the difficulties associated with this is that the number of increments taken for model 02 has not been sufficient for the ultimate load to be reached. In order to apply further load increments it would be necessary to repeat the complete analysis for the previous increments, and hence a considerable amount of extra computer time would be required for an extra three or four load increments.

In this case it was thought that the analysis of model 02 had been taken far enough to demonstrate the similarities and differences between the behaviour of models 01 and 02.

6.6 EFFECT OF VARIATION OF DOWELL FACTOR

In undertaking the analysis of a composite box one of the major problems encountered is the determination of the material properties for the cracked concrete. As described in chapter 4 these properties are based on a dowell factor and an aggregate interlock factor; increase or decrease of these factors will result in a corresponding increase or decrease of the shear stiffness of the cracked slab. In order to investigate the effect of variation of the slab shear stiffness model 01 under load case 3 was considered. The load-deflection curves for this case with dowell factors of 0.2 and 0.5 are plotted in fig. 6.17. (This variation is equivalent to a reduction of approximately 15 per cent in the shear stiffness of the cracked slab).

Fig. 6.17 shows that the reduction of the dowell factor from 0.5 to 0.2 leads to a slightly faster reduction in both the bending and torsional stiffness after cracking of the slab. Considering the large variation applied to the dowell factor the variations in the overall stiffness of the model are surprisingly small. There is virtually no effect on the ultimate load of the structure. The fact that the overall behaviour of the model is comparatively insensitive to these values is encouraging since their accurate evaluation is very difficult.

6.7 EFFECT OF VARIATION OF SHEAR CONNECTION STIFFNESS

It has already been shown (Figs 6.8 and 6.9) that there is a considerable difference between the torsional rigidities of the open and closed composite sections (models 01 and C1). The rigidity of the open section is likely to be greatly affected by the degree to which the concrete slab changes the steel from

an open section to a closed section. This degree of closure of the section is likely to be greatly affected by the stiffness of the shear connection between the steel and the concrete. In order to establish the effect of a variation in the shear connection stiffness on the behaviour of the open box model, the effect of doubling the shear connection stiffness of model 01 was investigated. Since the torsional behaviour is likely to be more seriously affected by variation of the shear connection properties than the bending behaviour, load case 4 was considered.

In the elastic region the change of shear connection stiffness caused virtually no change in the distribution of shear stress around the section, (figs 6.20 - 6.21), but considerable changes in the direct stress distribution were noted (figs 6.18 - 6.19). The distributions of direct stress show that, as the shear connection stiffness is increased, the section behaves more like a closed section than an open section, and hence the warping stresses decrease. The doubling of the shear connection stiffness considered here results in a decrease of approximately 25 per cent in the maximum warping stress. The increase in shear connection stiffness leads to only a very small, (about 7 per cent), increase in the maximum shear connector force; hence it can be seen that doubling the number of shear connectors on the top flange, will result in a decrease of about 45% in the load in each connector.

The load-deflection curves for the two connection stiffnesses (fig 6.22) shows that the beam with the stiff connection has a torsional rigidity about 5 per cent higher than that of the beam with the normal shear connection. Virtually no change was noted in the ultimate load of the section.

CHAPTER 7

CONCLUSIONS AND FUTURE WORK

7.1 CONCLUSIONS

The main conclusions drawn from the work described in this thesis are as follows:

(1) In chapter 2 upper and lower bound solutions to the ultimate load of a steel hollow section under bending, shear and torsion load have been derived. For boxes under bending and shear load it has been shown that the Heyman-Dutton empirical relation lies between the upper and lower bound solutions for all but very short boxes. For the 200mm x 300mm beam considered (fig 2.1) very short boxes may be taken to be those with depth to length ratios greater than 0.6. For boxes under combined uniaxial bending, shear and torsion, interaction curves have been plotted for three difference lengths of 300 mm x 200 mm and 200mm x 300mm rolled hollow sections. For the shorter beams, (relatively high shear forces), the difference between the upper and lower bound solutions is much larger than for the longer beams, suggesting that accurate prediction of the collapse load is more difficult for shorter beams. An illustration of the differences involved is that for a 300mm x 200mm beam of length 300mms the maximum difference between the upper and lower bounds was around 17%, compared with less than 3% for the 1200mm long beam.

In evaluating the lower bound solutions it has been assumed that a section is unable to carry any further torsion load when one web has reached full yield. In practice, whether or not a section will fail when this load is reached, is likely to be governed by the capacity of the section to redistribute the stresses caused by any further loading. This is likely to depend on the amount of frame action present, and on the rigidity of any diaphragms or bracing in the box.

(2) In chapter 3 a computer program, using the dynamic relaxation method, to solve the finite difference equations for a steel hollow section is described. Results from this analysis suggest that,

due to interaction between direct and shear stresses, the web failure mode may be of significance in a wider variety of beams than is suggested by the work in chapter 2. In order to fully establish the significance of this web failure mode a series of tests is required. Further theoretical work is required with a more detailed diaphragm model and also, possibly, taking account of frame action of the section.

(3) The series of tests on small-scale model composite box girders has demonstrated a number of important aspects of their behaviour. The bending tests on the closed composite box have demonstrated the importance of shear lag, particularly with regard to the loading on the shear connection. The torsion and eccentric load tests on the closed boxes have demonstrated the strength of this type of section in resisting torsion loads. The open box experiments have shown that, under a bending load, the behaviour of an open box section is almost the same as that of a similar closed box. The later tests showed that addition of quite a small torsion component of load, (for example that caused by placing the load over one web rather than over the longitudinal centreline), leads to very extensive cracking of the concrete slab. In both the eccentric load and torsion tests the ultimate strength of the open box was shown to be considerably lower than that of the corresponding closed box. For the models tested under eccentric load the ultimate load of the open box was 32 tons compared with 37 tons for the closed box, for the torsion tests the corresponding ultimate loads were 19 tons and 46 tons. The type of failure of the concrete slabs in these two open box tests has indicated that the strength of this type of section may be seriously affected by bending moments within the concrete slab.

(4) The dynamic relaxation program has been extended to analyse both open and closed composite box girders. Comparison of the results obtained using these programs with those obtained in the tests shows that good agreement is obtained for the closed box tests and also for the open box under bending load. For the open box under loadings containing a torsion component the ultimate load predicted by the theory is much higher than that measured

in the experiments; (e.g. for the torsion test 54 tons predicted by the theory compared with 19 tons measured in the experiment). The reason for the poor agreement in these two cases is the influence of the slab bending moments discussed above; the plane stress condition assumed in the theoretical work makes no allowance for the effects of these forces. It is thought likely that these bending moments will be greatly affected by the rigidity and positioning of any bracing or diaphragms present in the boxes.

(5) The finite difference programs have been used to analyse open and closed composite boxes of more realistic dimensions than those tested. The results indicate that, for an open box section, cracking of the concrete slab leads to a significant, but not catastrophic, loss of torsional rigidity (20 to 40 per cent, depending on the type of loading). In general the predicted ultimate loads of the open and closed boxes were similar for similar load combinations. In the light of the results of the experimental work it seems quite likely that, in practice, where there is a torsion component of load, the ultimate loads of the open boxes may be considerably reduced by bending stresses in the slab.

The effects, on the behaviour of an open box, of variation of parameters thought to be of significance to the torsional properties of the section were investigated. The most important of these properties was found to be the shear connection stiffness. It was found that variation of the shear connection stiffness leads to significant changes in the warping stresses in the section. This is likely to be of particular importance with regard to the cracking of the concrete slab. A second significance of the warping rigidity of the section is that, in practice, the fully restrained warping condition, assumed in the theoretical work, is not likely to be present; hence the increased tendency to warp, caused by a reduction in the shear connection stiffness, is likely to lead to a decrease in the overall stiffness of the section.

7.2 FUTURE WORK

The work described in this thesis has demonstrated the sensitivity of open composite boxes to torsion components of load.

The bending moments in the concrete slab (see conclusion (3)), which were found in the experimental work, may or may not be of significance in full size composite box girders. In order to investigate this further it would be necessary to undertake either some tests on large scale open box specimens, or a theoretical investigation which includes out of plane bending of the slab. It appears that the details of the diaphragms may significantly affect the behaviour of this type of section and hence these should be considered in some detail.

A considerable amount of work remains to be done on the influence of shear lag on the ultimate load behaviour of the shear connection, and particularly on the capacity of the connection to redistribute load after failure of one or more studs.

Another area requiring investigation is the influence, on the overall behaviour of the section, of buckling of either a web or the compression flange. Although the buckling behaviour of individual plates is now quite well understood little work has yet been done on the ability of a composite box section to redistribute loads released by the buckling of one plate.

References

1. Fairhurst, W.A. & Beveridge, A. The Superstructure of the Tay Road Bridge. Structural Engineer, Vol. 43. No. 3, March 1965.

2. Viest, I.M., Fountain, R.S. and Singleton, R.C. Composite Construction in Steel and Concrete. McGraw-Hill, 1958.

3. Nelson, H.M., Beveridge, A. and Arthur, P.D. Tests on a Model Composite Bridge Girder. Zurich, Int. Ass. for Bridge and Structural Engineering Publ. Vol 23, 1963, p. 263.

4. Billington, C.J. The Theoretical and Experimental Elastic Behaviour of Box Girder Bridges. Ph.D. Thesis, Univ. of London, 1974.

5. Gray, S.R., Clark, P.J. and Gent, A.R. Birkenhead-Mersey Tunnel Approach Viaducts. Structural Engineer, Vol 46, No. 12, Dec. 1968.

6. Cullen-Wallace, A.A. The White Cart Viaduct. Conf. on Steel Bridges, I.C.E. 1968 Session 2 paper 3.

7. Deuce, L.T.G. The Lofthouse Interchange Bridges. Conf. on Steel Bridges, I.C.E., 1968 Session 2 paper 5.

8. Murray, J. and Rigby, W.W. Design and Construction of Curved Steel Bridges in Lancs. Conf. on Steel Bridges, I.C.E., 1968 Session 2 paper 4.

9. Konishi, I., Yamada, Y. and Fukumoto, Y. On the Experimental Stress Analysis of a Single Composite Box Girder Bridge. Proceedings of the Symposium on Stress Measurements for Bridges and Structures. Japanese Society for the Promotion of Science, Tokyo, Dec. 1968.

10. Konishi, I., Komatsu, S. and Ohashi, M. Stress Analysis and Calculation for Design of Composite Box Girders. Trans. Japanese Society of Civil Engineers, No. 25, 1955 (In Japanese).

11. Barnard, P.R. A Series of Tests on Simply Supported Composite Beams. Journal, American Concrete Institute, Mar. 1965. p.443.

12. Chapman, J.C. Composite Construction in Steel and Concrete - The Behaviour of Composite Beams. Structural Engineer, Vol. 42, No. 4, April 1964.

13. Chapman, J.C. and Balakrishnan, S. Experiments on Composite Beams. Structural Engineer, Vol. 42, No. 11, Nov. 1964.

14. Johnson, R.P., Greenwood, R.D. and Van Dalen, K. Stud Shear Connectors in Hogging Moments Regions of Composite Beams. Structural Engineer, Vol. 47, No. 9, Sept. 1969.

15. Johnson, R.P., Van Dalen, K. and Kemp, A.R. Ultimate Strength of Composite Beams. Conf. on Structural Steelwork, I.C.E., 1966, Session 1 paper 3.

16. Zienkiewicz, O.C. The Finite Element Method in Engineering Science, McGraw-Hill, London, 1958.

17. Lim, P.T.K., Kilford, J.T. and Moffatt, K.R. Finite Element Analysis of Curved Box Girder Bridges. Proc. Int. Conf. on Developments in Bridge Design and Construction, Cardiff, Mar. 1971.

18. Chapman, J.C., Dowling, P.J., Lim, P.T.K. and Billington, C.J. The Structural Behaviour of Steel and Concrete Box Girder Bridges. Structural Engineer, Vol. 49, No. 3, Mar. 1971.

19. Lamas, A.R.G. Influence of Shear Lag on the Collapse of Wide-flanged Girders. Ph.D. Thesis, Univ. of London, 1979.

20. Newmark, N.M., Siess, C.D. and Viest, I.M. Tests and Analysis of Composite Beams with Incomplete Interaction. Proc. Soc. for Experimental Stress Analysis. Vol. 9, No. 1, 1951.

21. Moffatt, K.R. An Analytical Study of the Longitudinal Bending Behaviour of Composite Box Girder Bridges having Incomplete Interaction. Engineering Structures Laboratories, Imperial College, London, 1976, CESLIC Report CB1.

22. Hill, R. & Siebel, M.P.L. On Combined Bending and Twisting of Thin Tubes in the Plastic Range. Phil. Mag. Vol, 42. p.722, 1951.

23. Siebel, M.P.L. The Combined Bending and Twisting of Thin Cylinders in the Plastic Range. Journal of the Mechanics and Physics of Solids, Vol. 1, p. 189, 1953.

24. Gaydon, F.A. & Nuttall, H. On the Combined Bending and Twisting of Beams of Various Sections. Journal of the Mechanics and Physics of Solids, Vol. 6, p. 17, 1957.

25. Komatsu, S. & Sakimoto, T. Elasto-plastic Behaviour of Thin-walled Steel Tubes Under Combined Forces. Proc. Japanese Society of Civil Engineers. No. 235, Mar. 1975.

26. Hill, R. The Mathematical Theory of Plasticity. Oxford, Clarendon Press, 1950.

27. Neal, B.G. The Plastic Methods of Structural Analysis, 3rd (S.I.) Ed., London, Chapman & Hall, 1977.

28. Scarborough, J.B. Numerical Mathematical Analysis, 6th Ed., Baltimore, Johns Hopkins Press, 1966.

29. No ref. 29.

30. Chrisfield, M.A. Large Deflection Elasto-plastic Buckling Analysis of Plates using Finite Elements. T.R.R.L. Report 593, Transport and Road Research Laboratory, Crowthorne, Berkshire, 1973.

31. Harding, J.E., Hobbs, R.E. & Neal, B.G. The Elasto-plastic Analysis of Imperfect Square Plates under In-plane Loading. Proc. I.C.E., part 2 vol 63, March 1977.

32. Frieze, P.A., Hobbs, R.E. & Dowling, P.J. Application of Dynamic Relaxation to the Large Deflection Elasto-plastic Analysis of Plates. Computers and Structures, Vol. 8, No. 2, April 1978.

33. Cassell, A.C. Shells of Revolution under Arbitrary Loading and the use of Fictitious Densities in Dynamic Relaxation Proc. I.C.E. Vol. 45, Jan. 1970.

34. Moffatt, K.R. & Dowling, P.J. The Longitudinal Bending Behaviour of Composite Box Girder Bridges having Incomplete Interaction. The Structural Engineer, Vol. 46B, Sept. 1978.

35. Buckby, R.J. 'Topic for discussion at a meeting of Box Girder Research Panel at Warwick University on Tuesday 28th September 1976.'

36. Highway Structures Design Handbook, Vol. 2. United States Steel Corporation, 1965.

37. Dowling, P.J. Recent Developments on the Inelastic Analysis and Design of Plate & Box Girders. Proc. Int. Colloquium on Stability of Structures Under Static and Dynamic Loads. Washington, March 1977.

38. Mattock, A.H. & Johnstone, S.B. Behaviour Under Load of Composite Box Girder Bridges. J. Structural Div. A.S.C.E. Vol. 94, No. ST10, Oct. 1968.

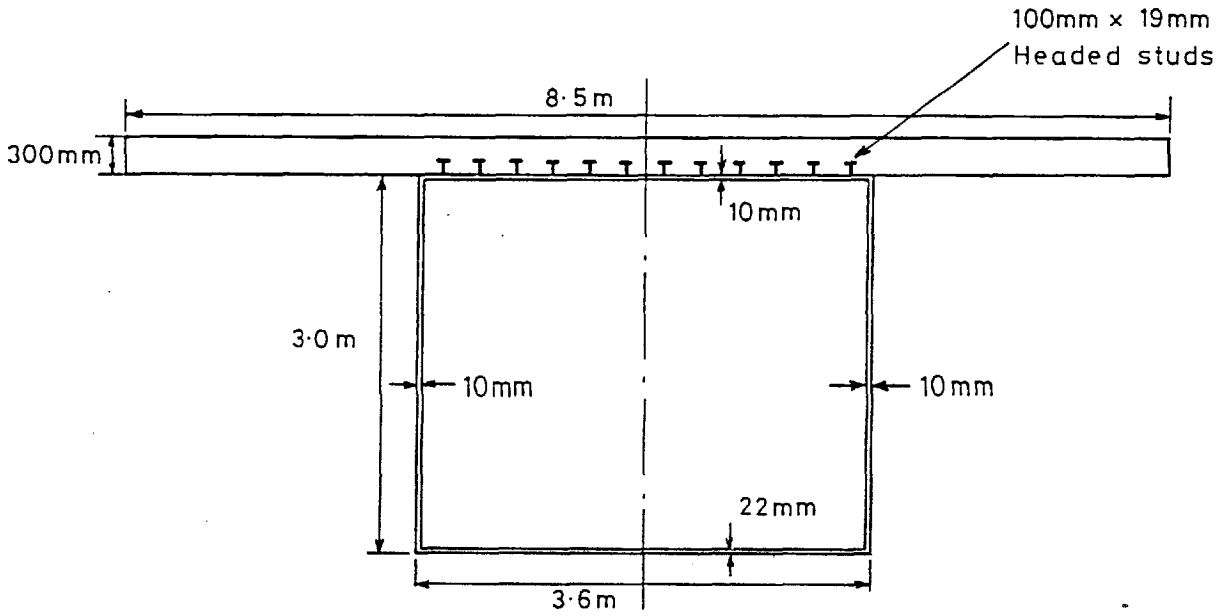

Fig 1·1 Cross-section of typical closed composite box girder (simplified)

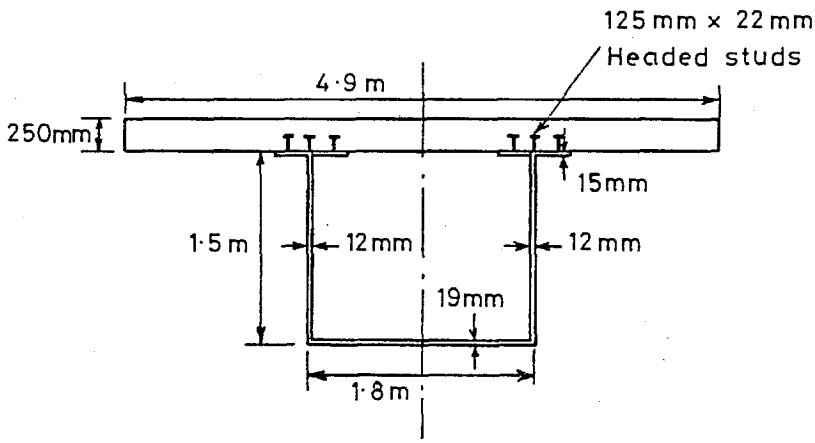

Fig 1·2 Cross-section of typical open composite box girder (simplified)

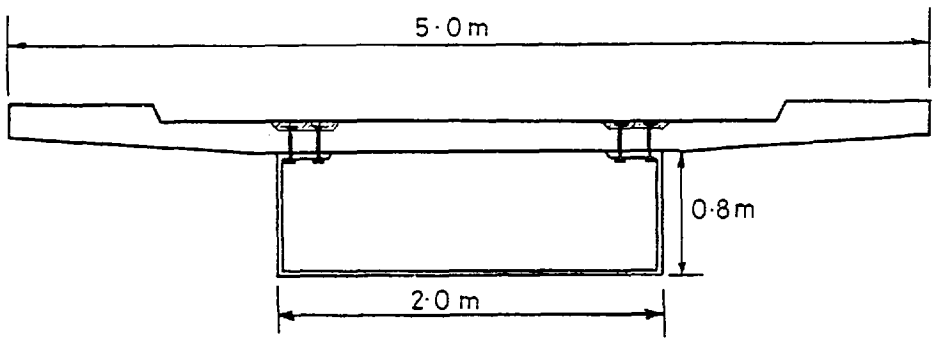

Fig 1·3 Simplified cross-section of curved viaduct ramp, Hanover Germany

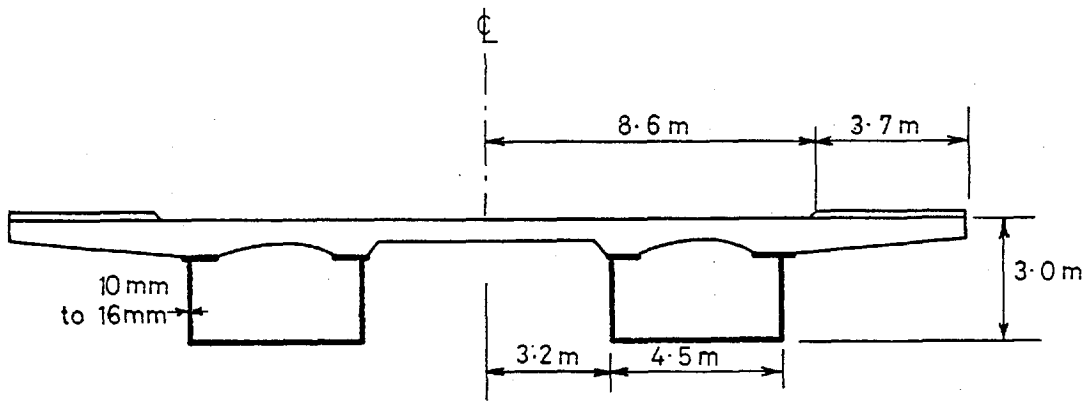

Fig 1·4 Simplified cross-section of Schloss bridge, Germany

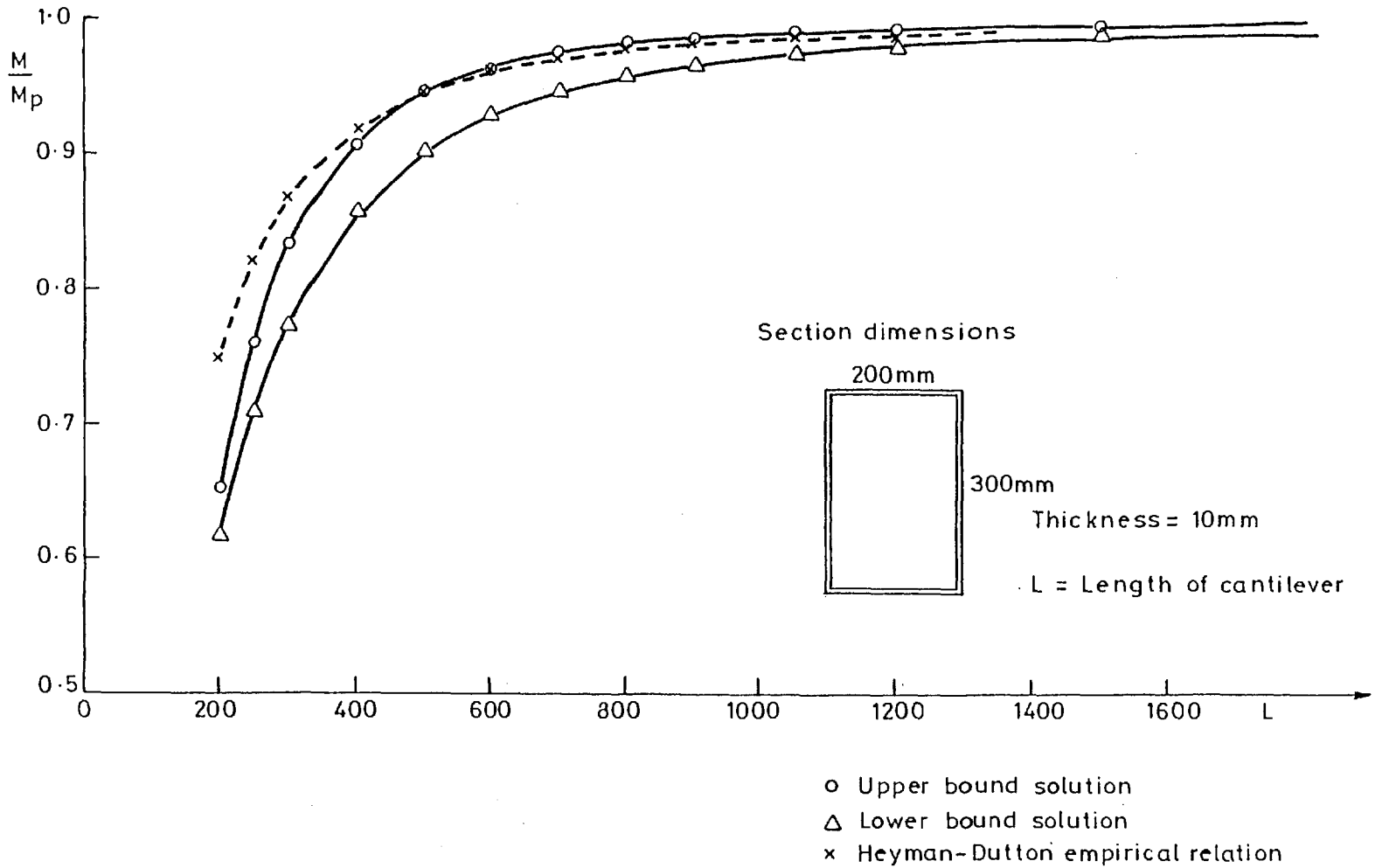

Fig 2·1 Comparison of various results for bending and shear

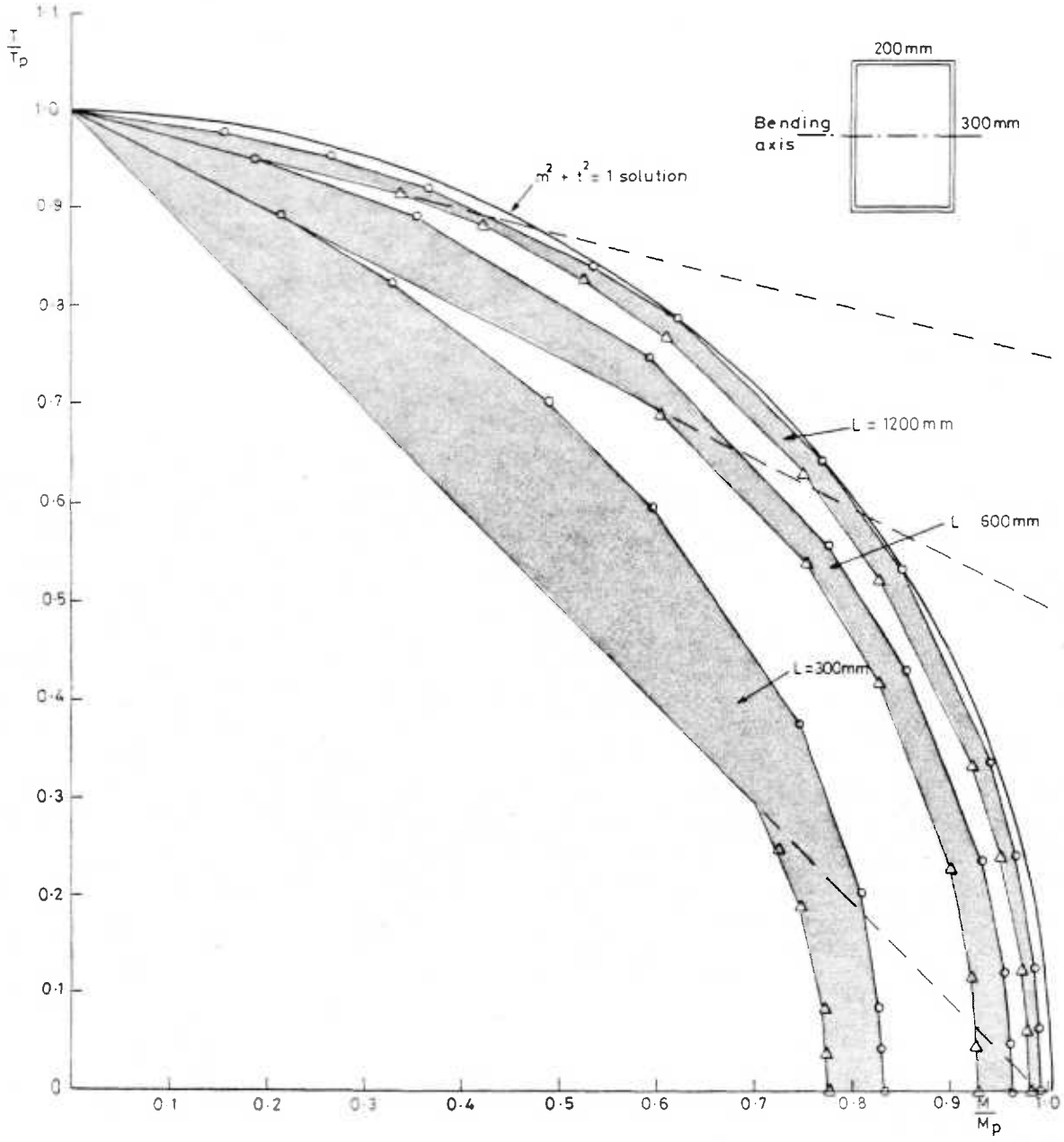

T = Ultimate torque in presence of moment M & associated shear force
M = Ultimate moment in presence of torque T & associated shear force
M_p = Plastic moment under pure bending
T_p = Plastic torque
L = Cantilever length (moment / shear force)
o = Upper bound solution
Δ = Lower bound (overall failure) solution
– – – Lower bound (web failure) solution

Fig 2·2 Interaction curve for section
200mms × 300mms of uniform thickness

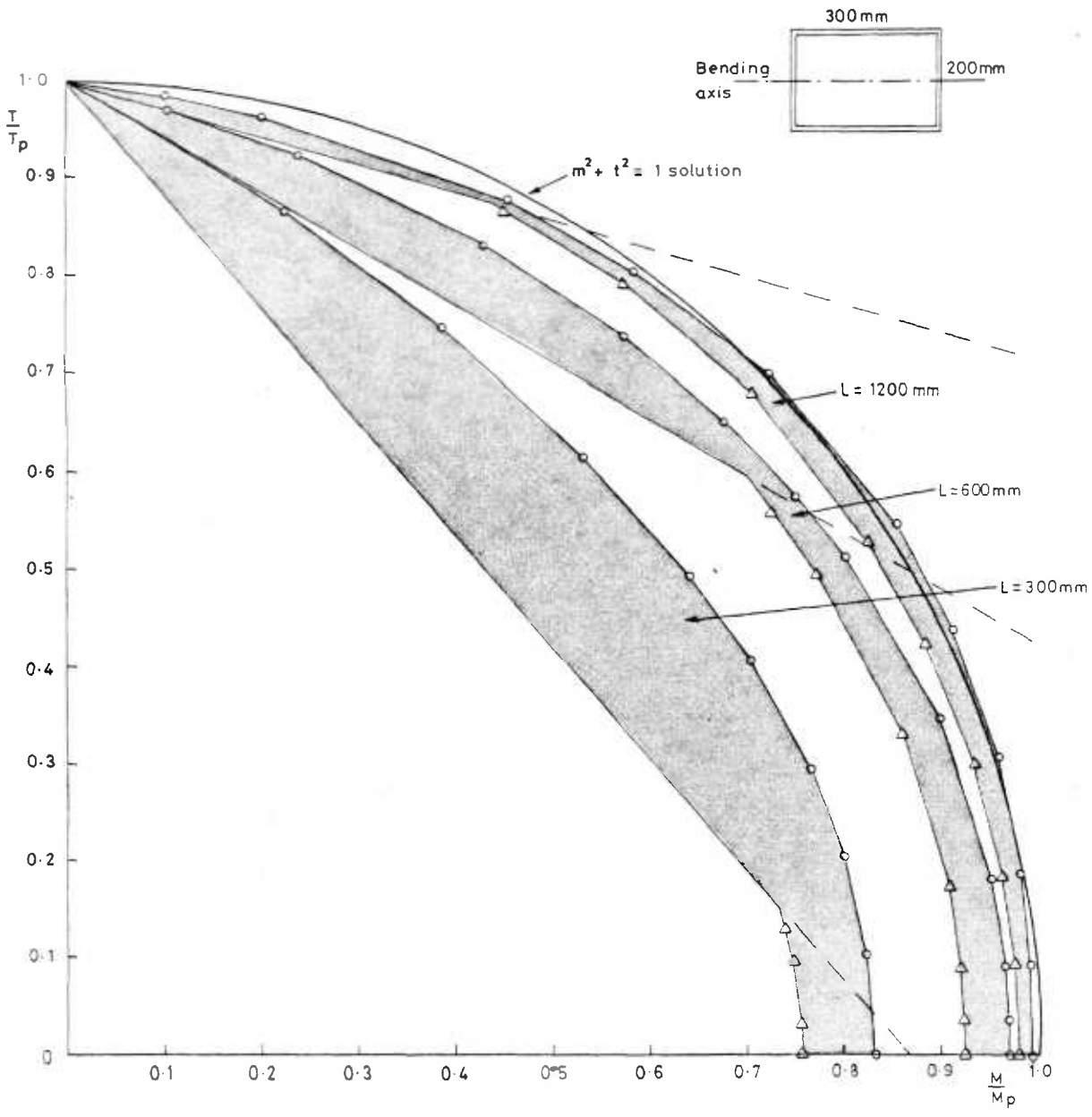

T = Ultimate torque in presence of moment M & associated shear force
M = Ultimate moment in presence of torque T & associated shear force
M_p = Plastic moment under pure bending
T_p = Plastic torque
L = Cantilever length (moment / shear force)
o = Upper bound solution
Δ = Lower bound (overall failure) solution
– – – Lower bound (web failure) solution

Fig 2·3 Interaction curve for section
300mms × 200mms of uniform thickness

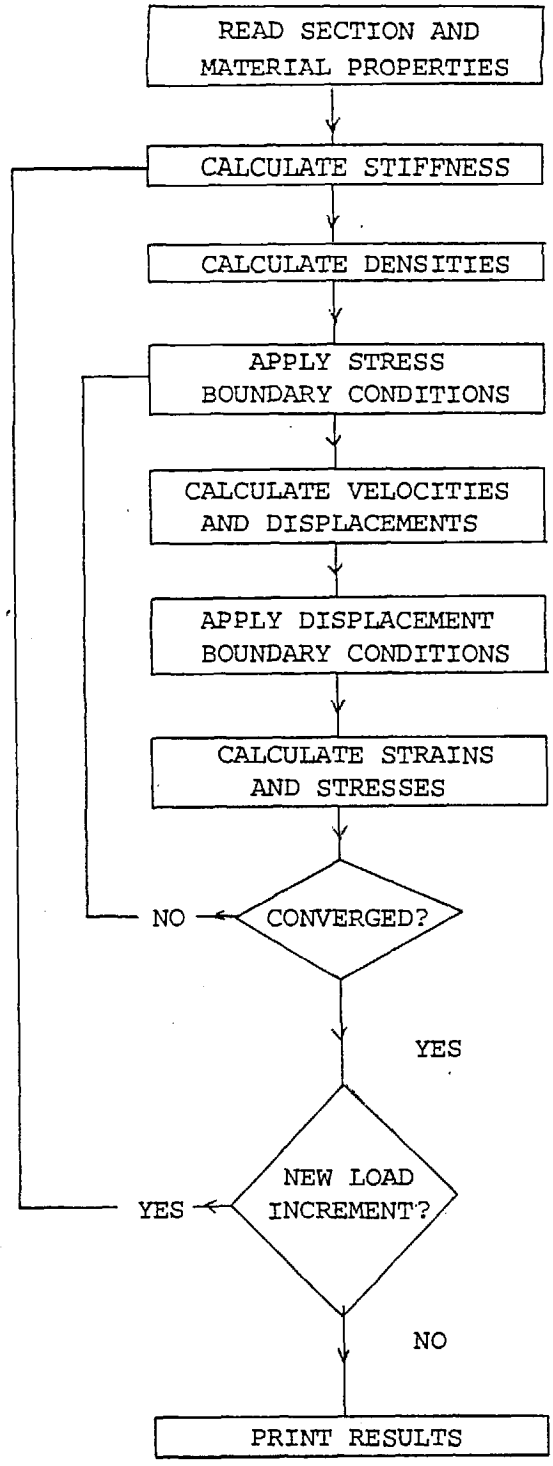

Fig 3.3 Flow chart for D.R. method

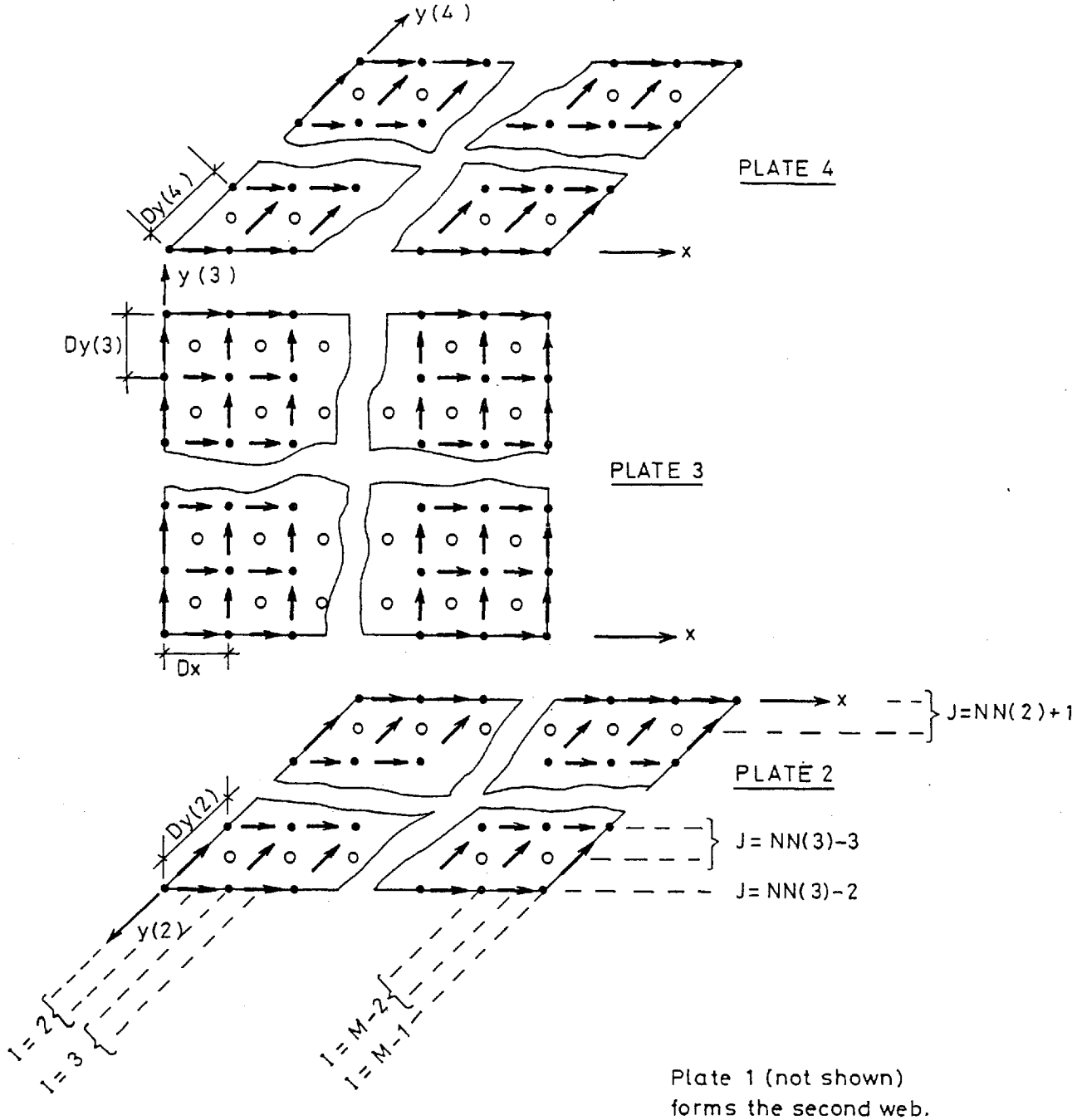

Fig 3·4 Finite difference mesh details

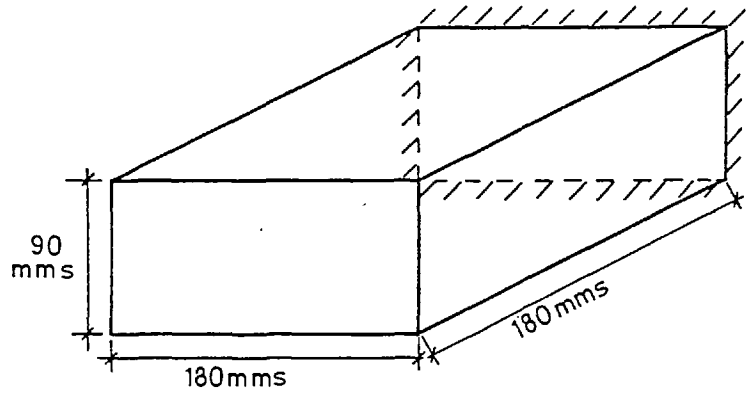

All plates 1·8 mms thick

Fig 3·5 Beam used for mesh size study

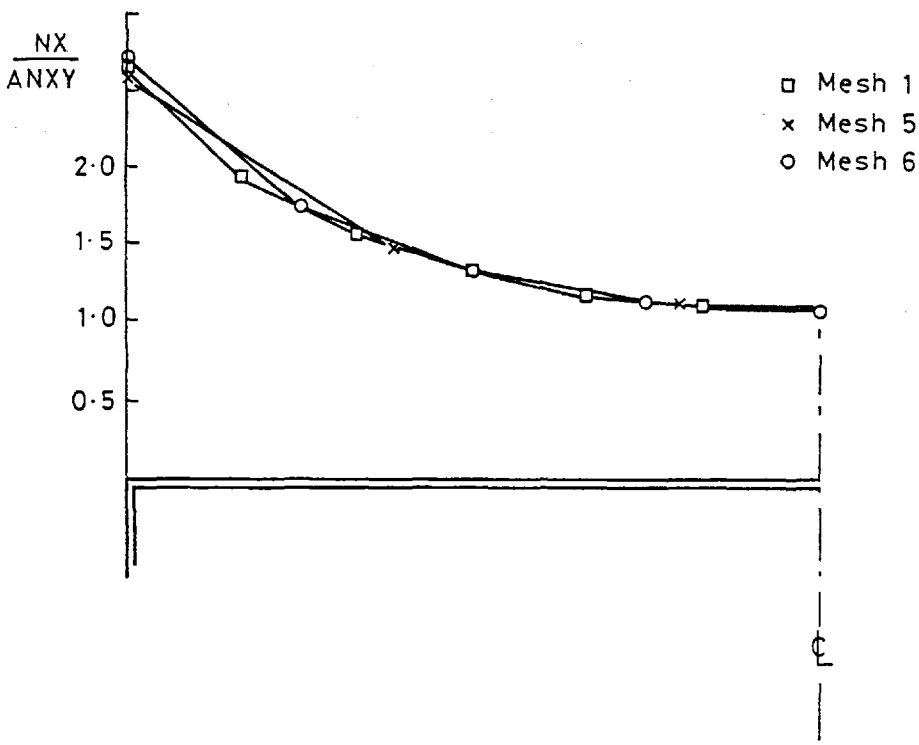

NX = Direct stress at support
ANXY = Applied shear stress

Fig 3·6 Effect of mesh size on elastic stresses at support

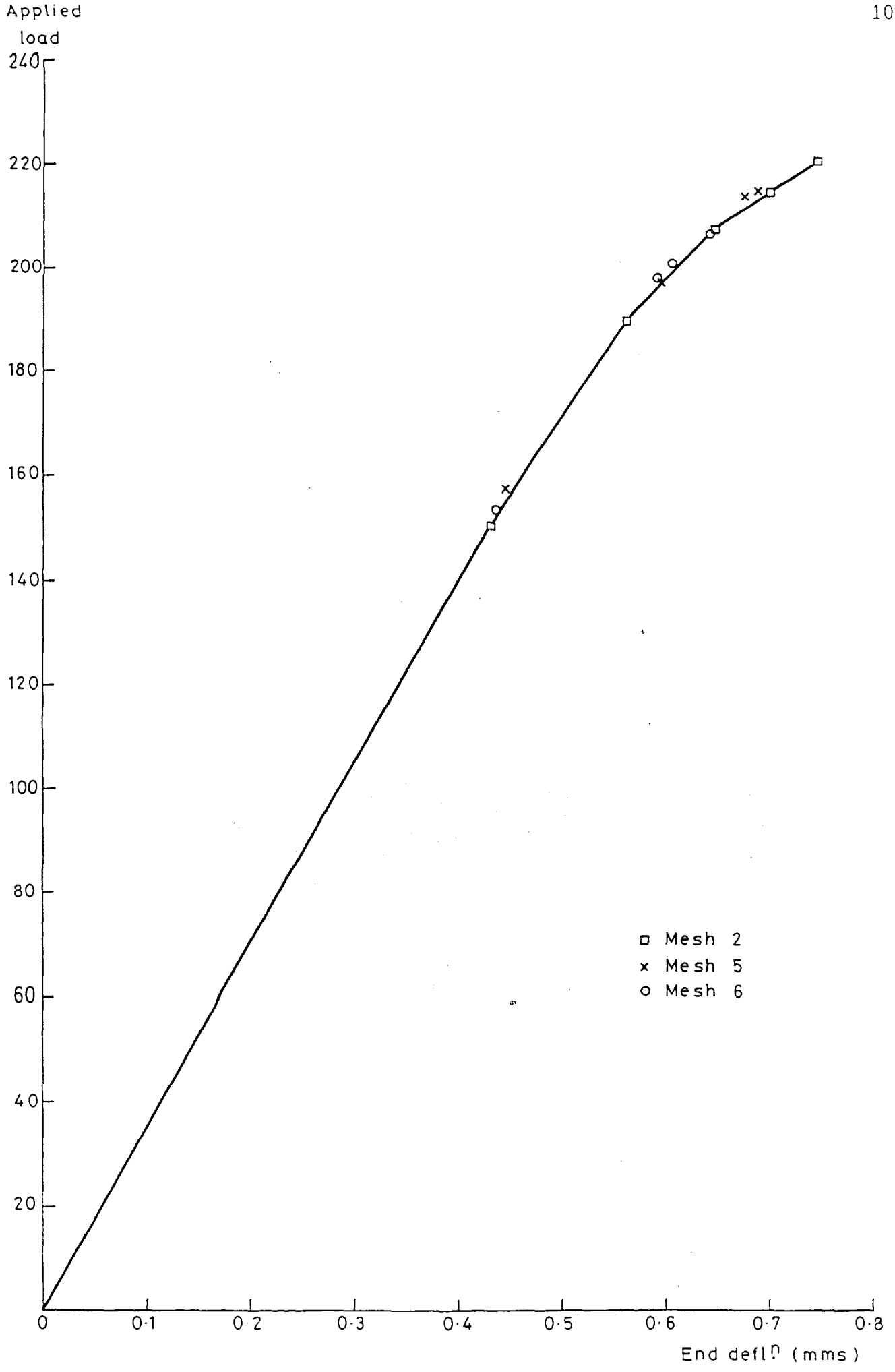

Fig 3·7 Comparison of load-deflection curves for various mesh sizes

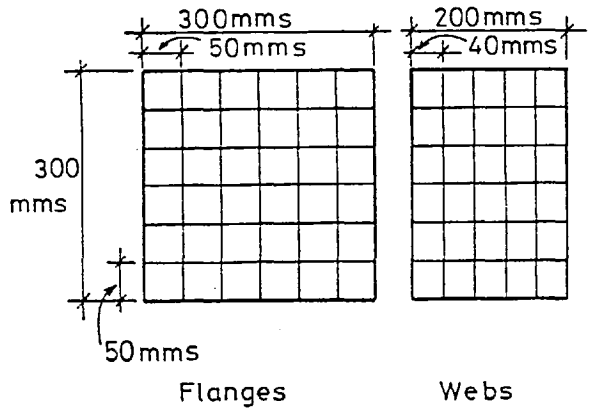

(a) MODEL 1

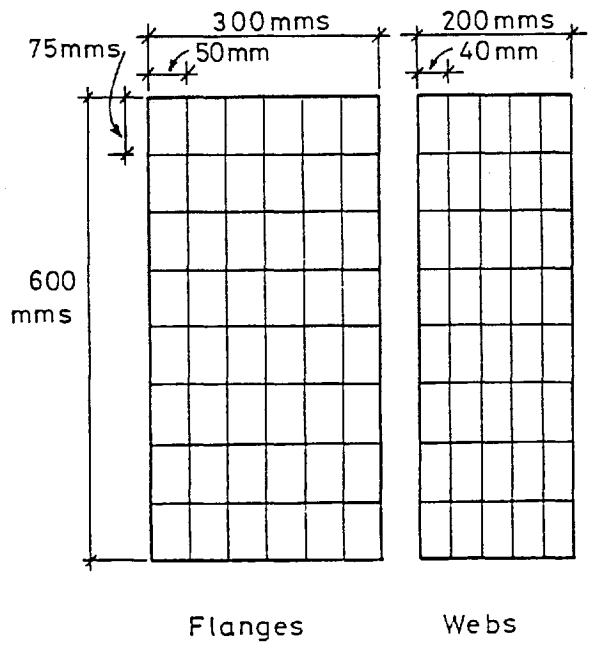

(b) MODEL 2

Fig 3·8 Finite difference meshes used for steel section study

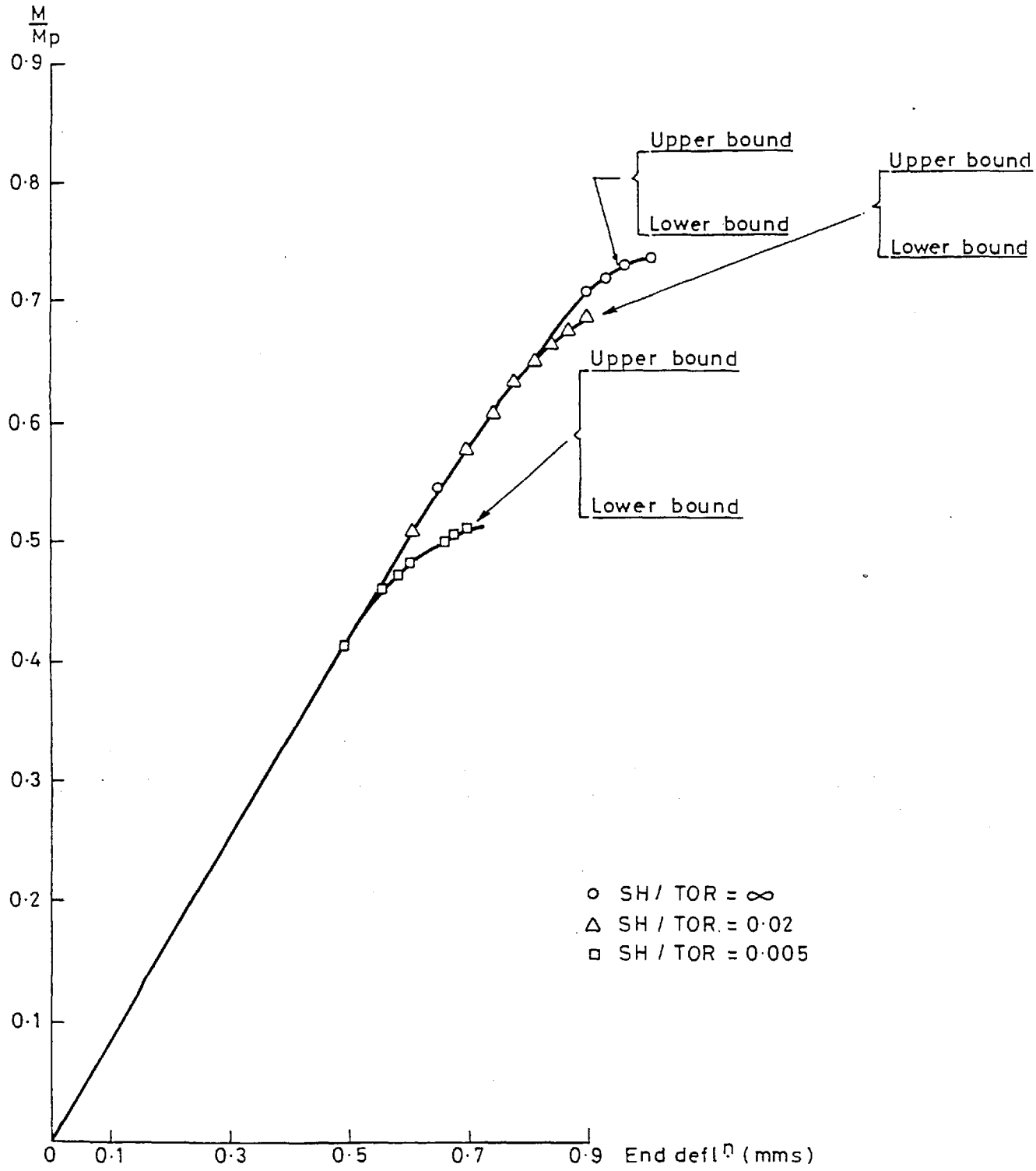

Fig 3·9 Load-end deflection curves for section 300mms × 200mms, 300mms long

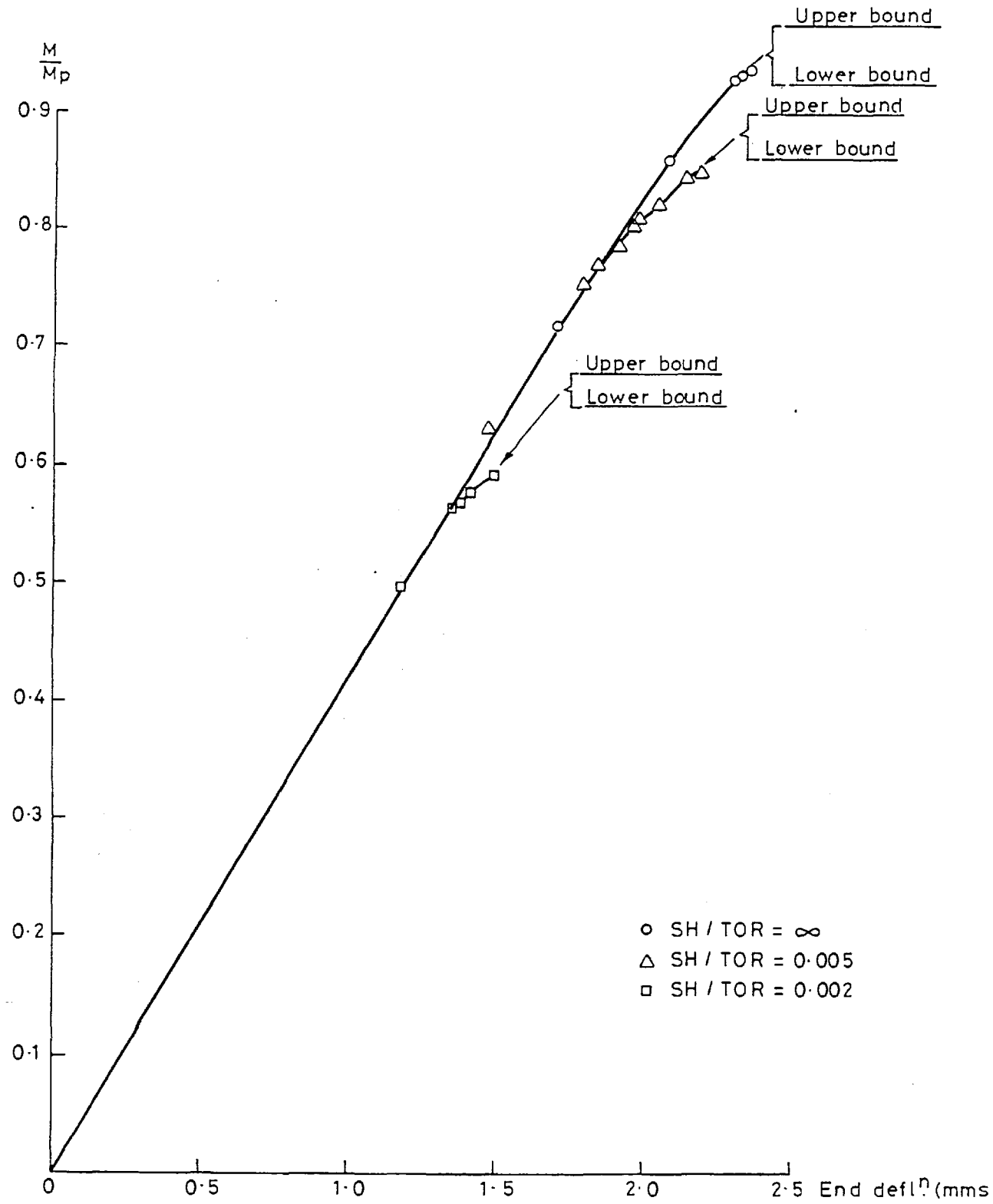

Fig 3·10 Load-end deflection curves for section 300 mms × 200 mms, 600 mms long

Section 300×200×10 L=300

△ Lower bound
× Upper bound
○ D.R. program
⊛ Lower bound web failure - stress distⁿ not applicable

DIRECT STRESS SHEAR STRESS

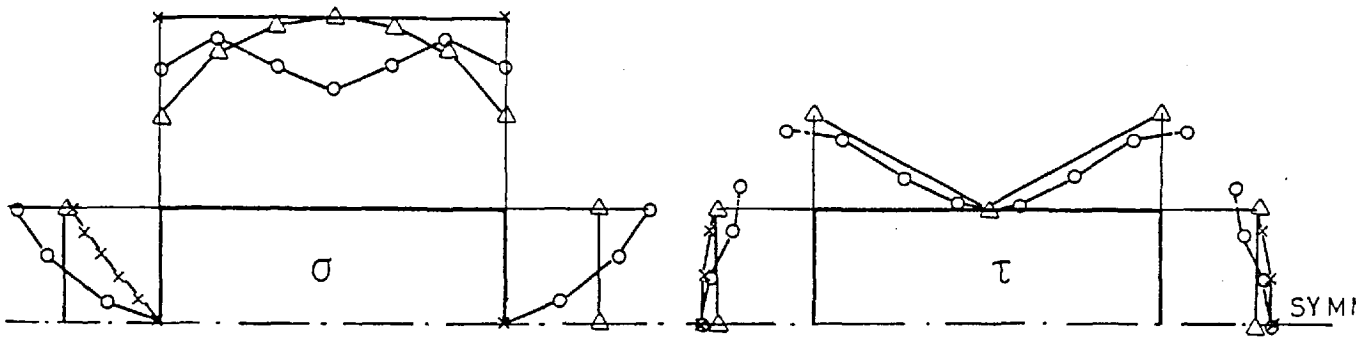

(a) BENDING ONLY

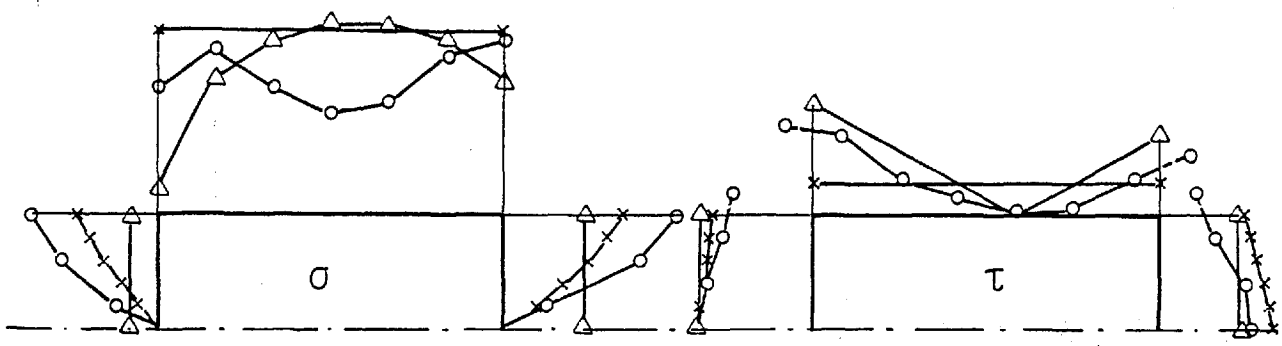

(b) SH/TOR = 0·02

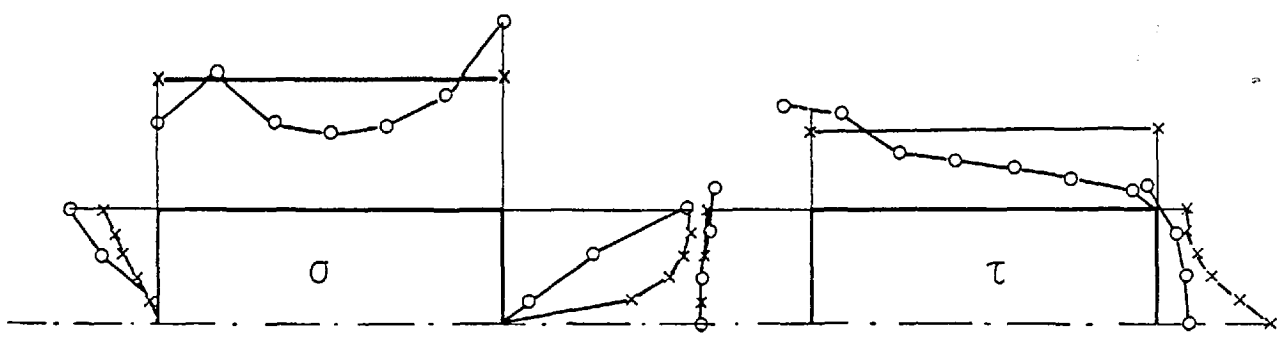

(c) SH/TOR = 0·005 ⊛

Fig 3·11 Stress distributions at ultimate load by various methods

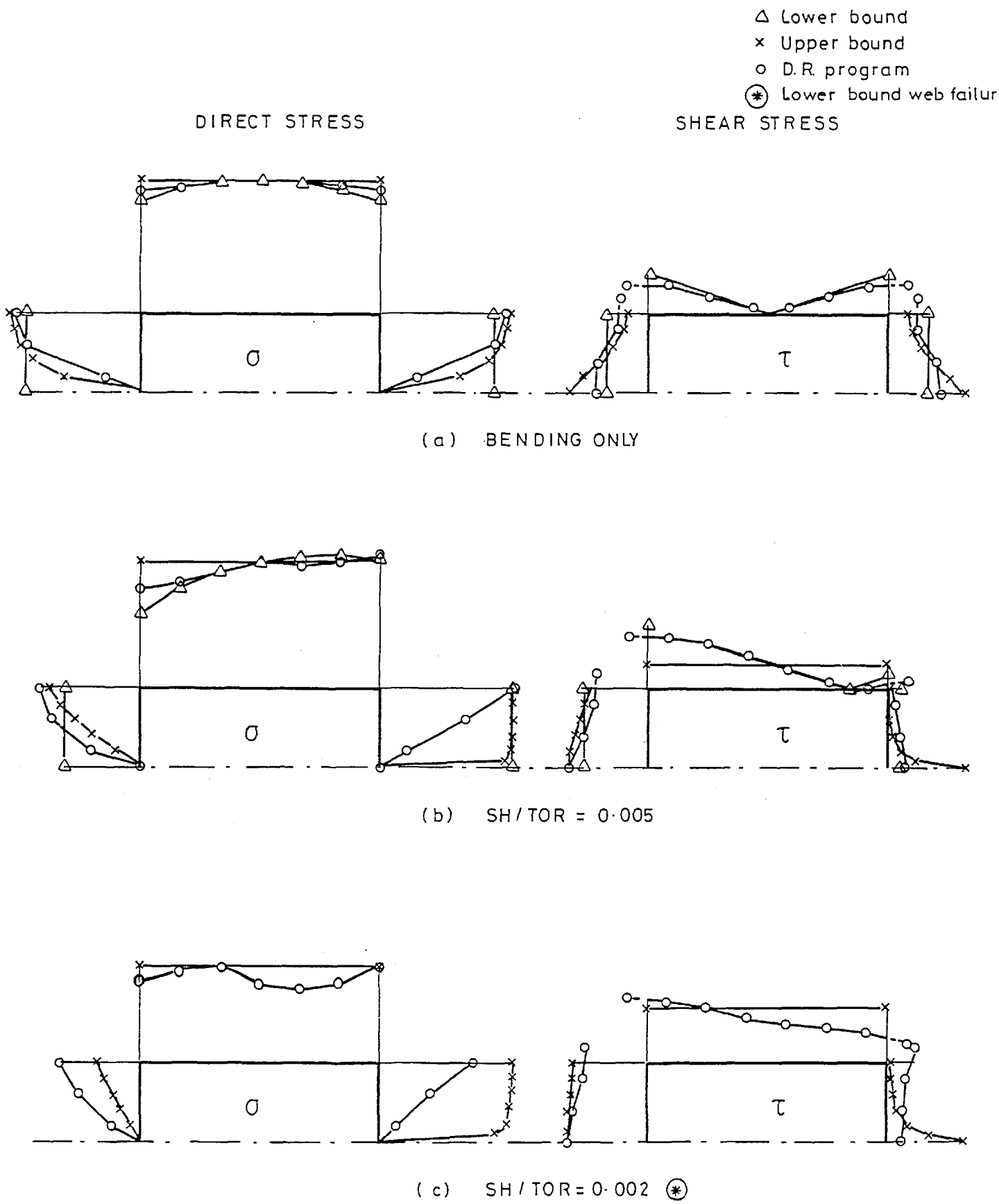

Fig 3·12 Stress distributions at ultimate load section 300×200×10 L=600

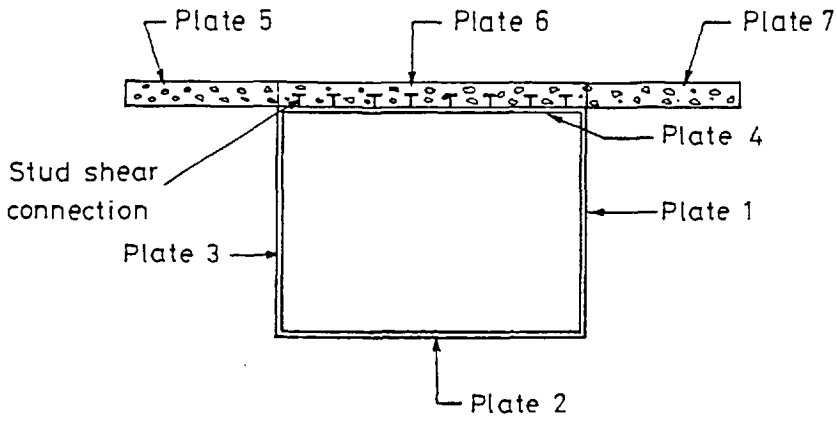

Fig 4·1 Simplified cross-section of a typical closed composite box girder

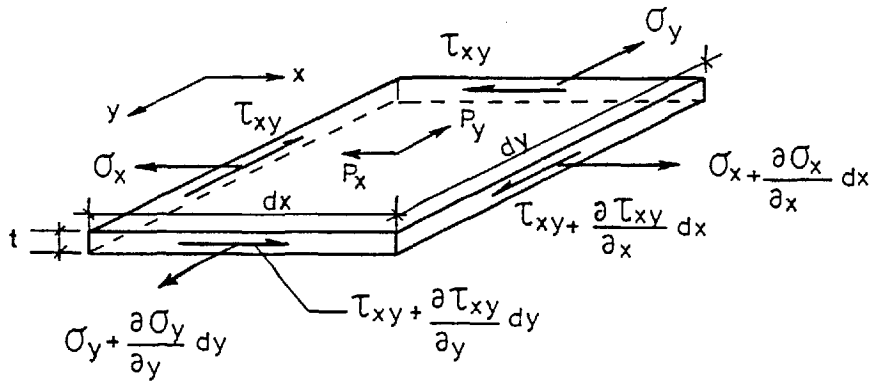

Fig 4·2 Stresses on a section of plate 4

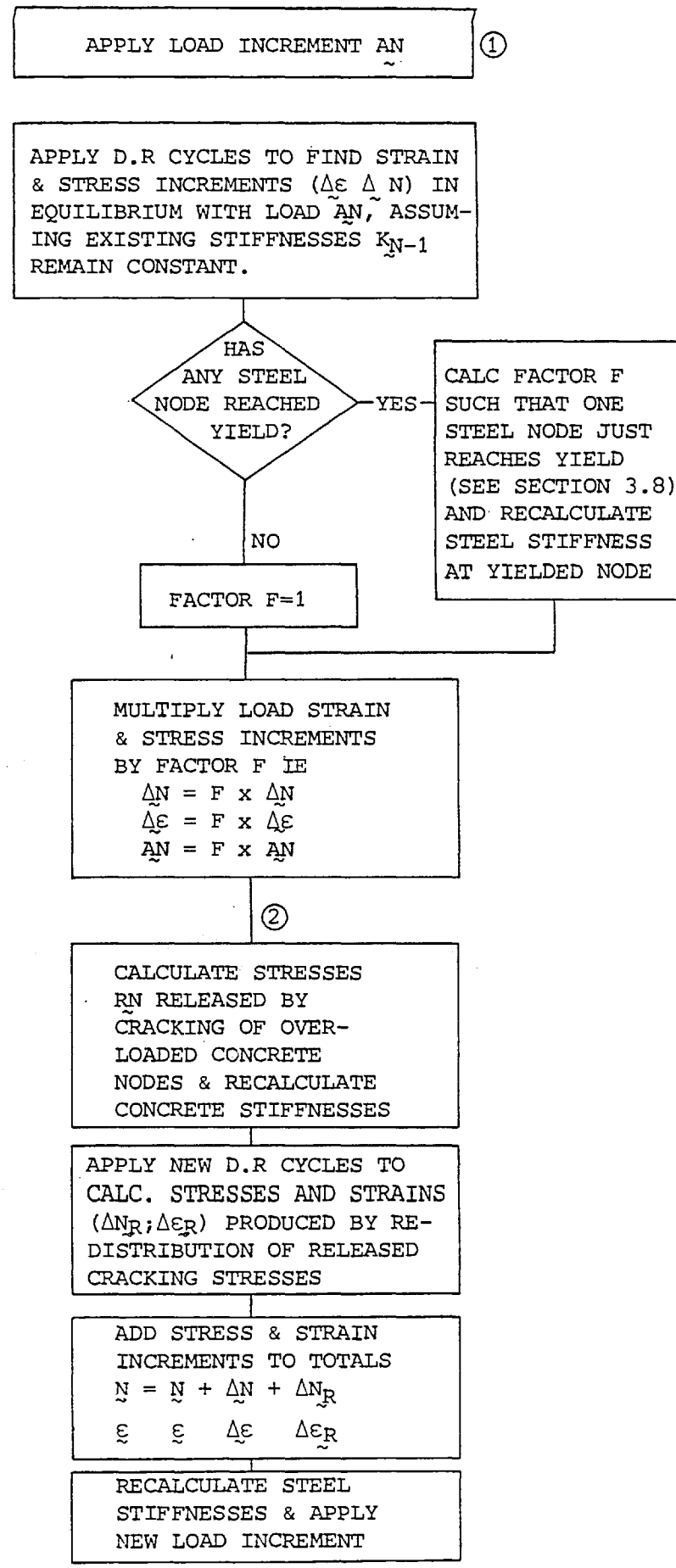

For notes (1) and (2) see text.

FIG 4.3 FLOW CHART SHOWING LOAD INCREMENTATION METHOD FOR COMPOSITE BOX PROGRAMS

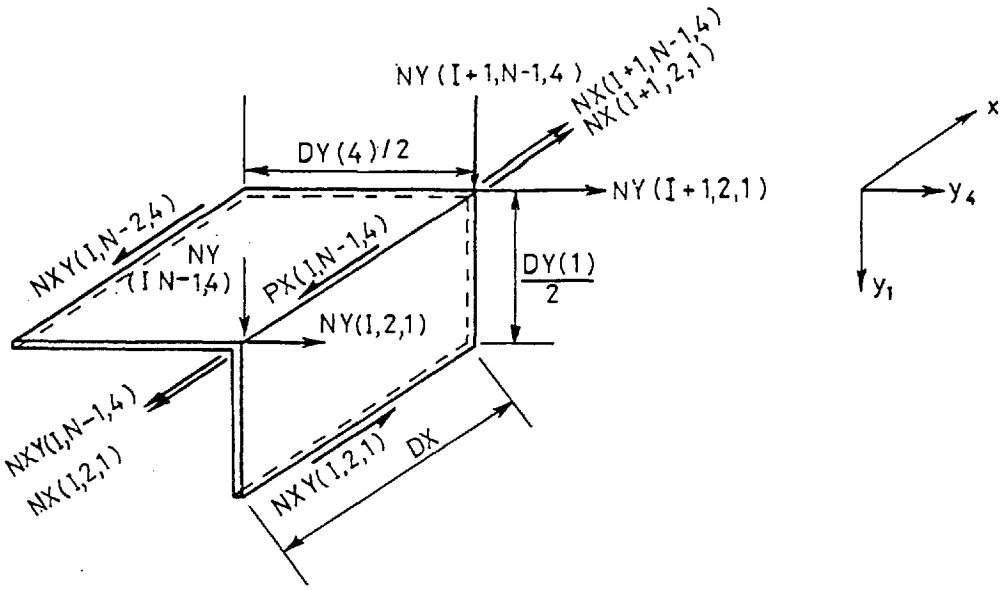

Fig 4·4 Stresses at typical section of junction of plates 1 & 4

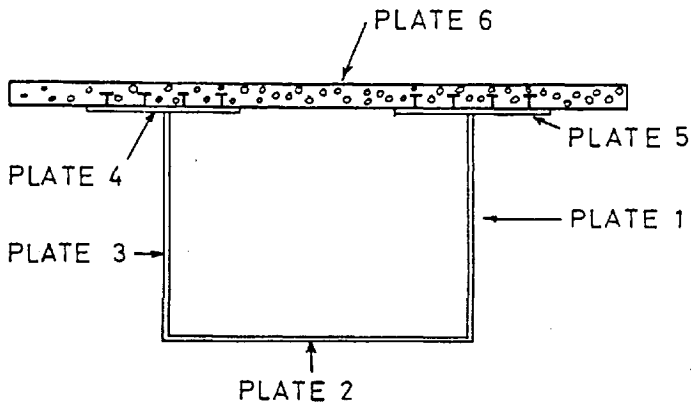

Fig 4·5 Simplified cross-section of a typical open composite box girder

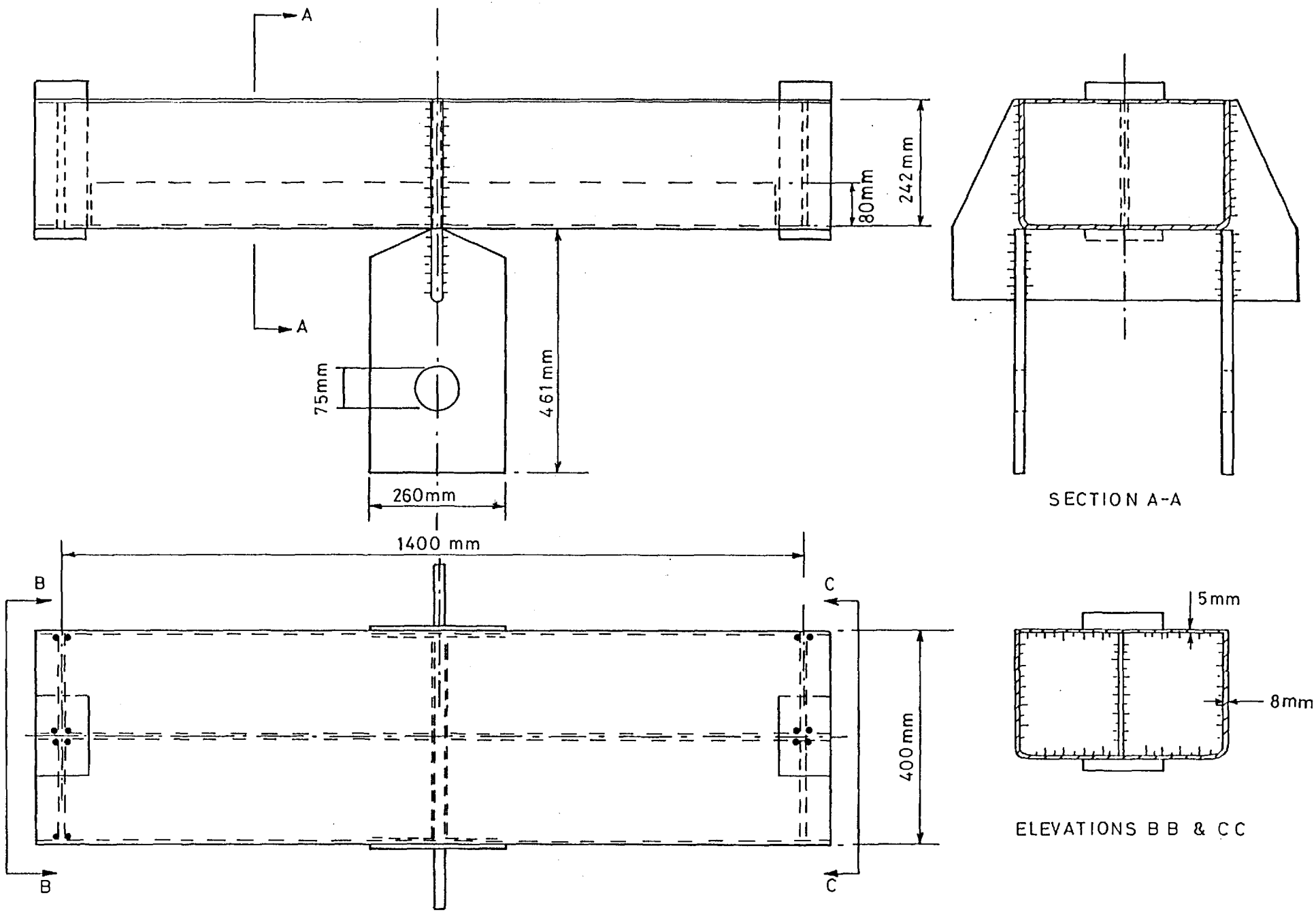

Fig 5·1 Details of closed box section

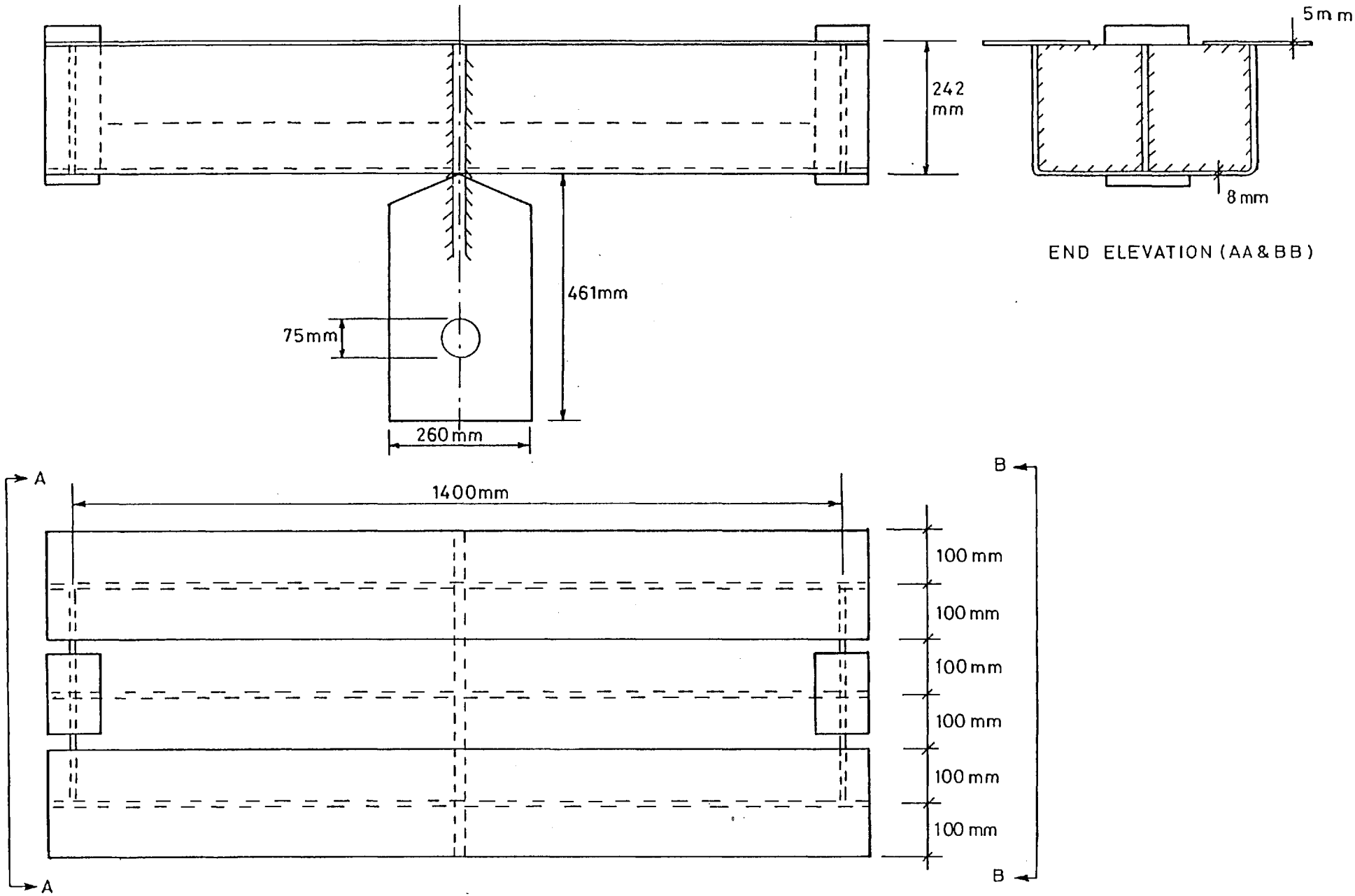

Fig 5·2 Details of open box section

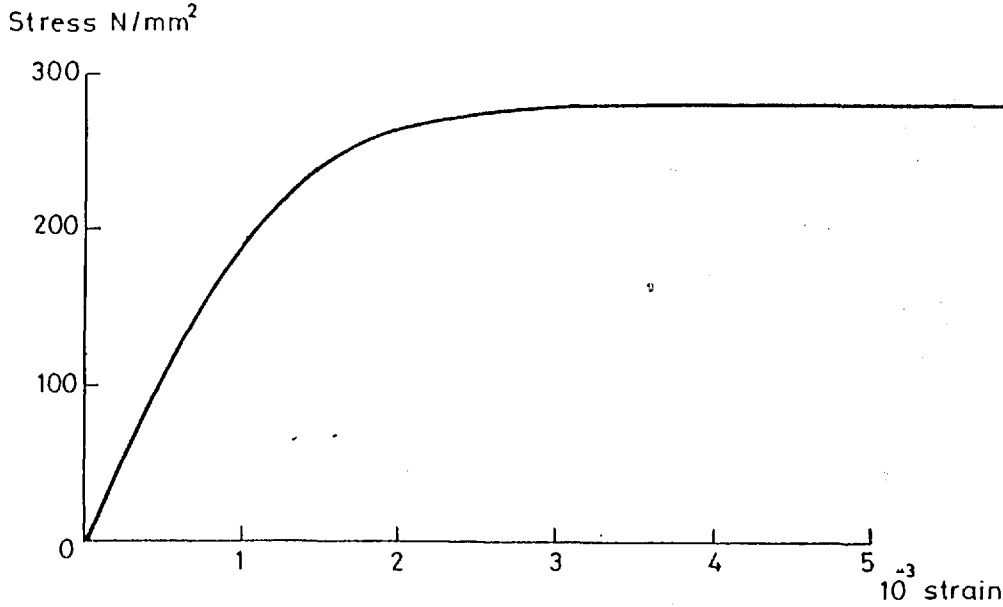

Fig 5·3 Top flange steel

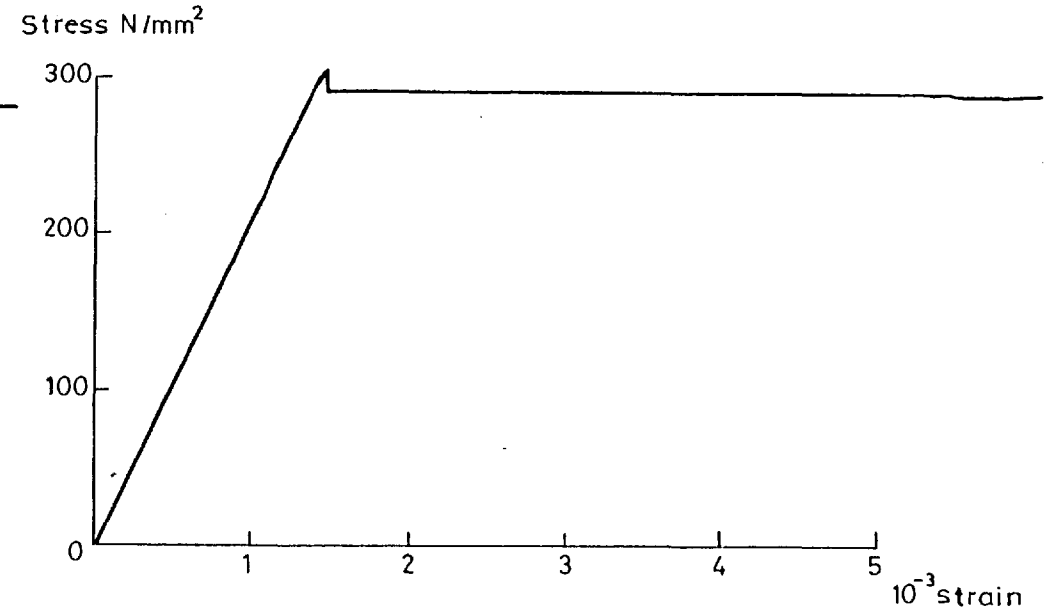

Fig 5·4 Webs & bottom flange

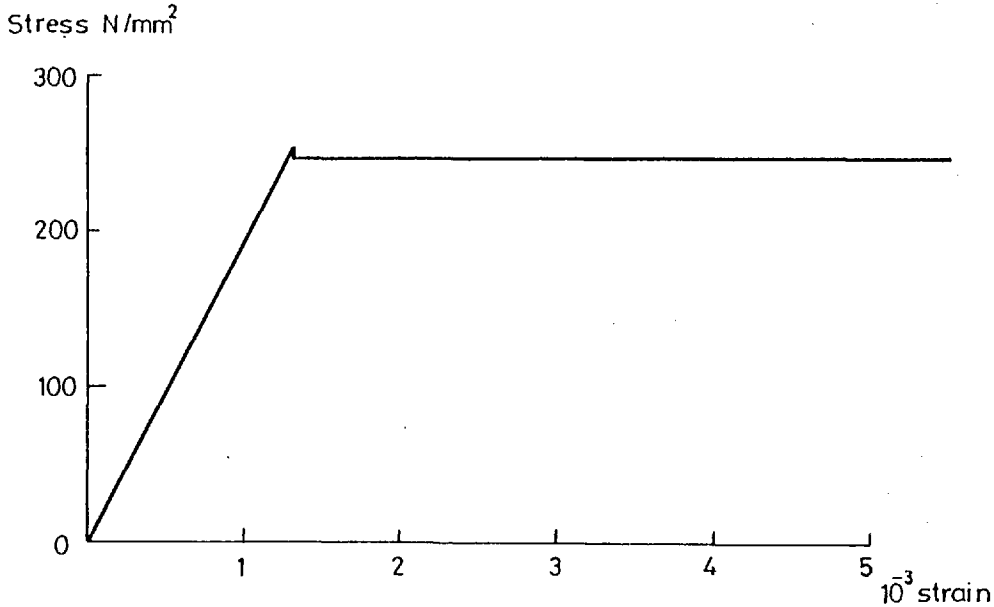

Fig 5·5 Stiffener

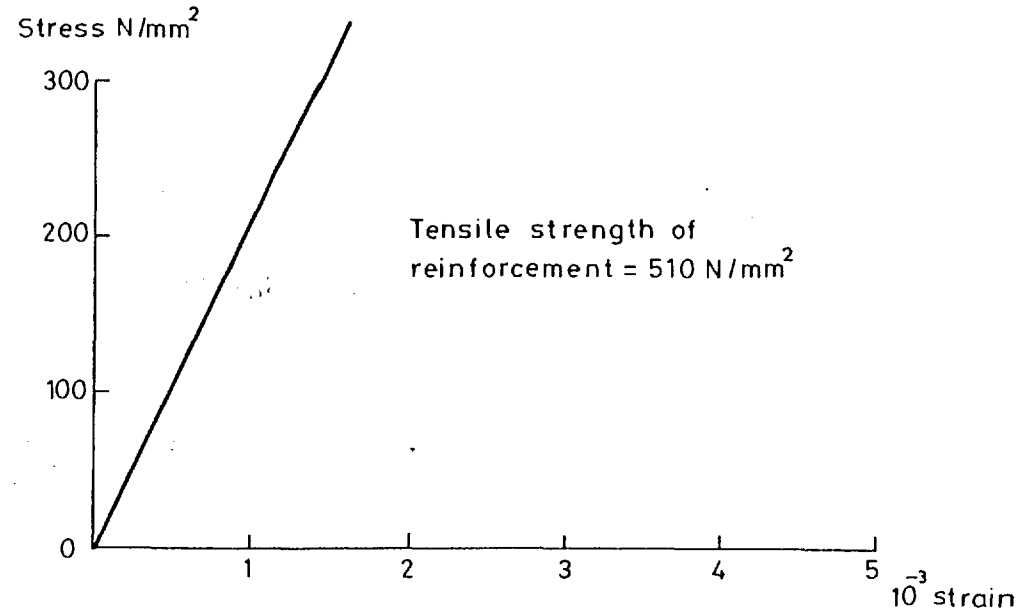

Fig 5·6 Reinforcing mesh

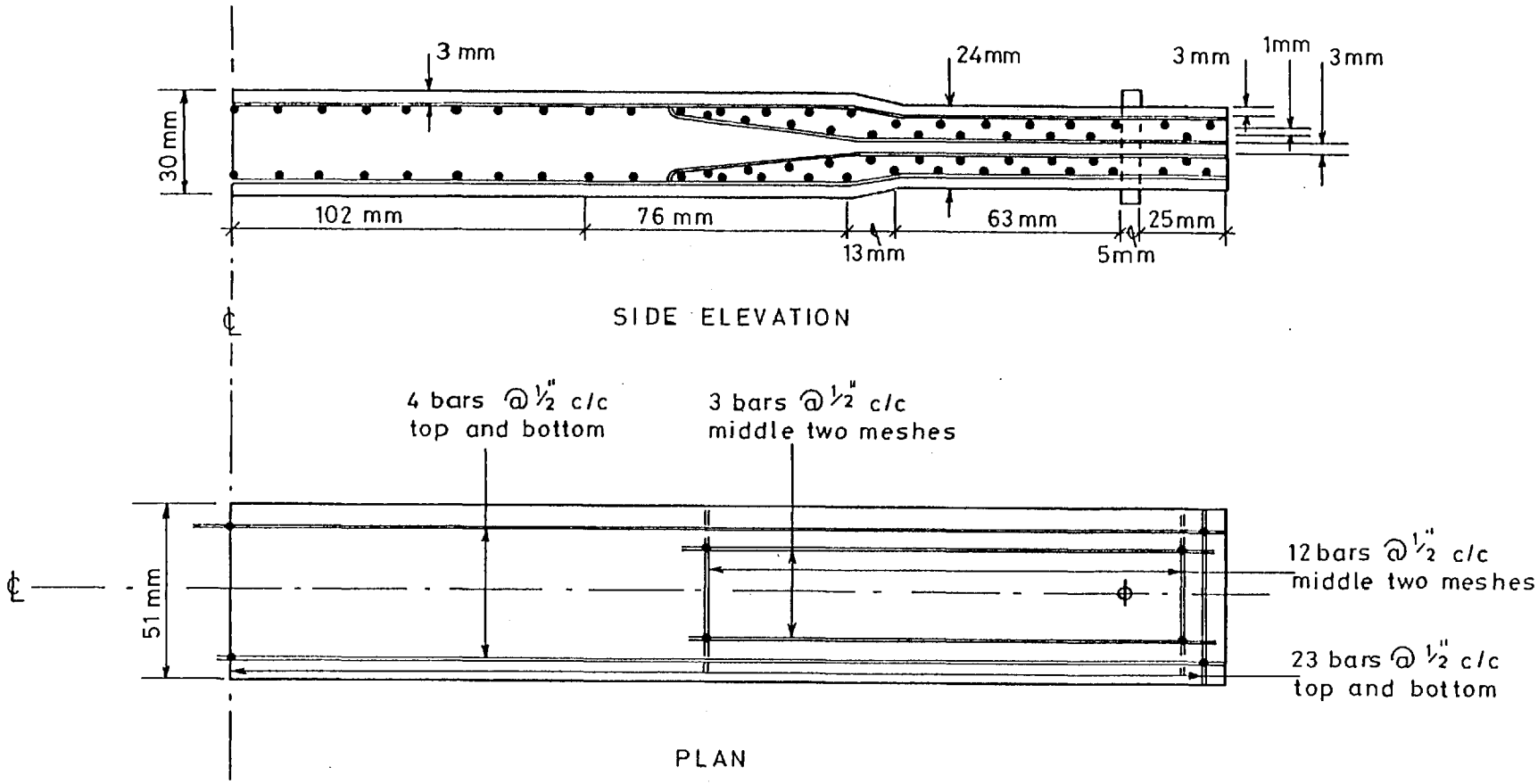

Fig 5·7 Details of concrete tensile specimens

Scale 1:2

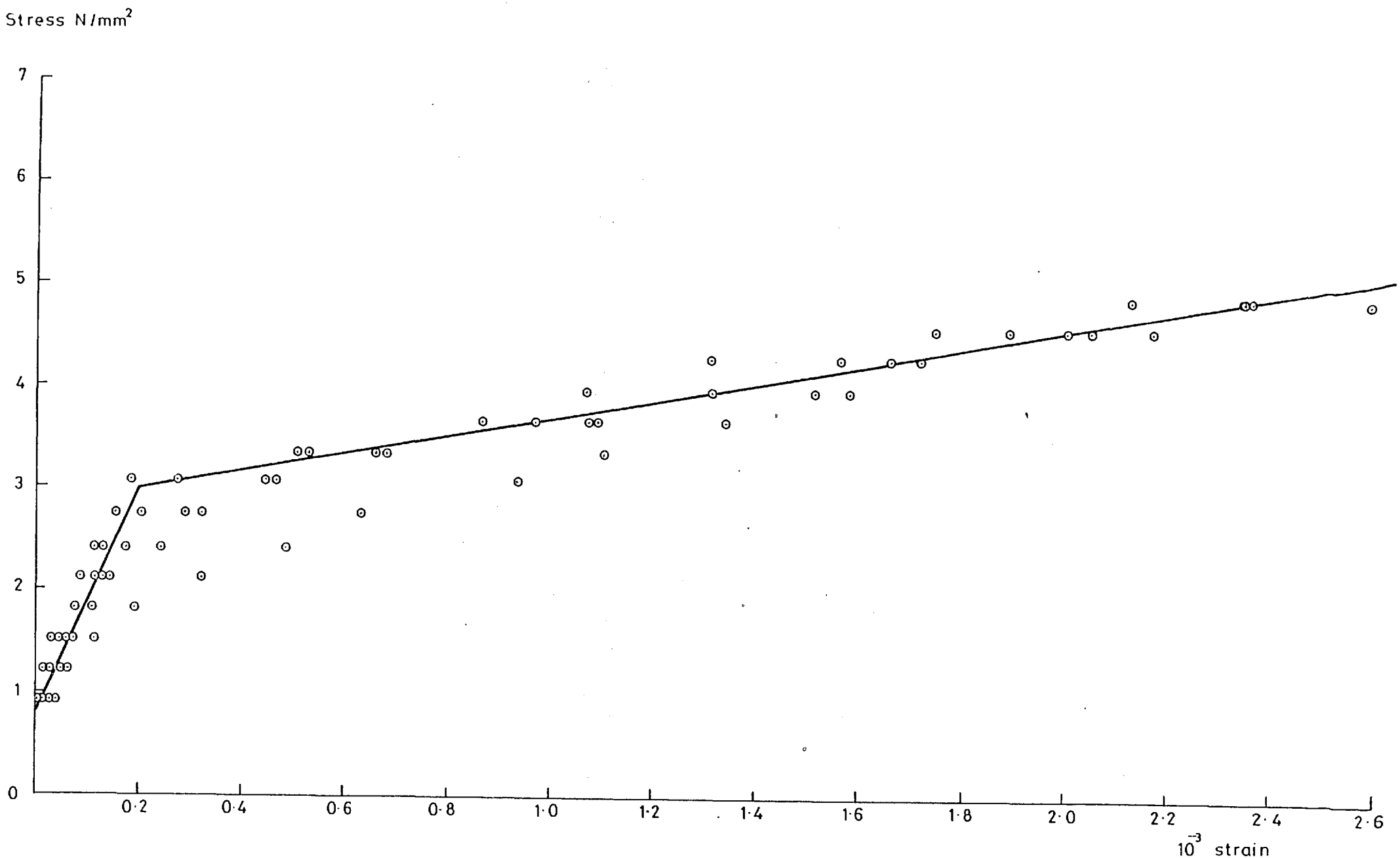

Fig 5·8 Concrete tensile test results

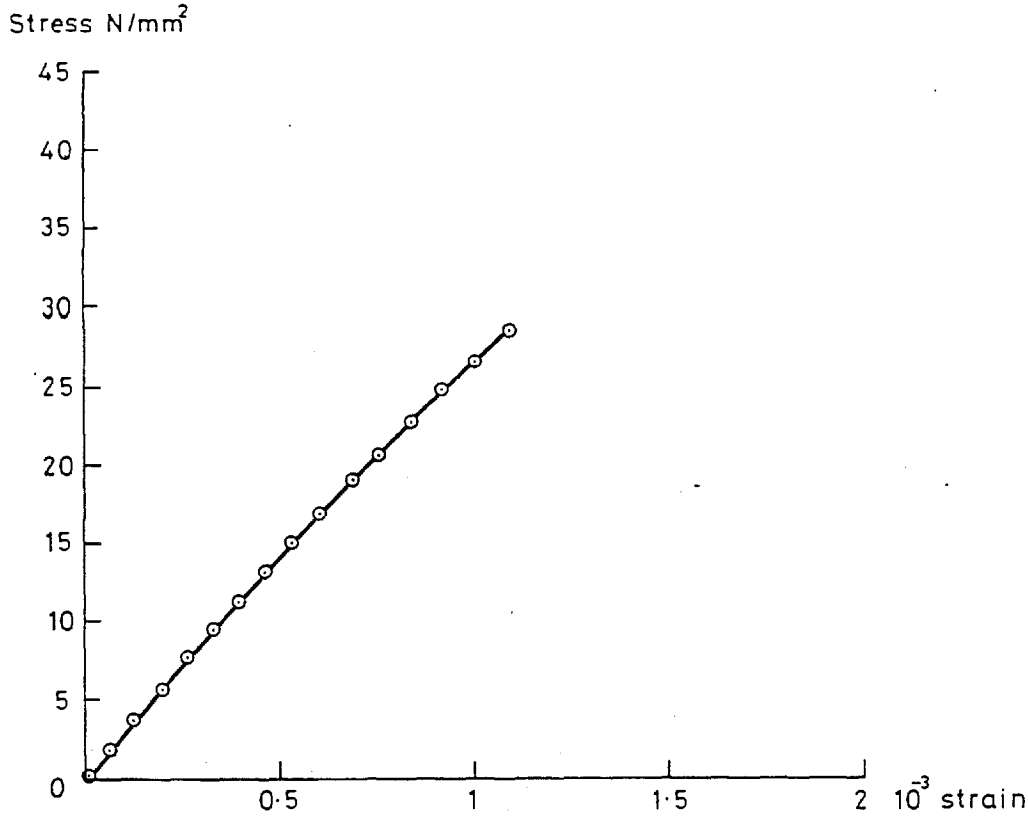

Fig 5·9 Concrete stress-strain curve (compression)

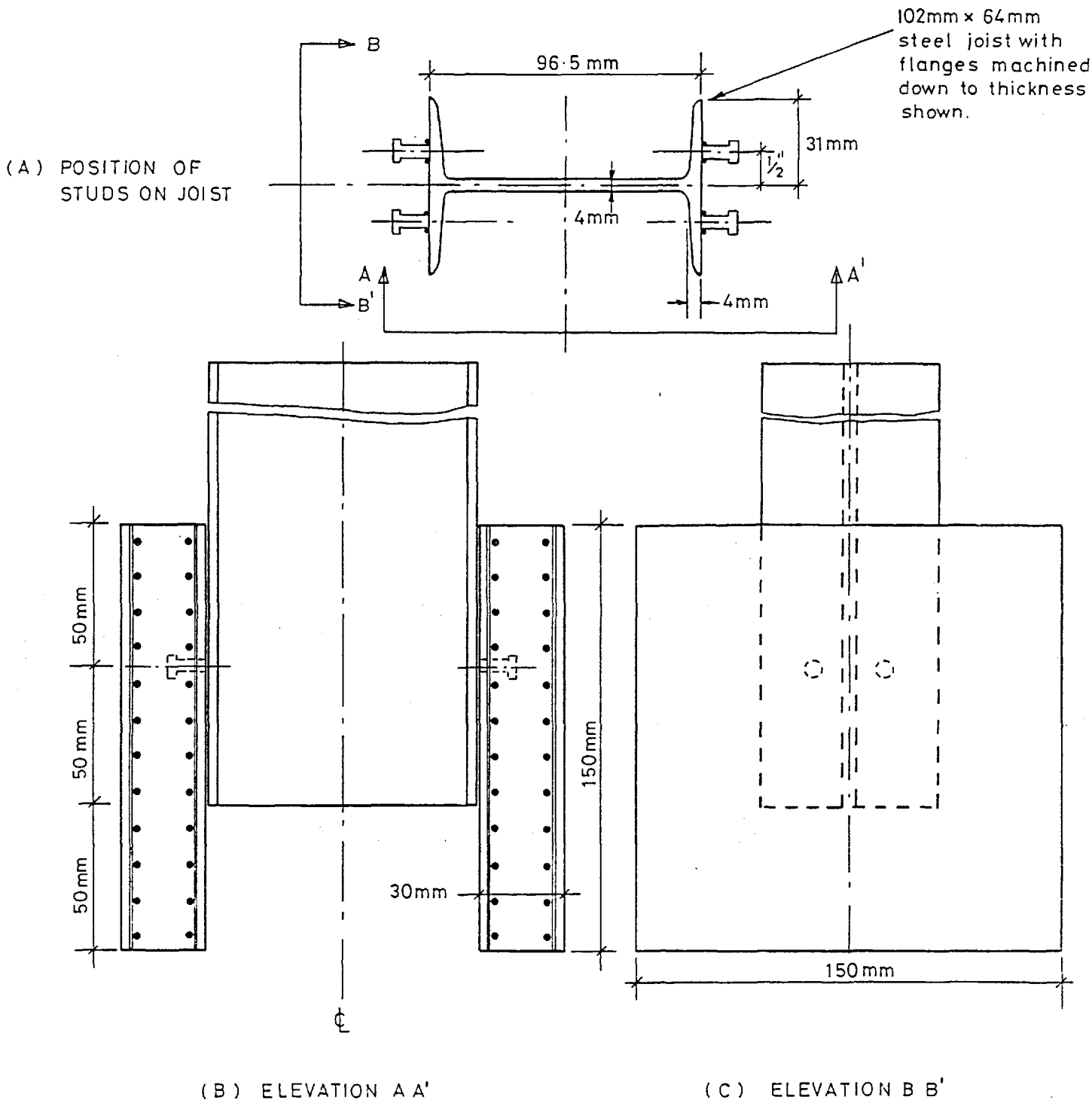

Fig 5·10 Push-out test specimen

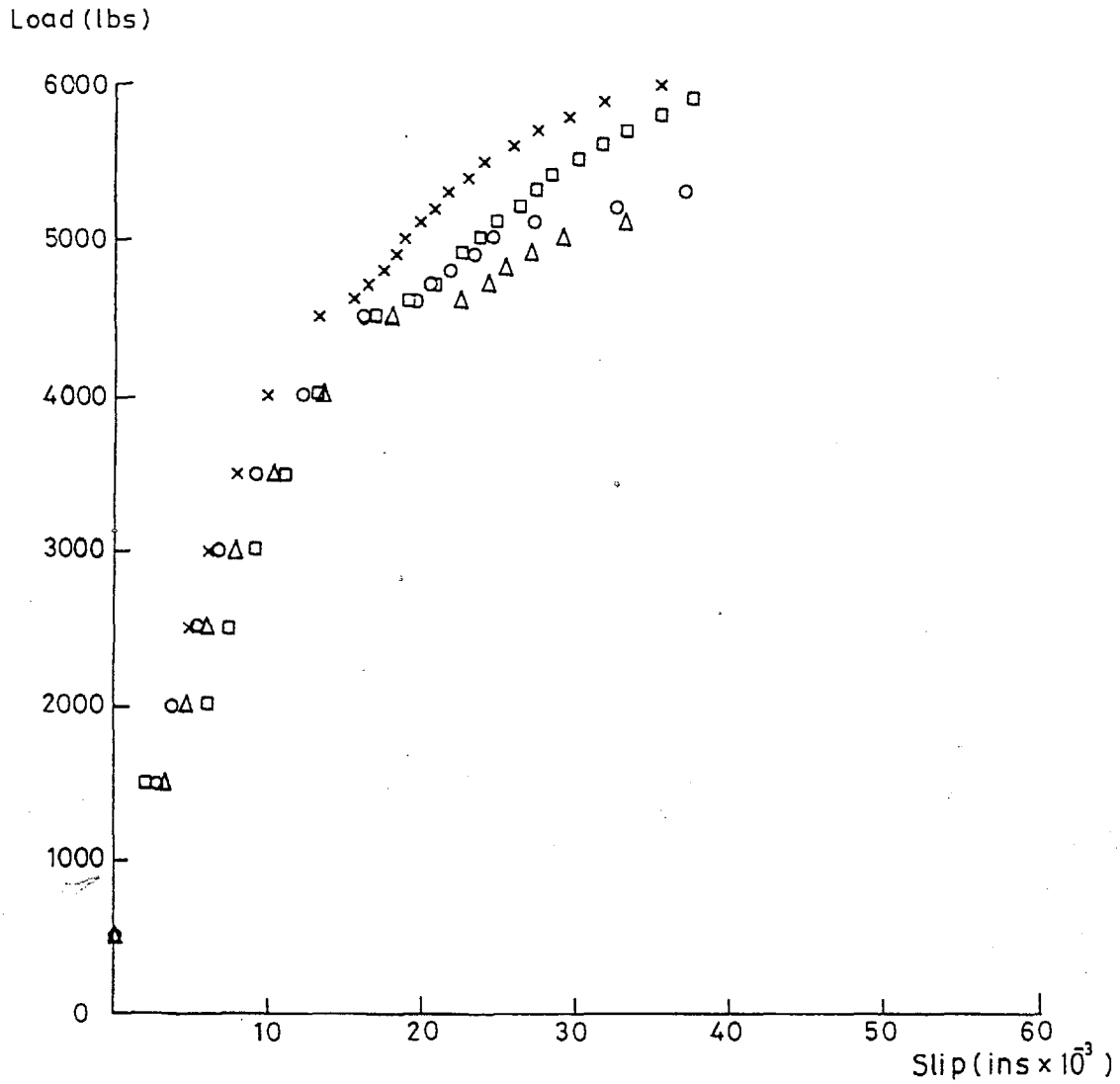

Fig 5·11 Pushout test results

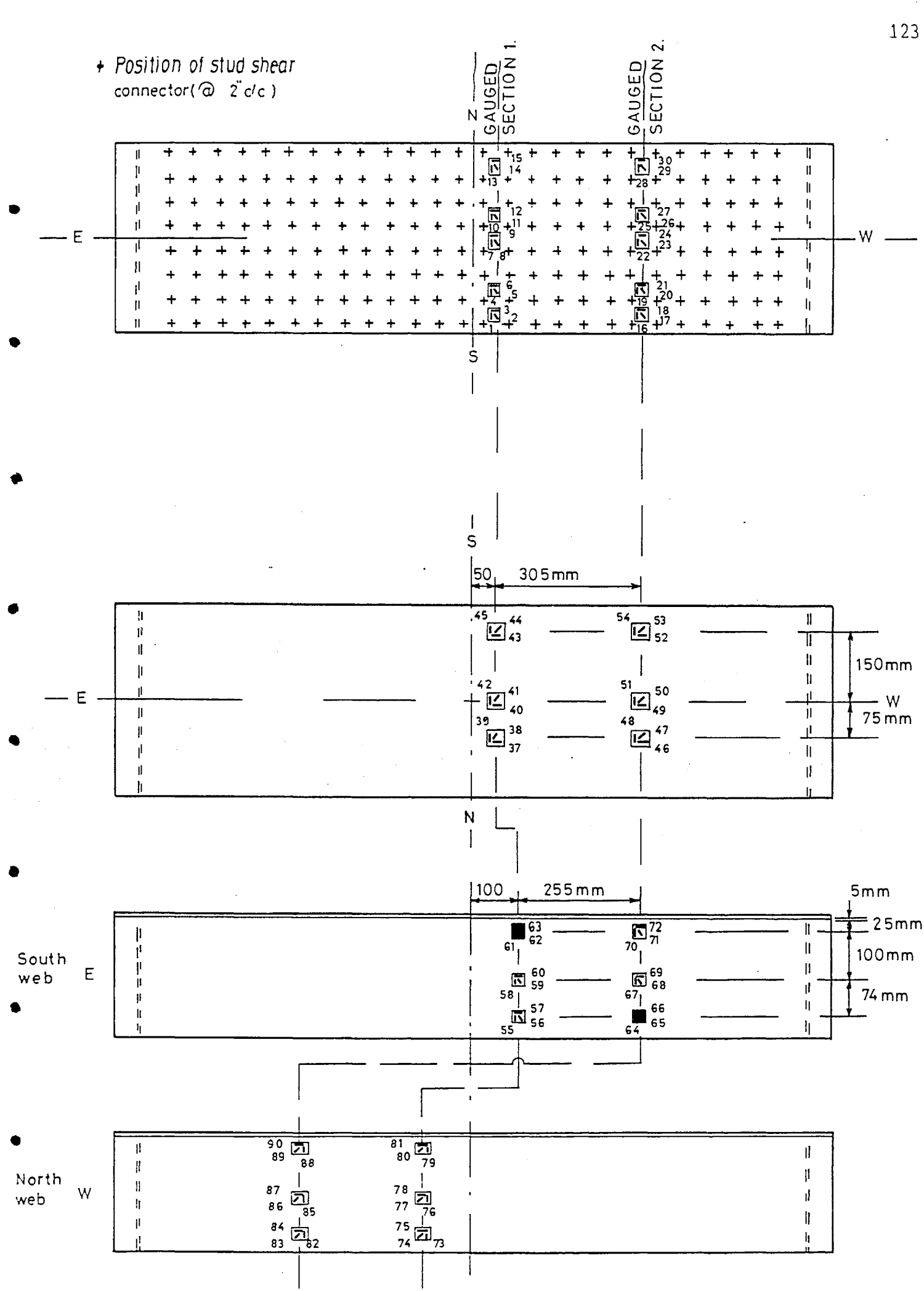

Fig 5·12 Closed box strain gauge positions

Scale 1:10

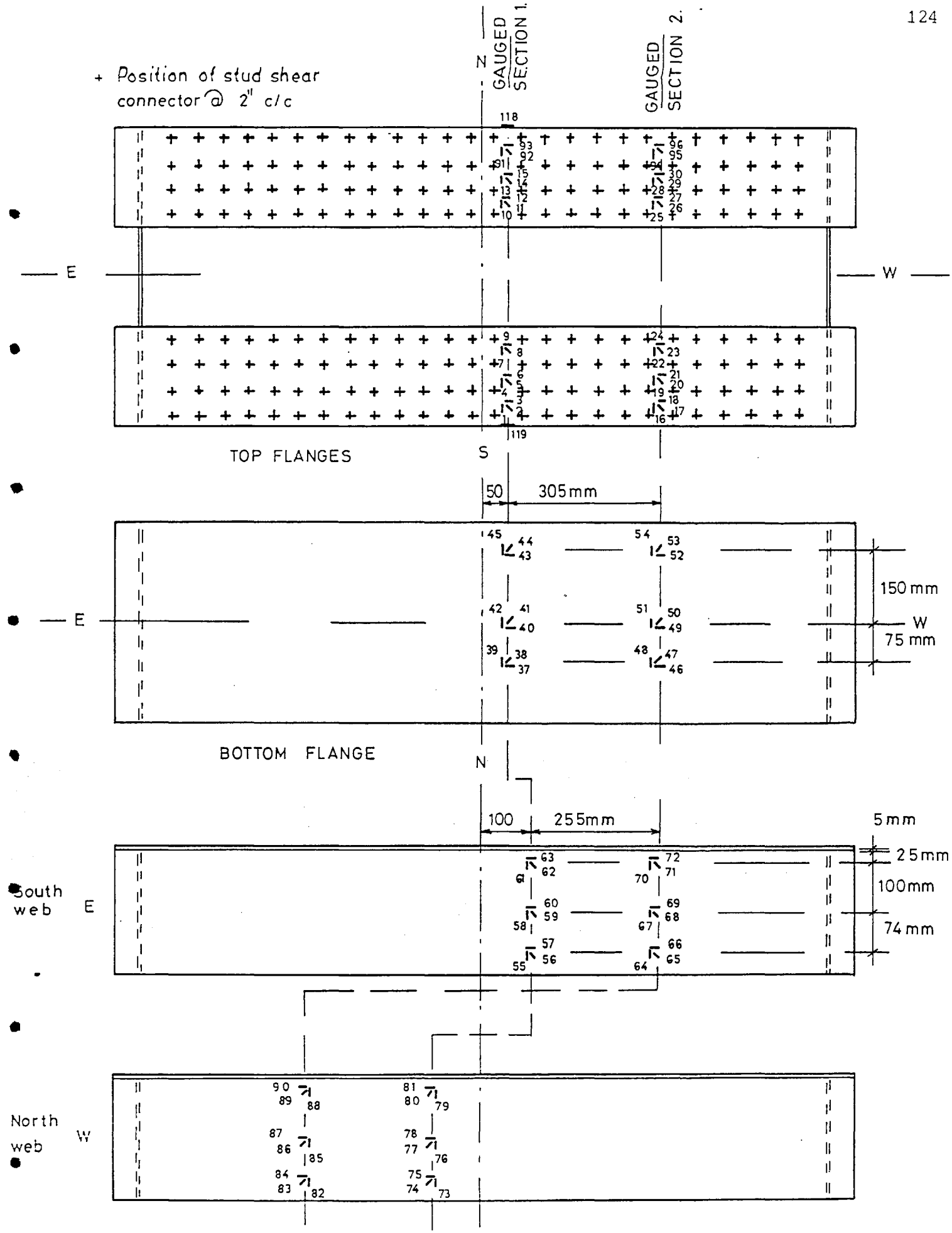

Fig 5·12a. Open box strain gauge positions

Scale 1:10

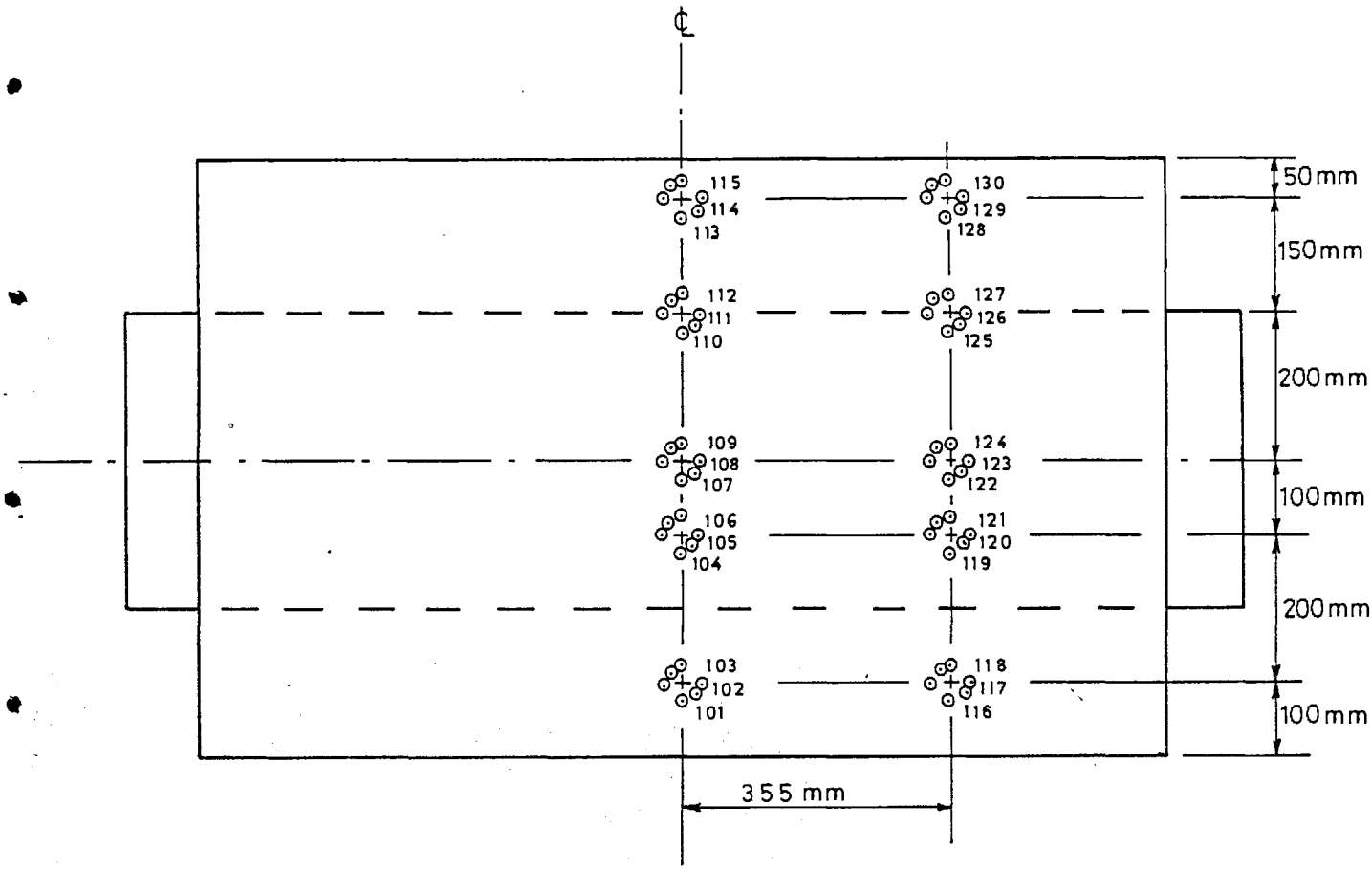

⊙ Demec gauge point (2"gauge length)

Fig 5·13 Strain gauges on concrete

Scale 1:10

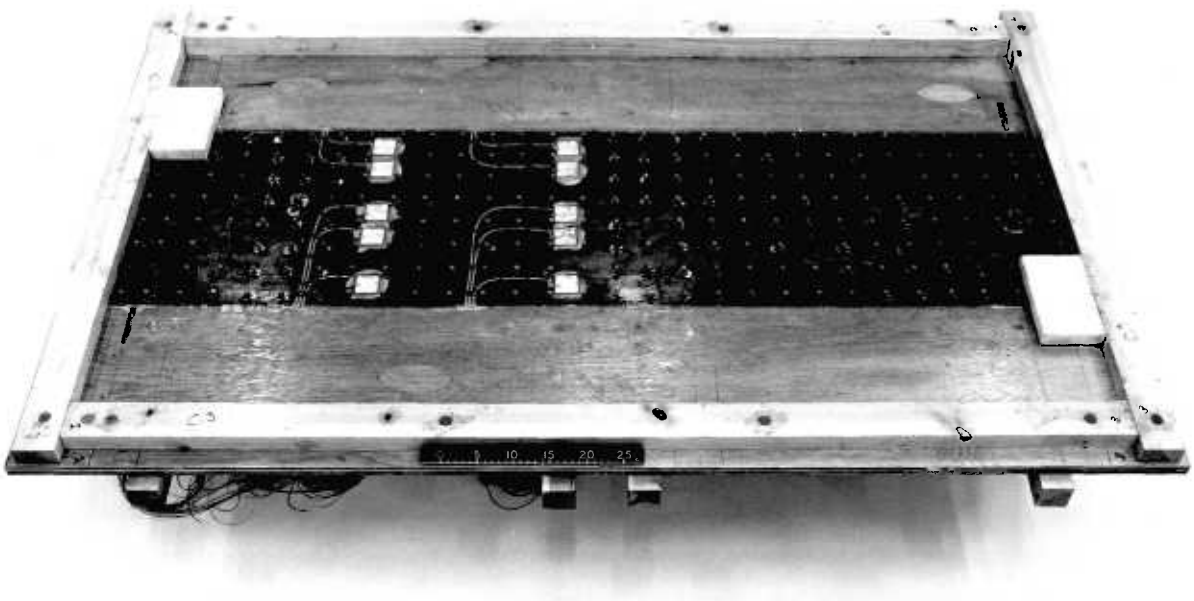

Fig 5.14 Formwork for closed box model

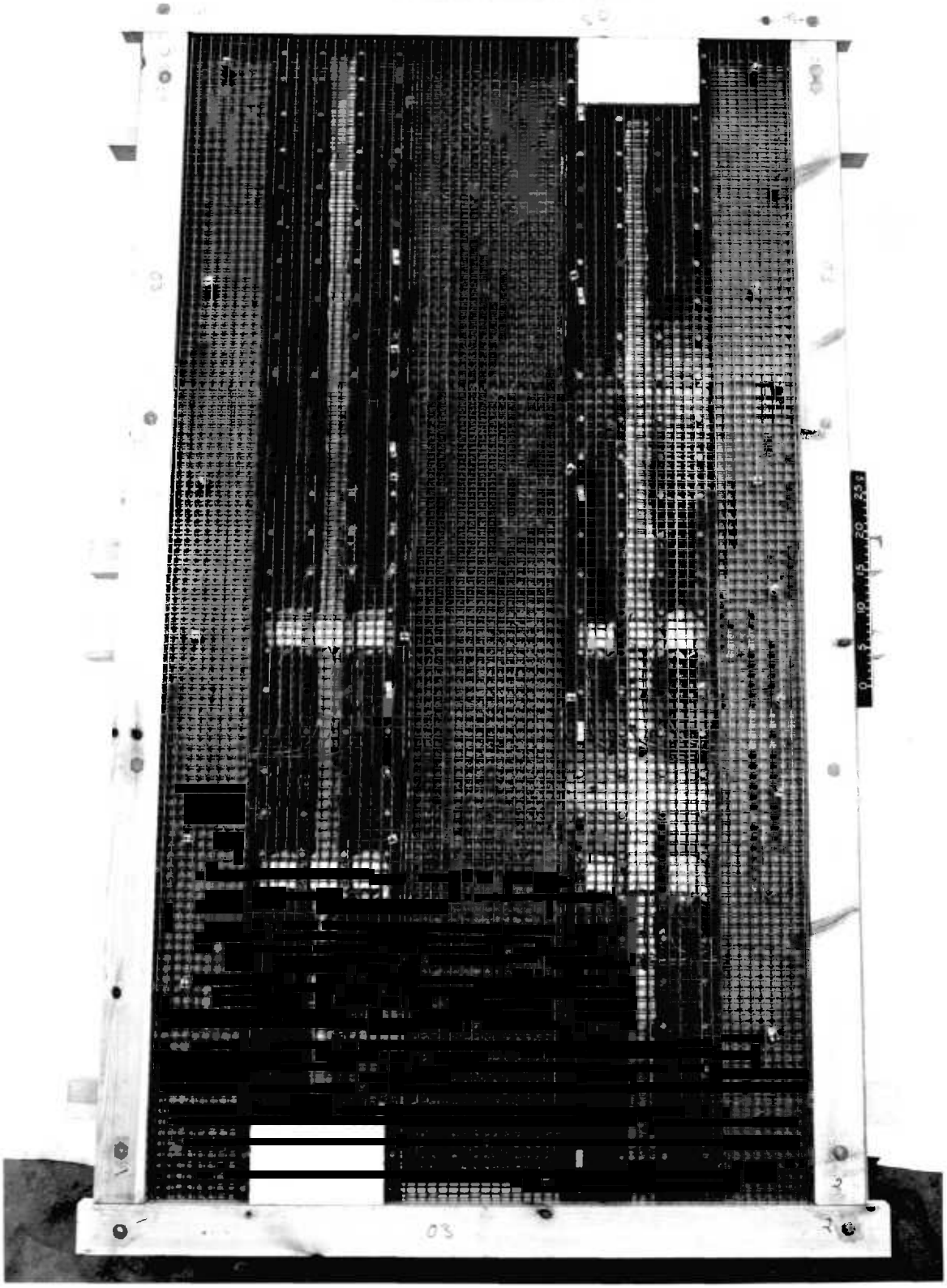

Fig 5.15 Formwork and reinforcement for open box model

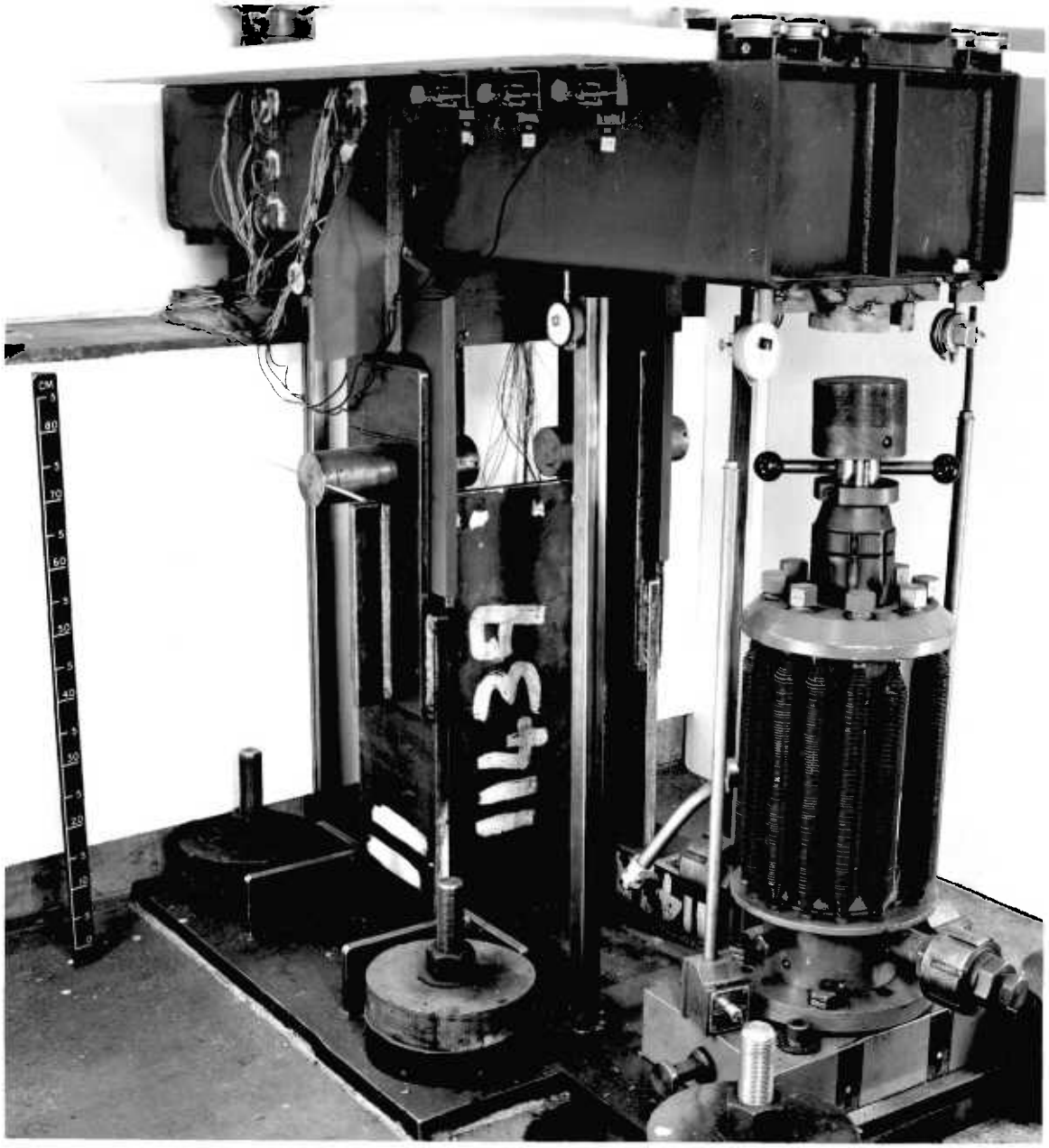

Fig 5.16 Photograph of central support rig

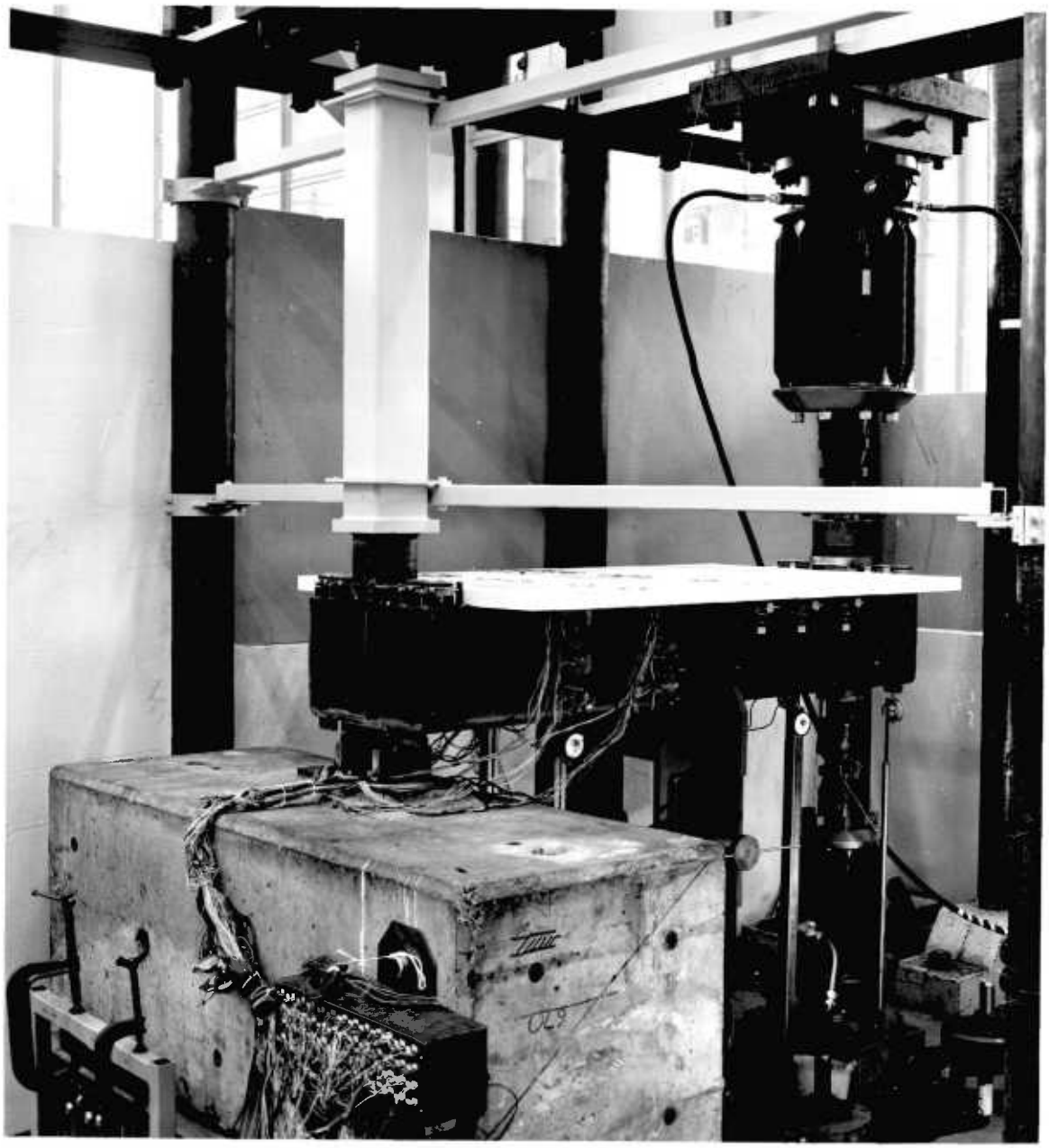

Fig 5.17 Loading arrangement for ultimate load test

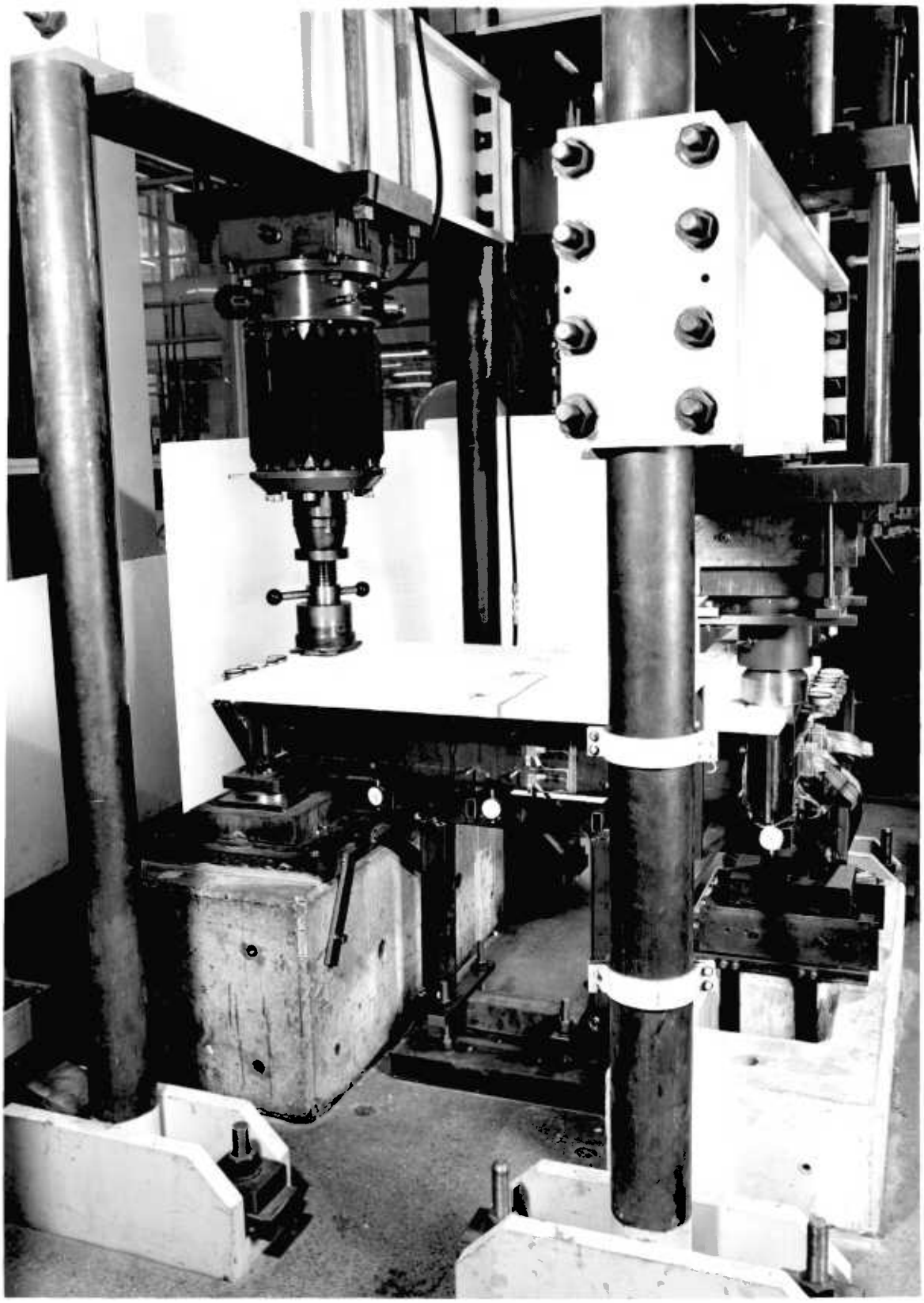

Fig 5.18 General view of torsion rig

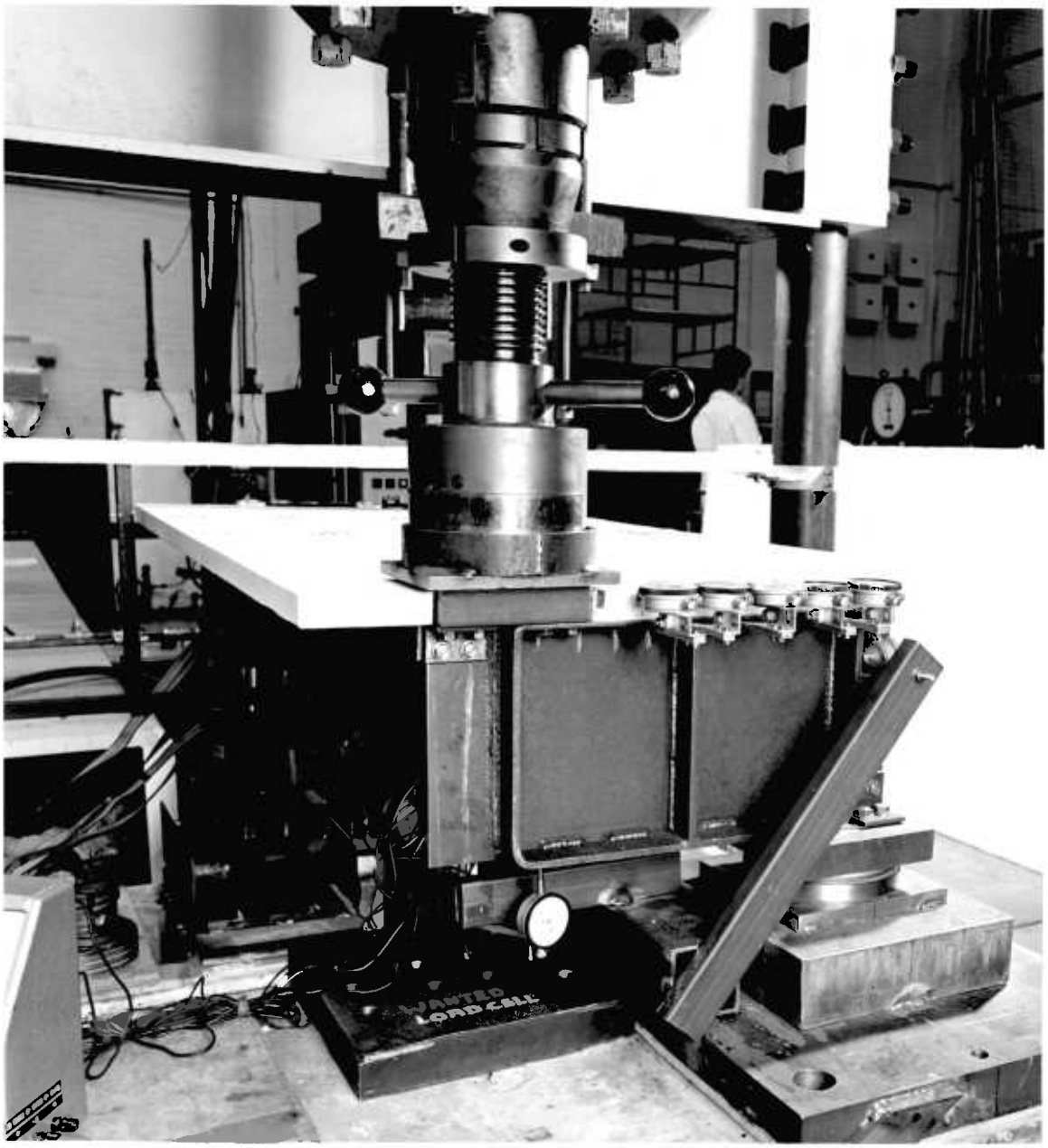

Fig 5.19 Loaded end of model C3

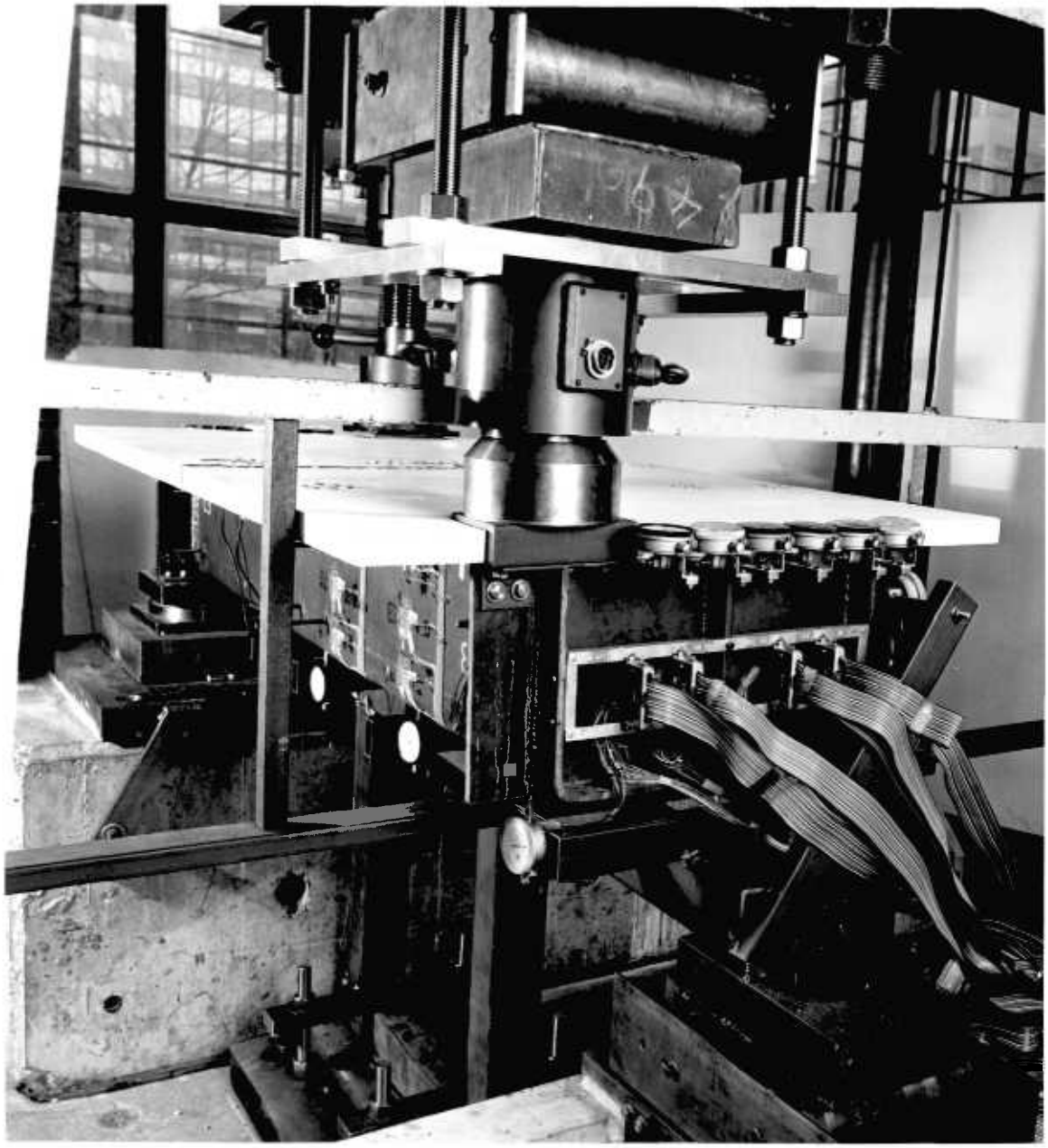

Fig 5.20 Supported end of model C3

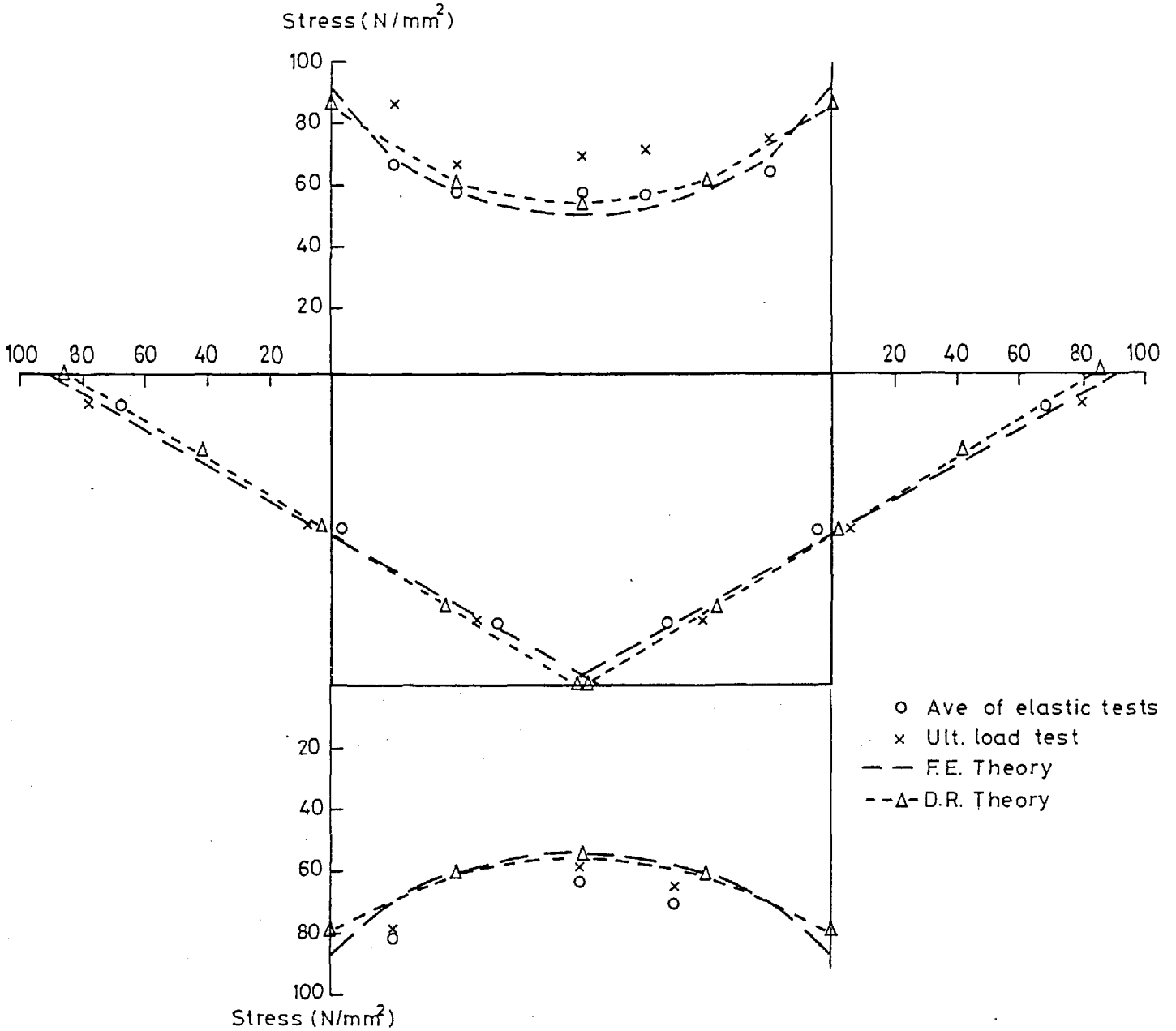

Fig 5·21 Test C1 Longitudinal stress distribution at gauged section 1 for 10 ton end load

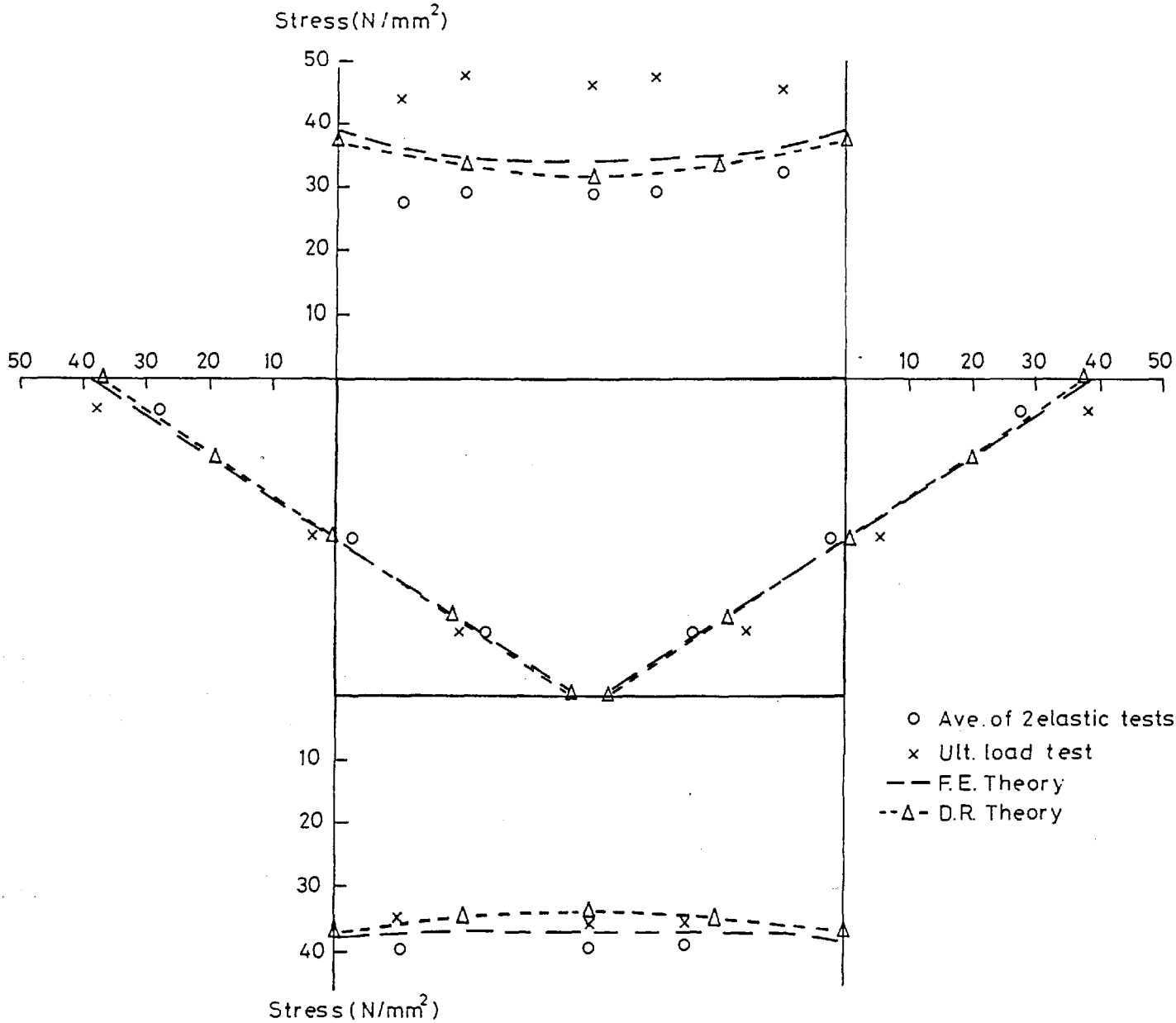

Fig 5·22 Test C1 Longitudinal stress distribution at gauged section 2 for 10 ton end load

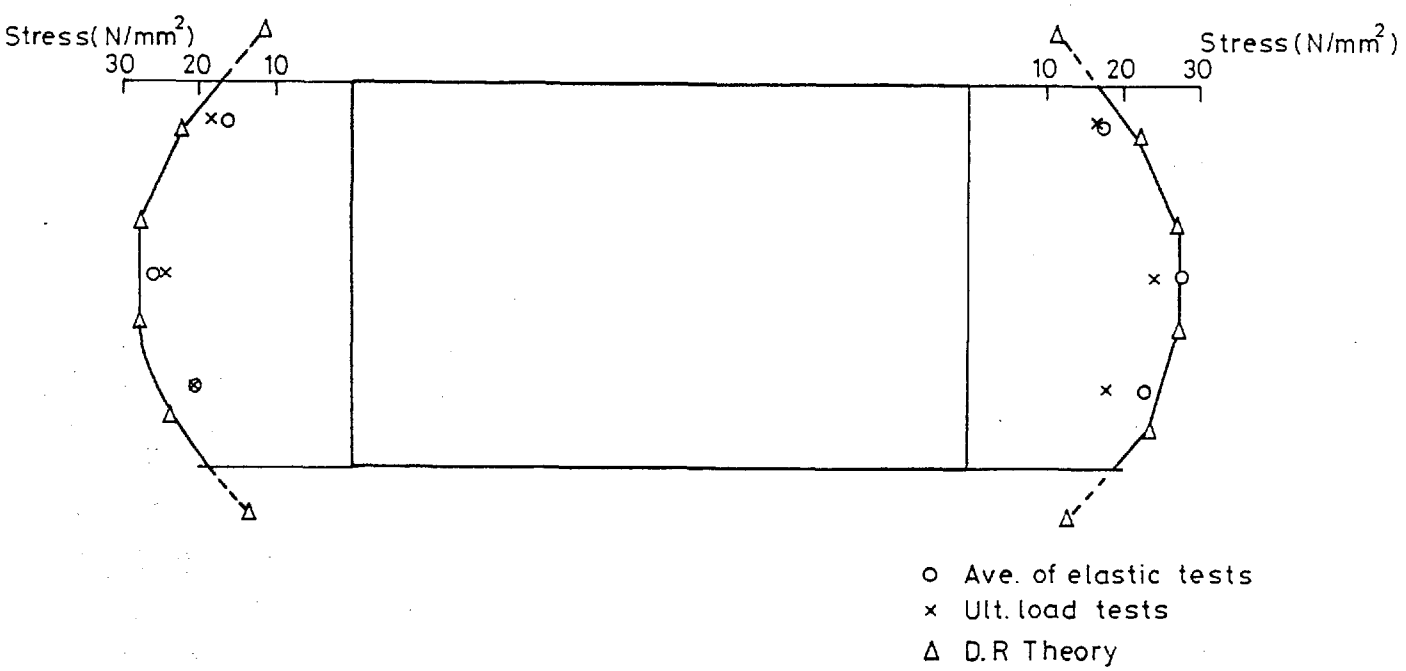

Fig 5·23 Test C1 Shear stress distribution at gauge section 1 for 10 ton end load

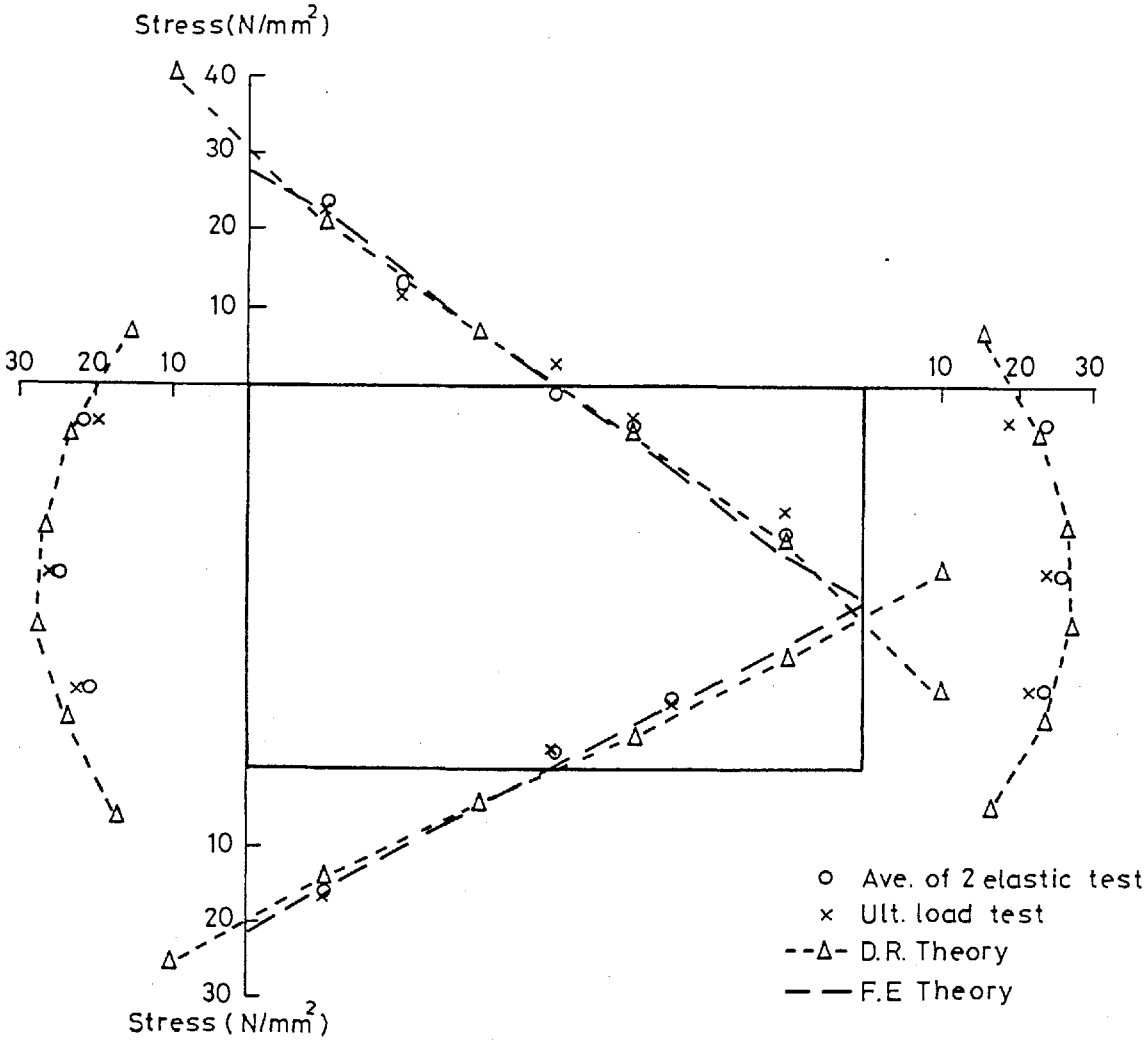

Fig 5·24 Test C1 Shear stress distribution at gauged section 2 for 10 ton end load

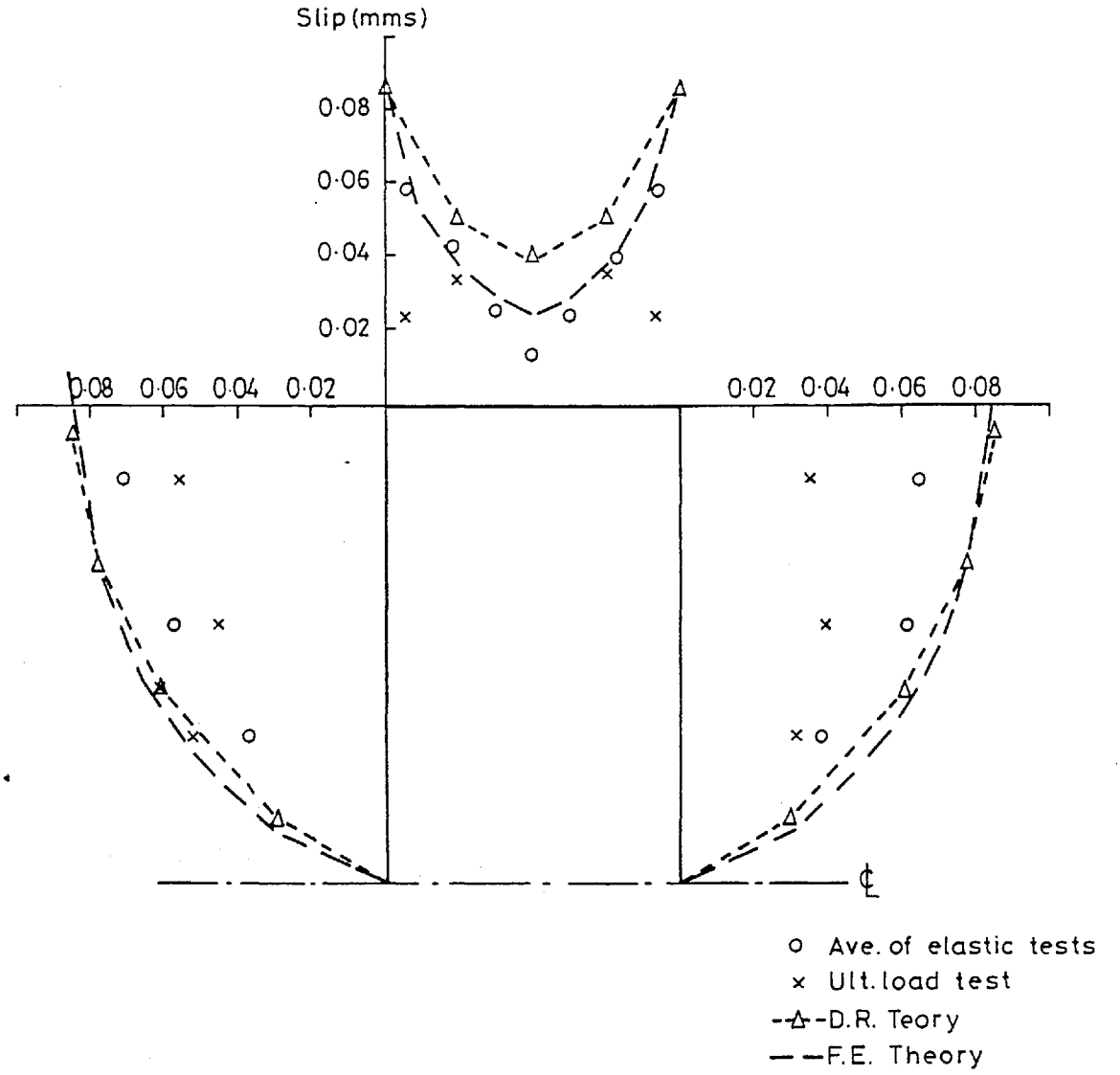

Fig 5·25 Test C1 Distribution of longitudinal slip for 10 ton end load.

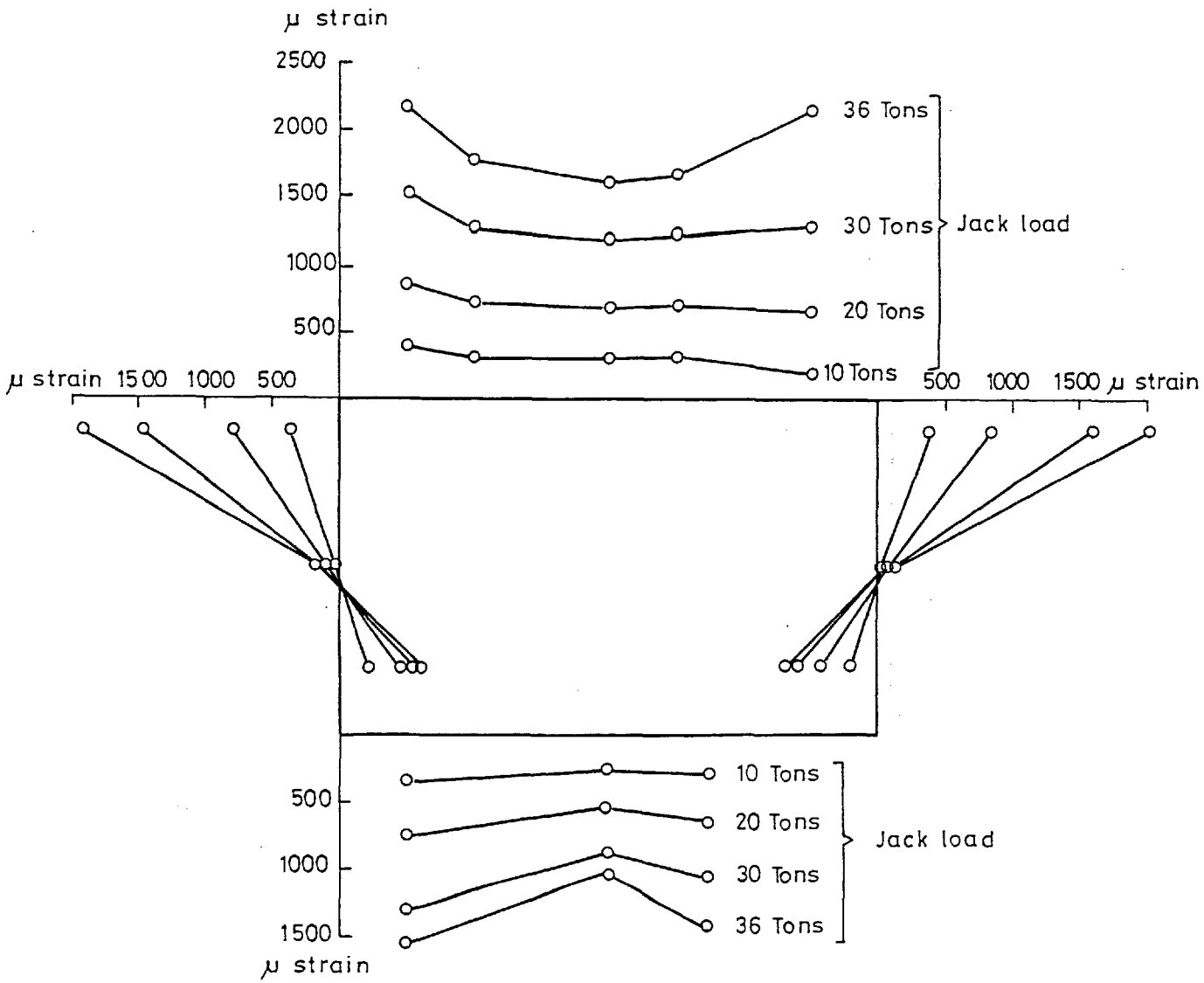

Fig 5·26 Test C1 Longitudinal strain distribution at gauged section 1 for various applied loads

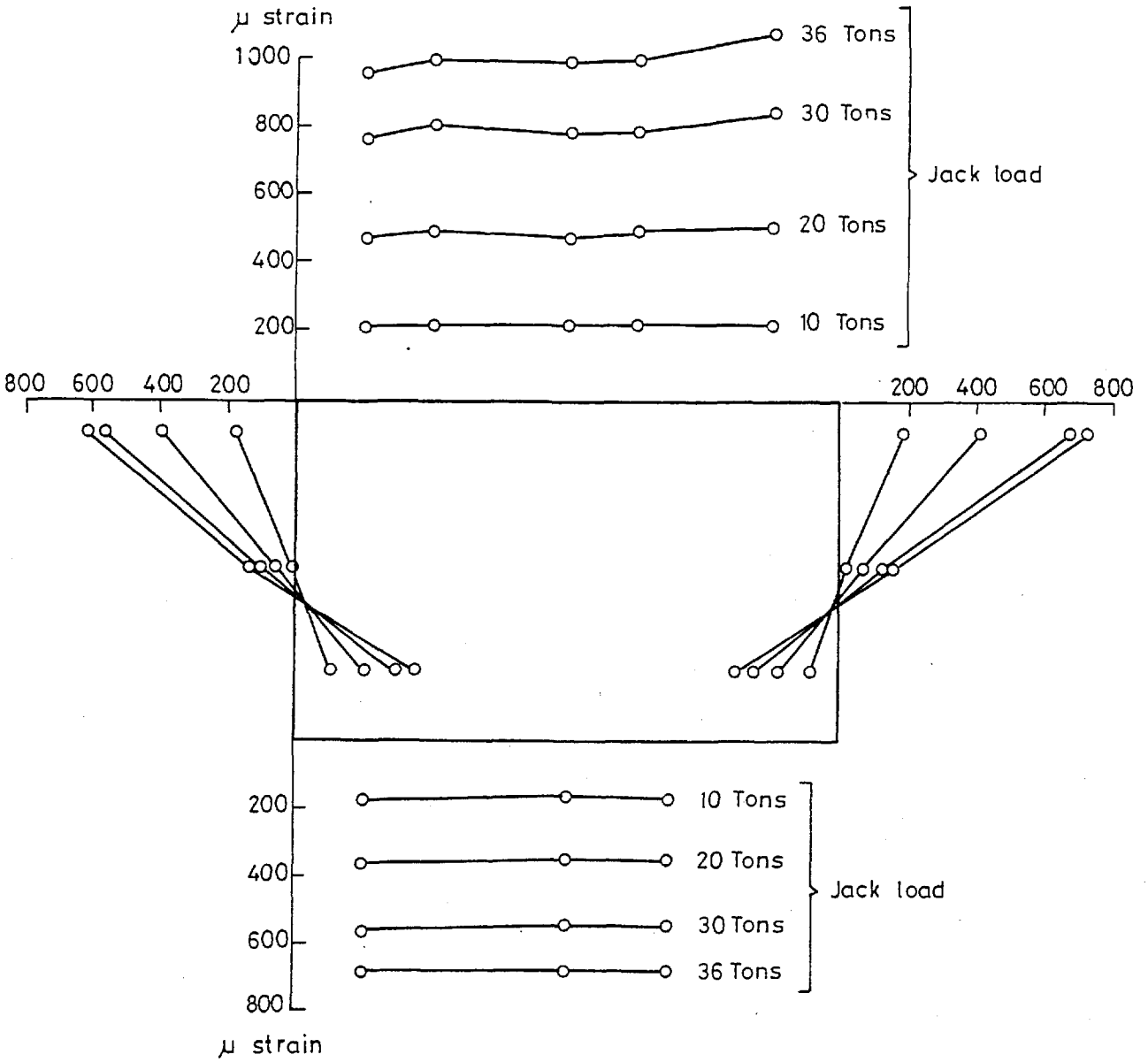

Fig 5·27 Test C1 Longitudinal strain distribution at gauged section 2 for various applied loads

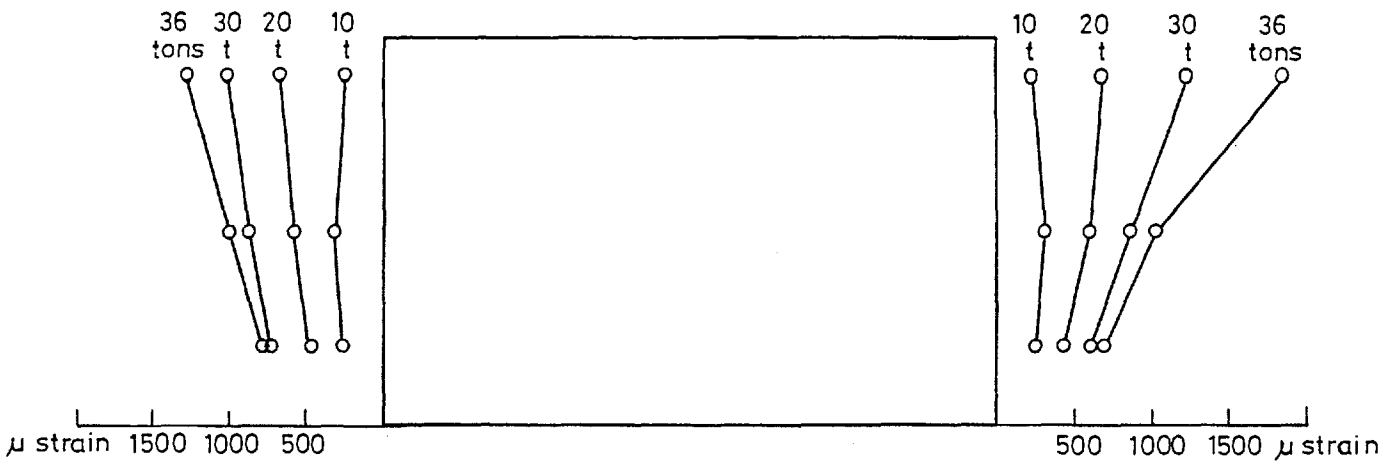

Fig 5·28 Test C1 Shear strain distribution at gauged section 1 for various applied loads

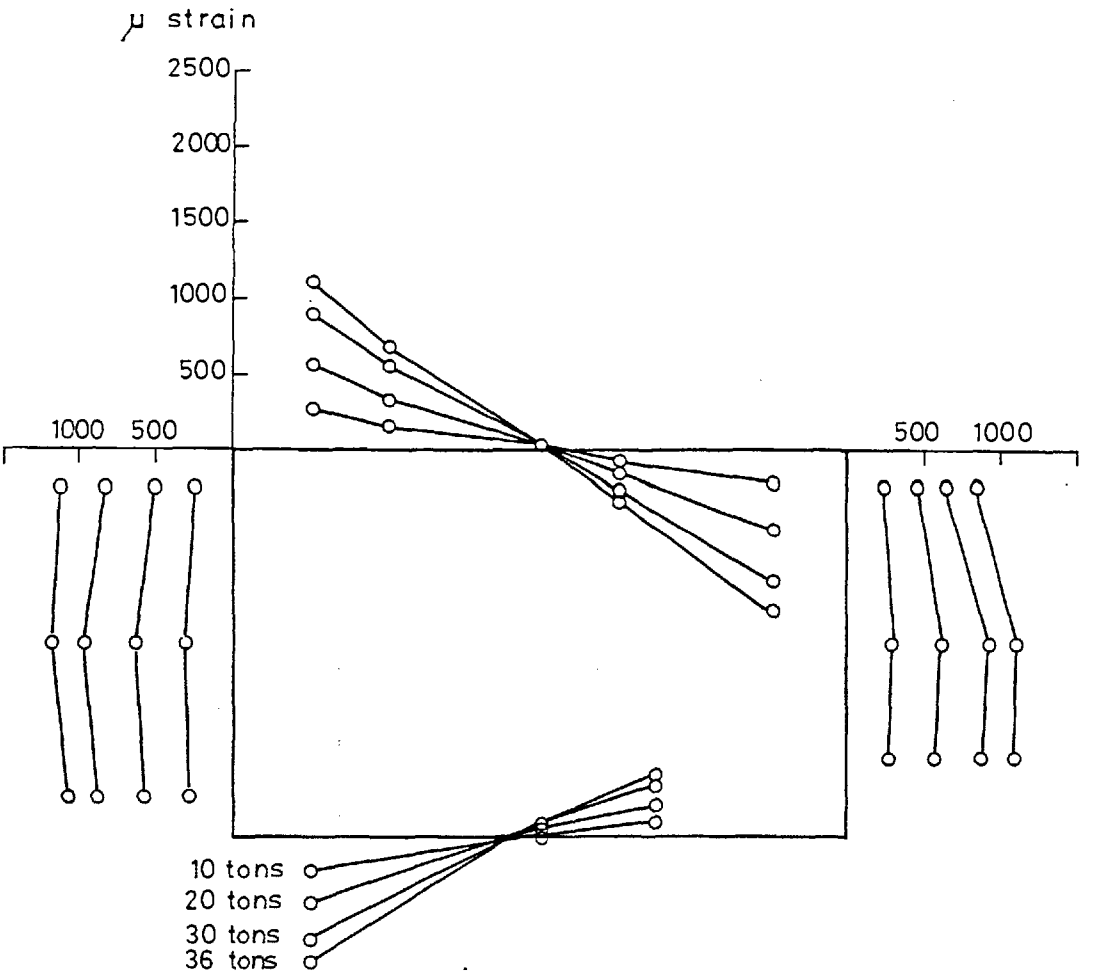

Fig 5·29 Test C1 Shear strain distribution at gauged section 2 for various applied loads

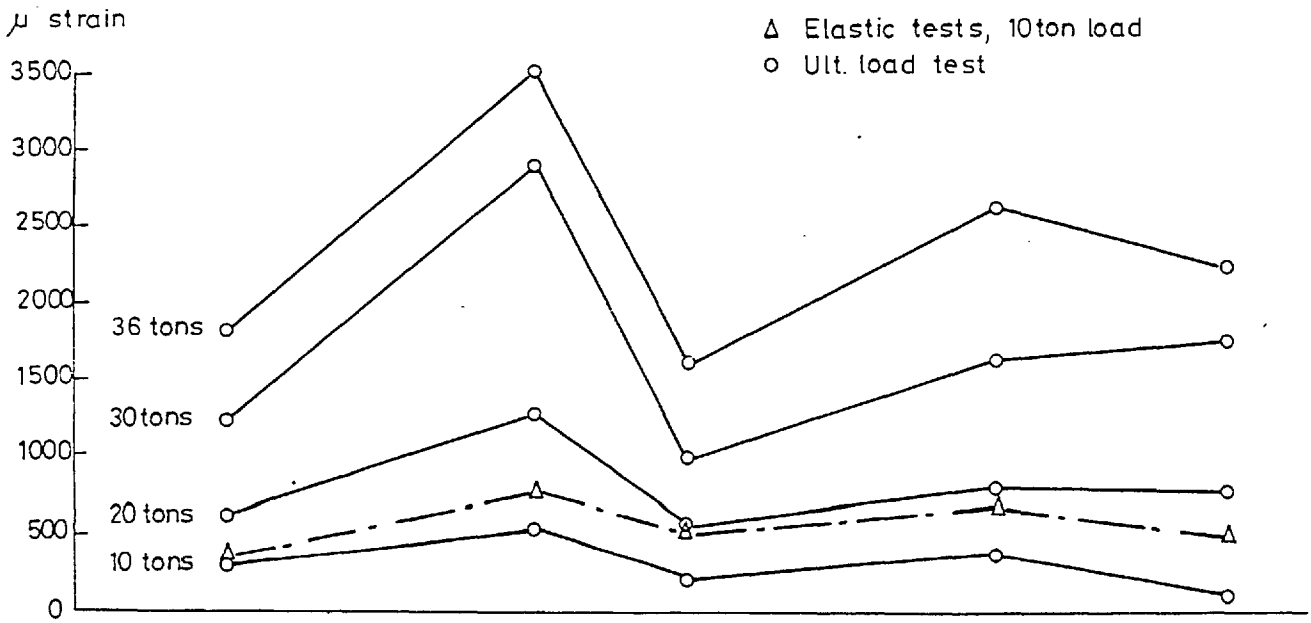

Fig 5·30 Test C1 Longitudinal slab strains at gauged section 1 for various loads

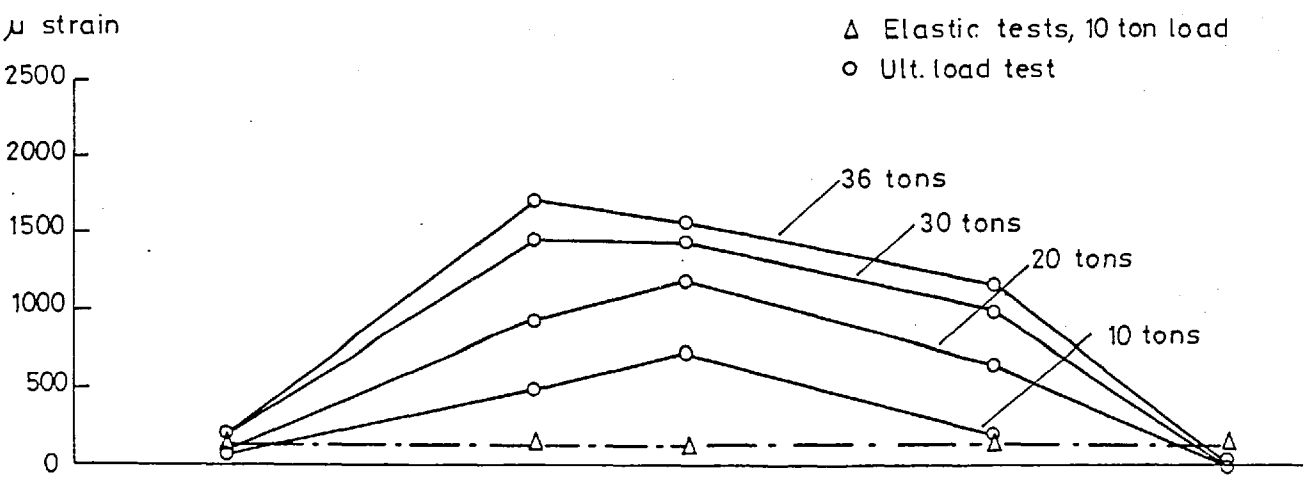

Fig 5·31 Test C1 Longitudinal slab strains at gauged section 2 for various loads

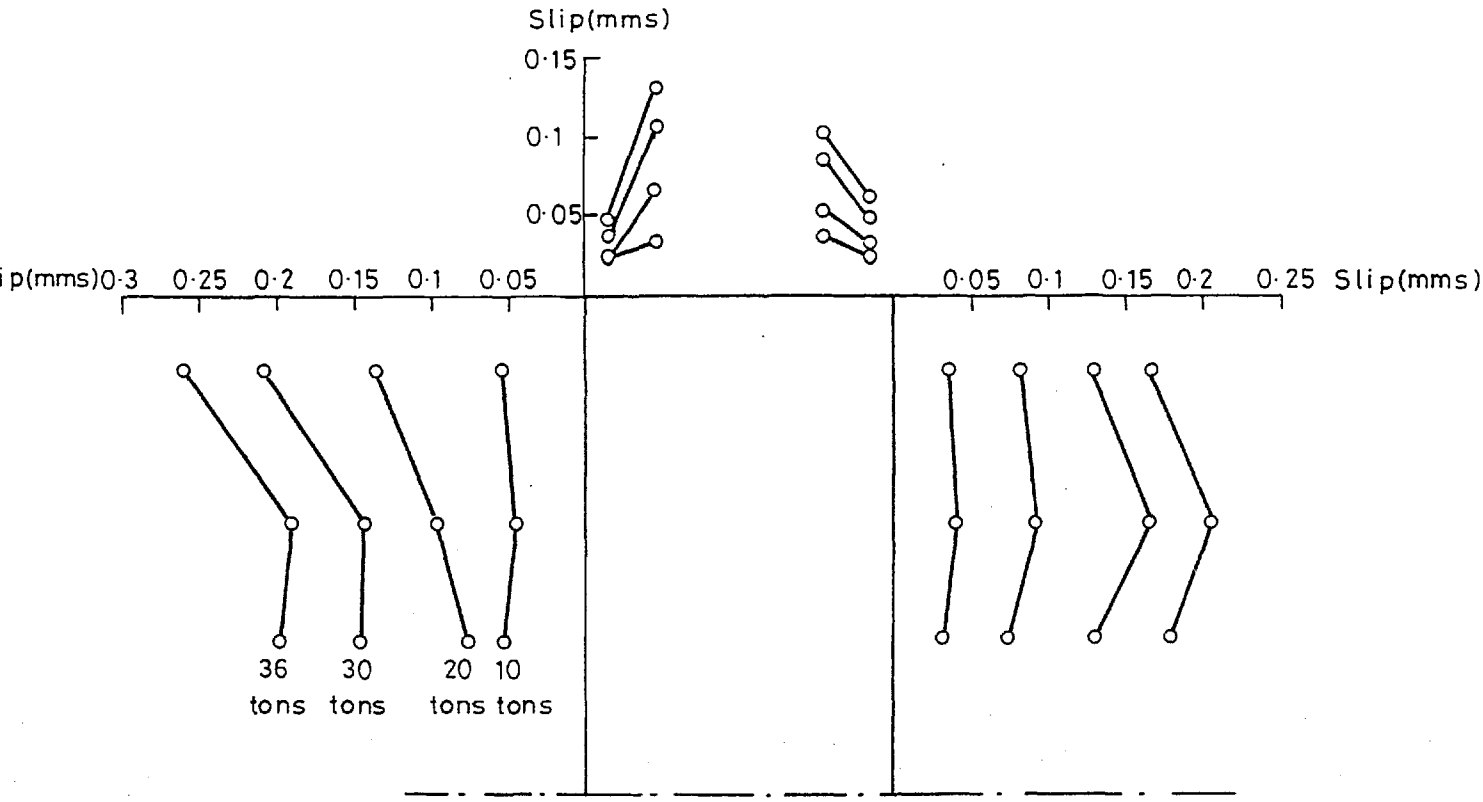

Fig 5·32 Test C1 Longitudinal slip distribution for various applied loads

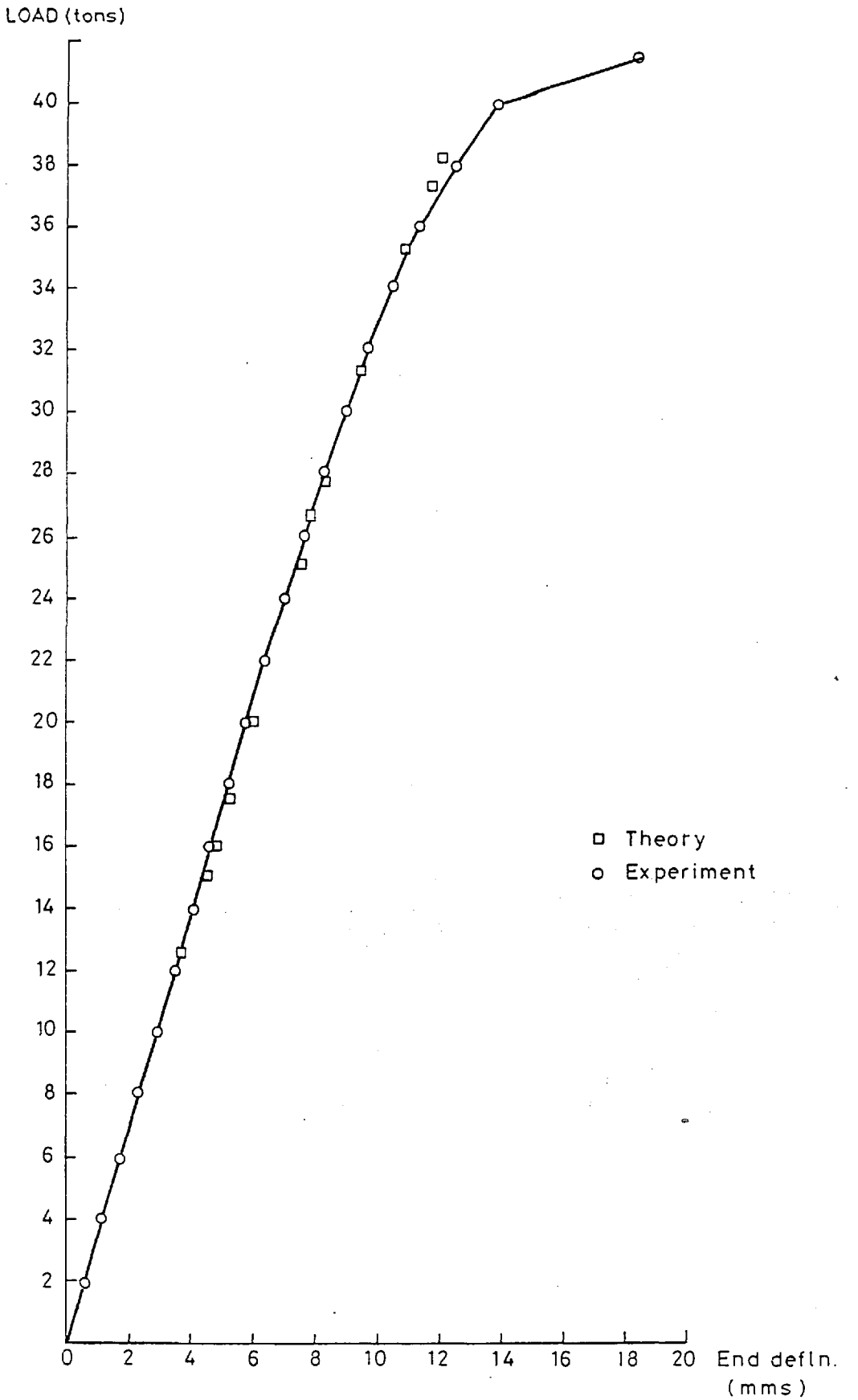

Fig 5·33 Test C1 Load - end deflection curve

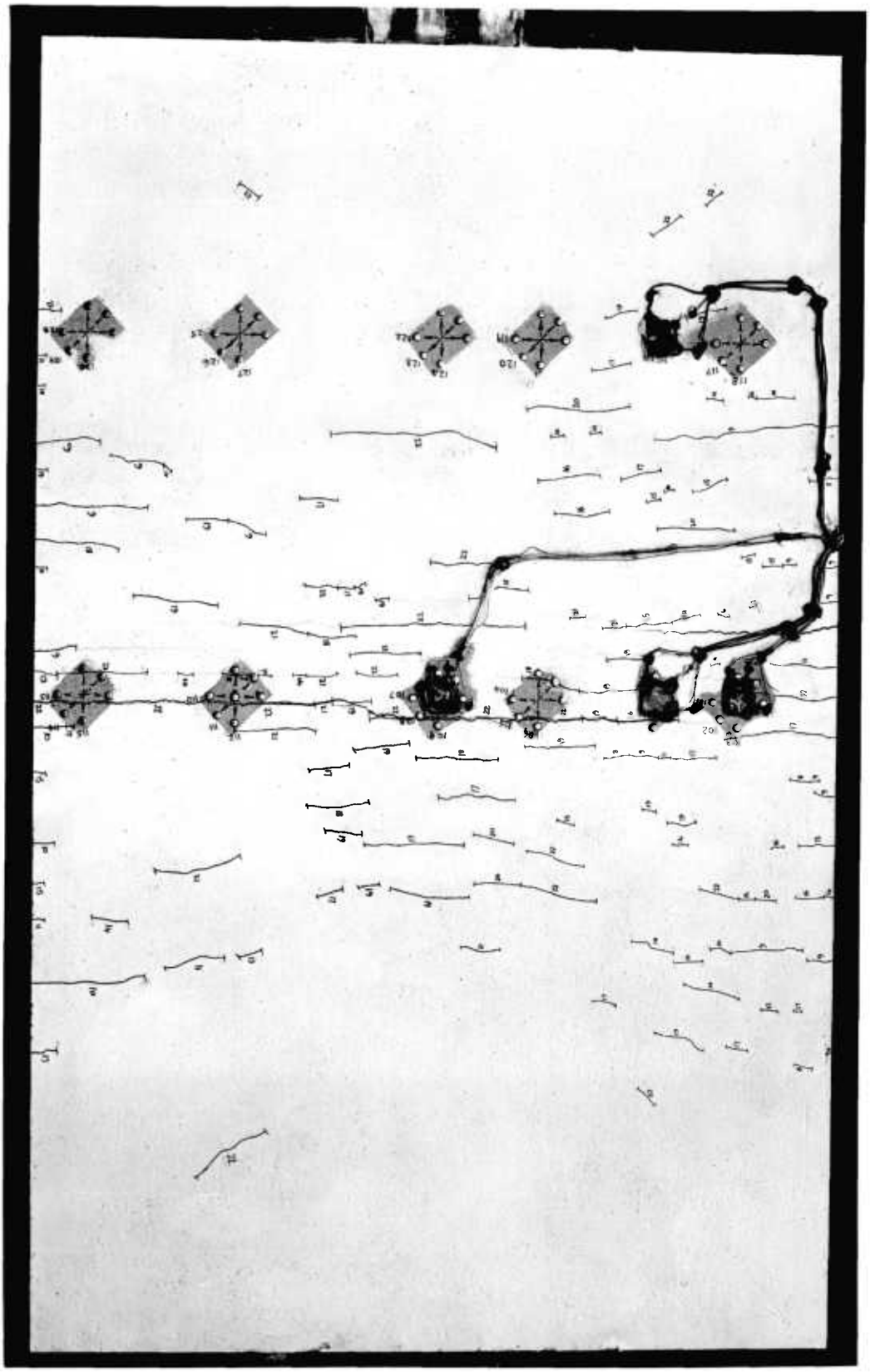

Fig 5.34 Test C1, photograph of cracked slab.

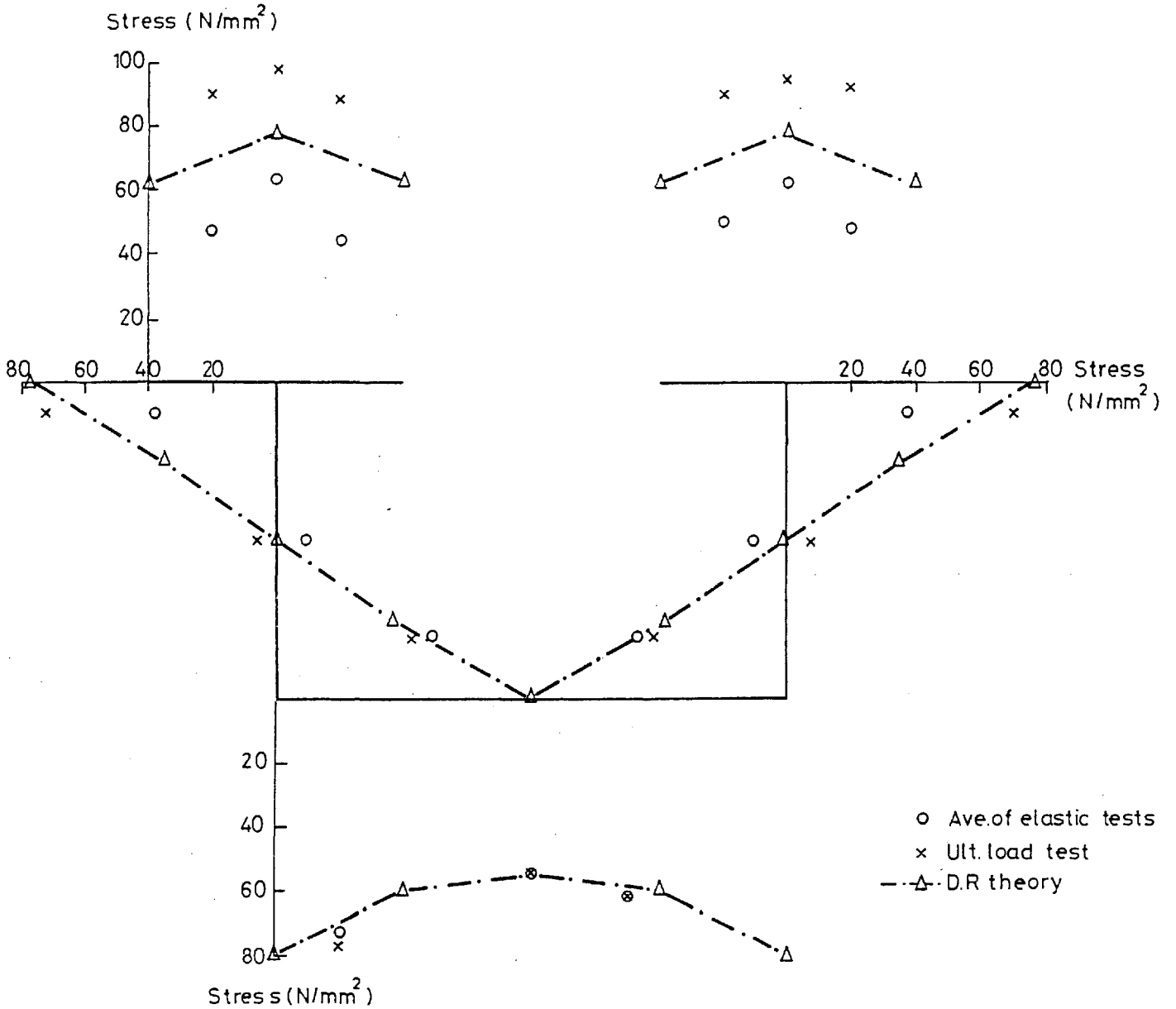

Fig 5·35 Test 01 Longitudinal stress distribution at gauged section 1 for 10 ton end load

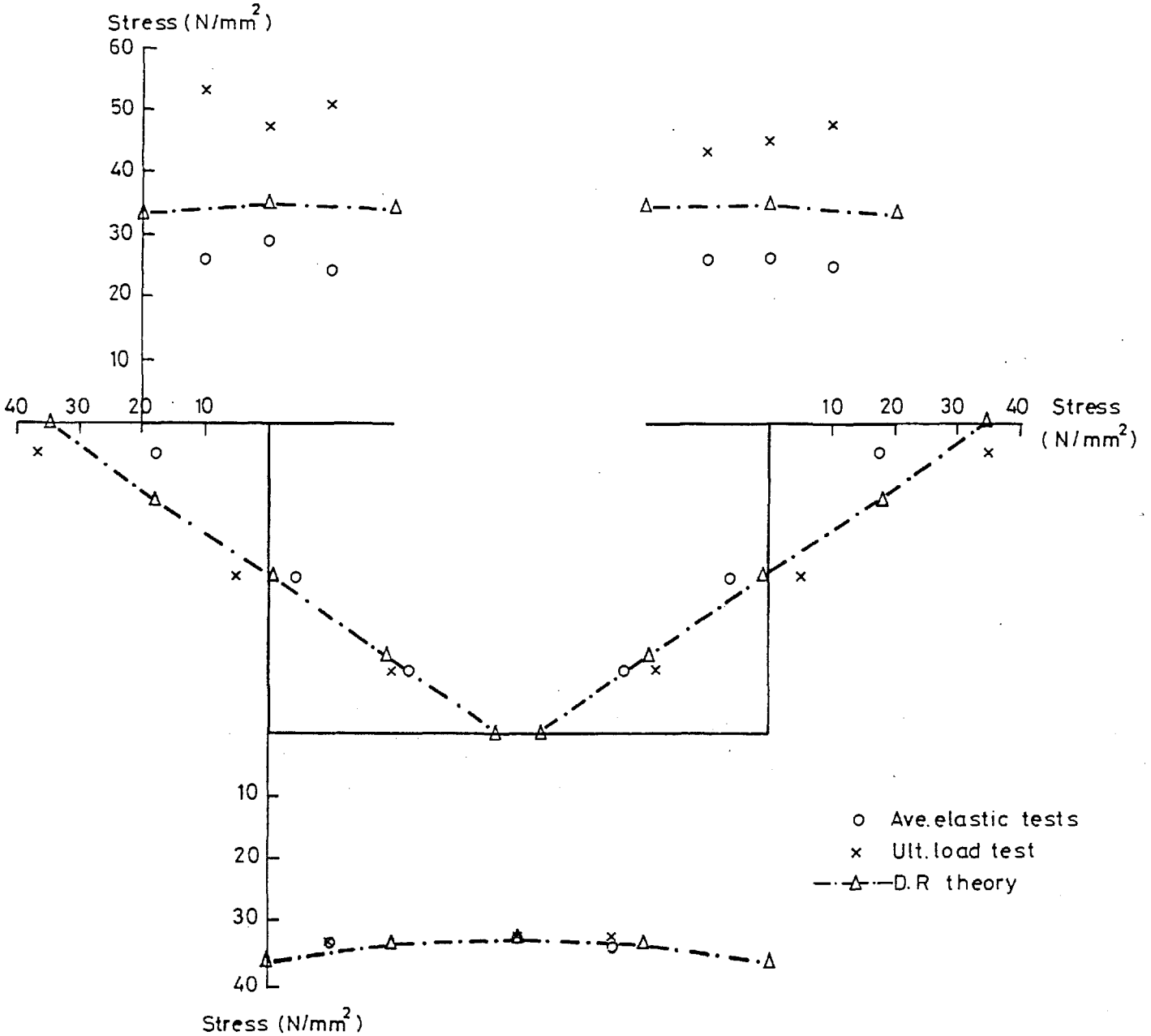

Fig 5·36 Test 01 Longitudinal stress distribution at gauged section 2 for 10 ton end load

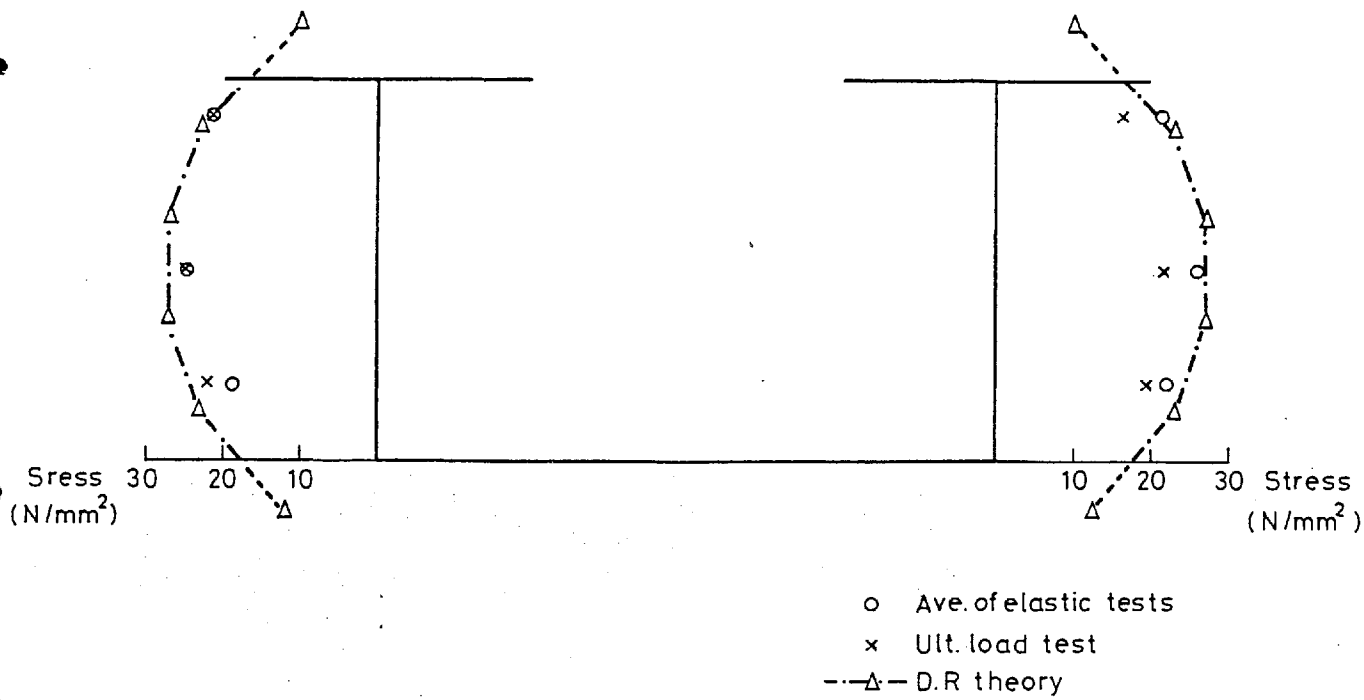

Fig 5·37 Test 01 Shear stress distribution at gauged section 1 for 10 ton end load

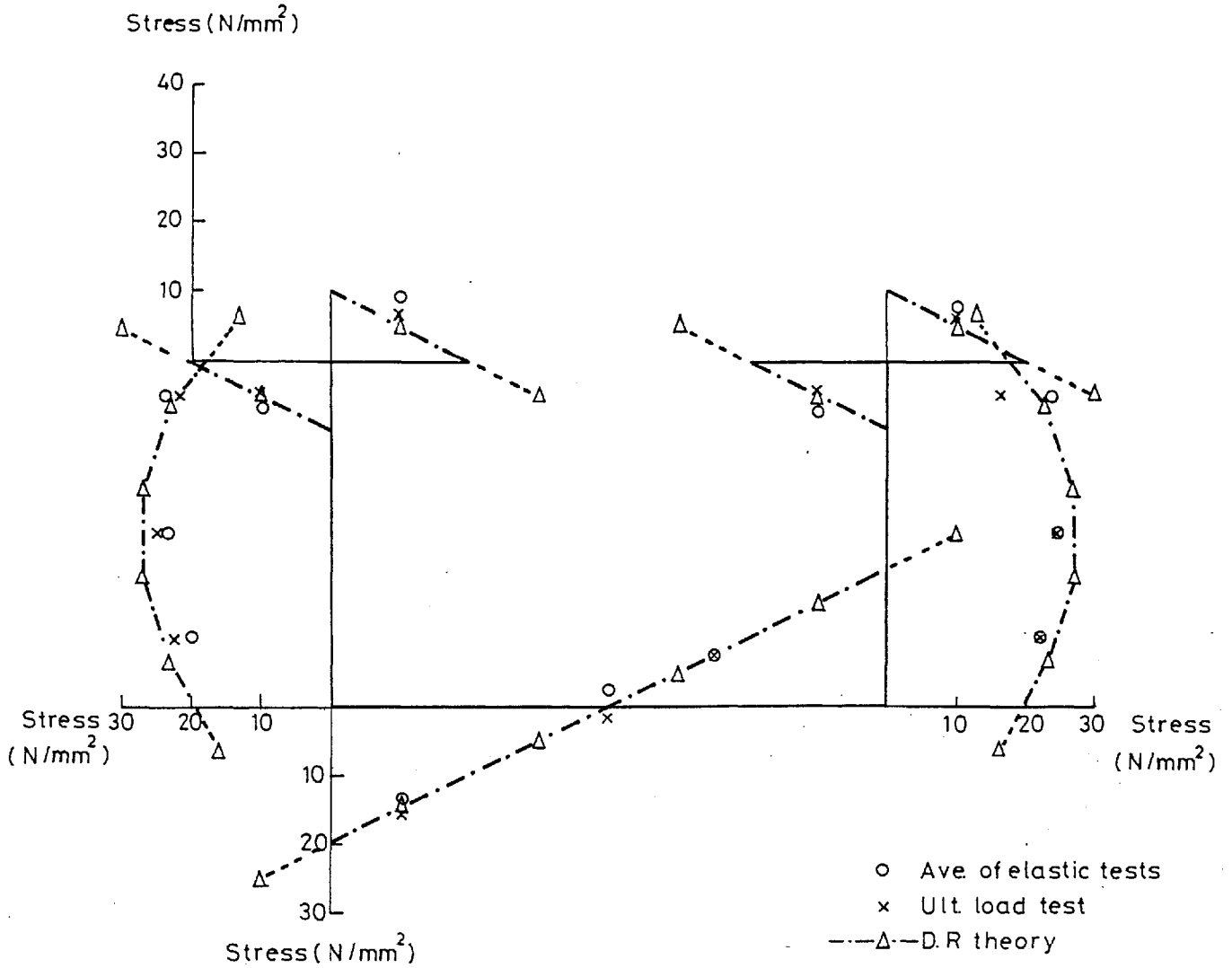

Fig 5·38 Test 01 Shear stress distribution at gauged section 2 for 10 ton end load

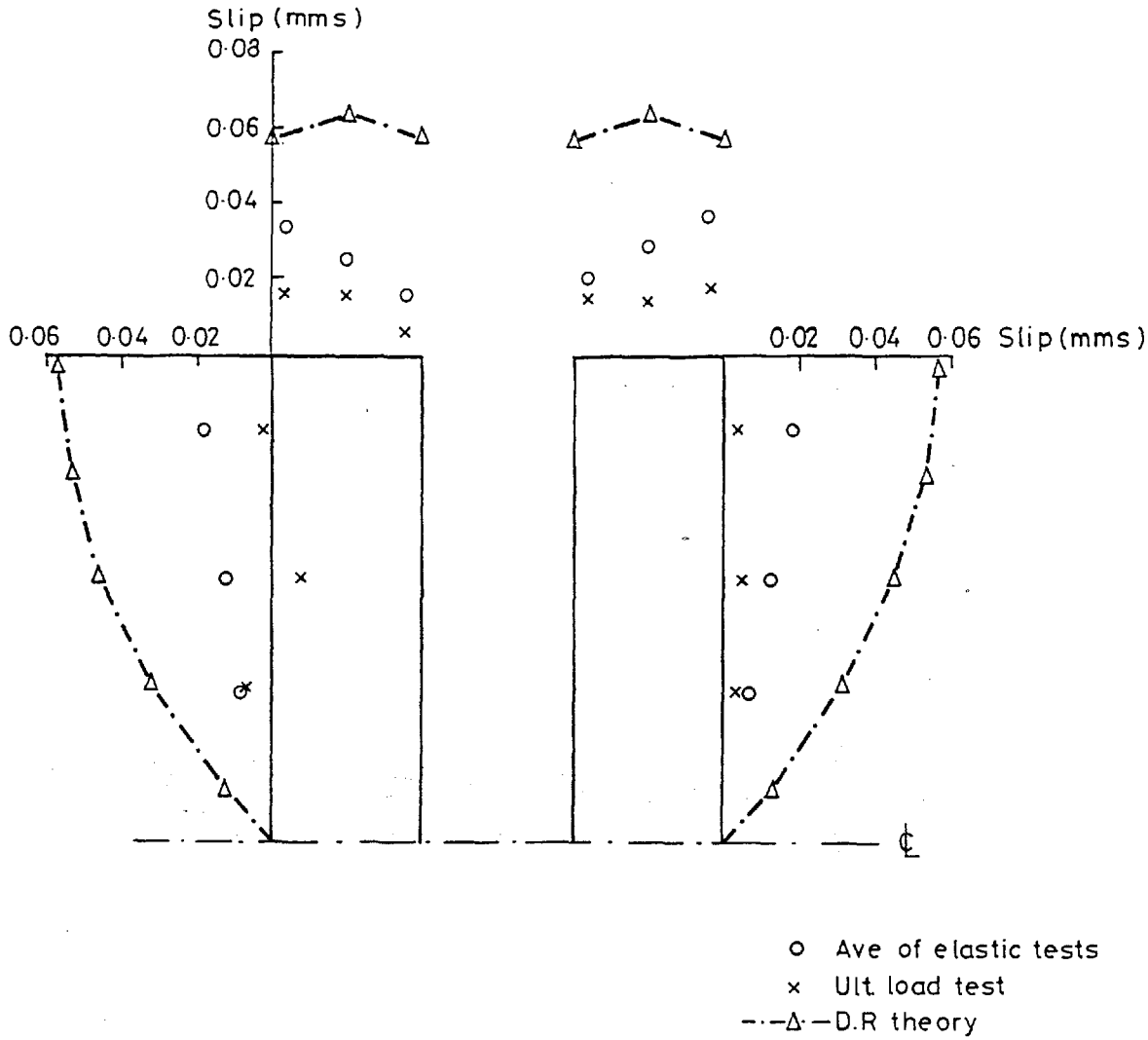

Fig 5·39 Test 01 Distribution of longitudinal slip for 10 ton end load

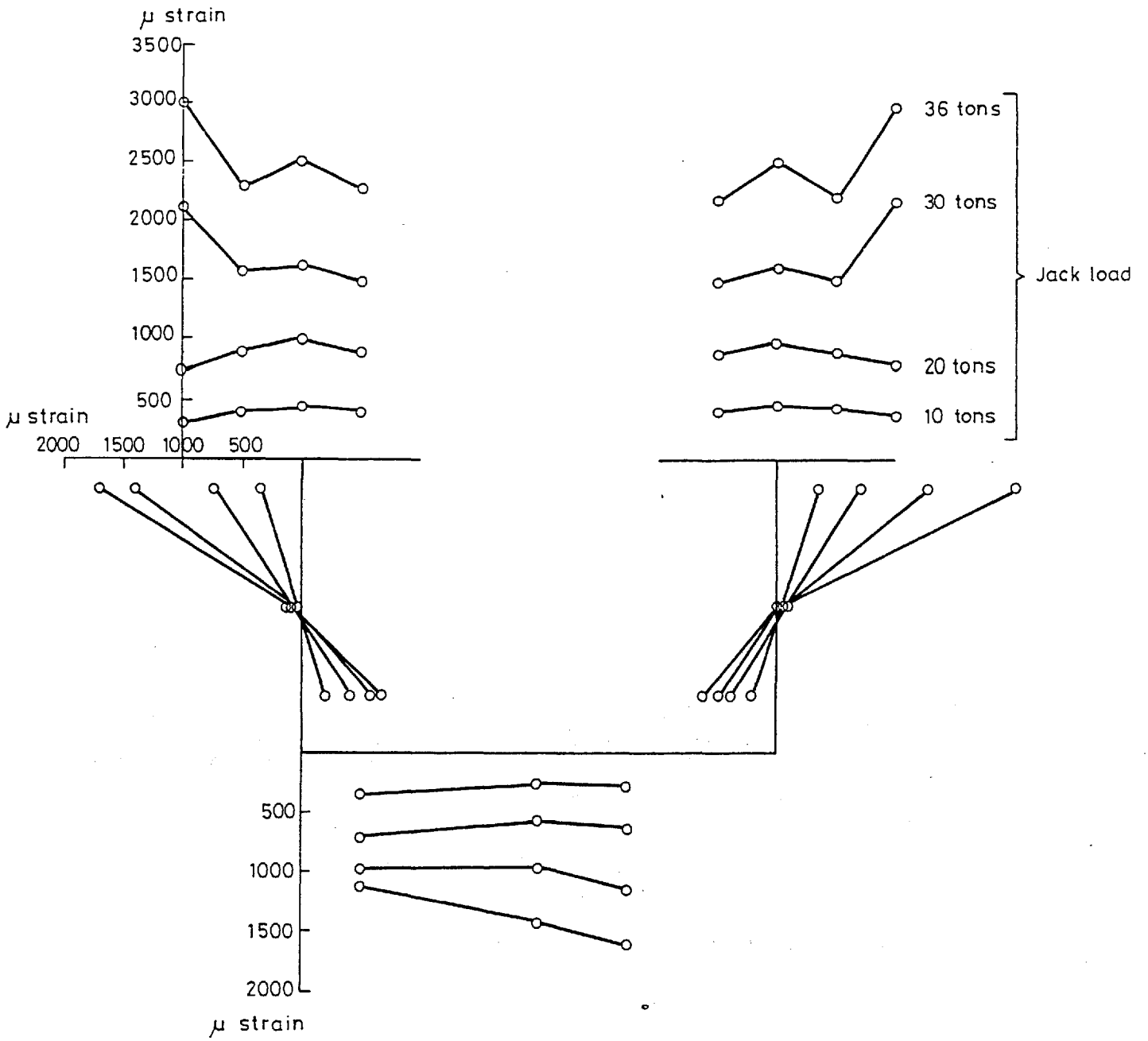

Fig 5·40 Test 01 Longitudinal strain distribution at gauged section 1 for various applied loads

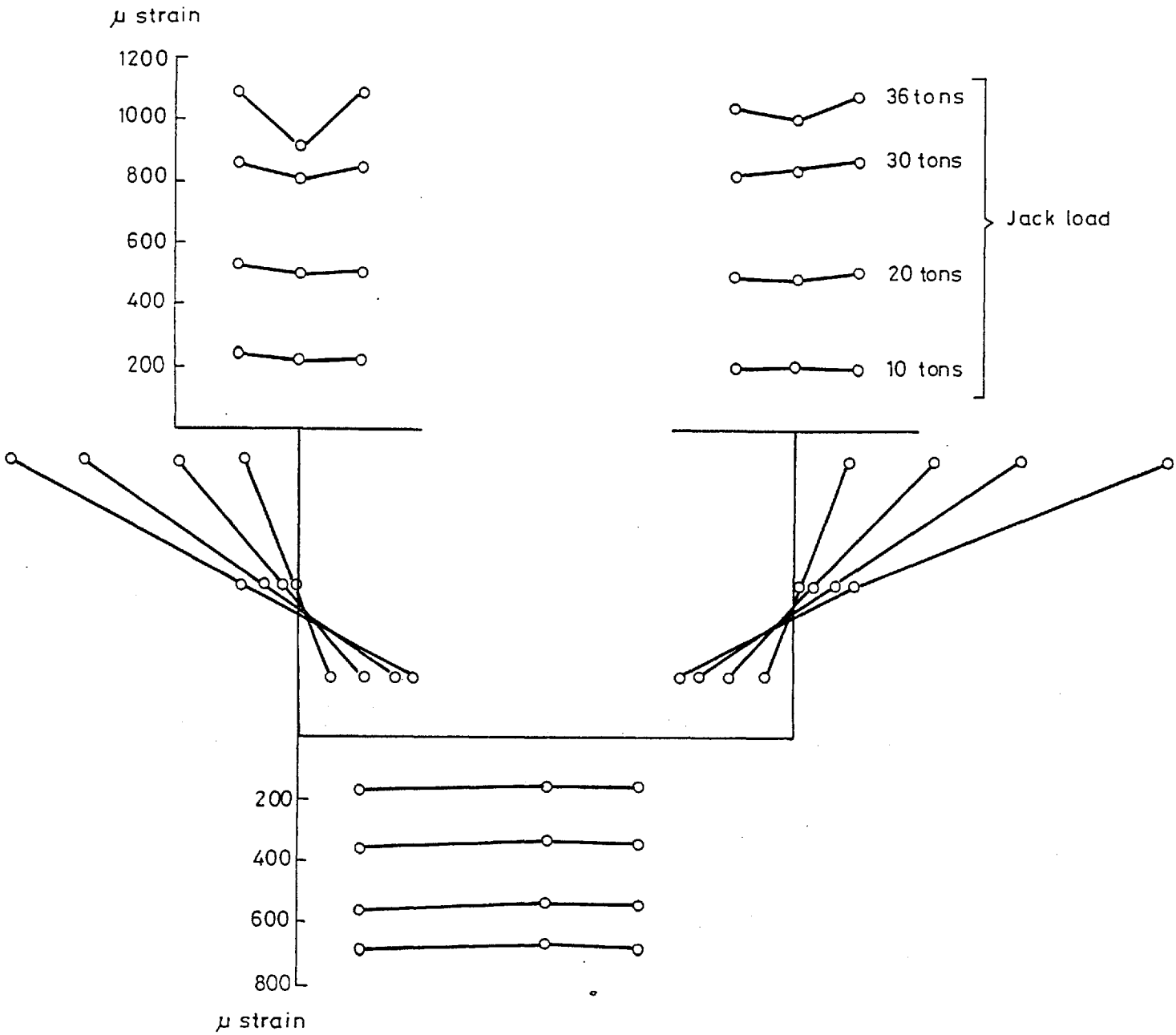

Fig 5·41 Test 01 Longitudinal strain distribution at gauged section 2 for various applied loads

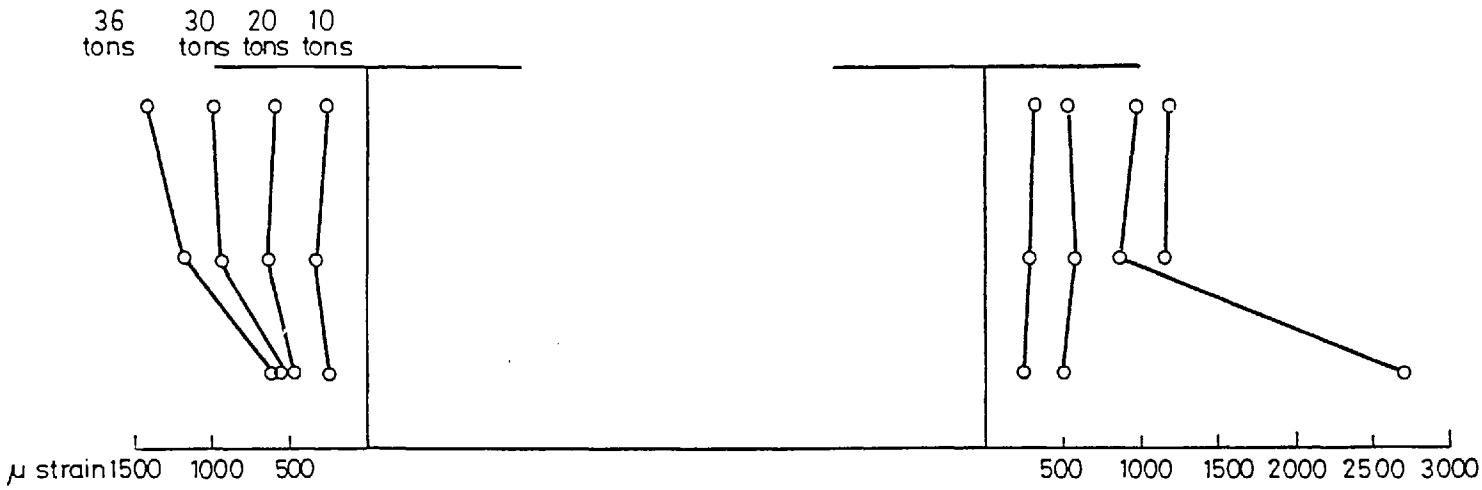

Fig 5·42 Test 01 Shear strain distribution at gauged section 1 for various applied loads

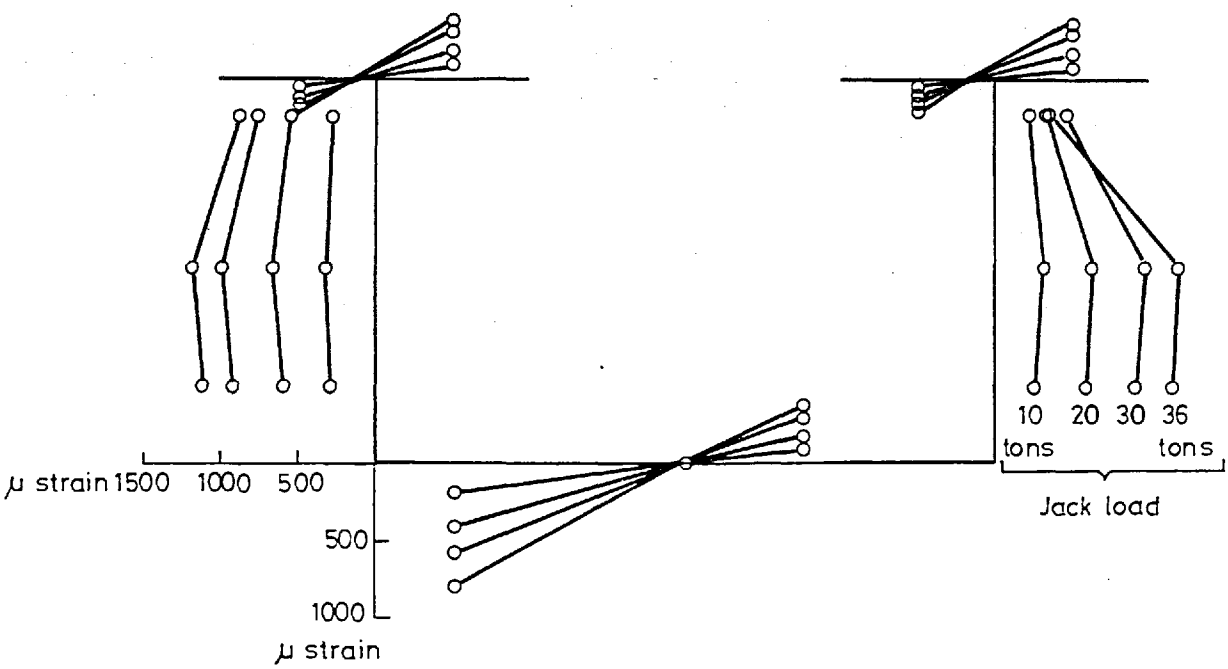

Fig 5·43 Test 01 Shear strain distribution at gauged section 2 for various applied loads

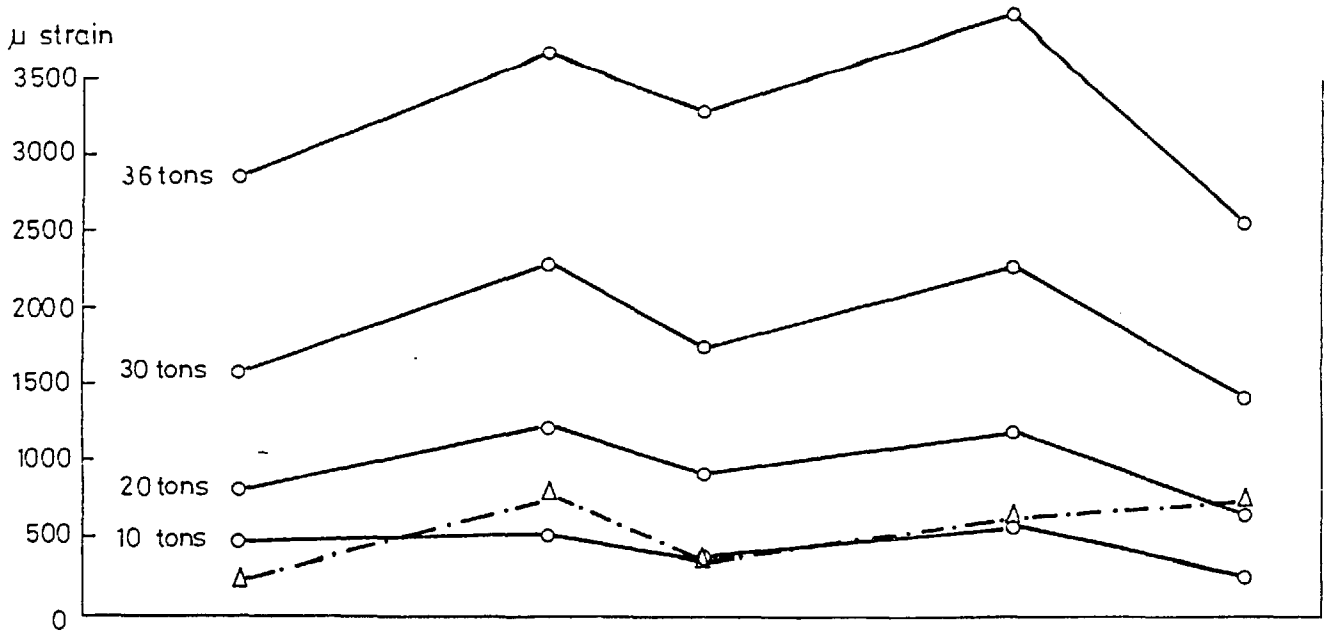

Fig 5·44 Test 01 Longitudinal slab strains at gauged section 1 for various loads

Δ = Elastic tests, 10 ton loads
o = Ult. load test

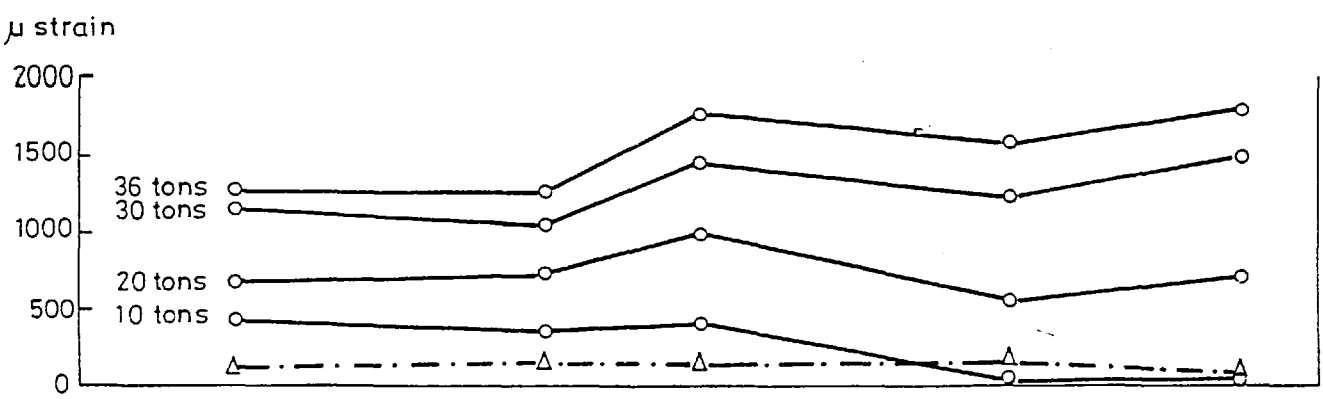

Fig 5·45 Test 01 Longitudinal slab strains at gauged section 2 for various loads

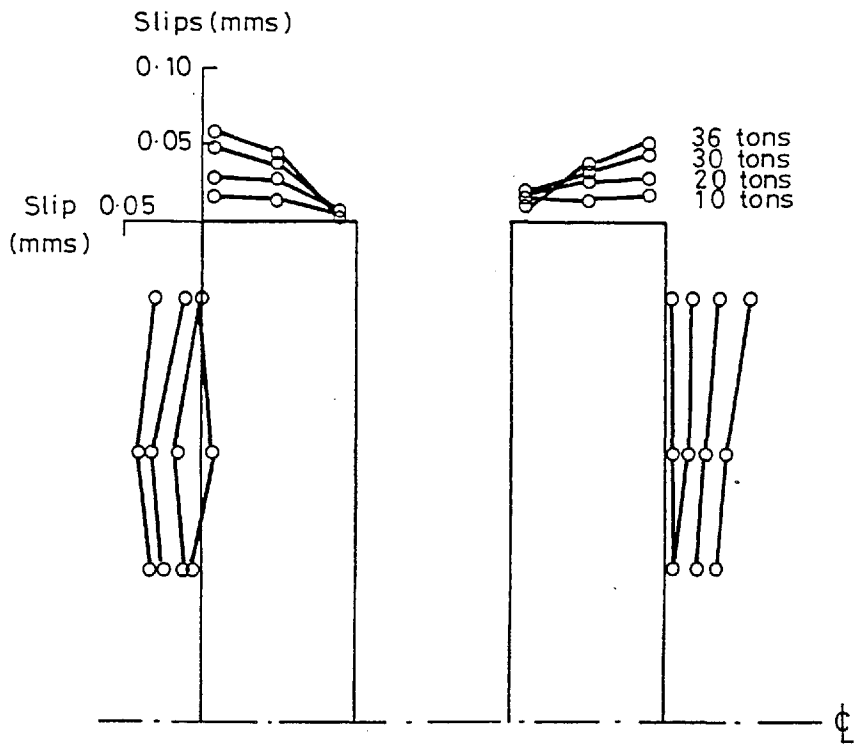

Fig 5·46 Test 01 Longitudinal slip distribution for various applied loads

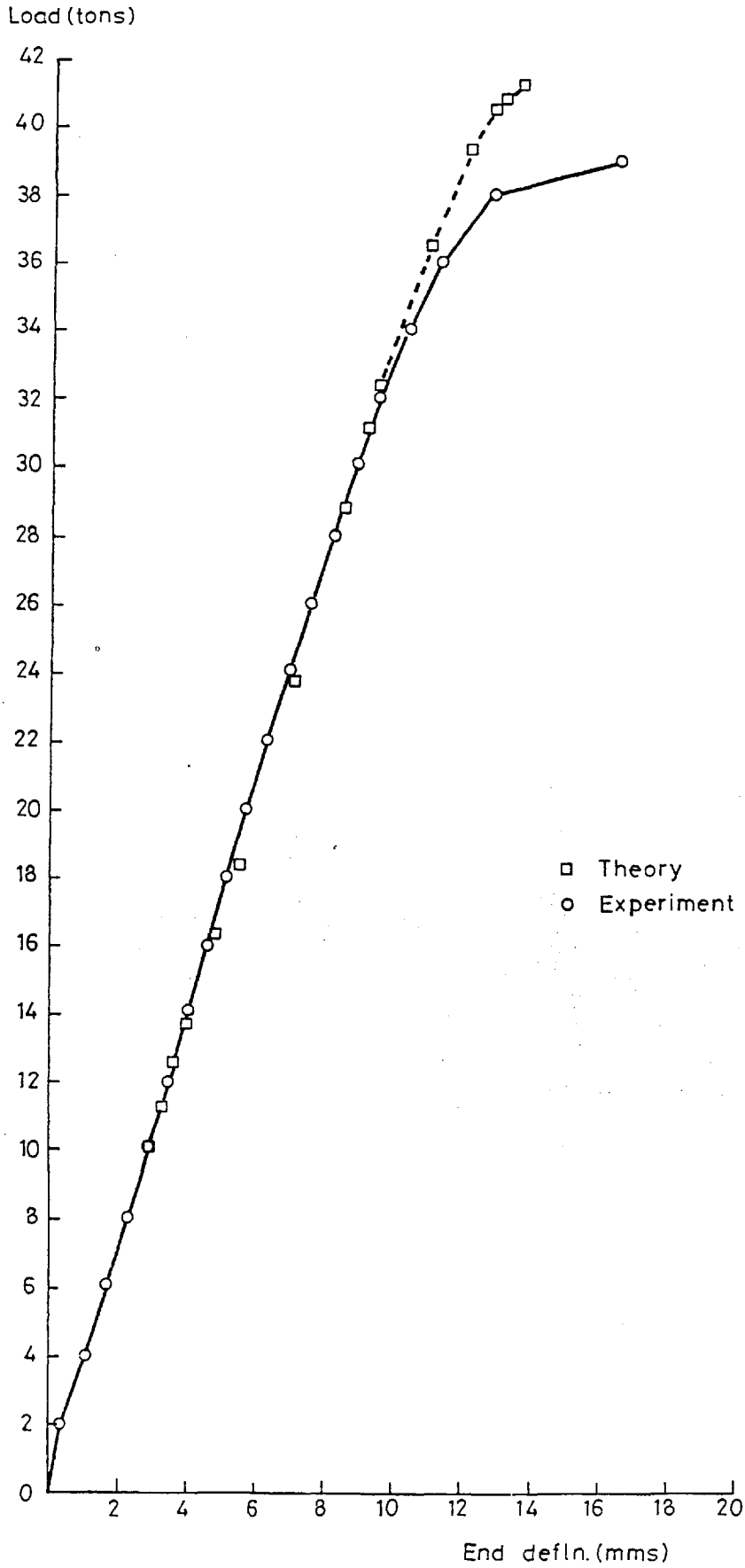

Fig 5·47 Test 01 Load-end deflection curve

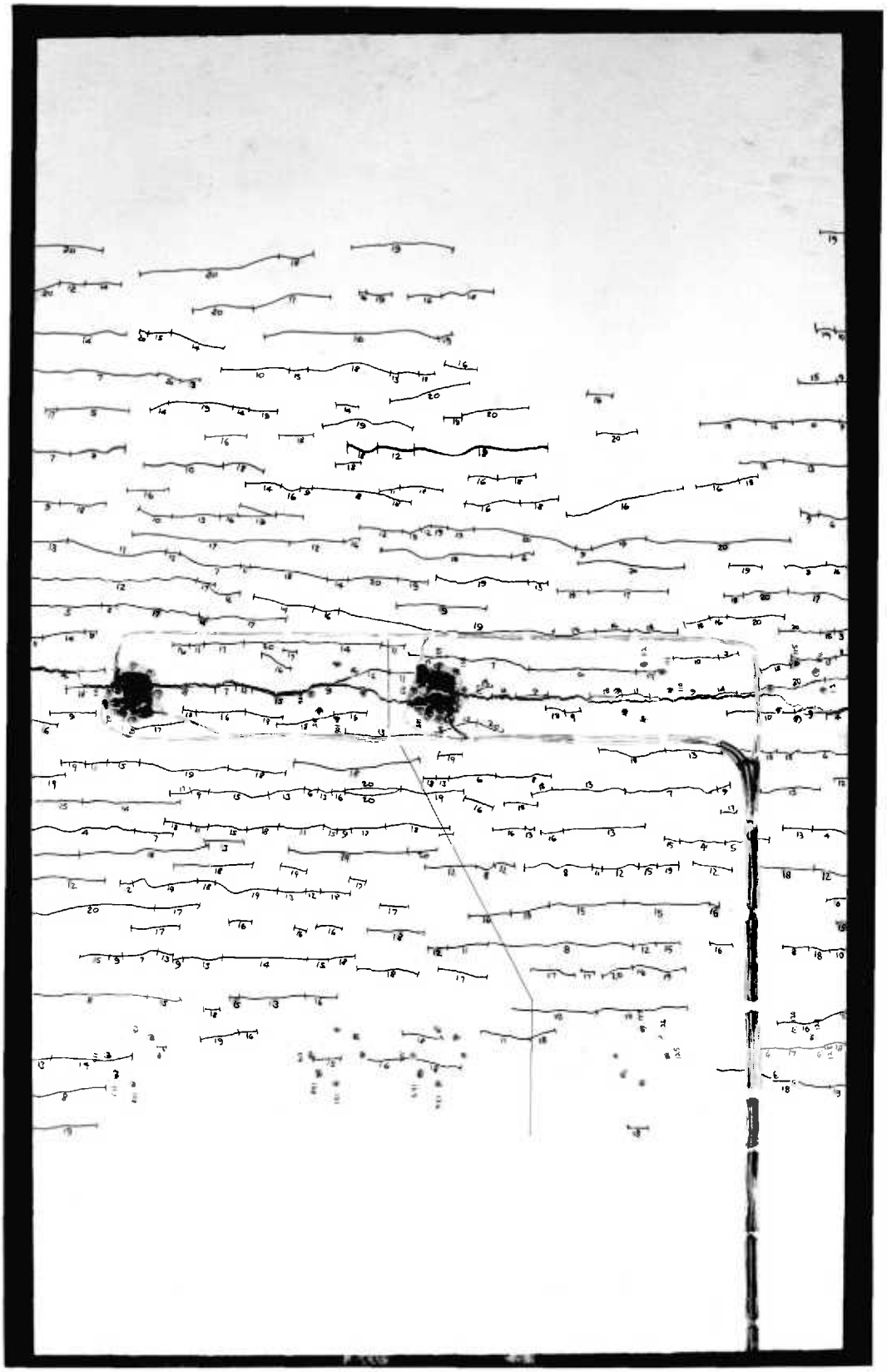

Fig 5.48 Test 01, photograph of cracked slab.

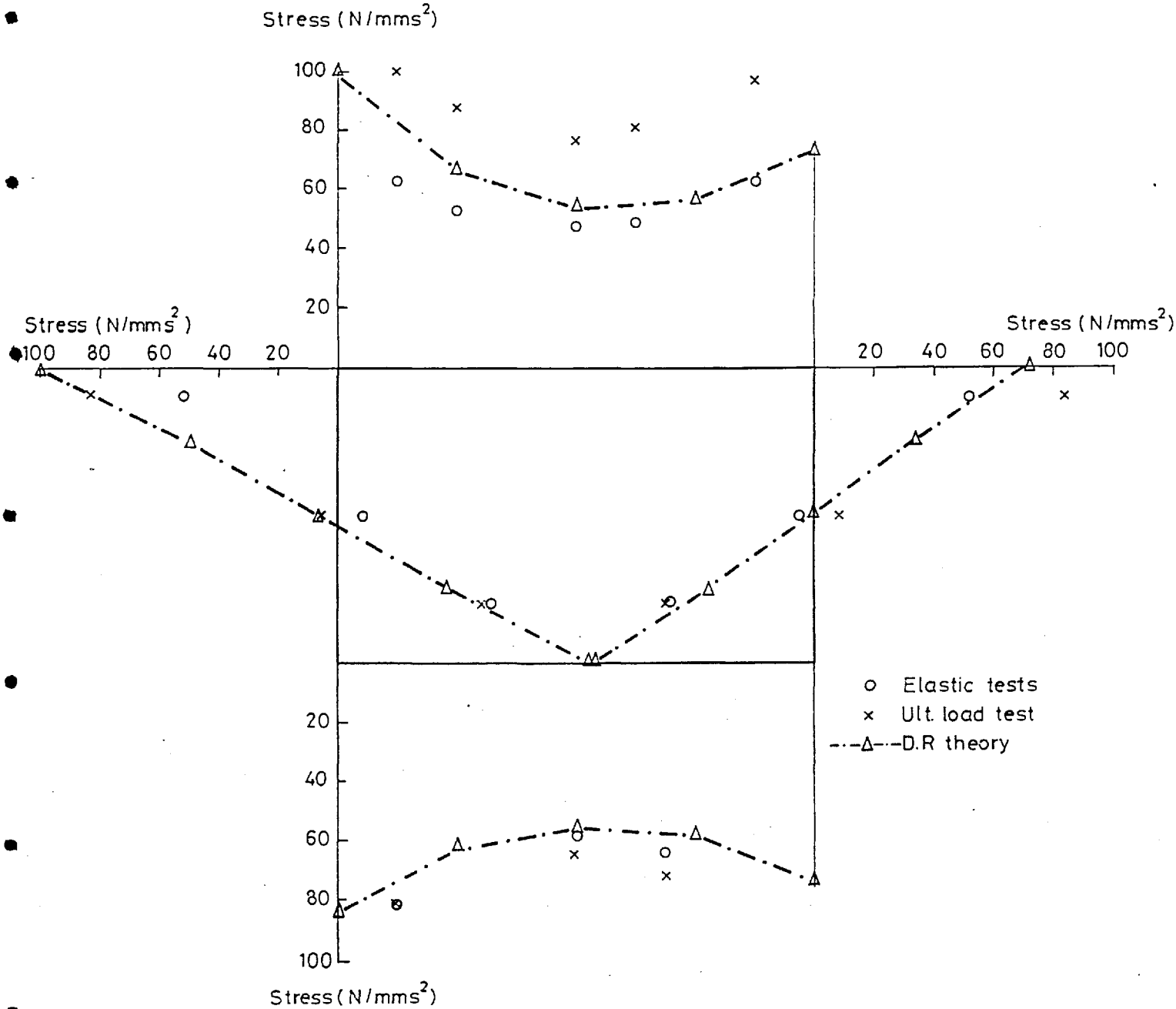

Fig 5·49 Test C2 Longitudinal ress distribution at gauged section 1 for 10 ton end load

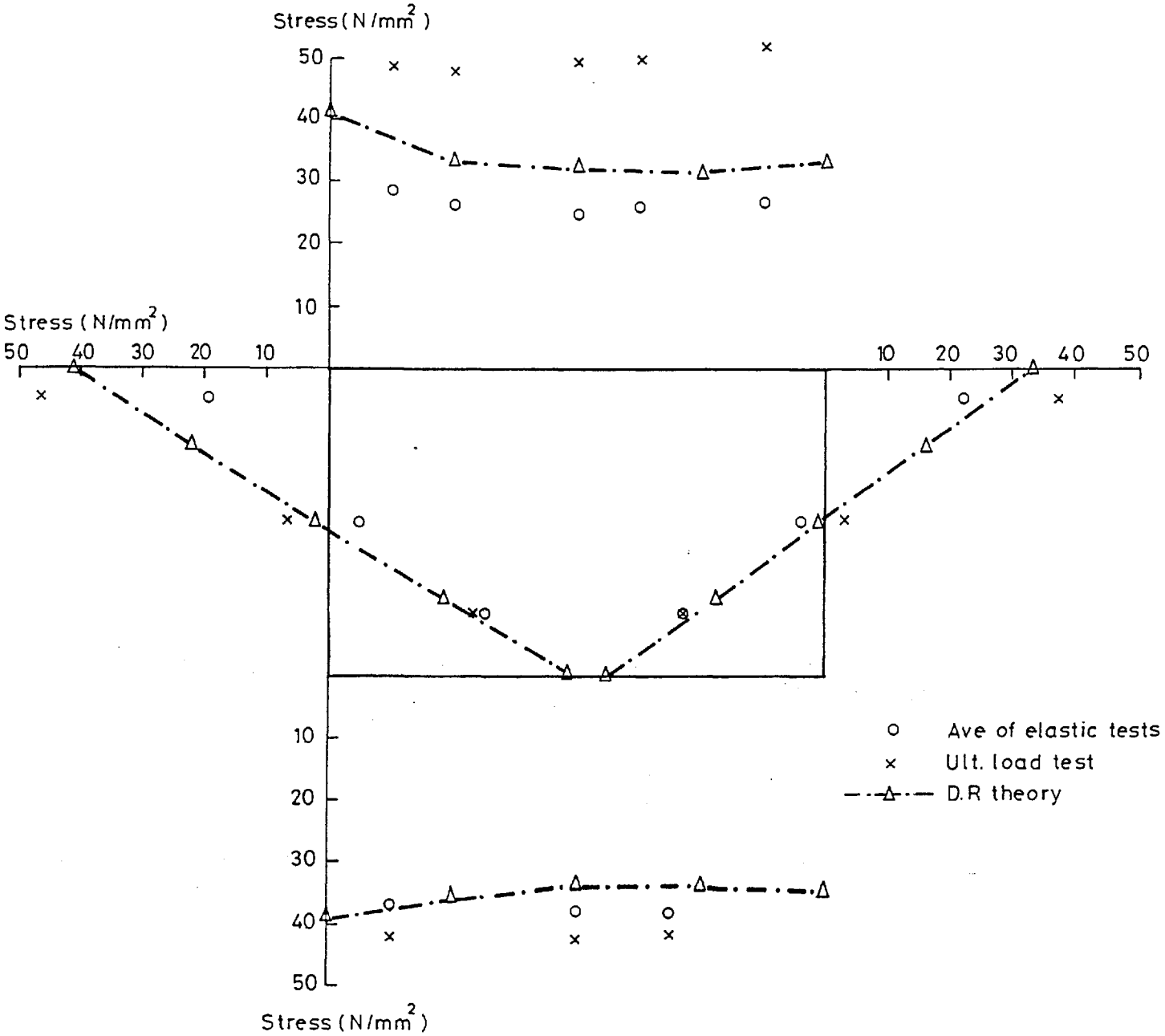

Fig 5·50 Test C2 Longitudinal stress distribution at gauged section 2 for 10 ton end load

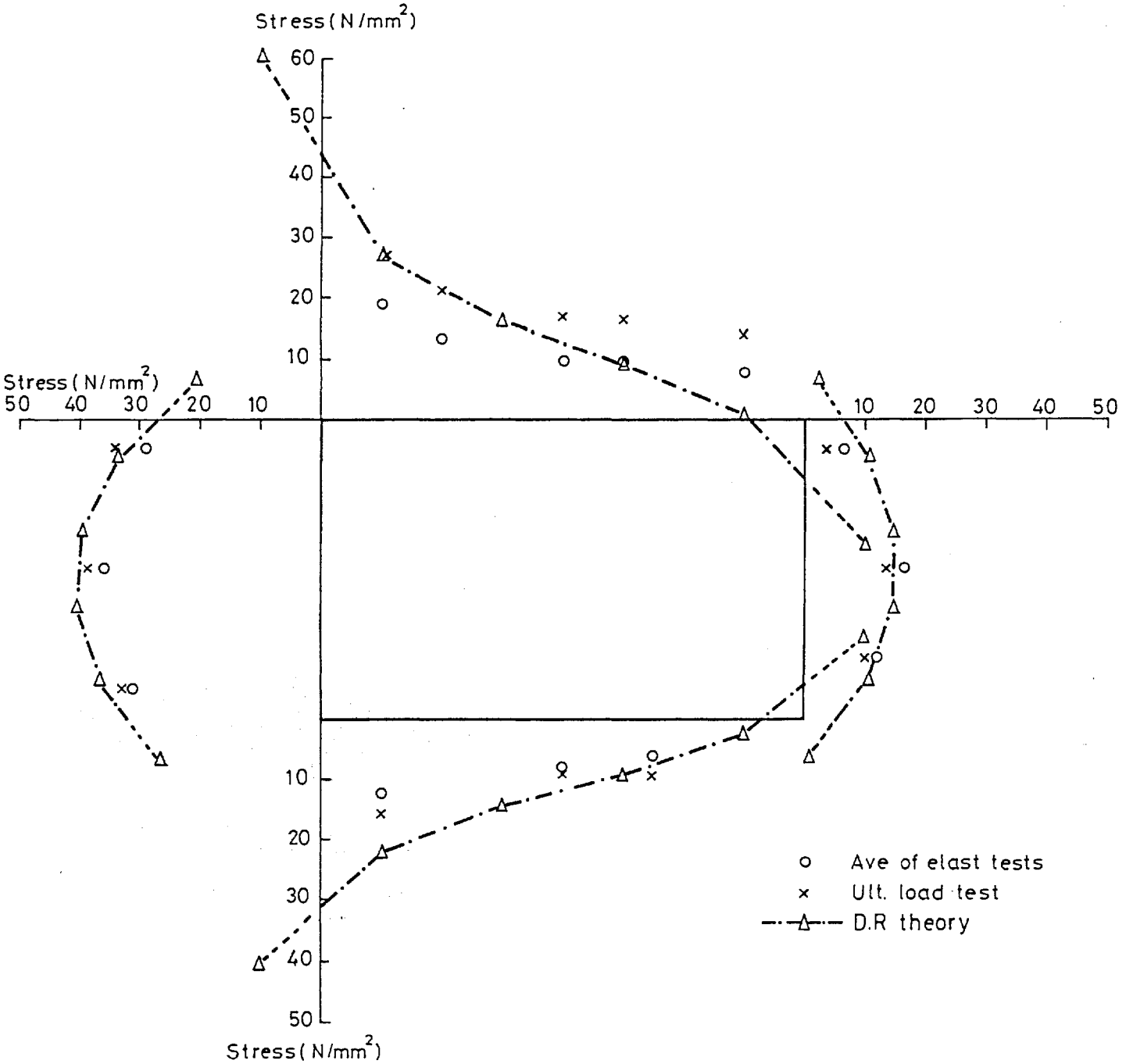

Fig 5·51 Test C2 Shear stress distribution at gauged section 1 for 10 ton end load

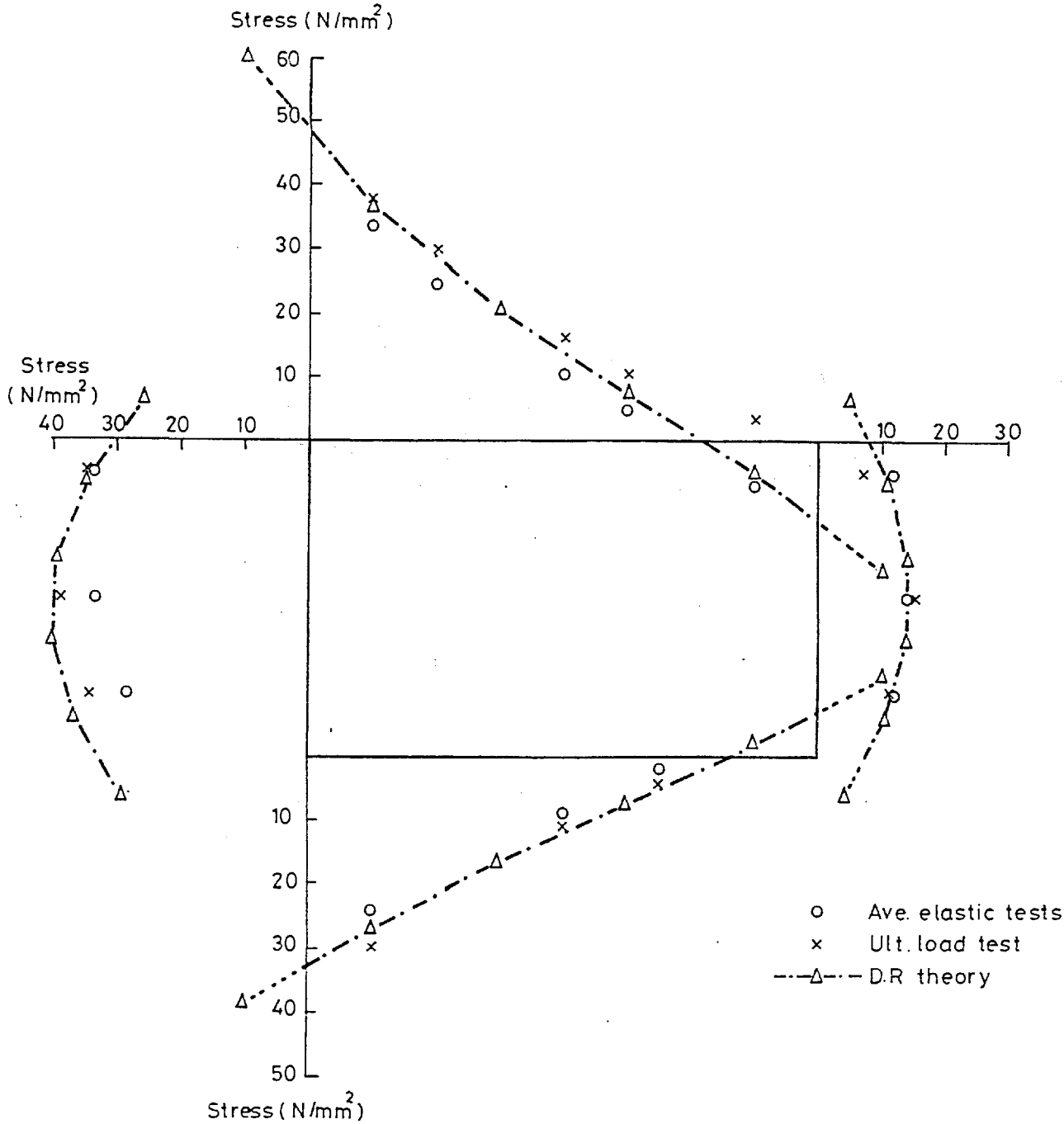

Fig 5·52 Test C2 Shear stress distribution at gauged section 2 for 10 ton end load

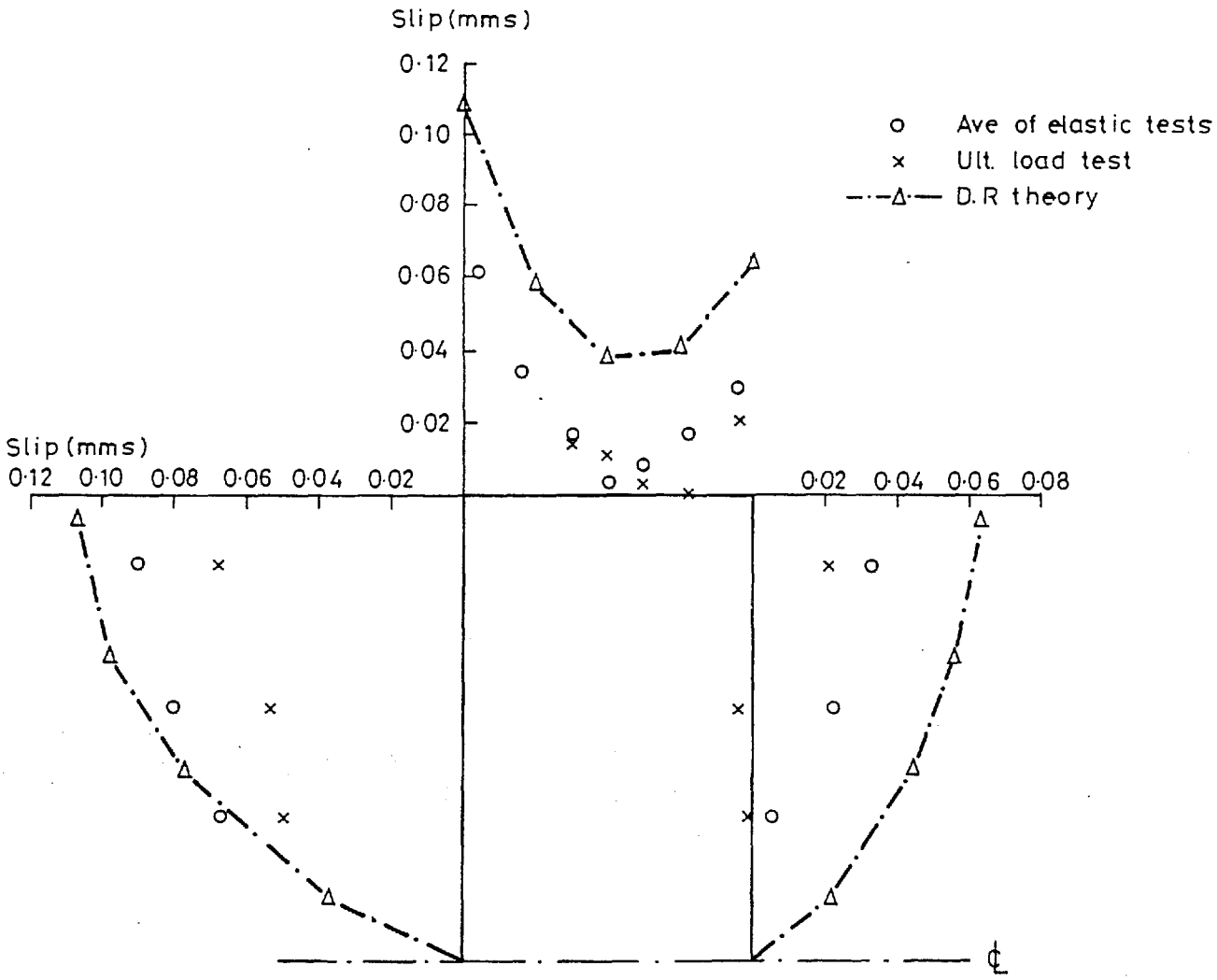

Fig 5·53 Test C2 Distribution of longitudinal slip for 10 ton end load

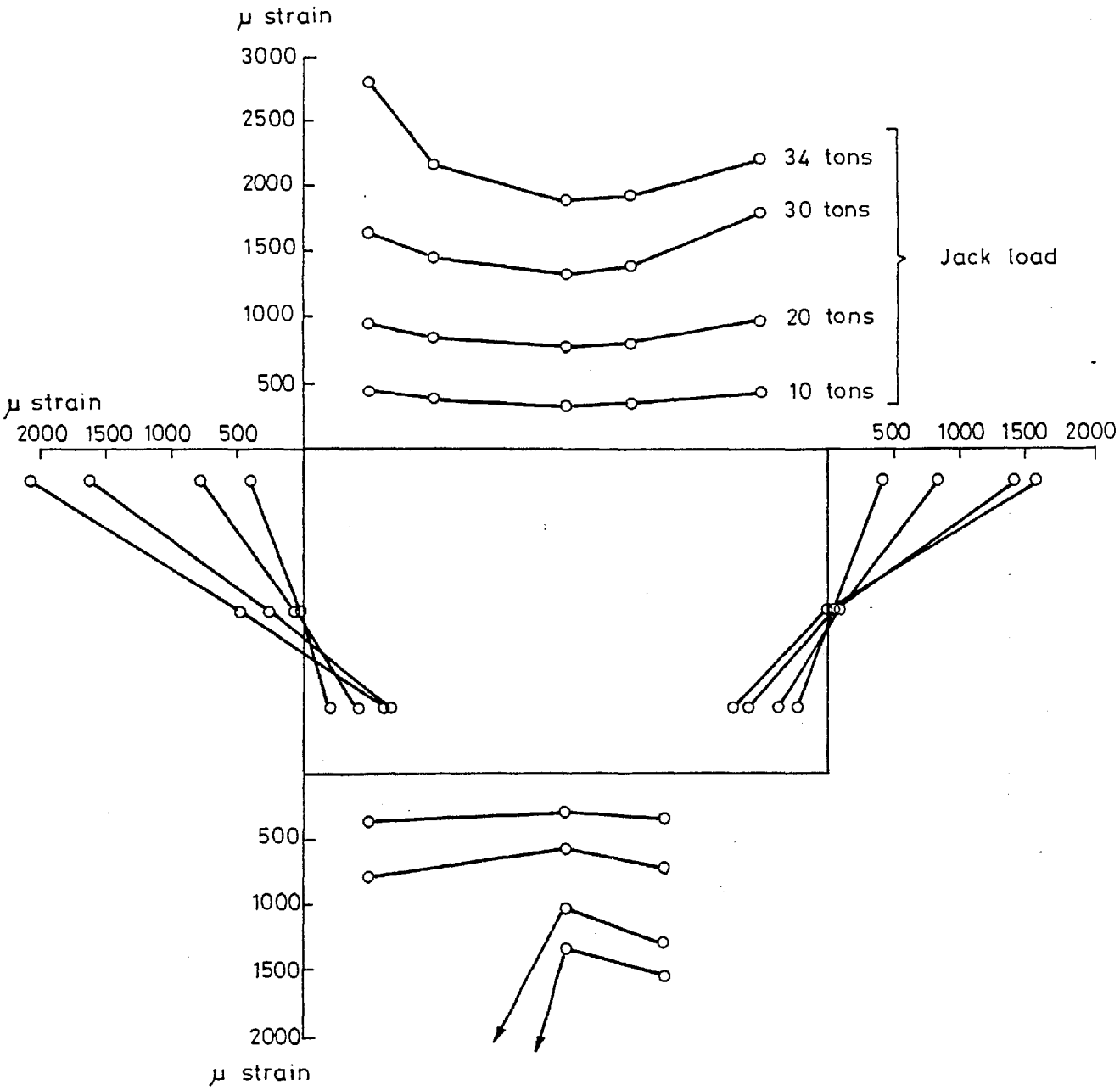

Fig 5·54 Test C2 Longitudinal strain distribution at gauged section 1 for various applied loads

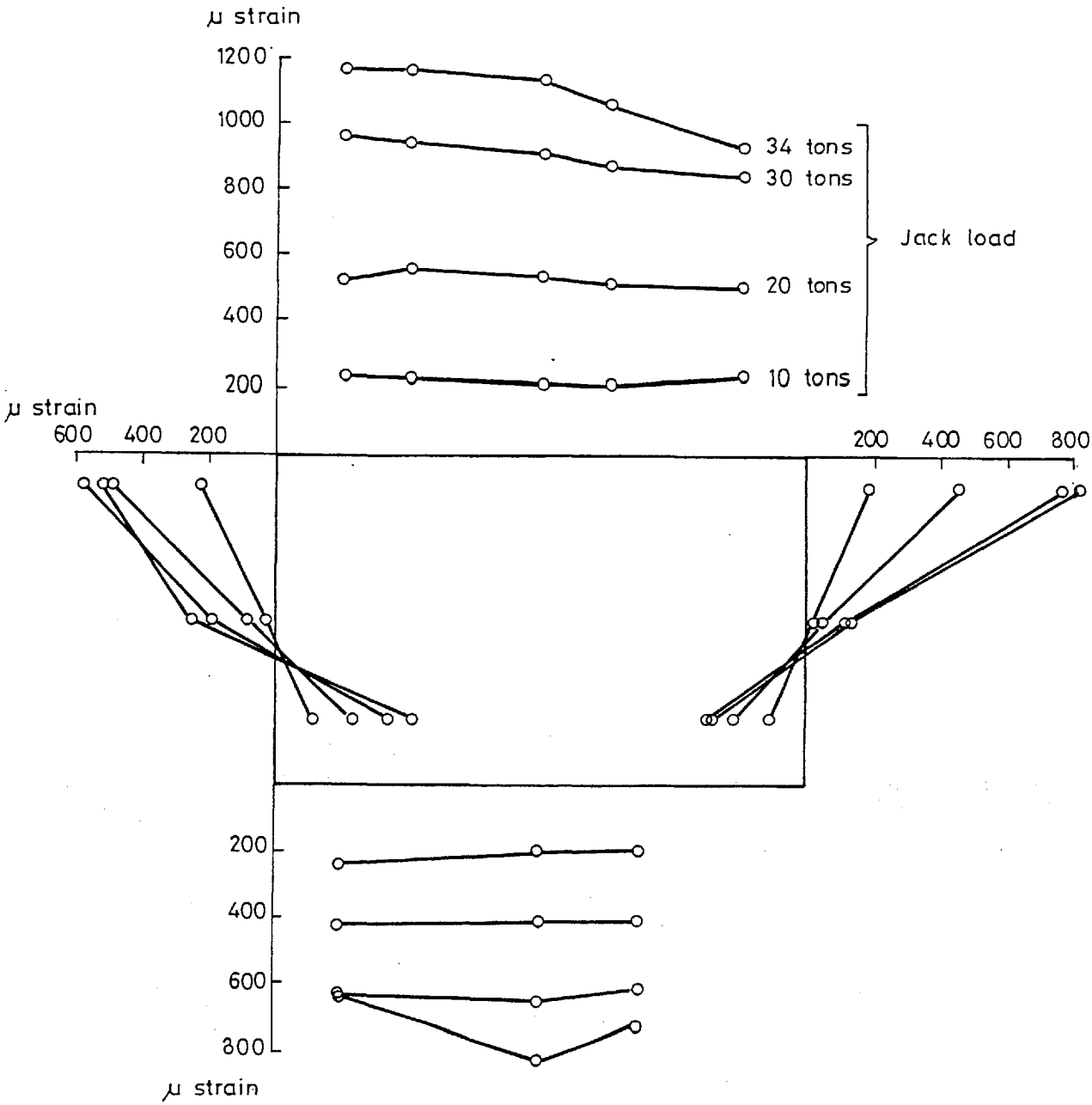

Fig 5·55 Test C2 Longitudinal strain distribution at gauged section 2 for various loads

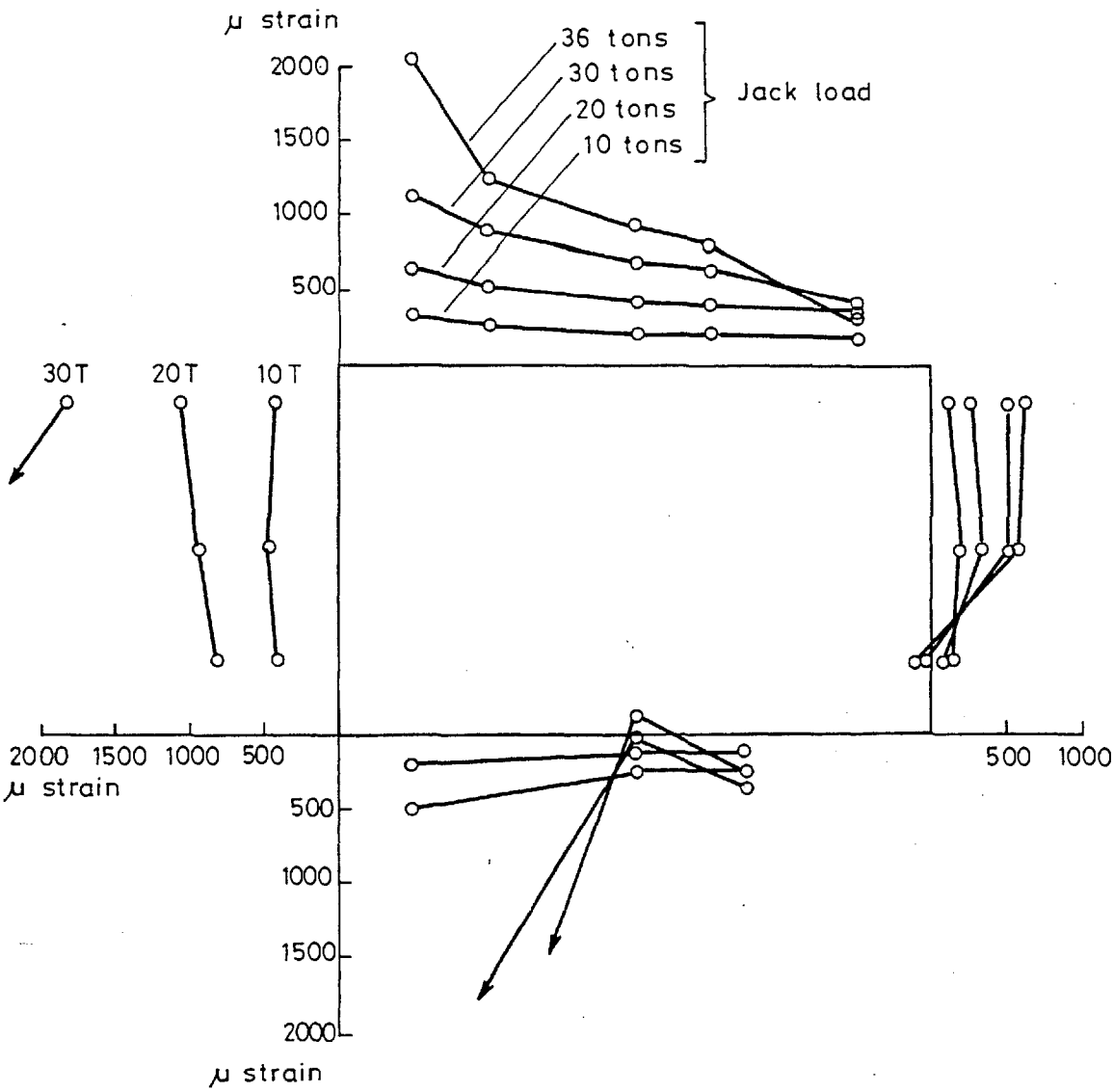

Fig 5·56 Test C2 Shear strain distribution at gauged section 1 for various loads

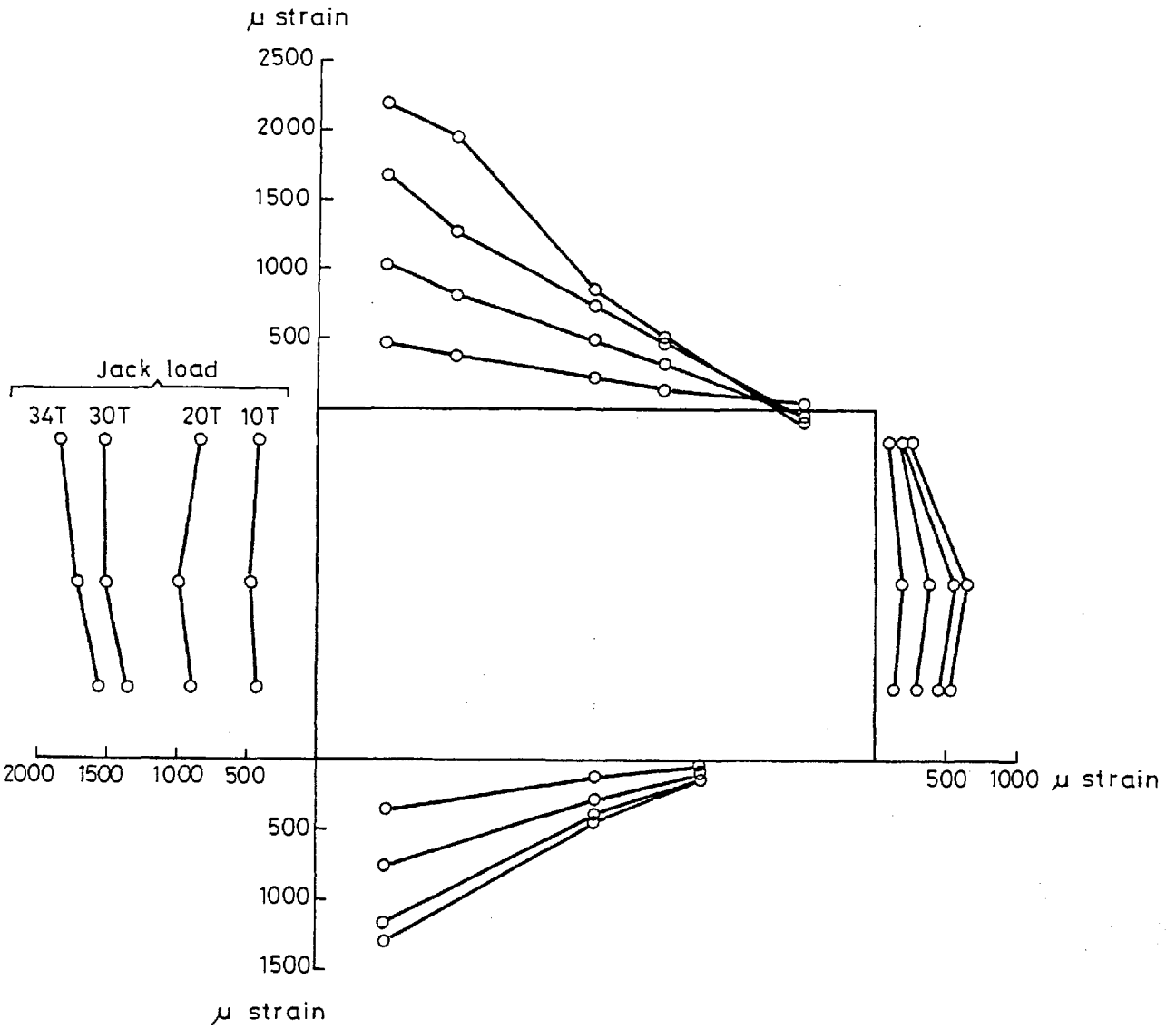

Fig 5·57 Test C2 Shear strain distribution at gauged section 2 for various loads

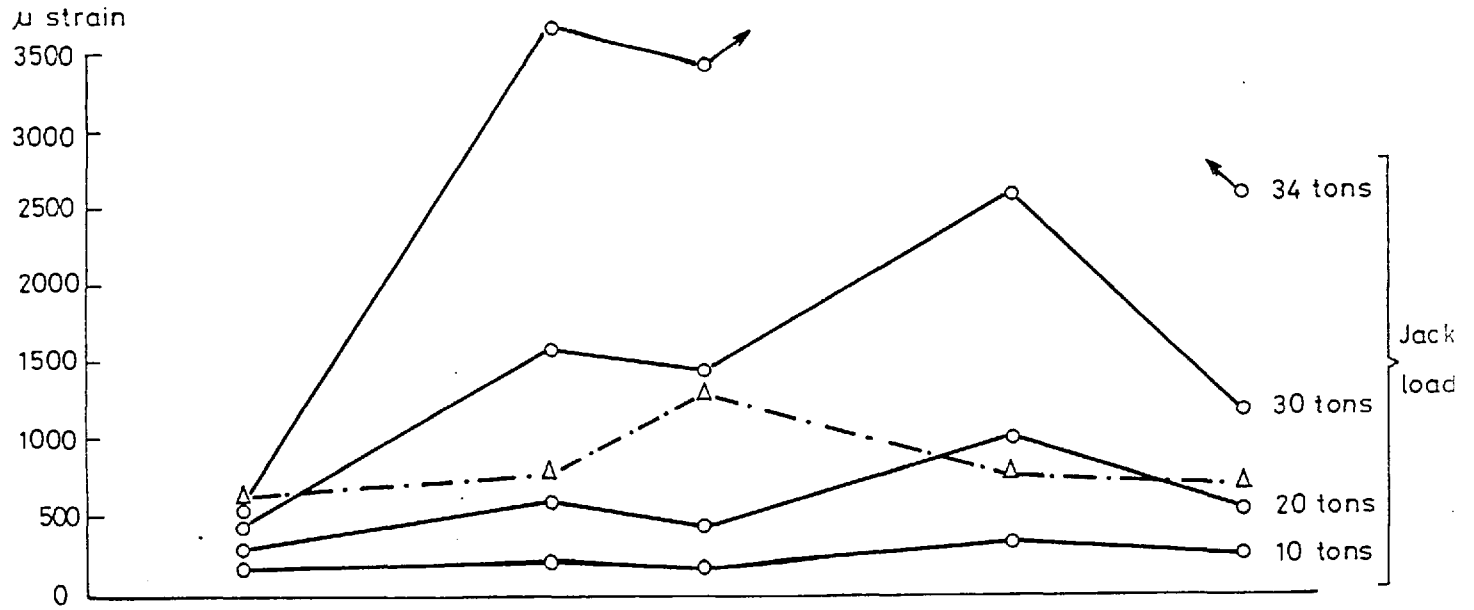

Fig 5·58 Test C2 Longitudinal slab strains at gauged section 1 for various loads

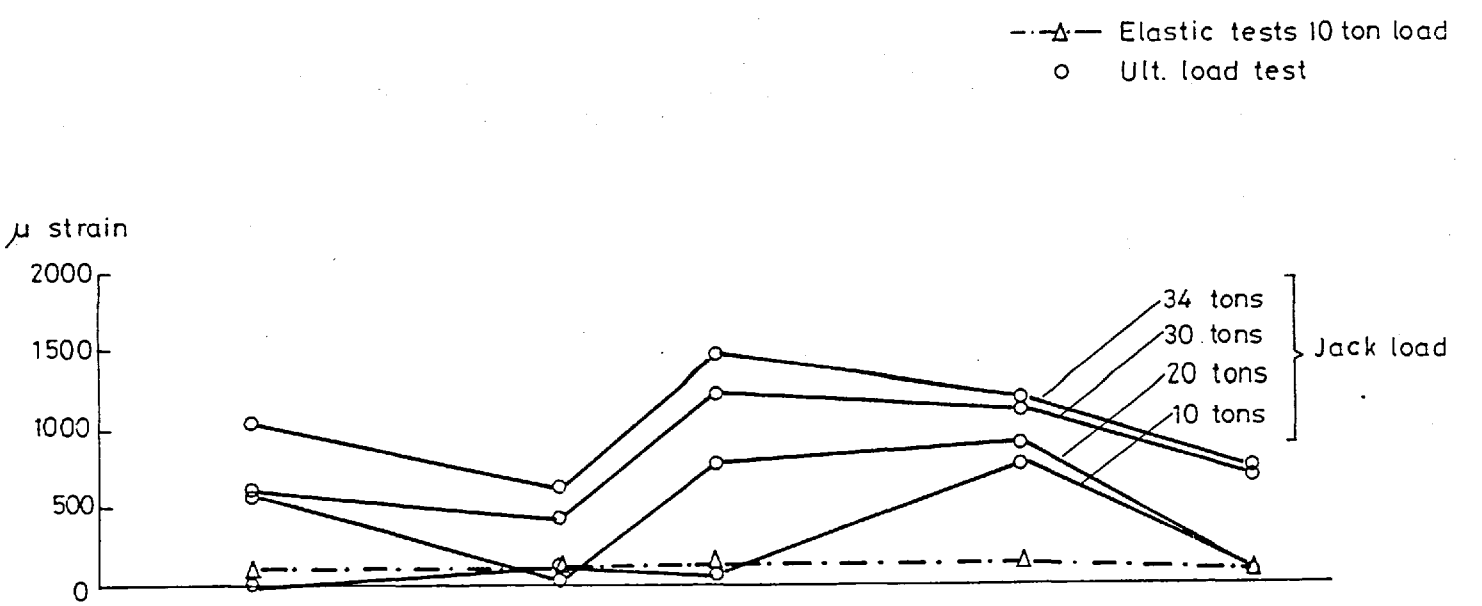

Fig 5·59 Test C2 Longitudinal slab strains at gauged section 2 for various loads

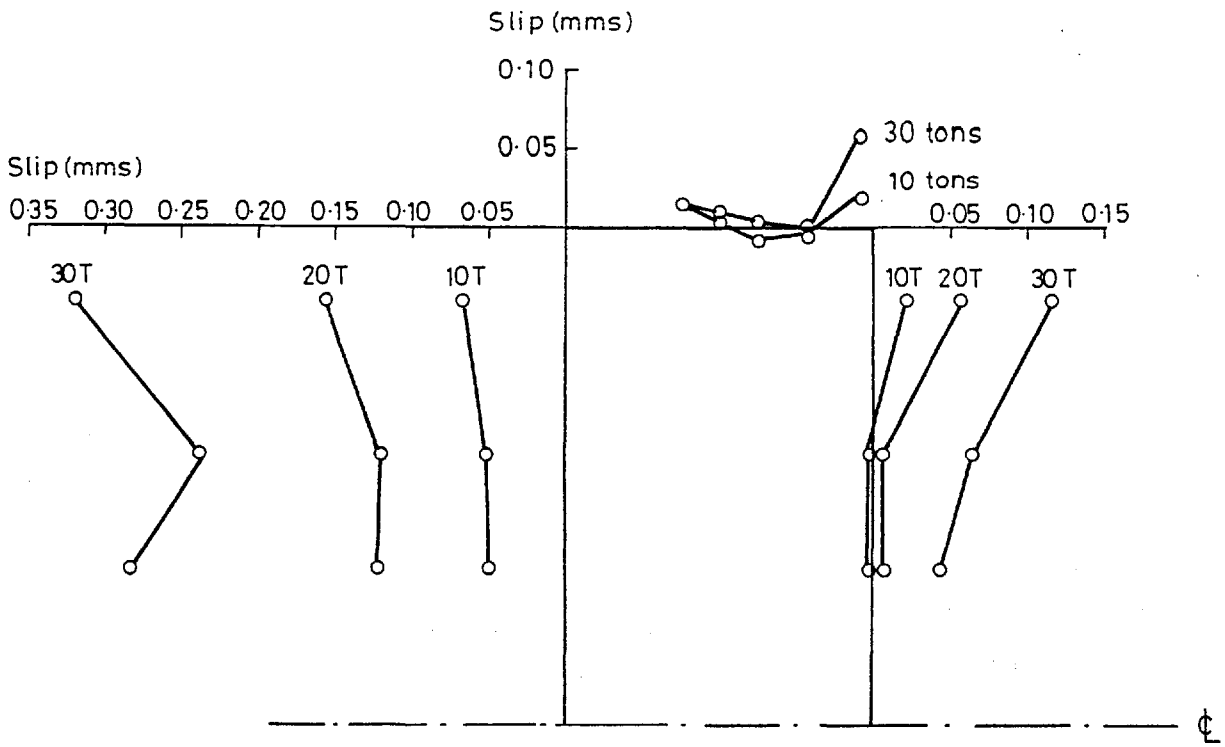

Fig 5·60 Test C2 Longitudinal slip distribution for various applied loads

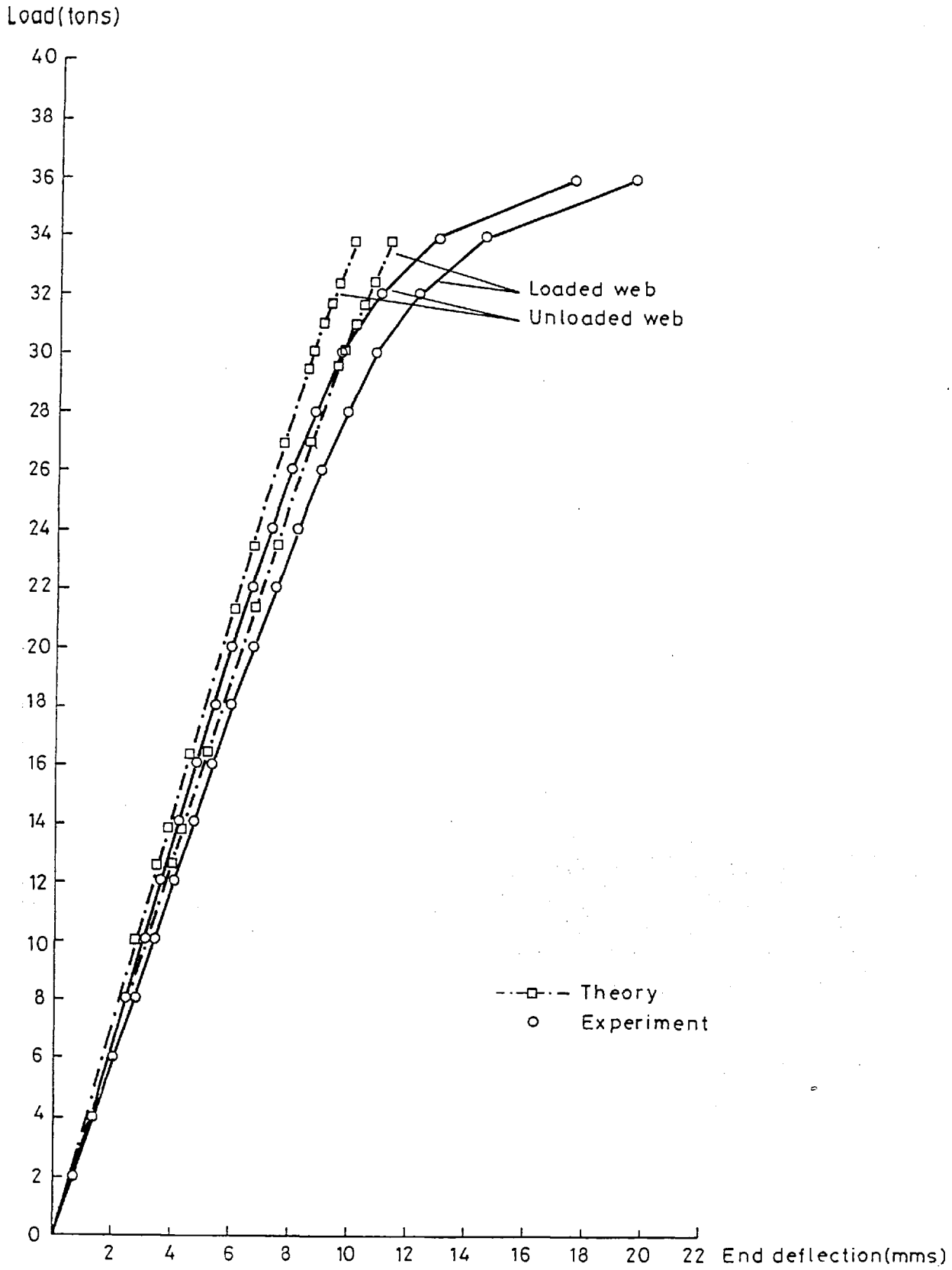

Fig 5·61 Test C2 Load-end deflection curves

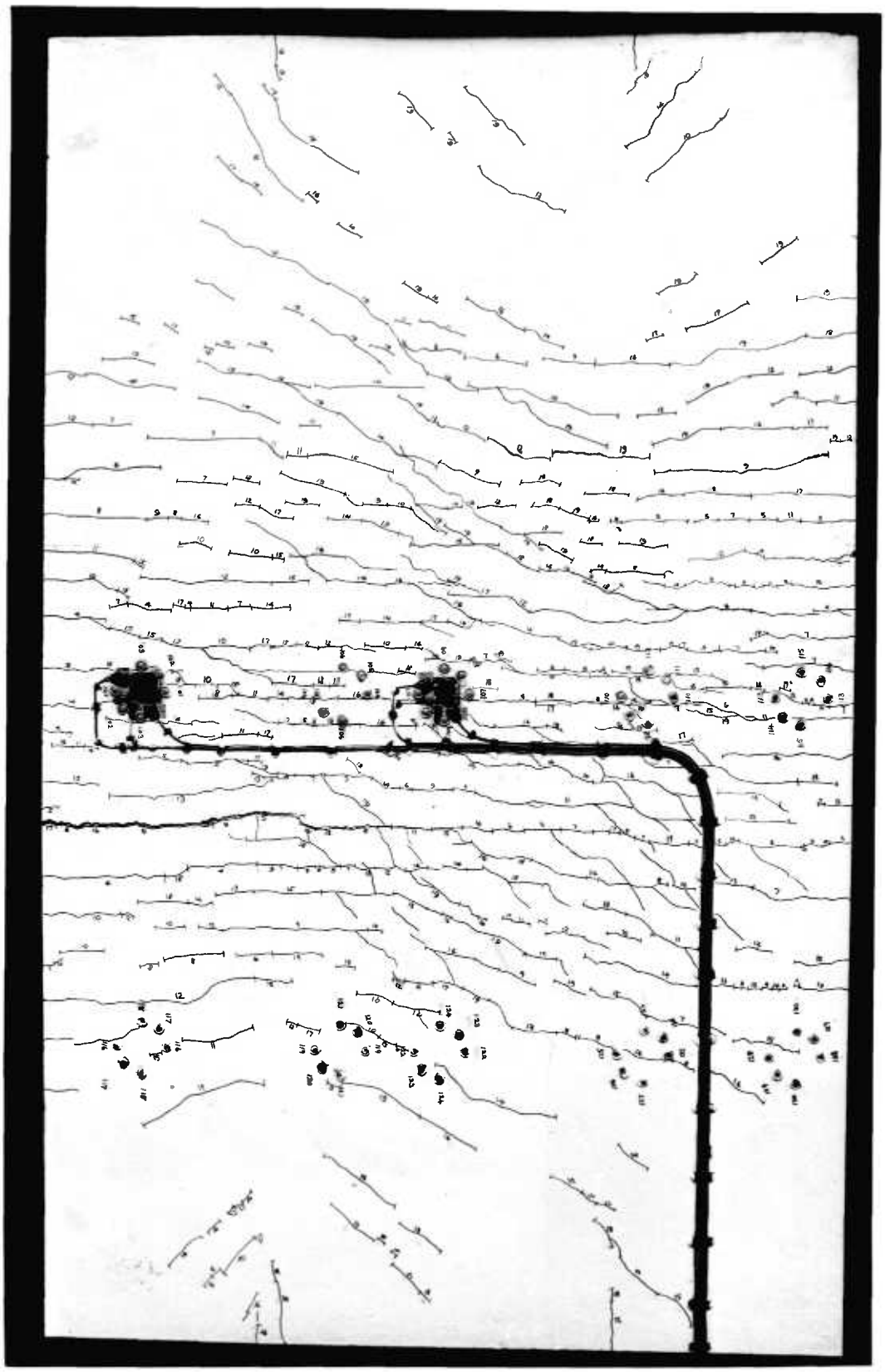

Fig 5.62 Test C2, photograph of cracked slab.

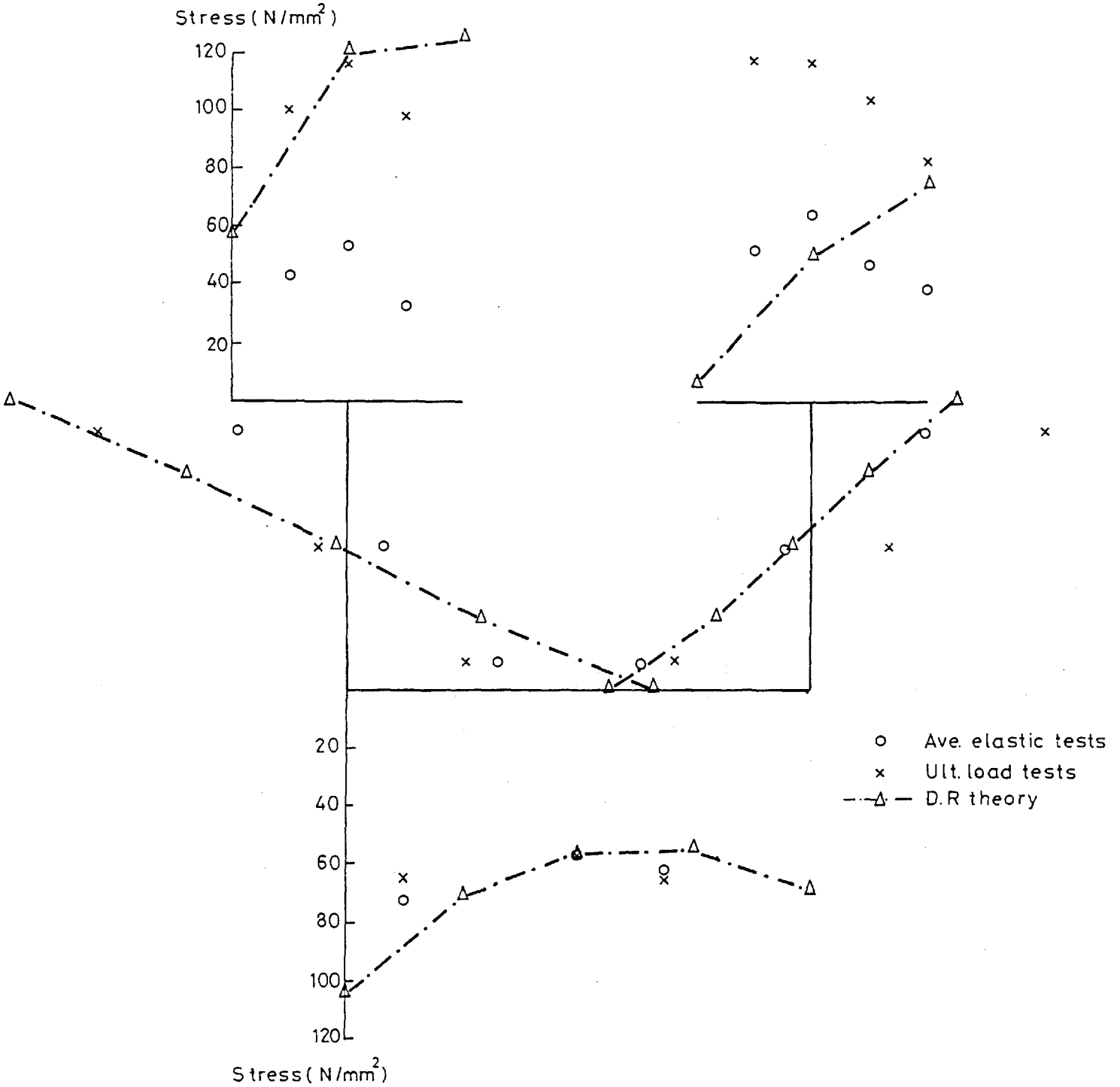

Fig 5·63 Test 02 Longitudinal stress distribution at gauged section 1 for 10 ton load

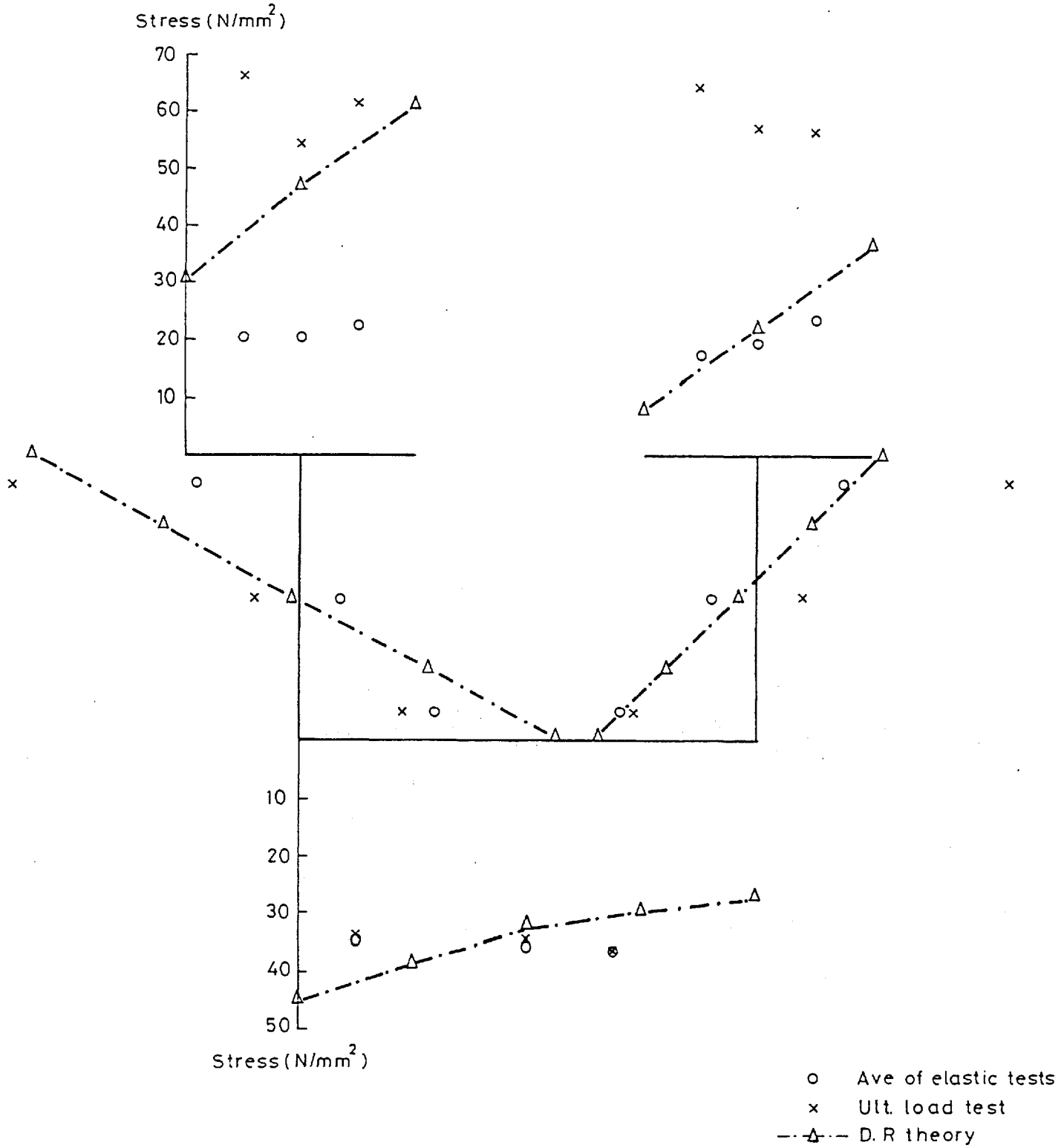

Fig 5·64 Test 02 Longitudinal stress distribution at gauged section 2 for 10 ton load

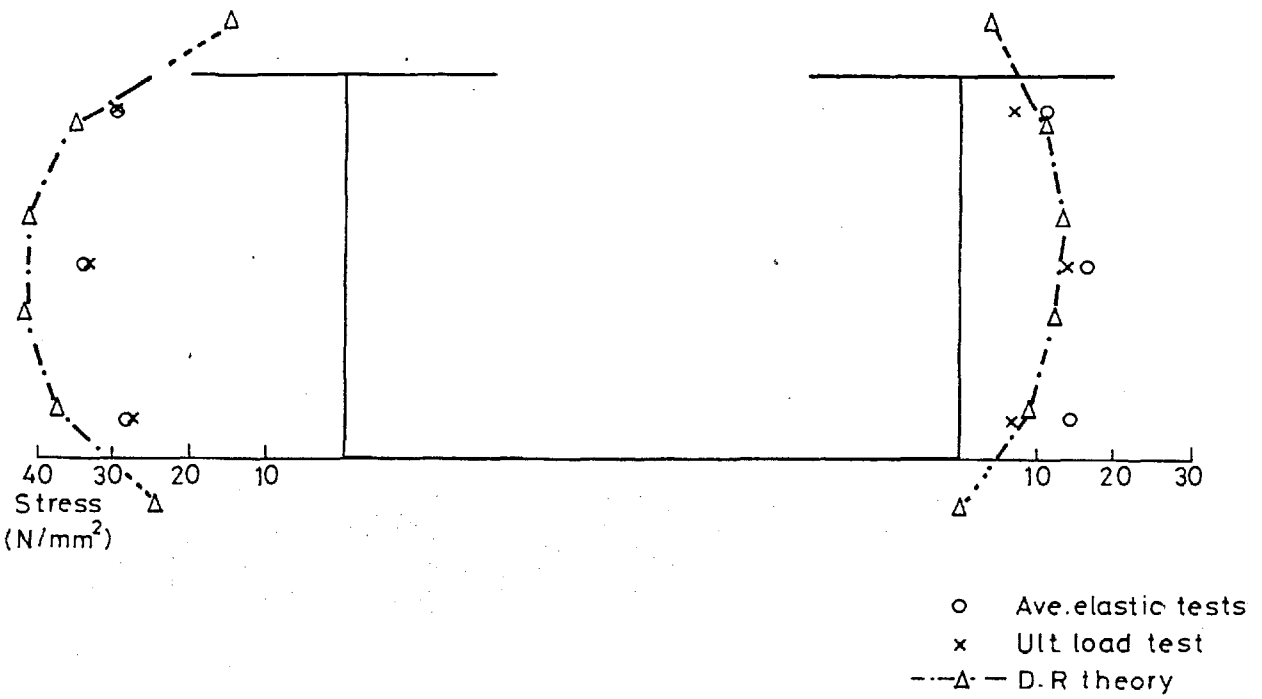

Fig 5·65 Test 02 Shear stress distribution at gauged section 1 for 10 ton end load

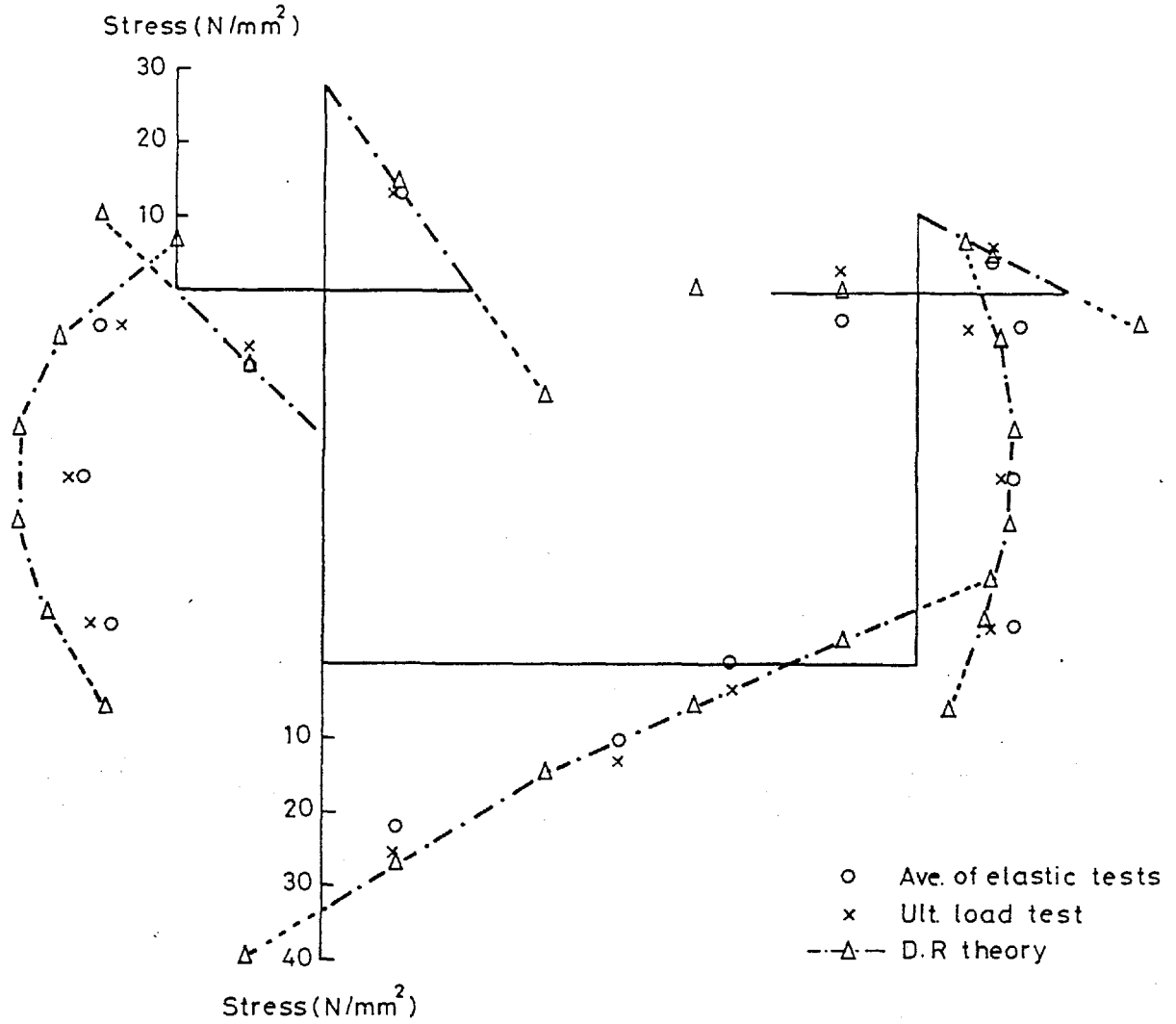

Fig 5·66 Test 02 Shear stress distribution at gauged section 2 for 10 ton load

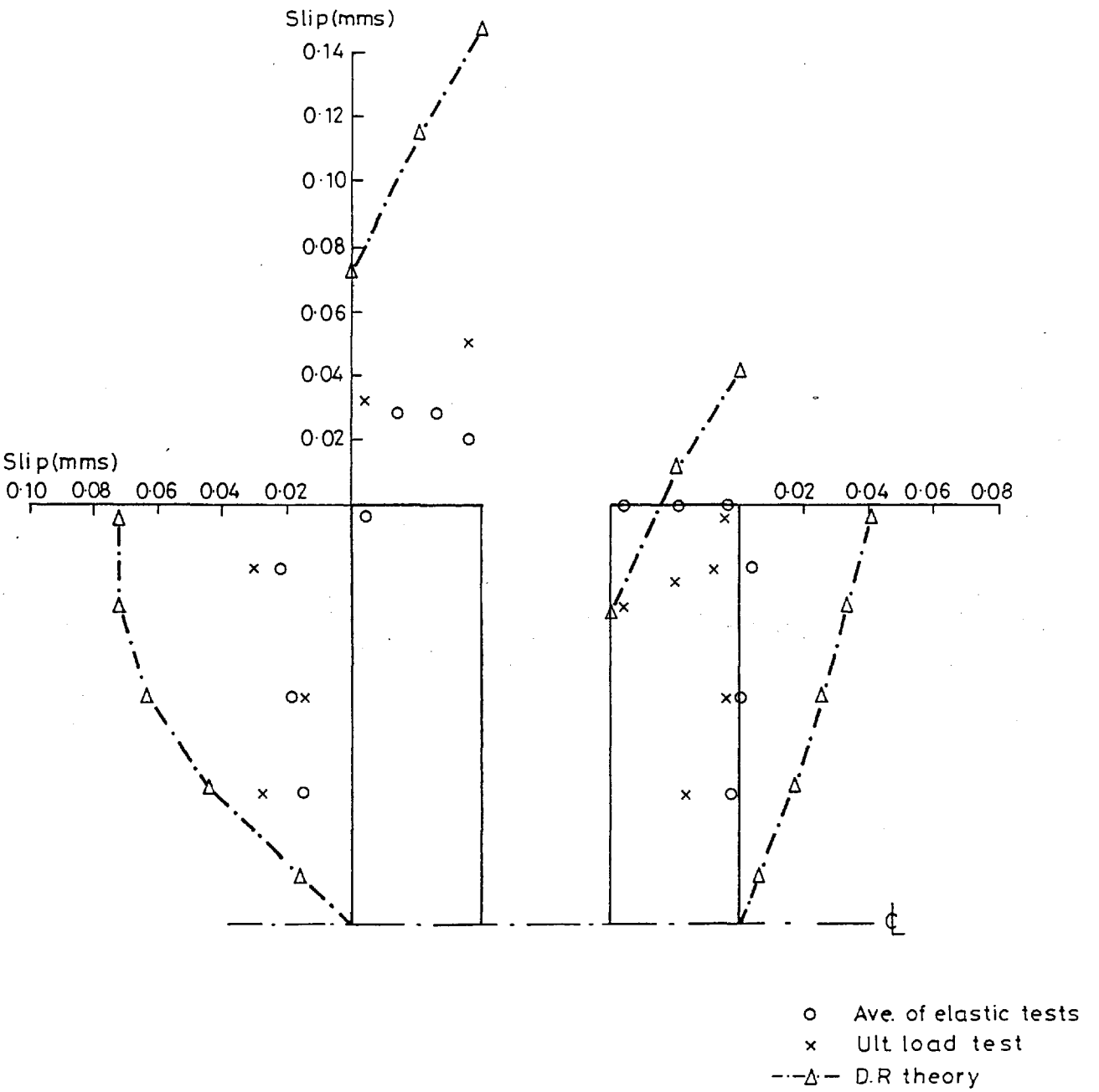

Fig 5·67 Test 02 Distribution of longitudinal slip for 10 ton load

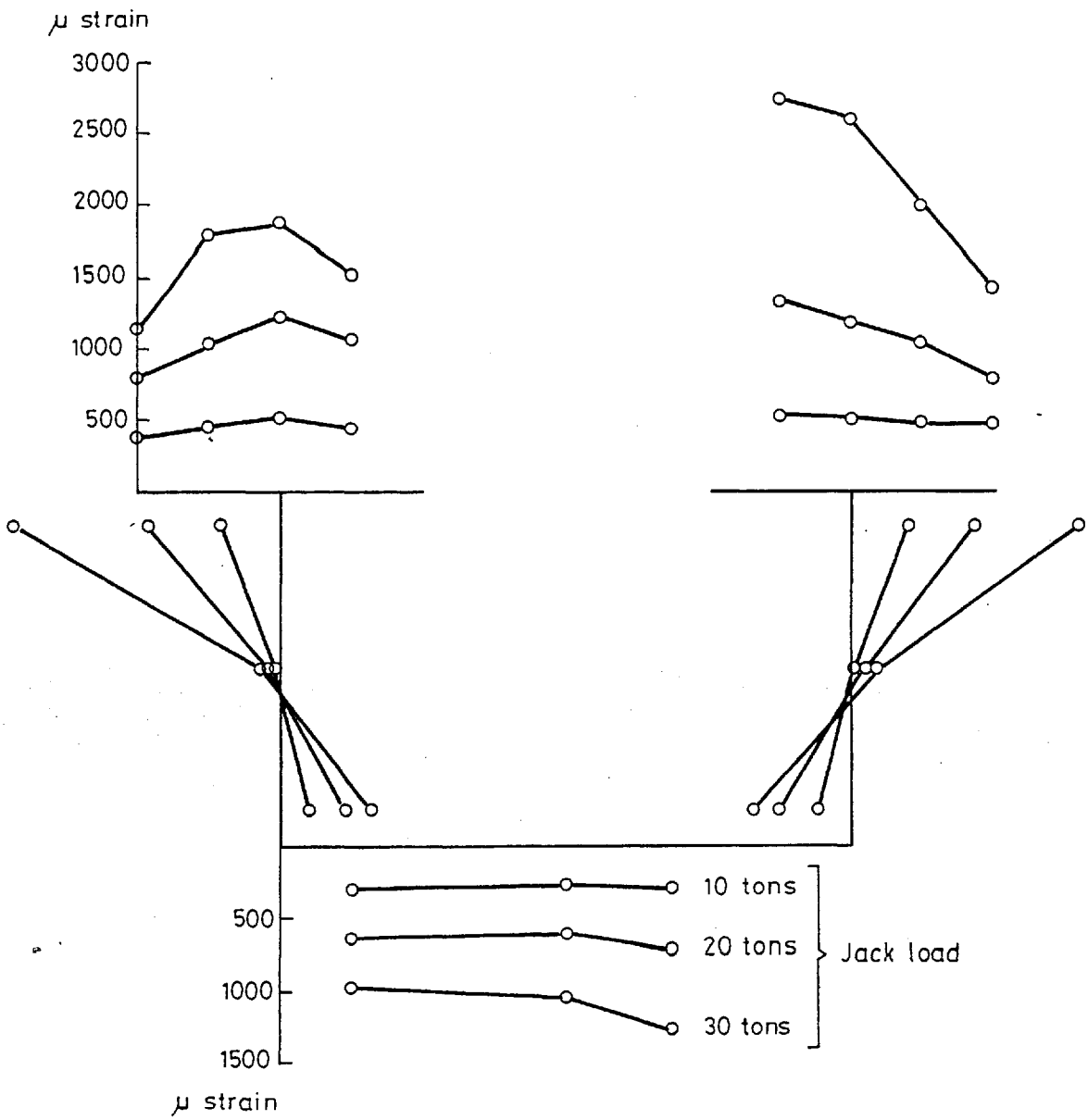

Fig 5·68 Test 02 Longitudinal strain distribution gauged section 1 for various applied loads

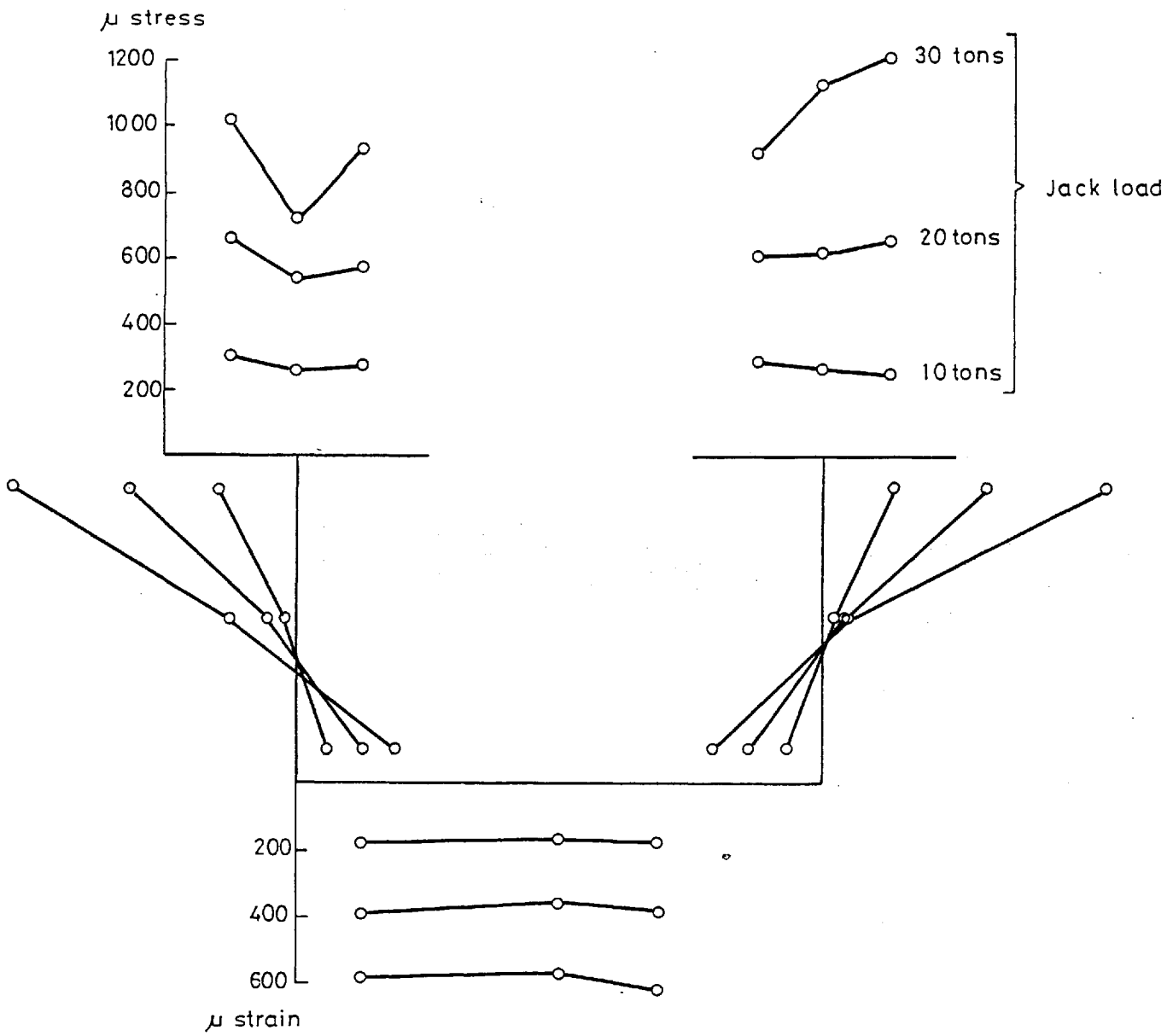

Fig 5·69 Test 02 Longitudinal strain distribution at gauged section 2 for various applied loads

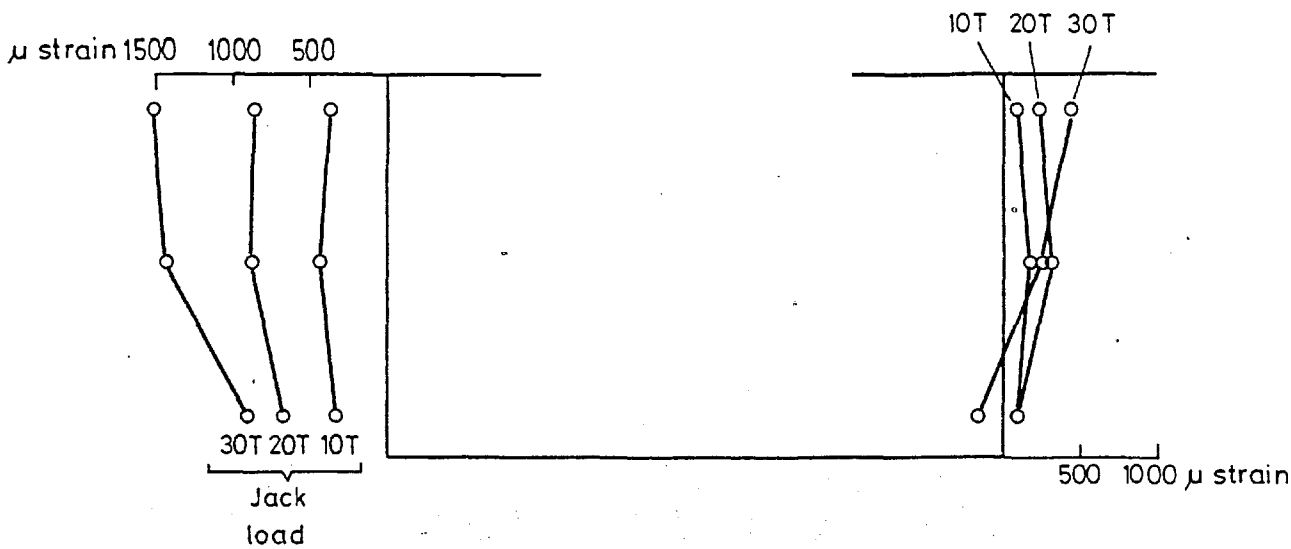

Fig 5·70 Test 02 Shear strain distribution at gauged section 1 for various applied loads

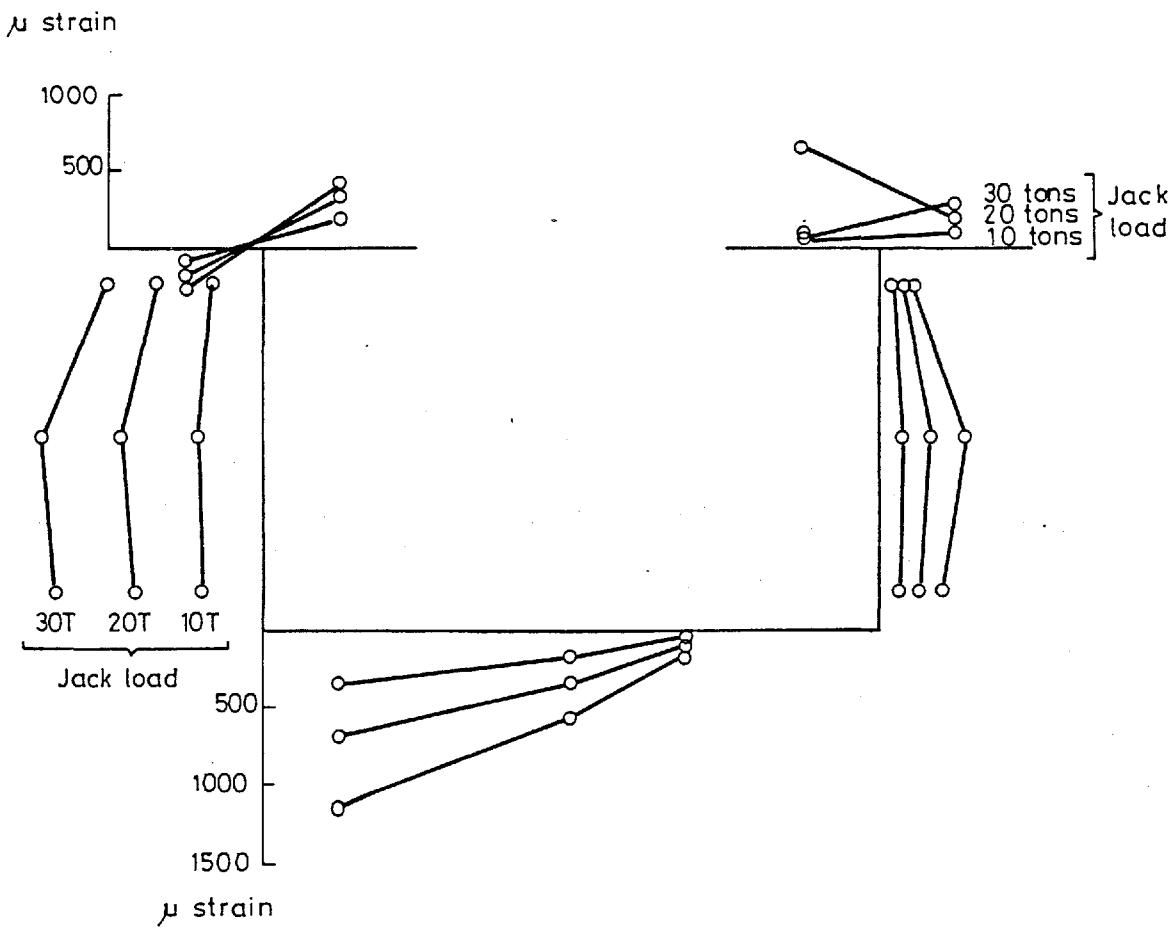

Fig 5·71 Test 02 Shear strain distribution at gauged section 2 for various loads

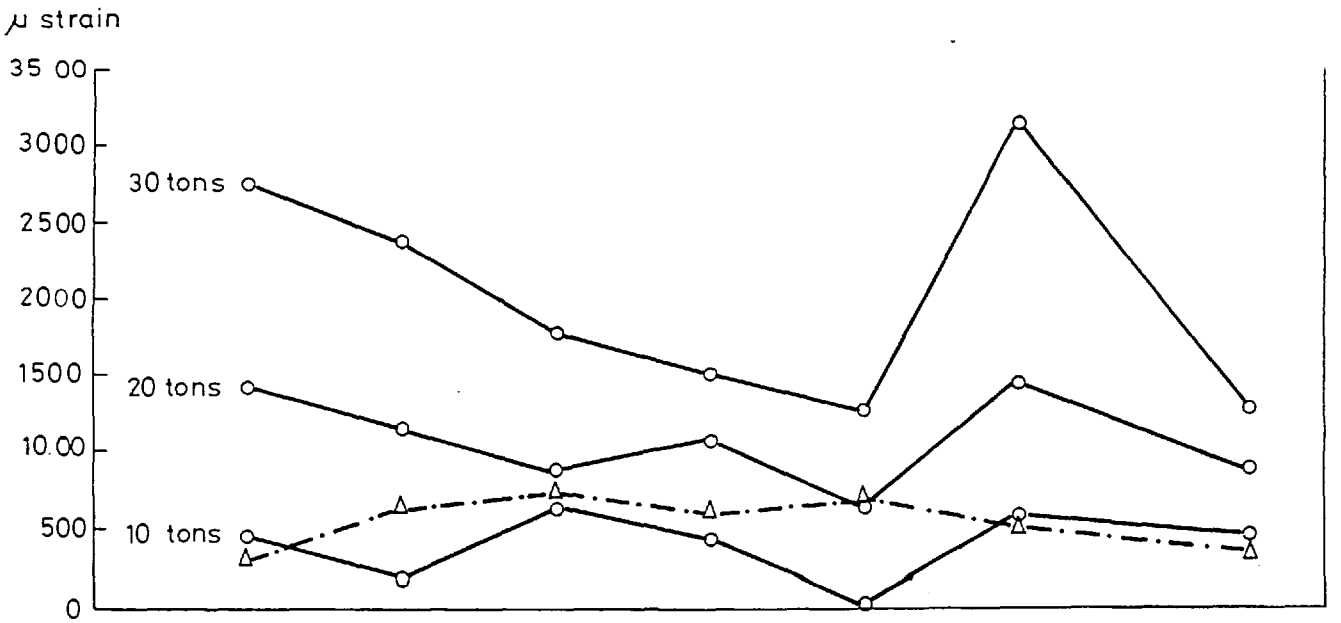

Fig 5·72 Test 02 Longitudinal slab strains at gauged section 1 for various loads

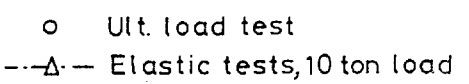

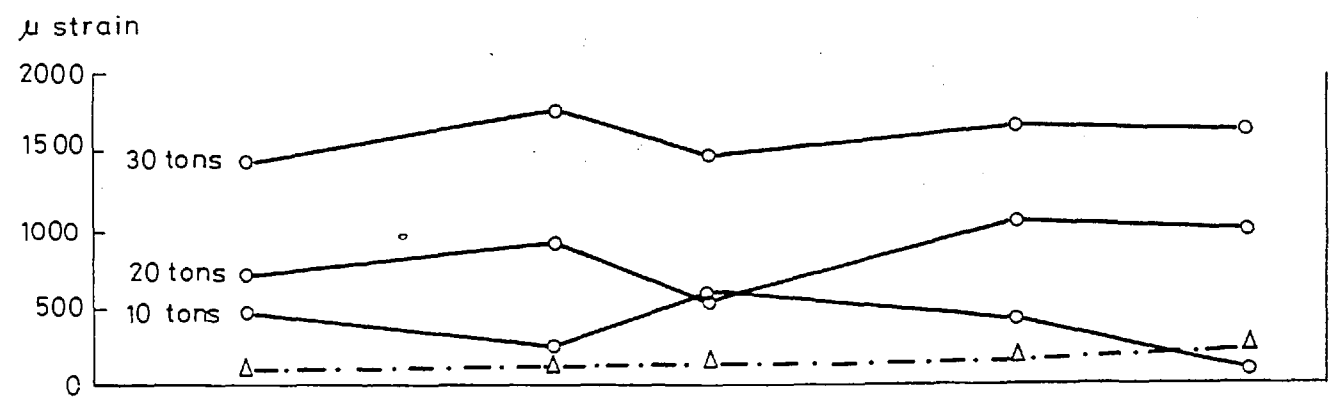

Fig 5·73 Test 02 Longitudinal slab strains at gauged section 2 for various loads

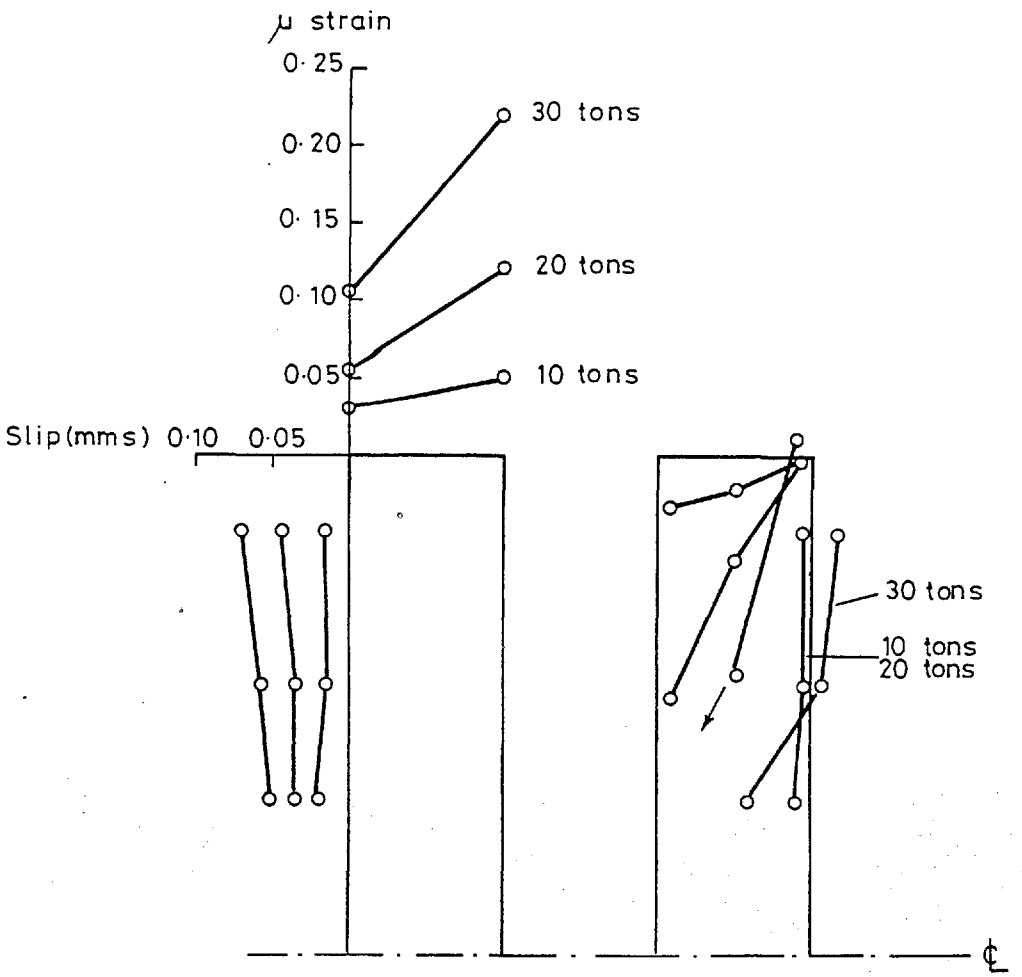

Fig 5·74 Test 02 Longitudinal slip distribution for various applied loads

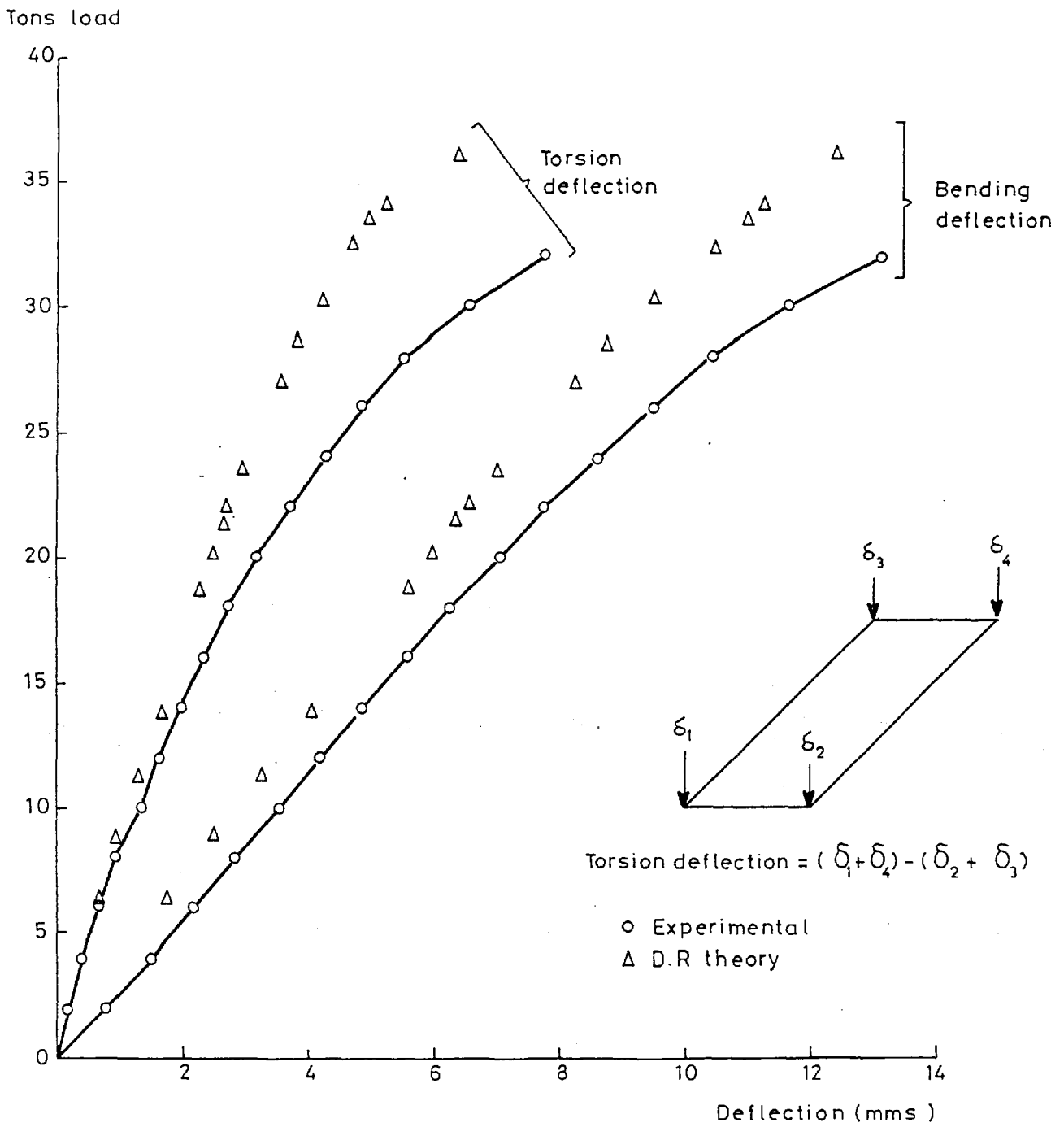

Fig 5·75 Test 02 Load-deflection curves

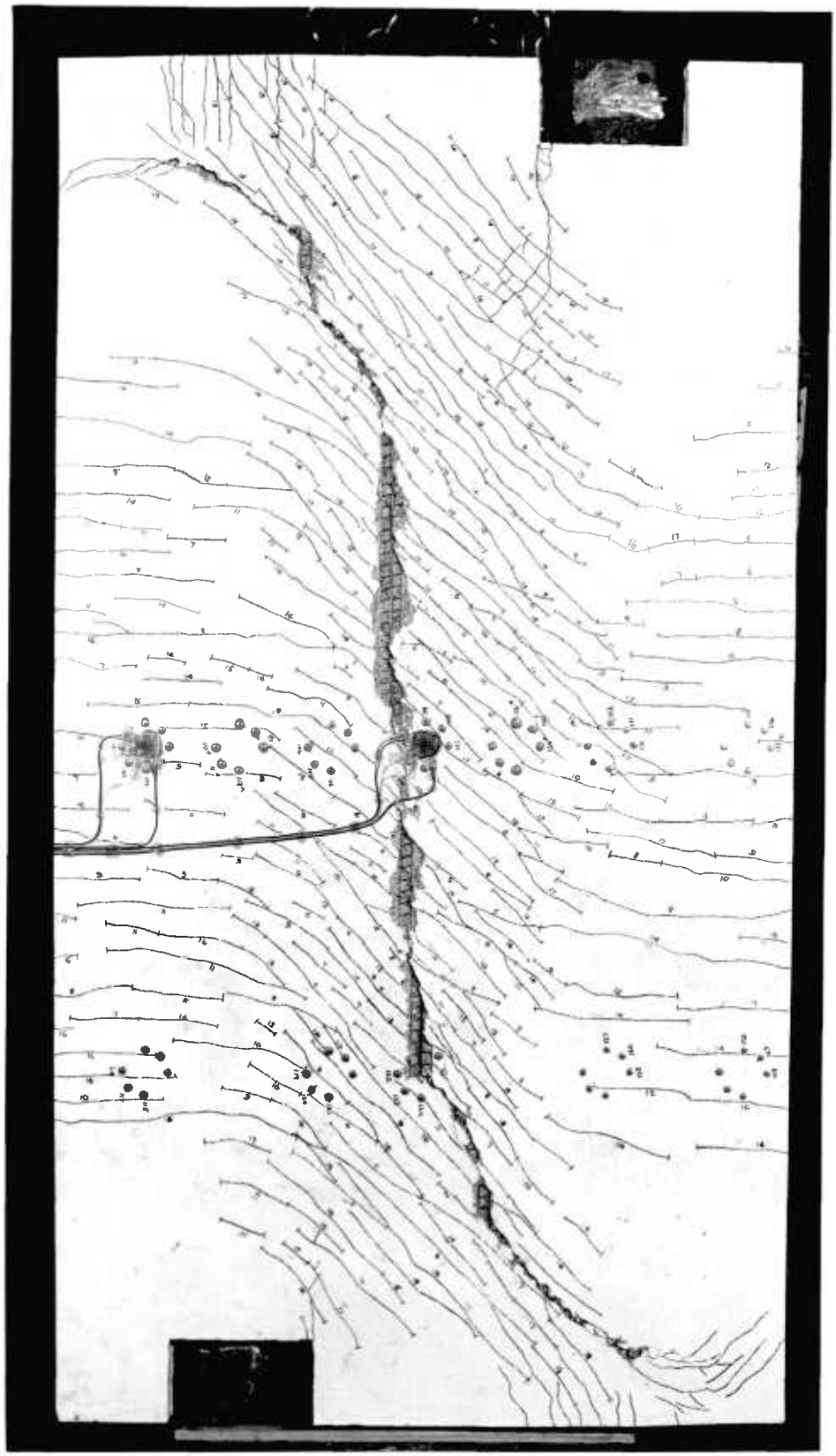

Fig 5.76 Test O2, photograph of cracked slab.

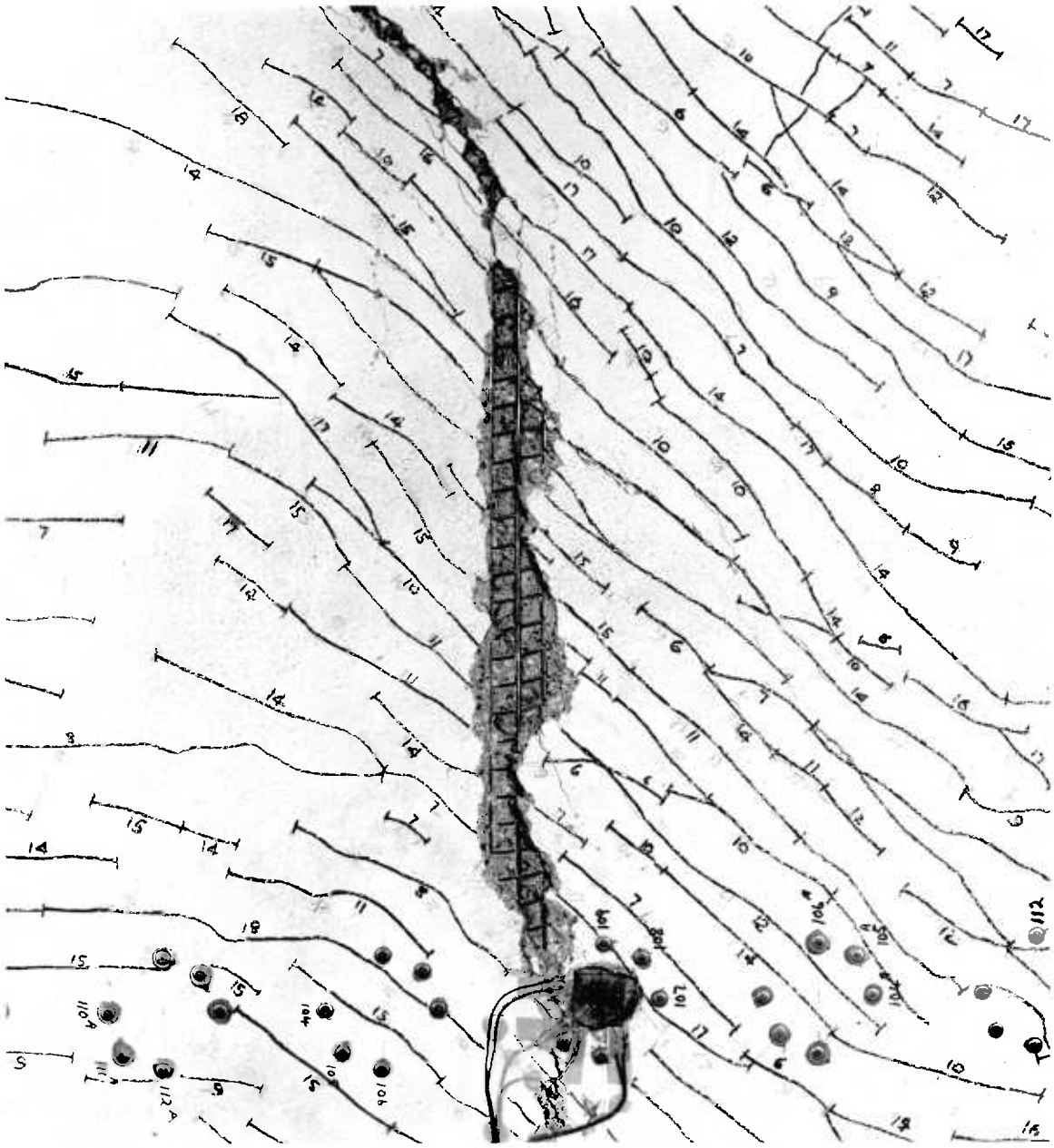

Fig 5.76A Test O2, detail of cracked slab.

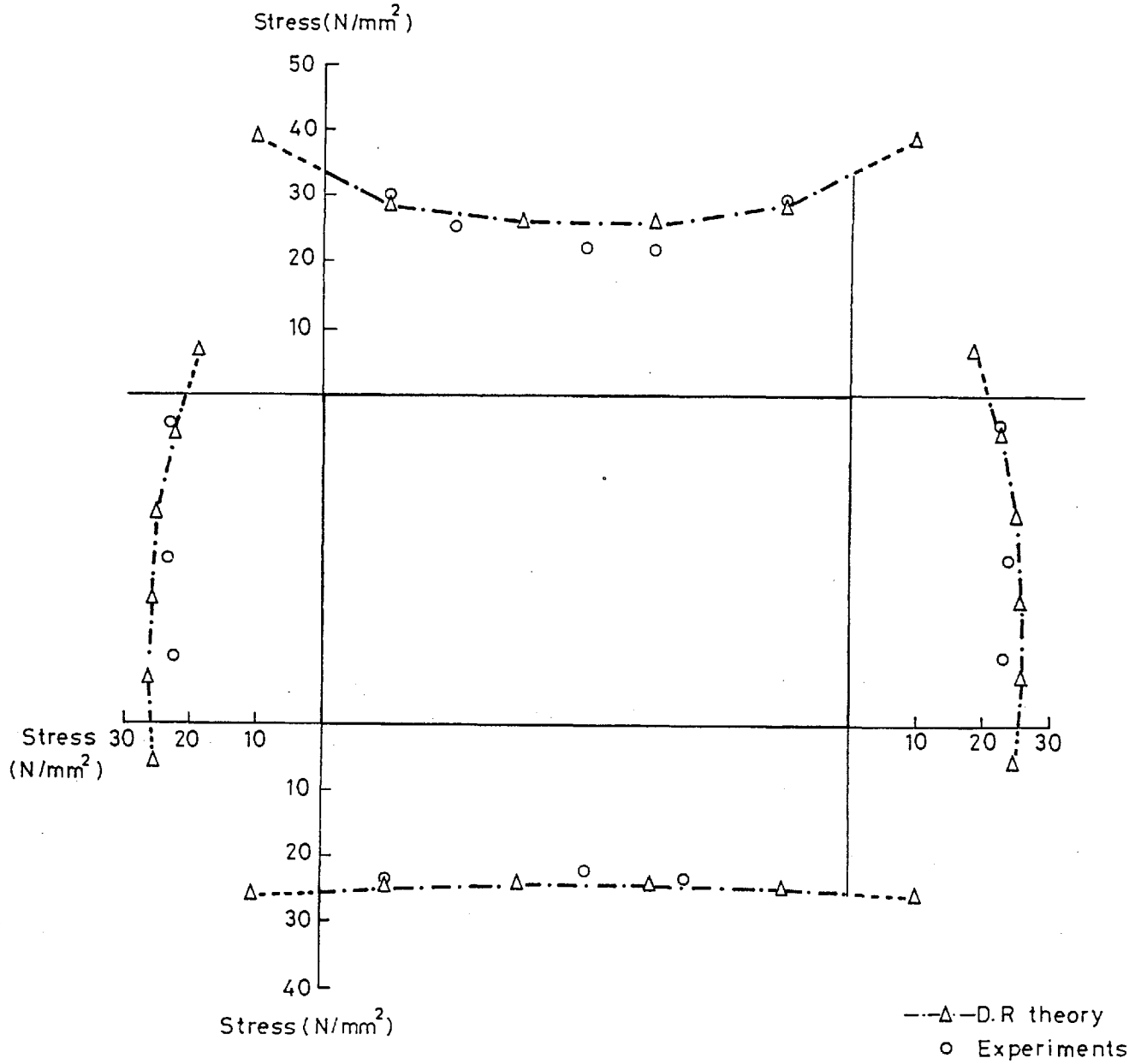

Fig 5·77 Test C3 Shear stress distribution at gauged section 1 for 10 ton jack load

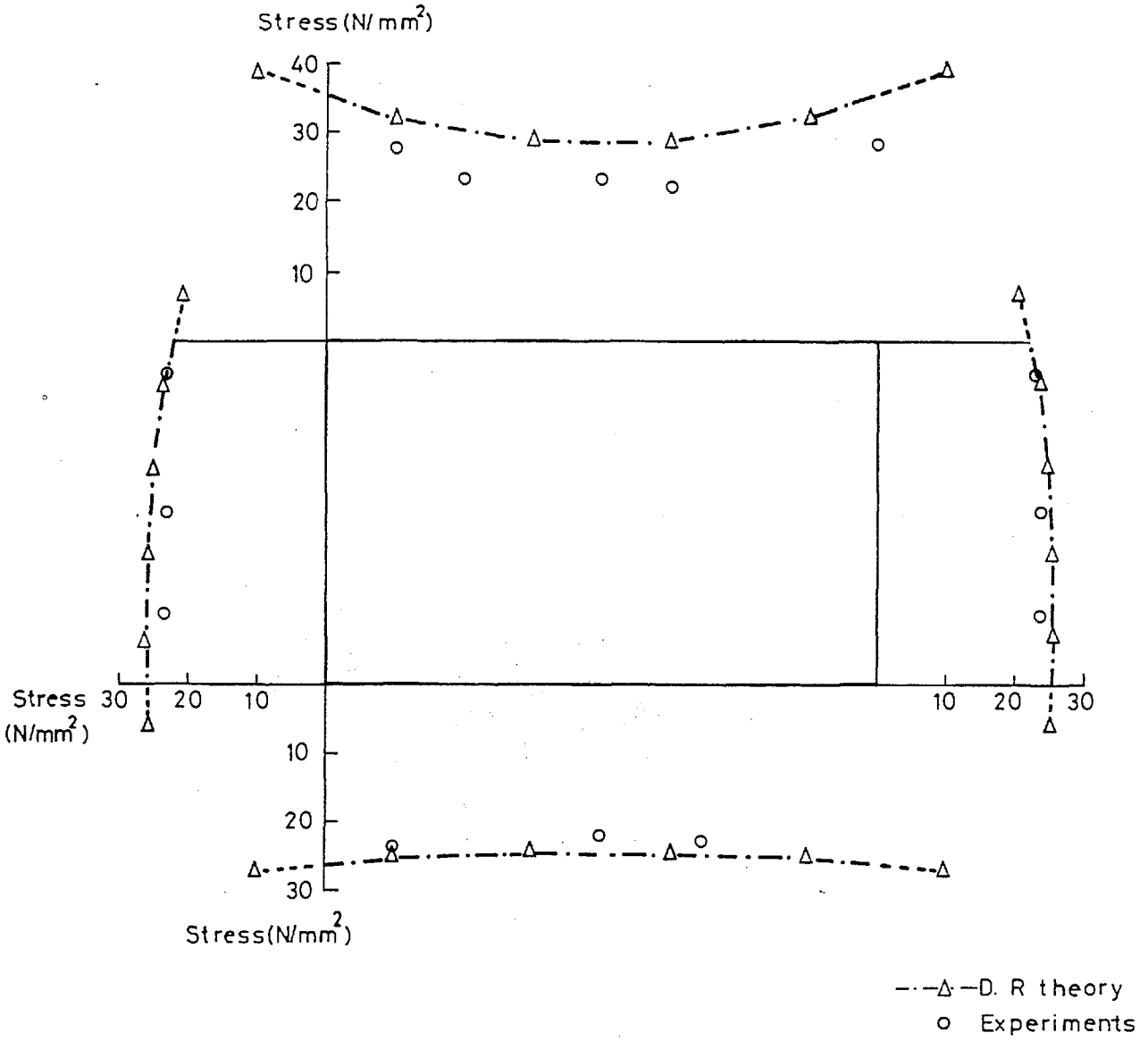

Fig 5·78 Test C3 Shear stress distribution at gauged section 2 for 10 ton jack load

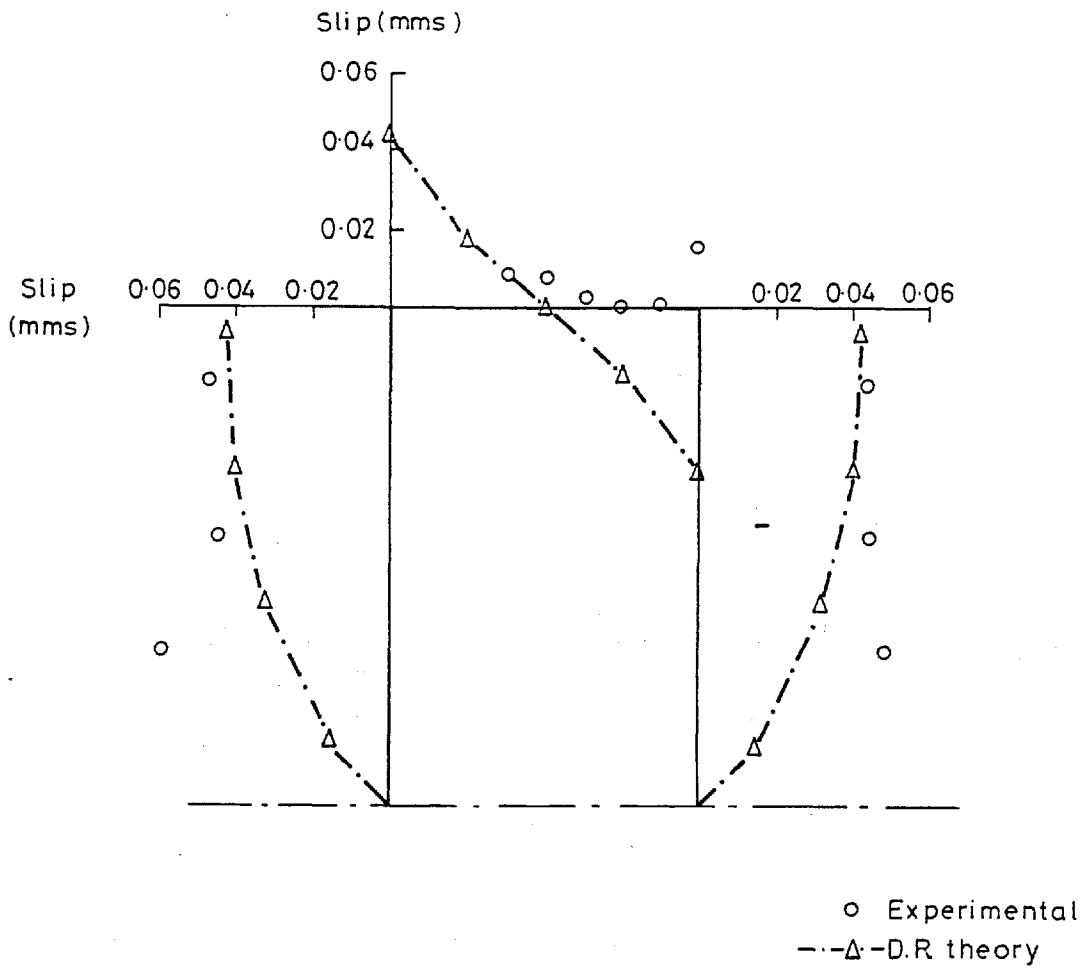

Fig 5·79 Test C3 Longitudinal slip distribution for 10 ton jack load.

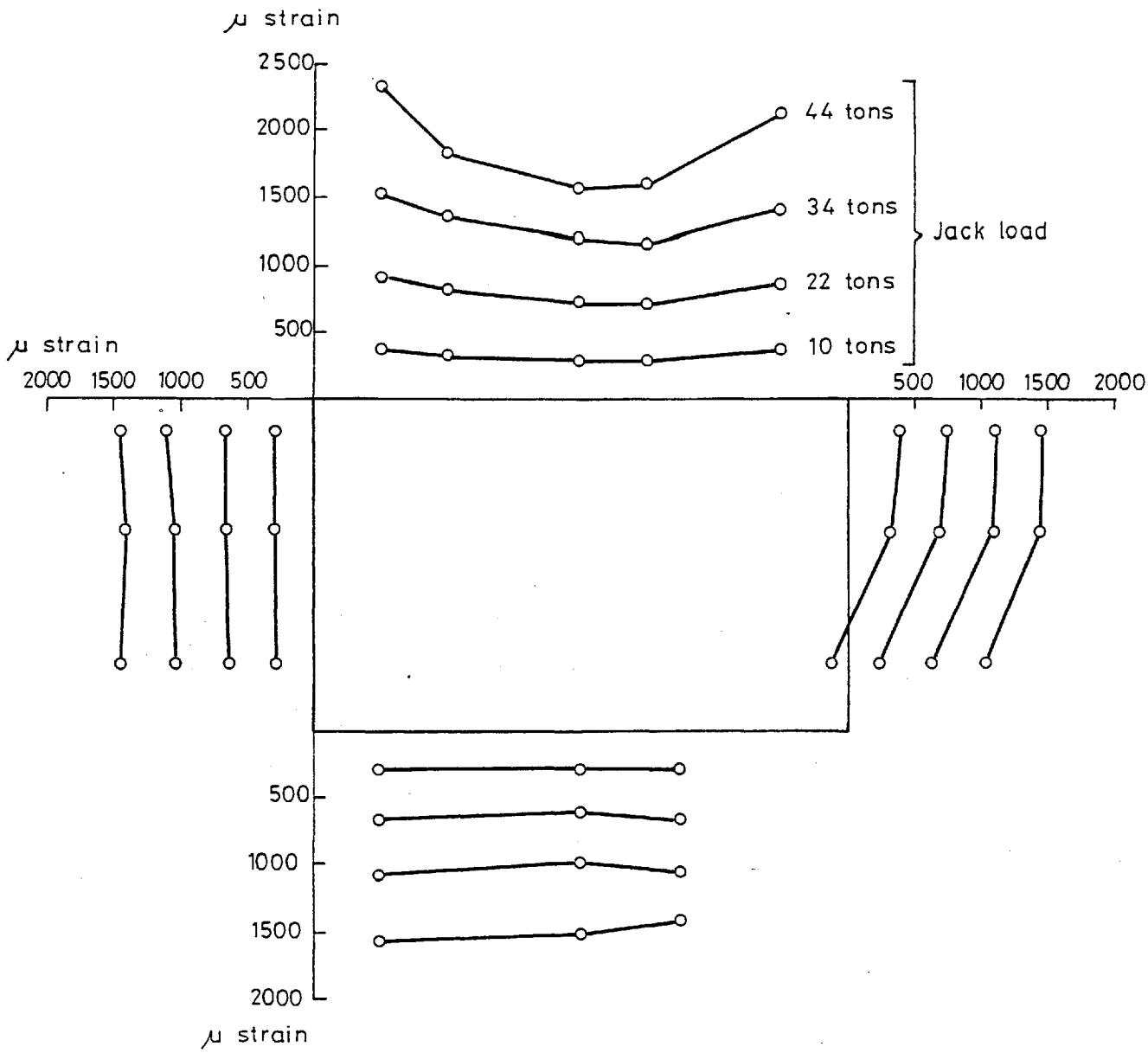

Fig 5·80 Test C3 Shear strain distribution at gauged section 1 for various applied loads

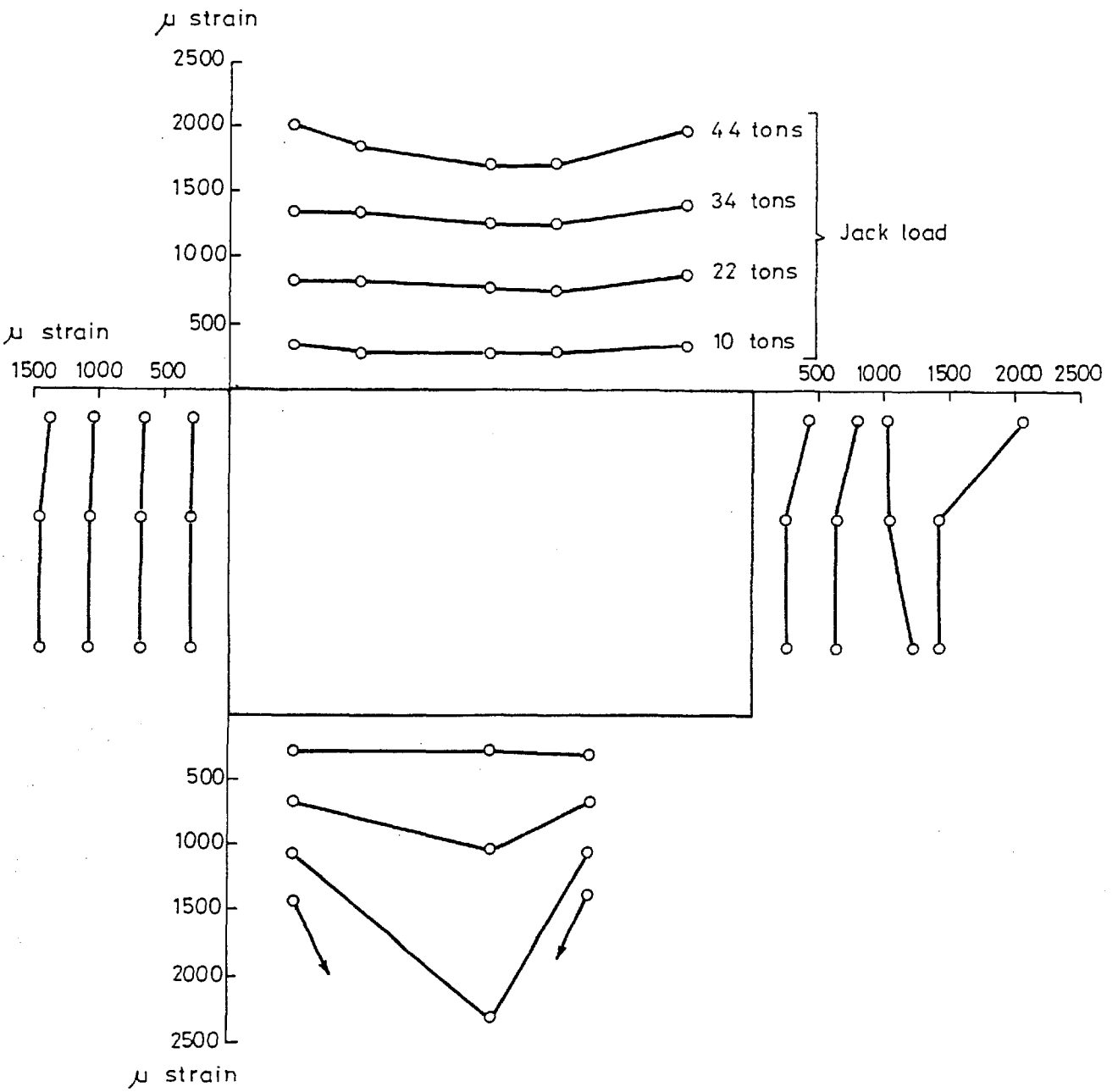

Fig 5·81 Test C3 Shear strain distribution at gauged section 2 for various applied loads

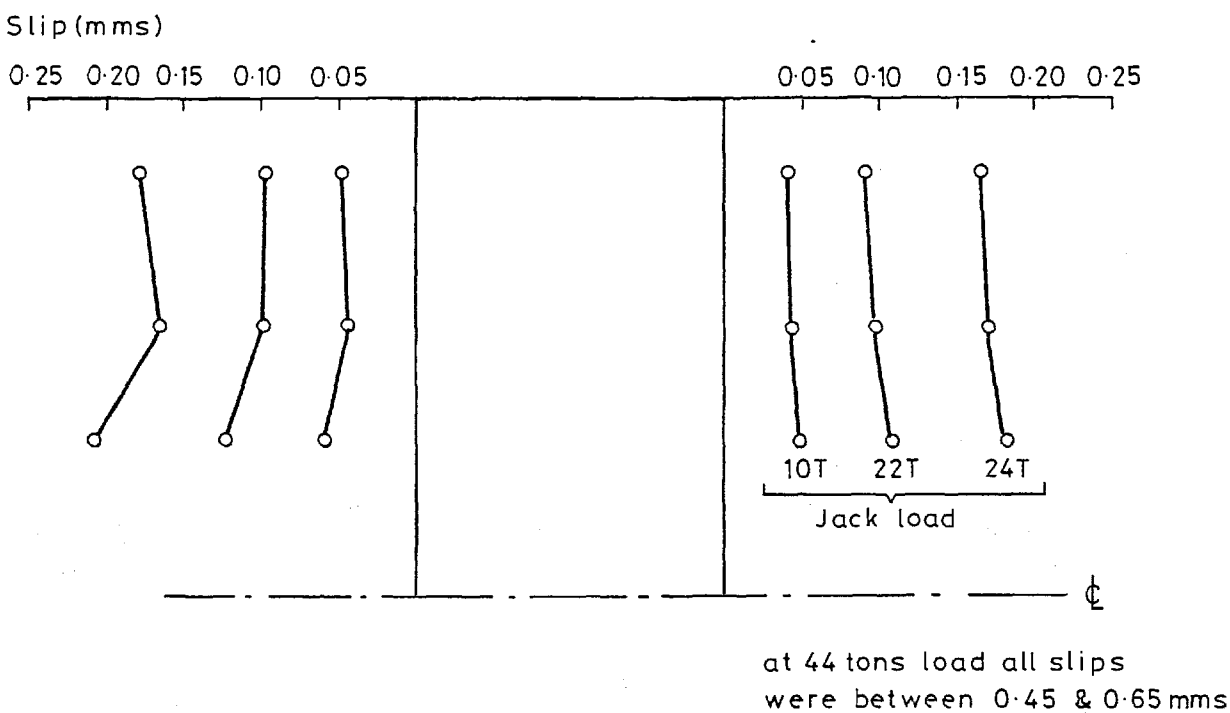

Fig 5·82 Test C3 Distribution of longitudinal slip for various applied loads

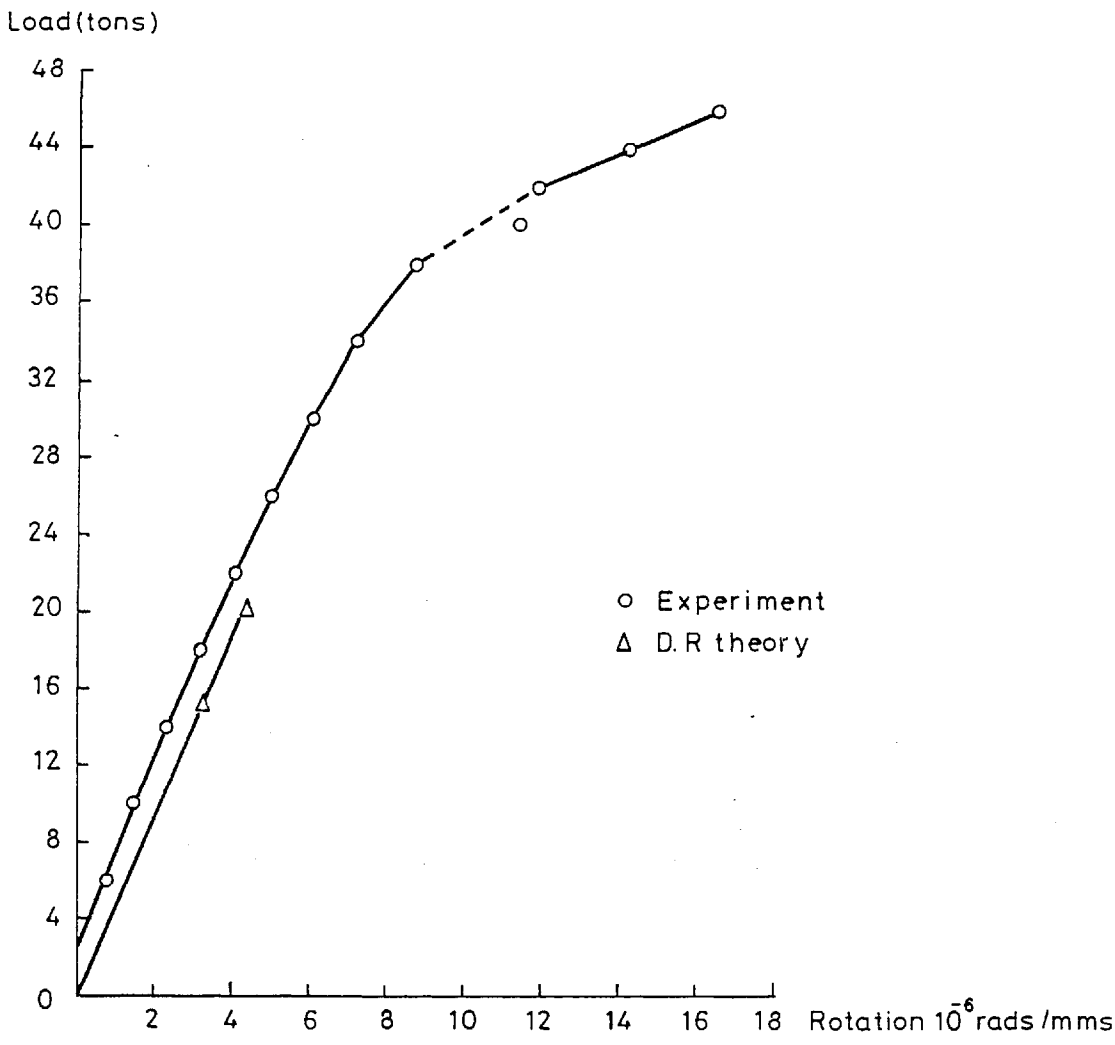

Fig 5·82a Test C3 Load-rotation curves

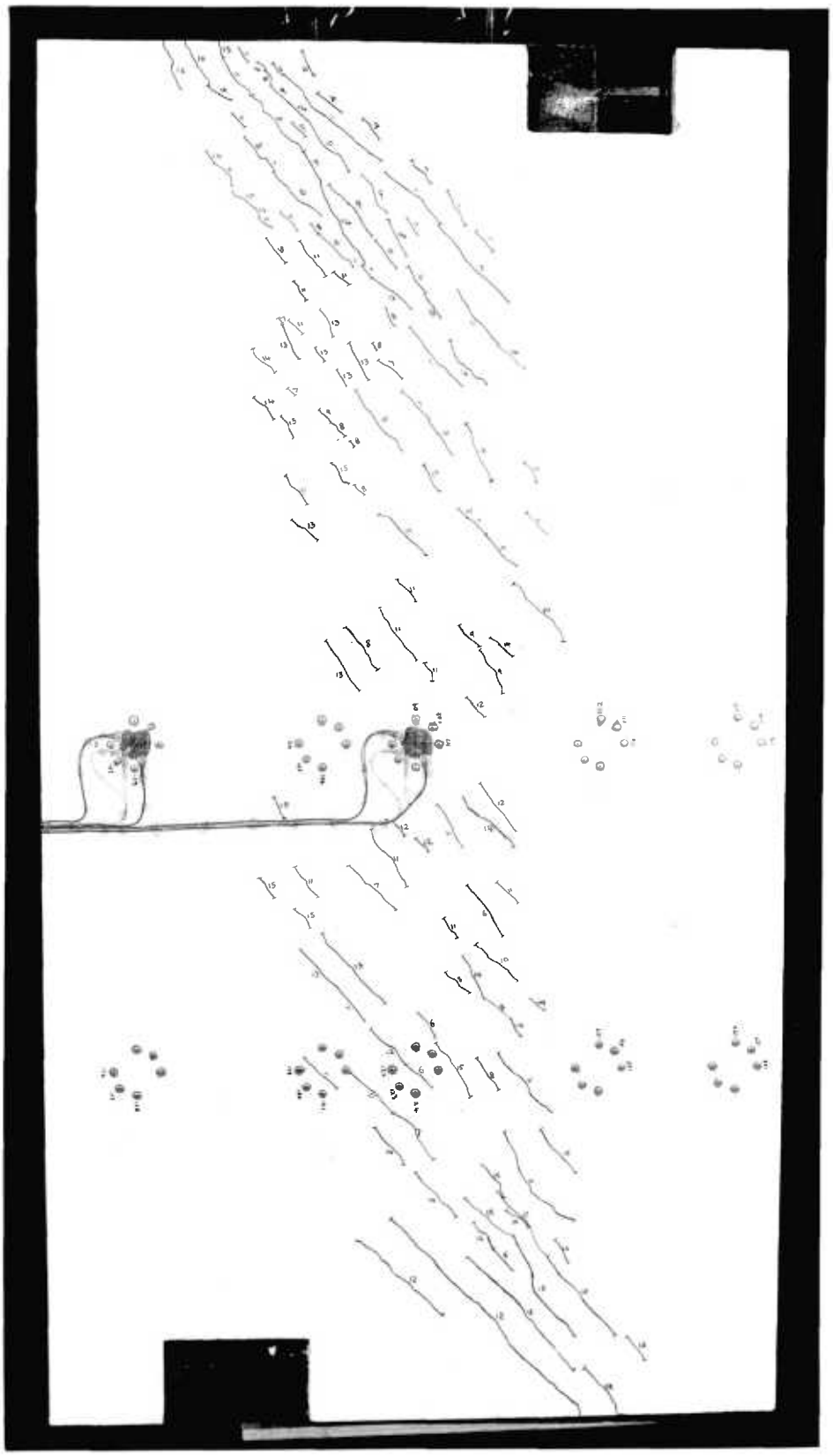

Fig 5.83 Test C3 photograph of cracked slab.

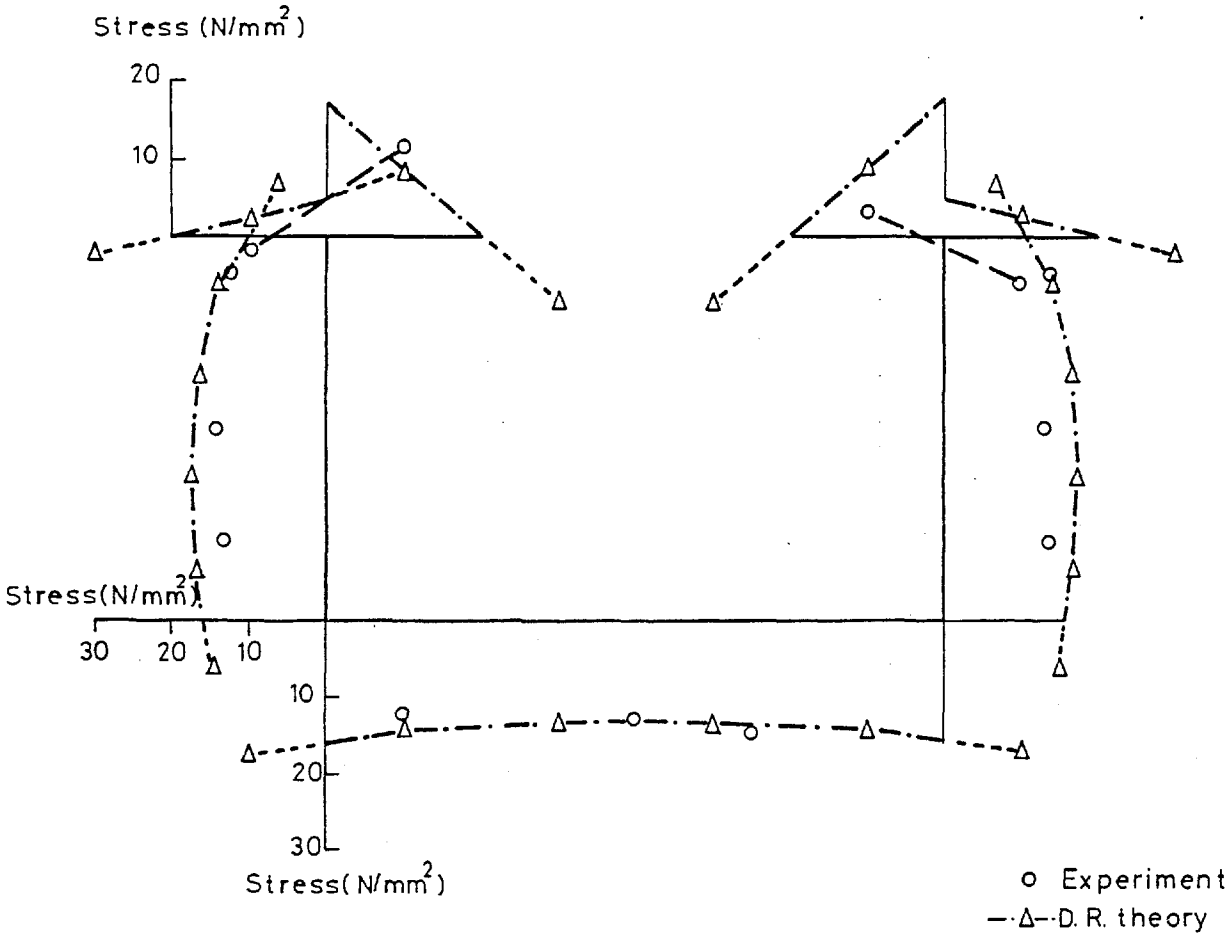

Fig 5·84 Test 03 Shear stress distribution at gauged section 1 for 6 ton jack load

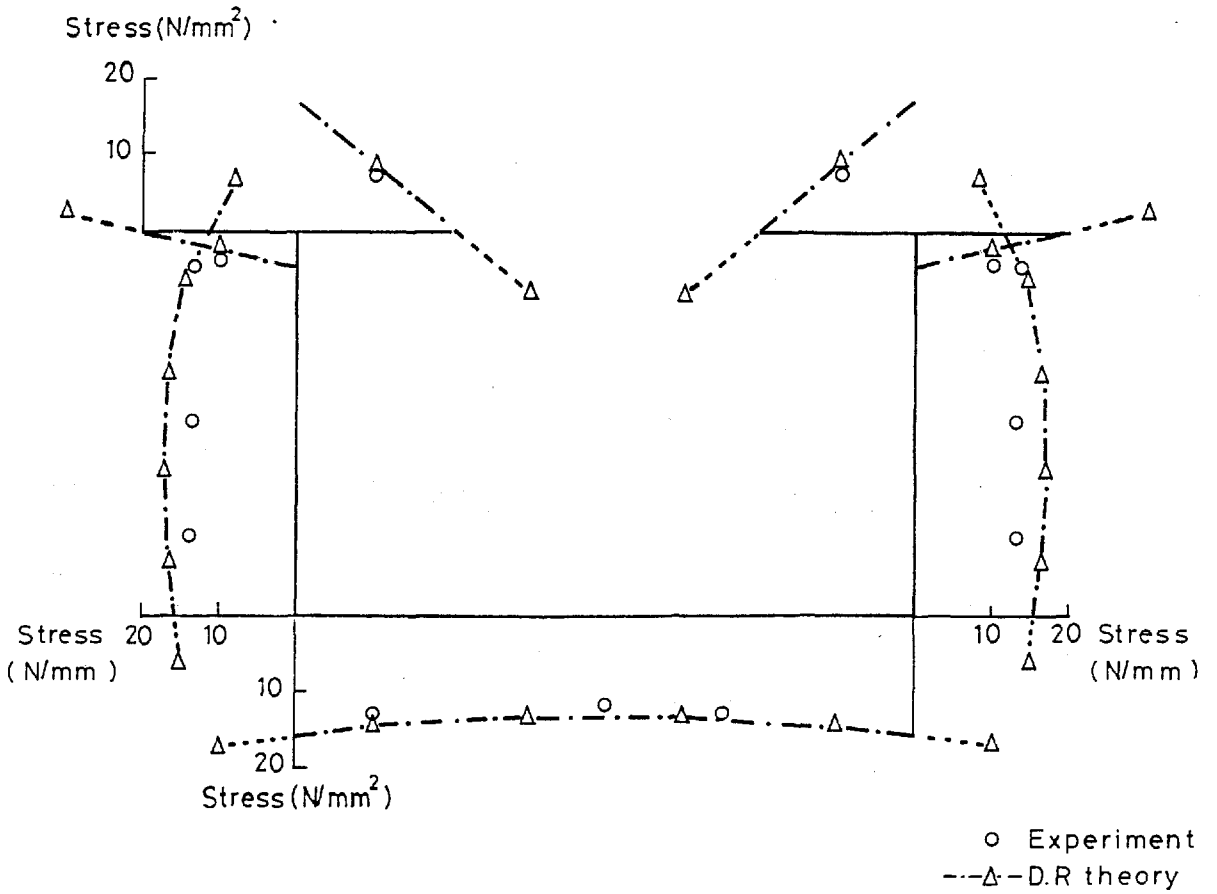

Fig 5·85 Test 03 Shear stress distribution for 6 ton jack load

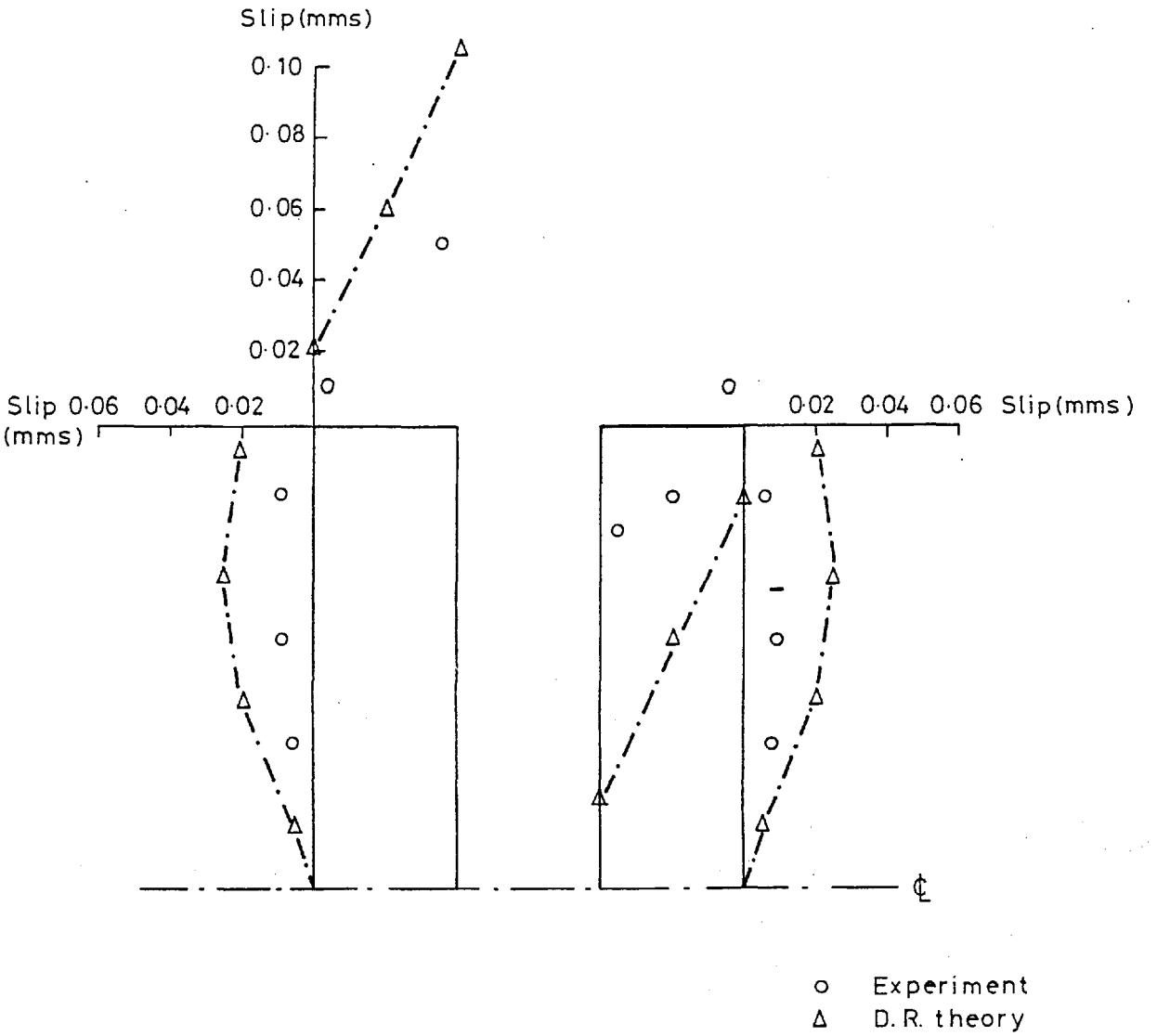

Fig 5·86 Test 03 Longitudinal slip distribution for 6 ton jack load

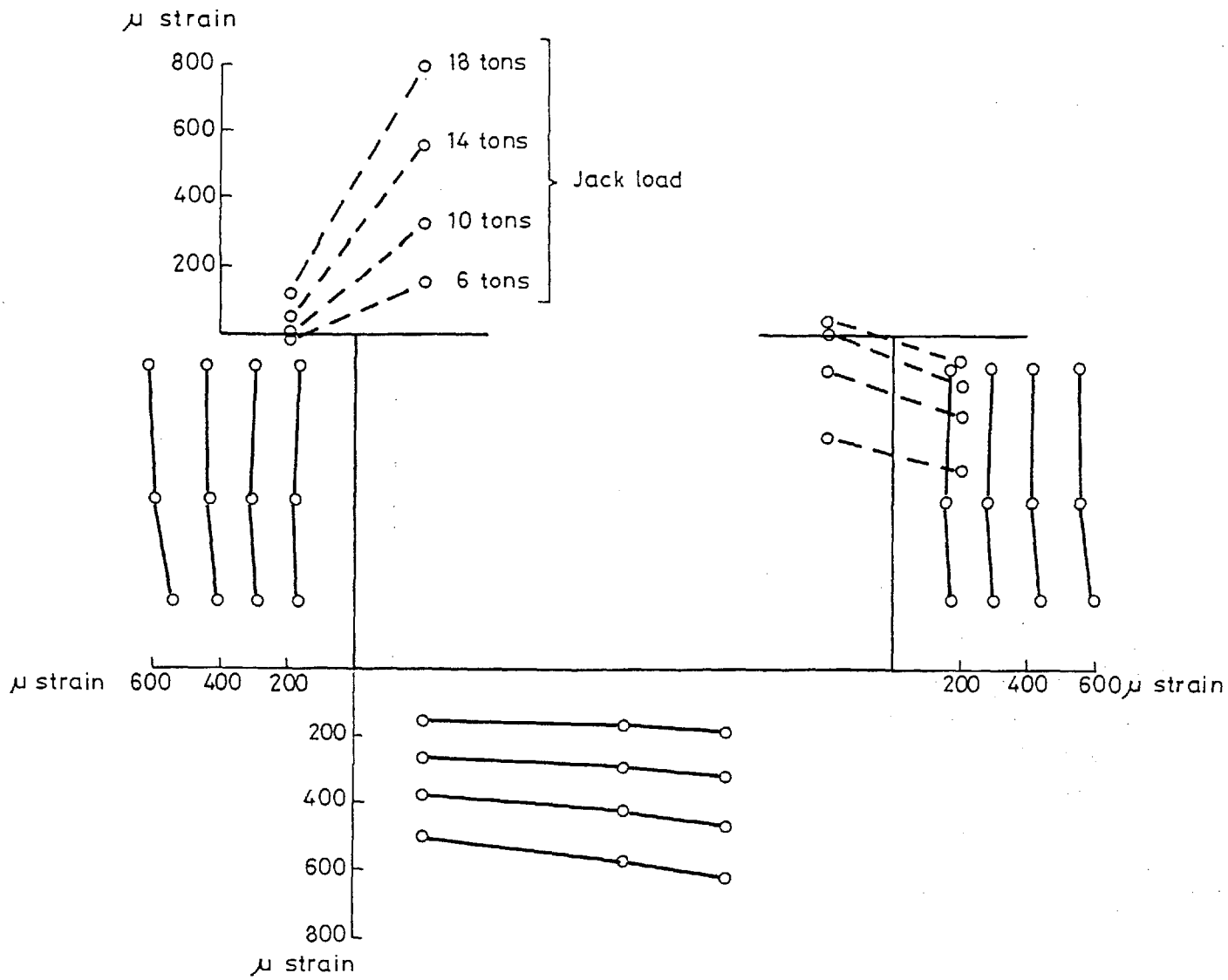

Fig 5·87 Test 03 Shear strain distribution at section 1 for various applied loads

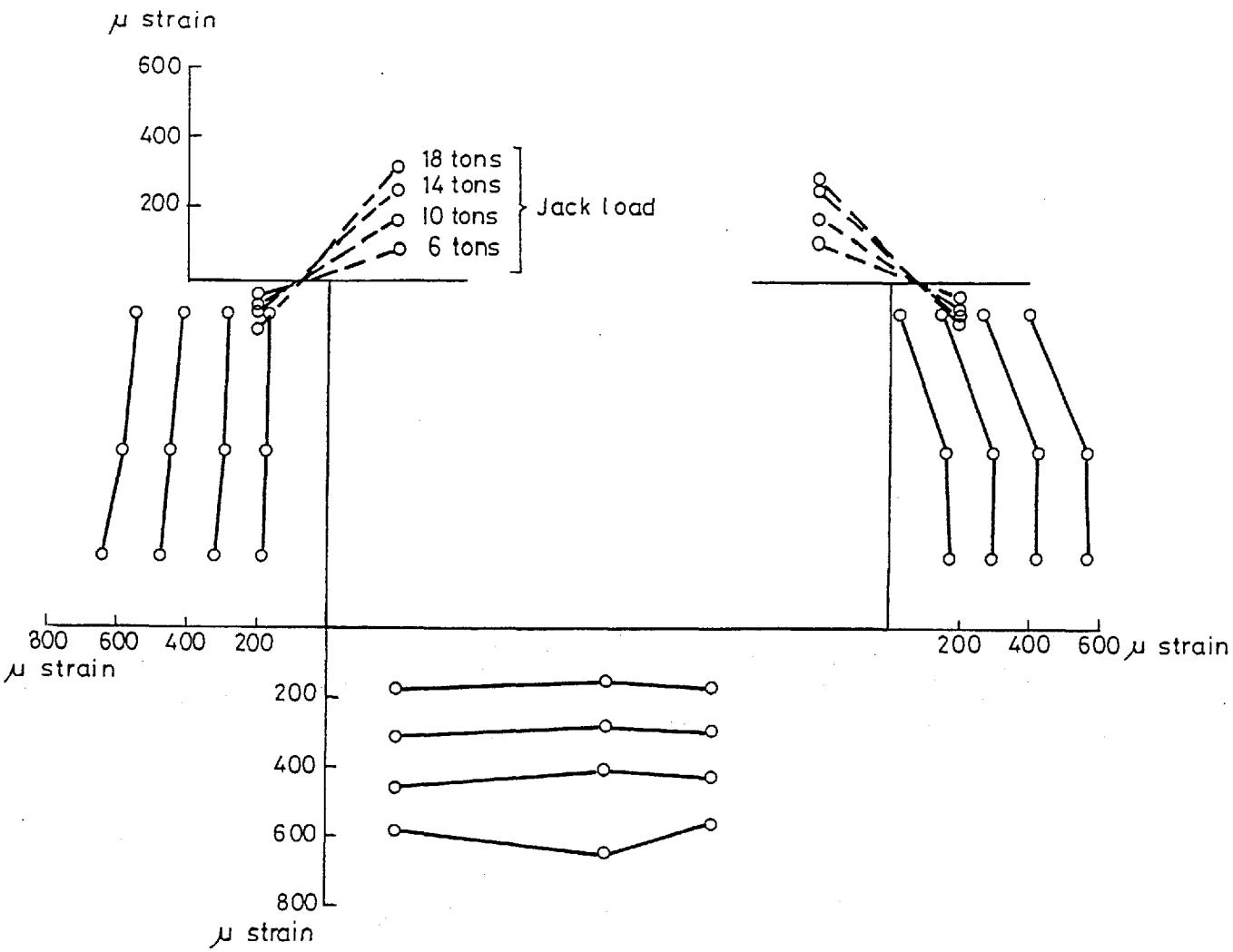

Fig 5·88 Test 03 Shear strain distribution at gauged section 2 for various applied loads

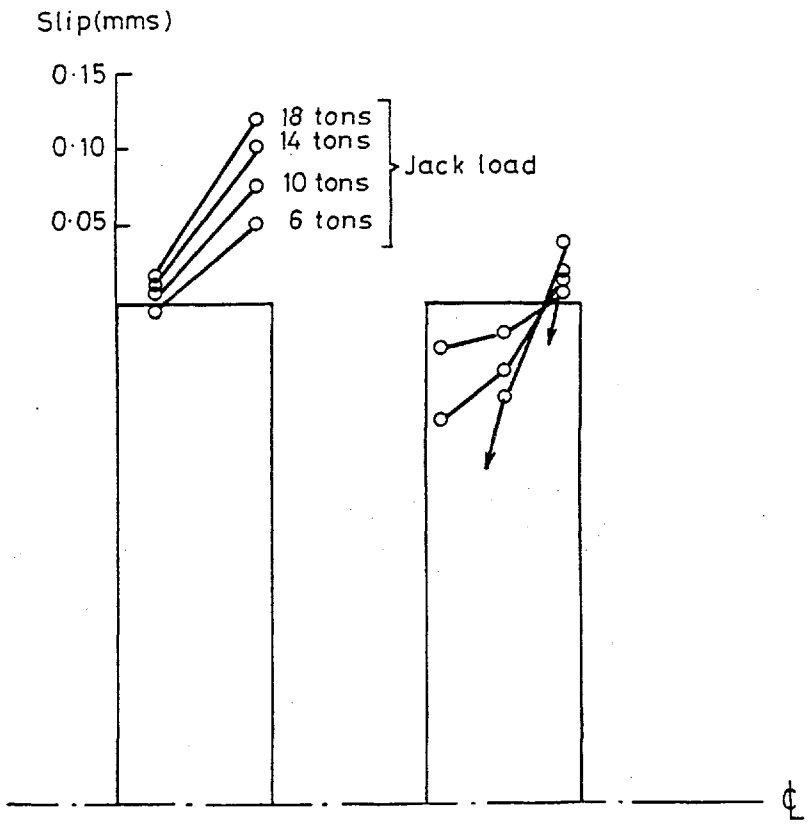

Fig 5·89 Test 03 Distribution of longitudinal slip at box end for various applied loads

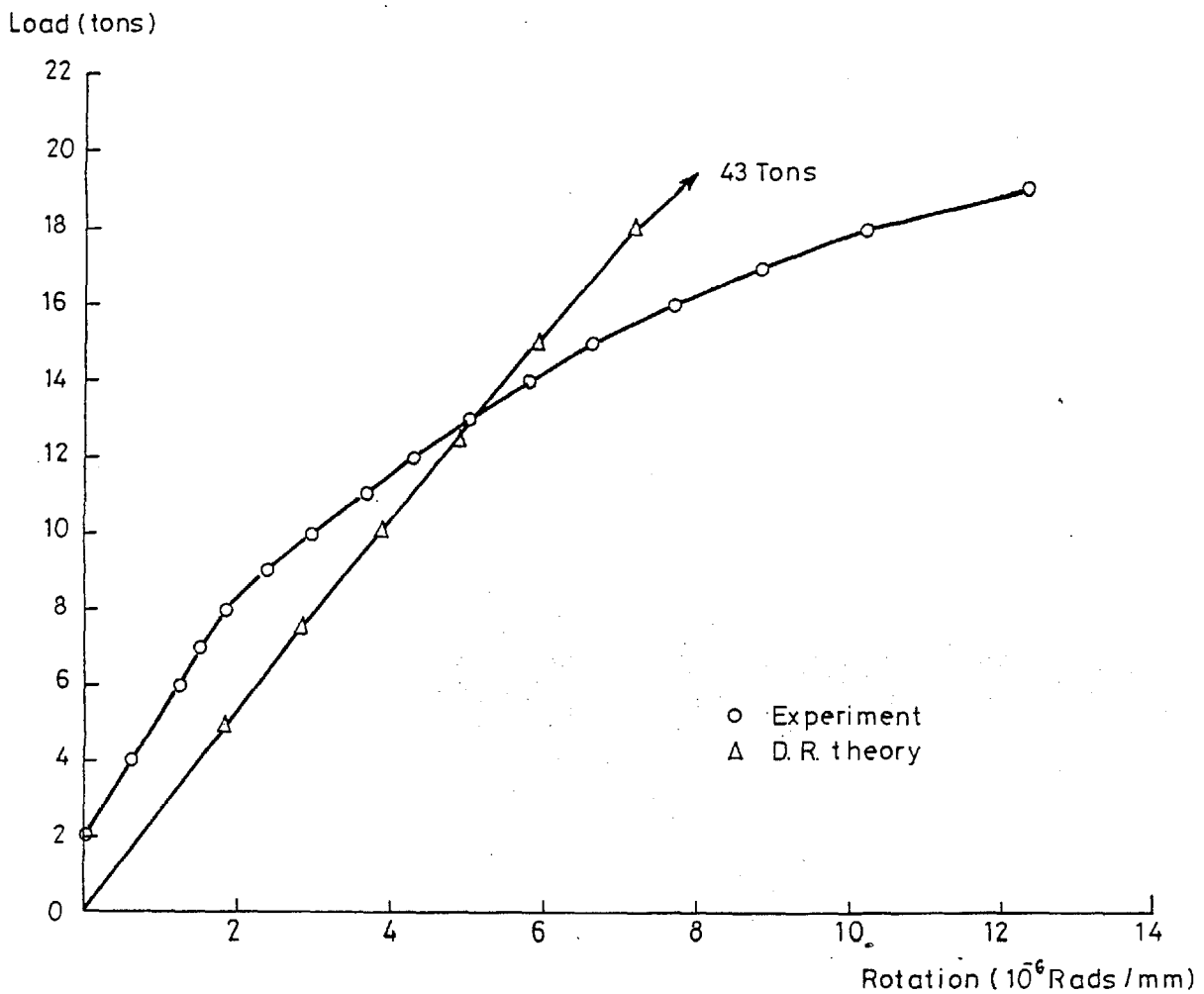

Fig 5·90 Test 03 Load-rotation curves

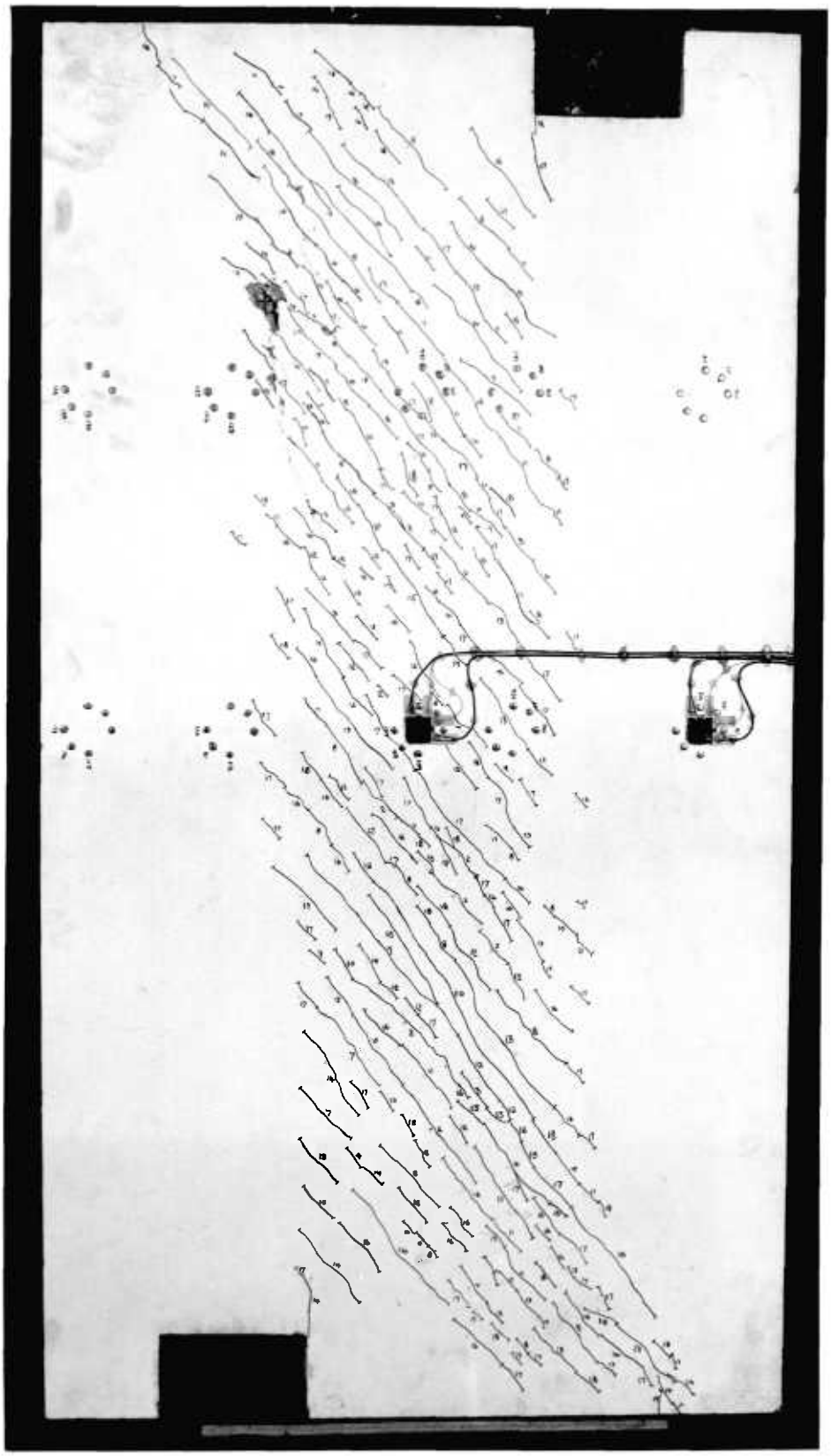

Fig 5.91 Test 03 photograph of cracked slab.

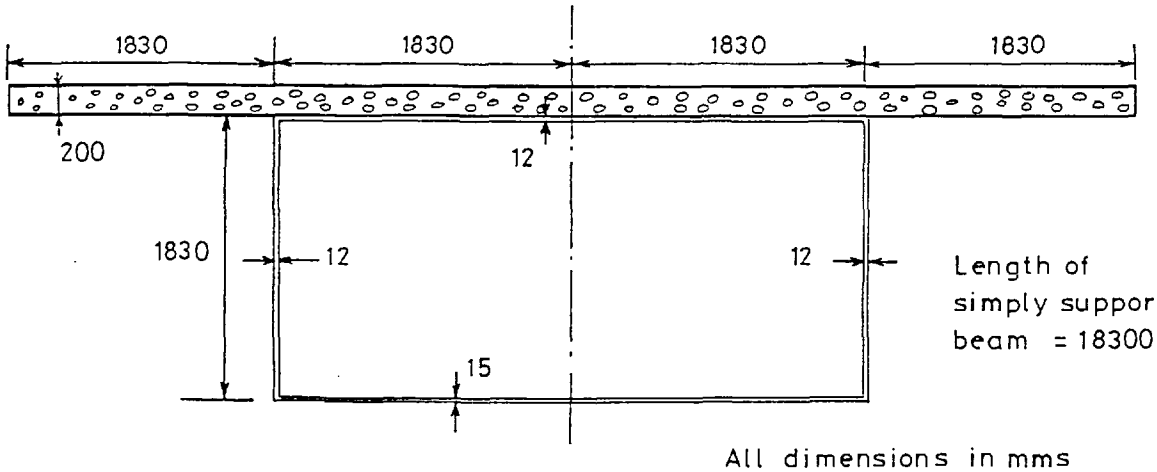

Material properties

Steel
- Modulus of elasticity 207000 N/mm^2
- Poissons ratio 0·3
- Yield stress 250 N/mm^2

Concrete
- Modulus of elasticity 16000 N/mm^2
- Poissons ratio 0·2
- Cracking stress 3 N/mm^2

Reinforcement in slab 1% long. & trans.
Shear connection stiffness 1·06 N/mm/mm^2
Dowell factor 0·4
AGG^T interlock factor 0·4

Fig 6·1 Details of closed box model C1

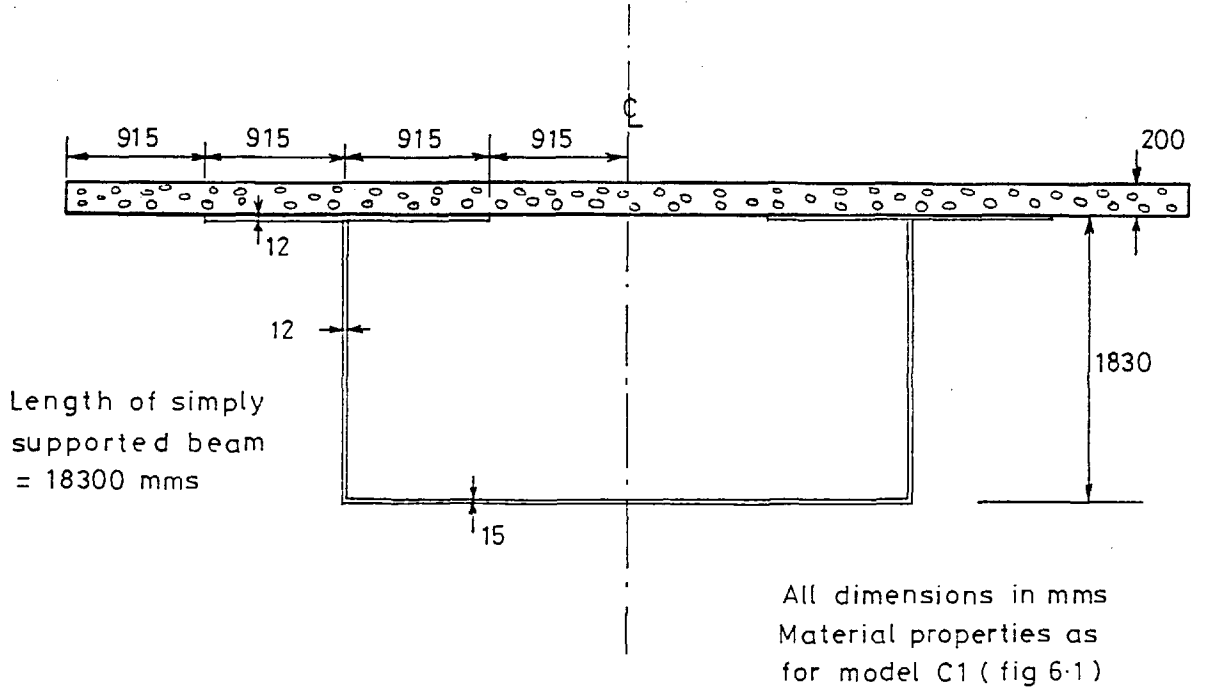

Fig6·2 Details of open box model 01

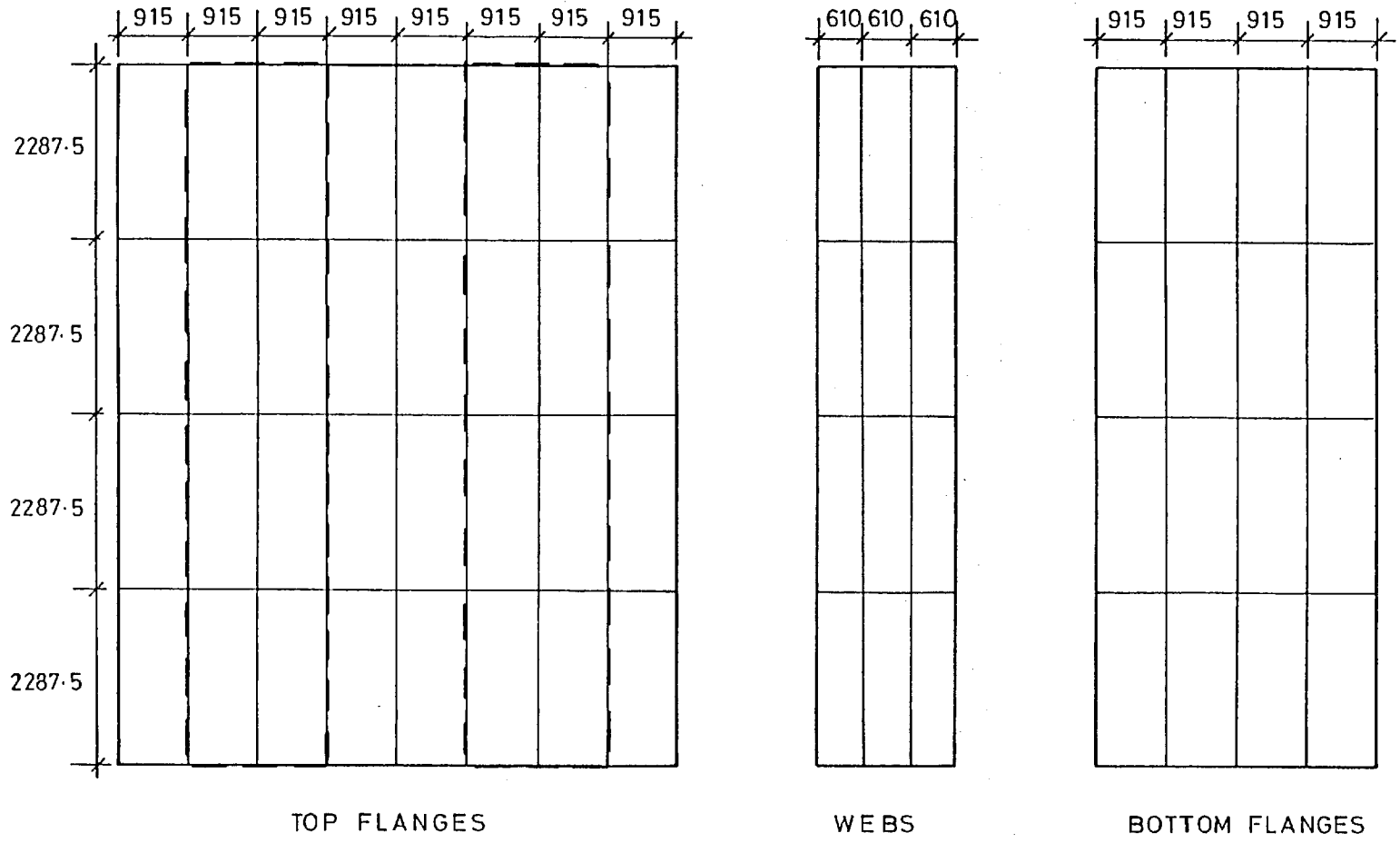

Fig 6·3 Coarse mesh for open box

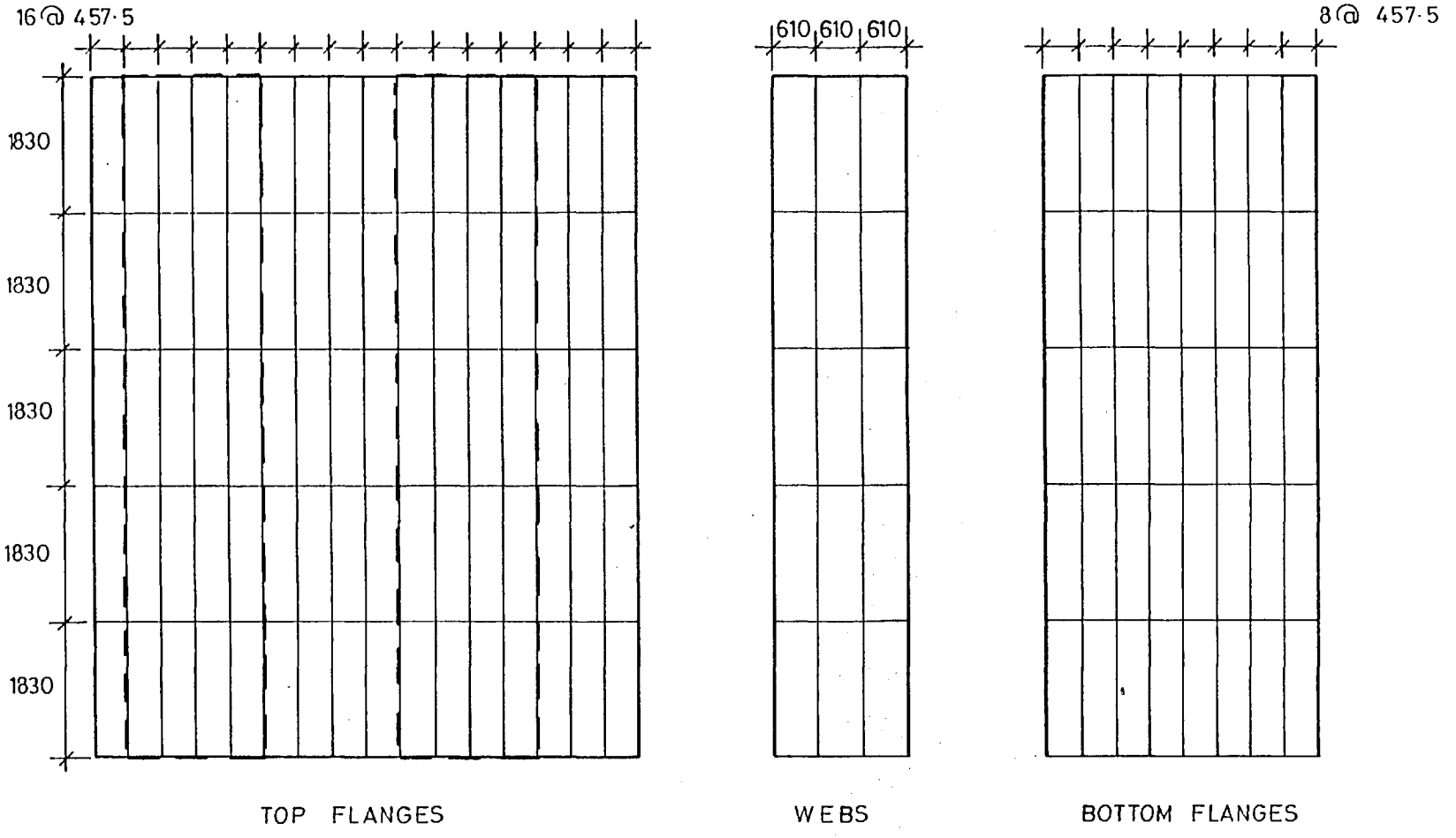

Fig 6·4 Fine mesh for open box

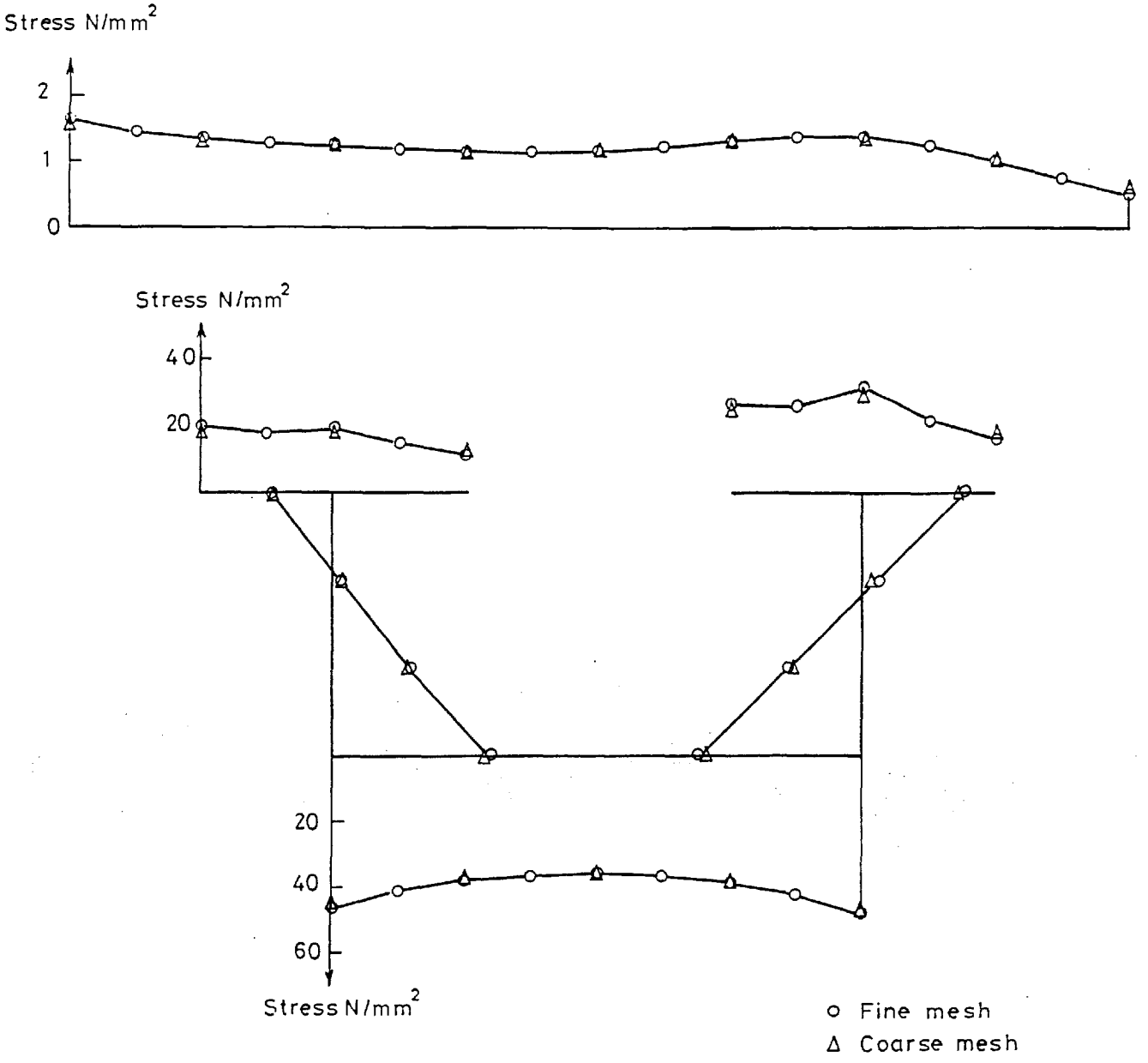

Fig 6·5 Comparison of ℄ longitudinal stress distributions for fine & coarse meshes

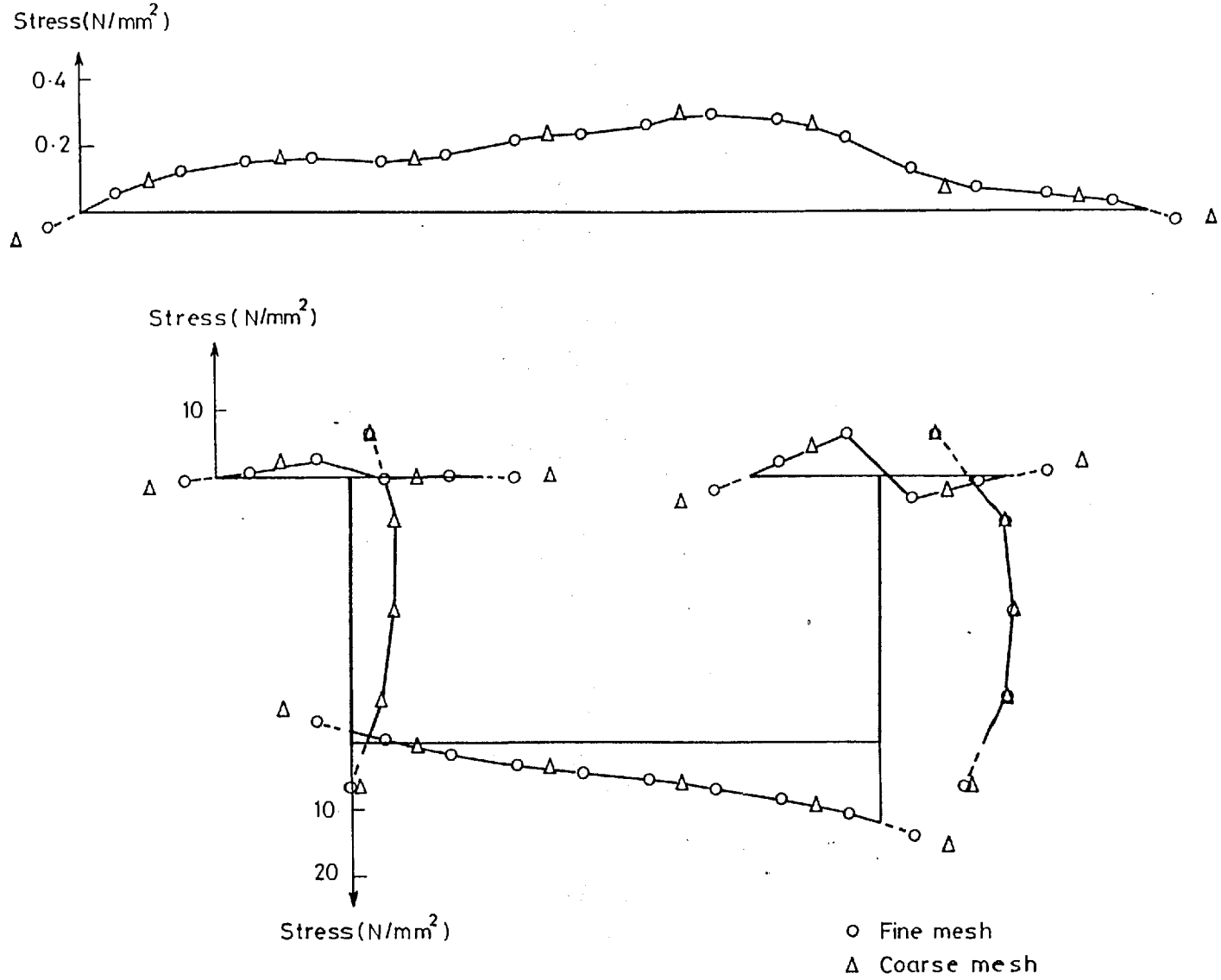

Fig 6·6 Comparison of ℄ shear stress distributions for fine & coarse meshes

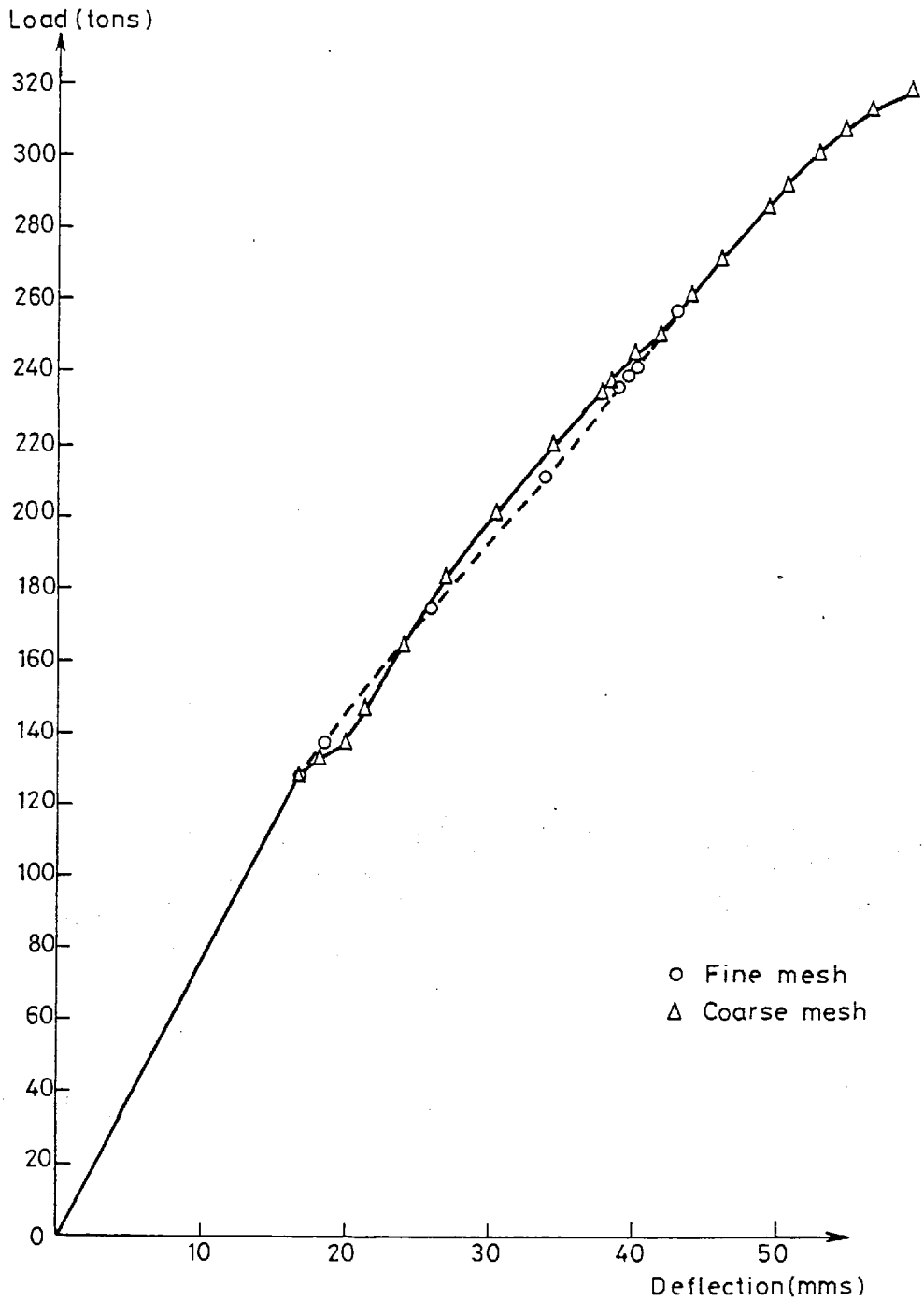

Fig 6·7 Comparison of load-deflection curves for fine and coarse meshes

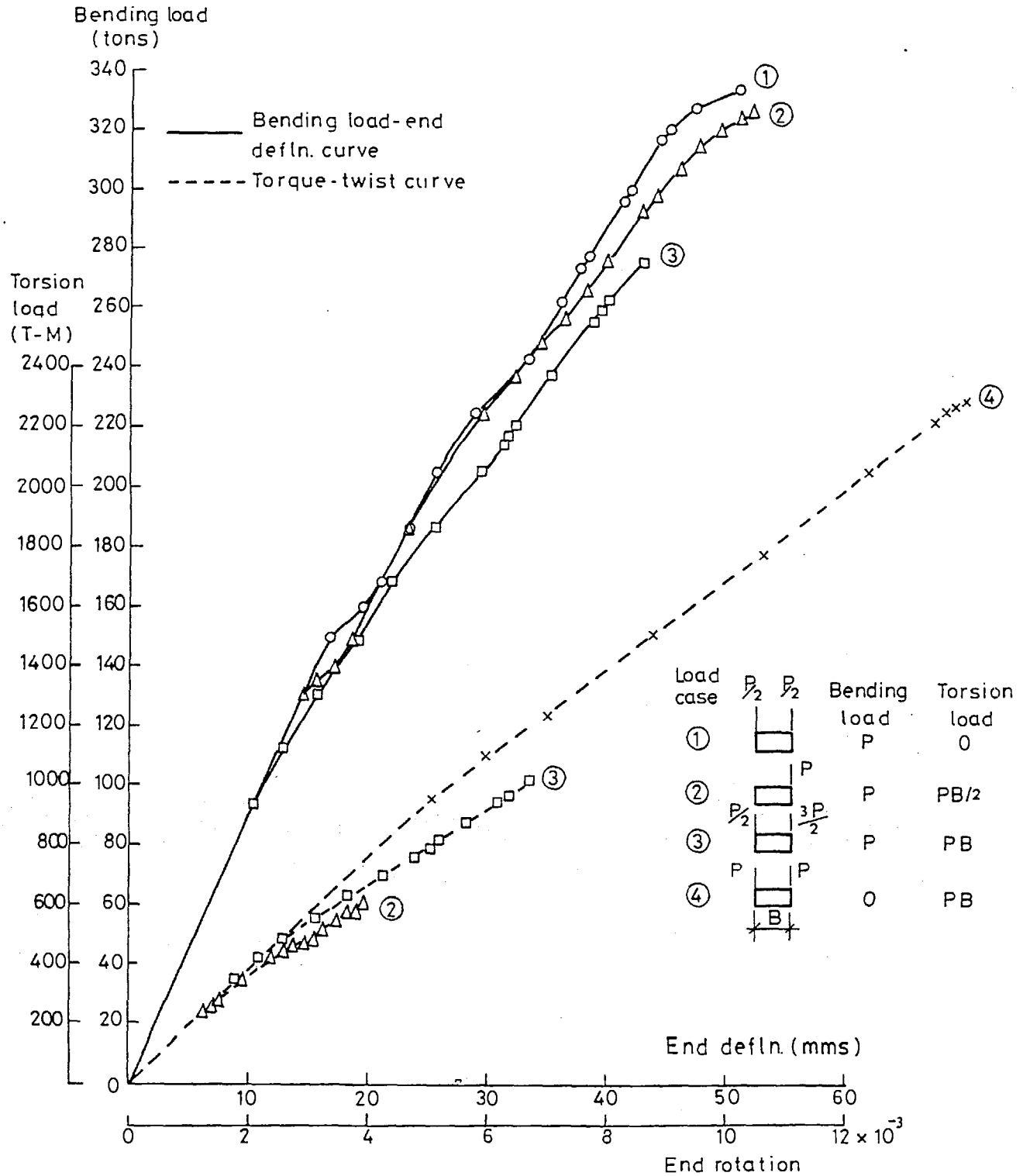

Fig 6·8 Behaviour of box 01 under various load combinations

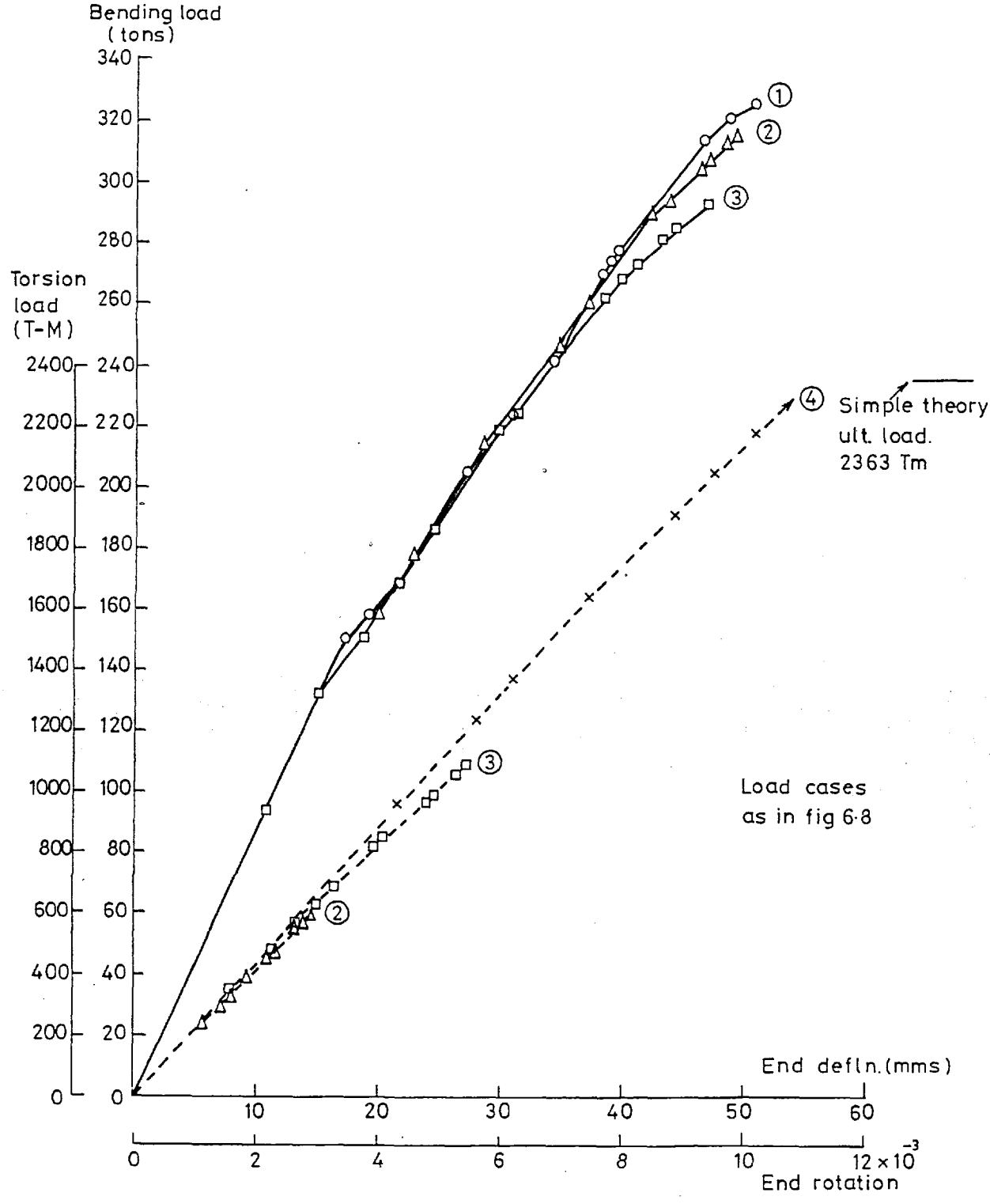

Fig 6·9 Behaviour of box C1 under various load combinations

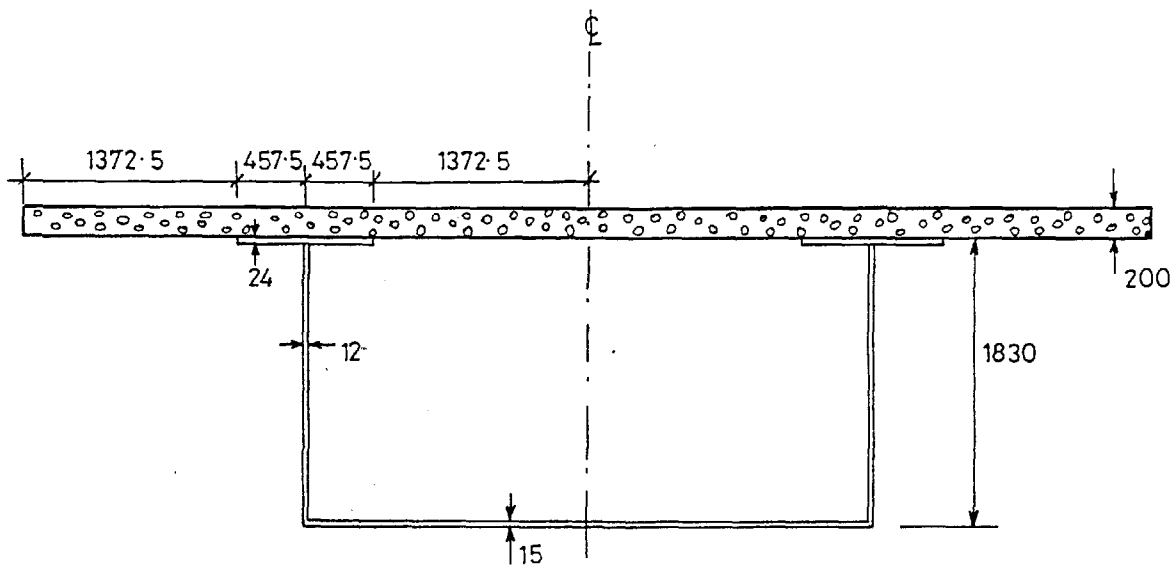

Fig 6·11 Cross-section of model 02

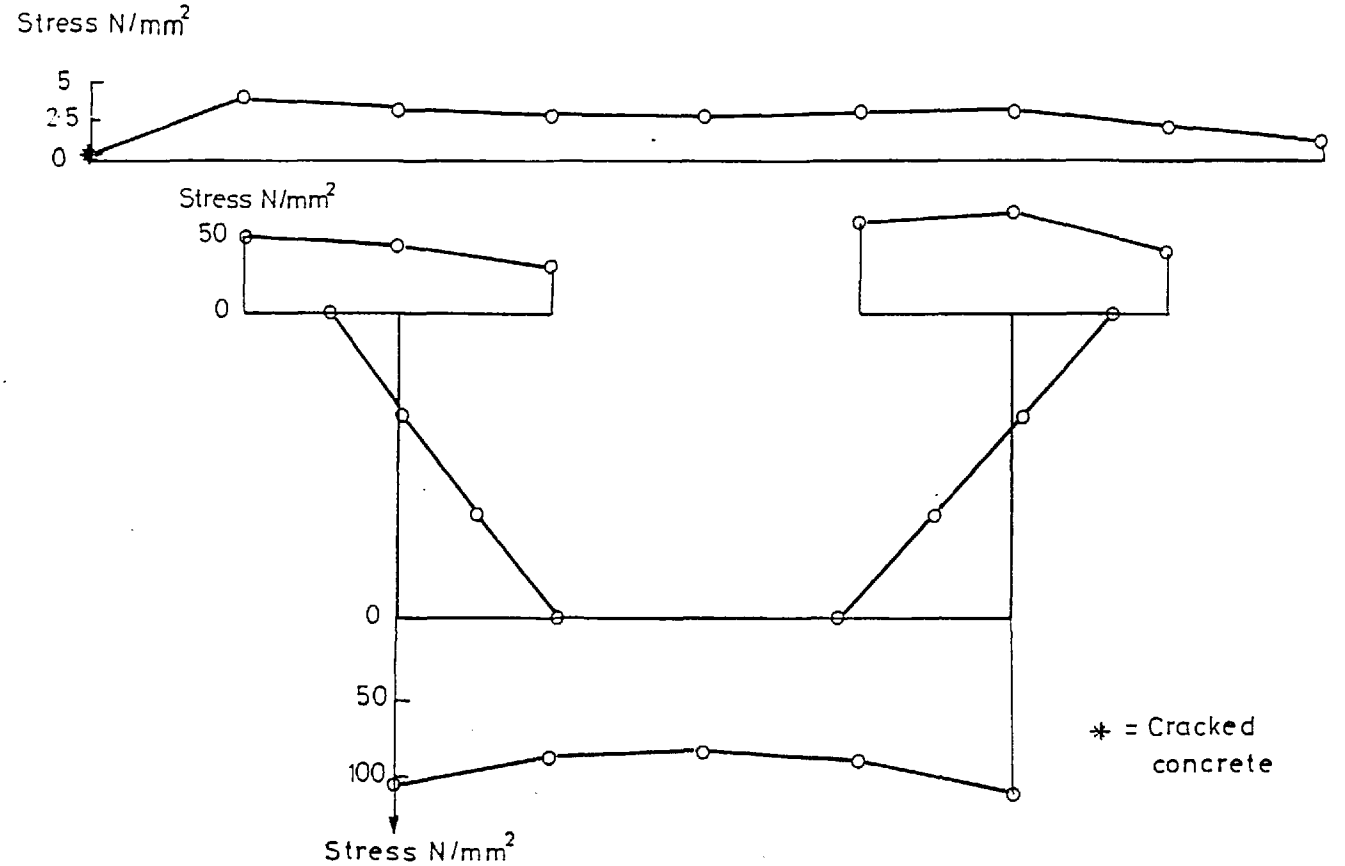

Fig 6·12 Box 01 Direct stress distribution at ℄ under load case 2

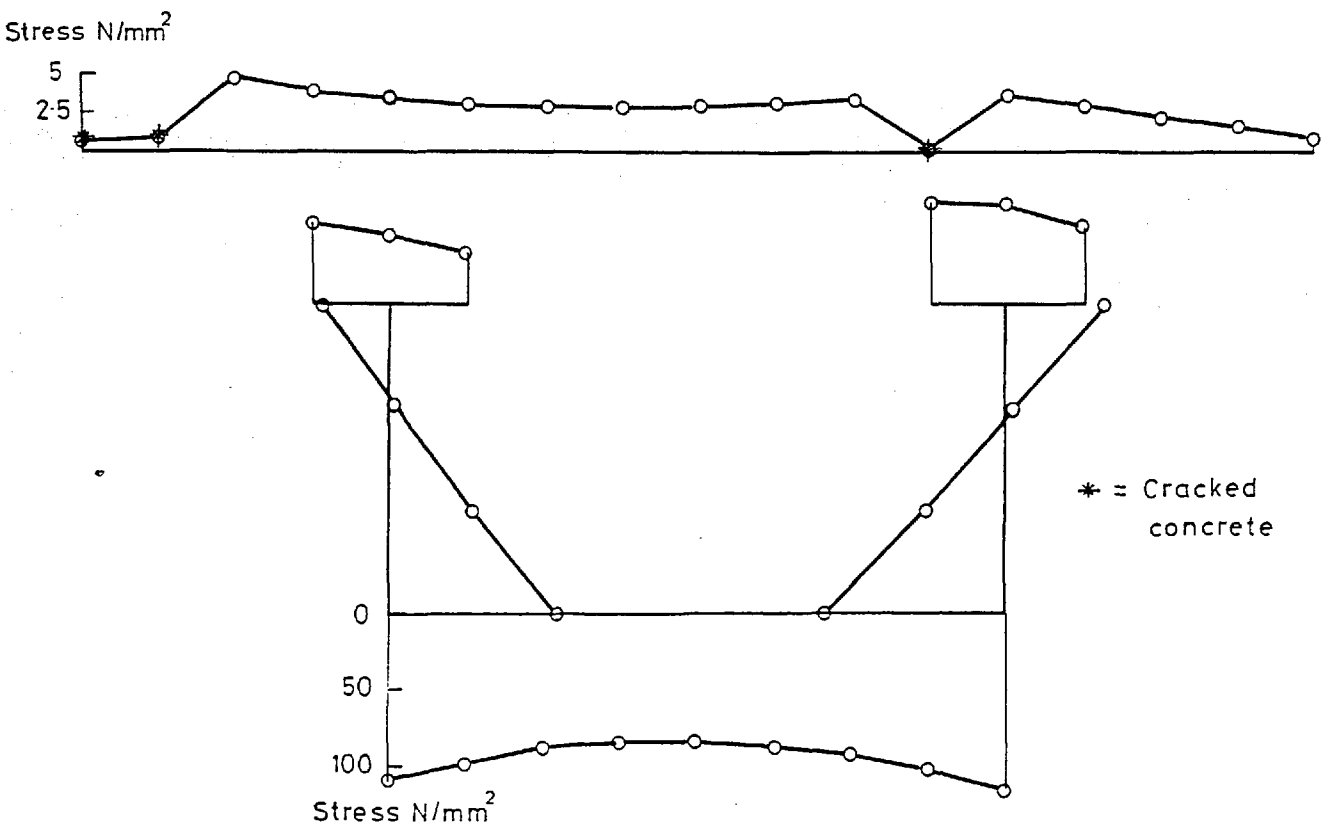

Fig 6·13 Box 02 Direct stress distribution at ℄ under load case 2

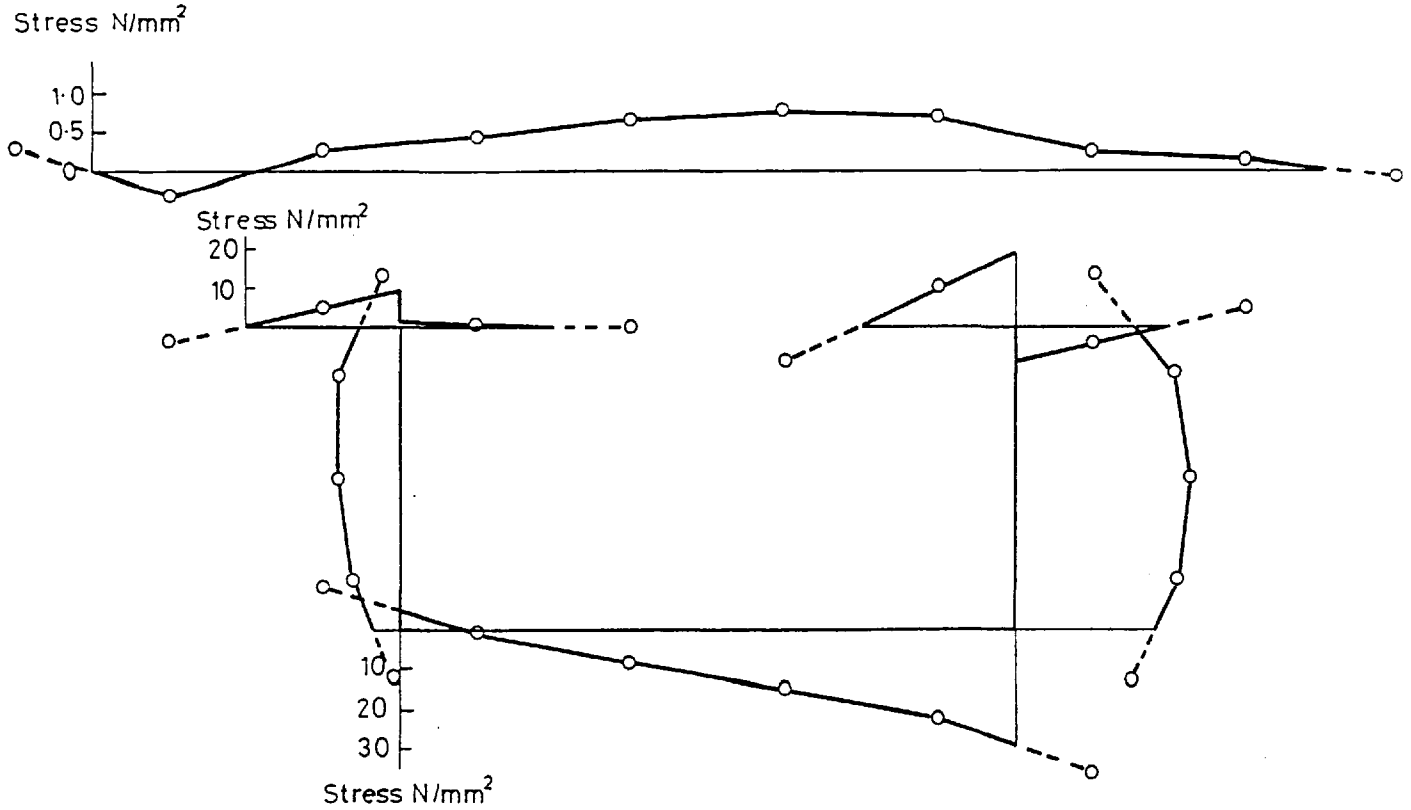

Fig 6·14 Box 01 Shear stress distribution at ℄ under load case 2

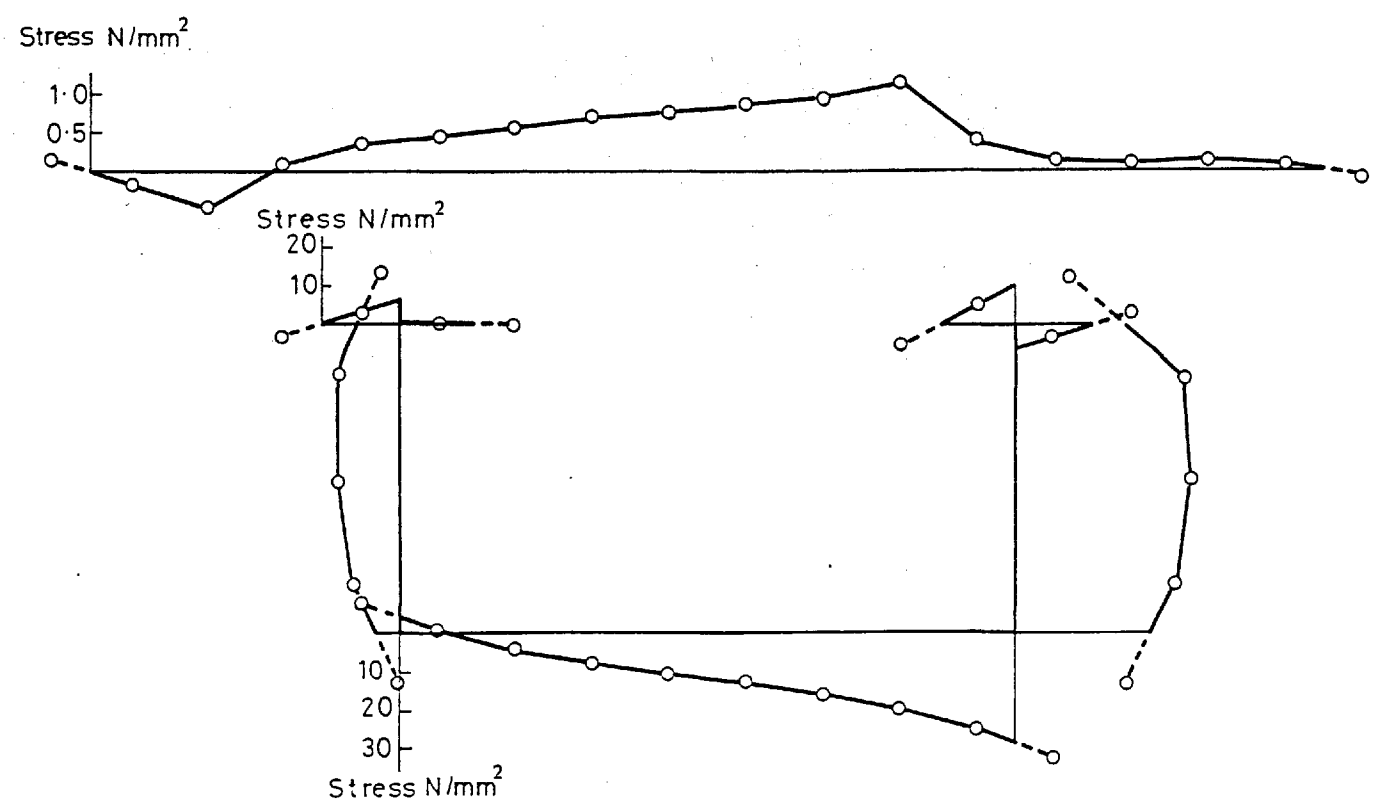

Fig 6·15 Box 02 Shear stress distribution at ℄ under load case 2

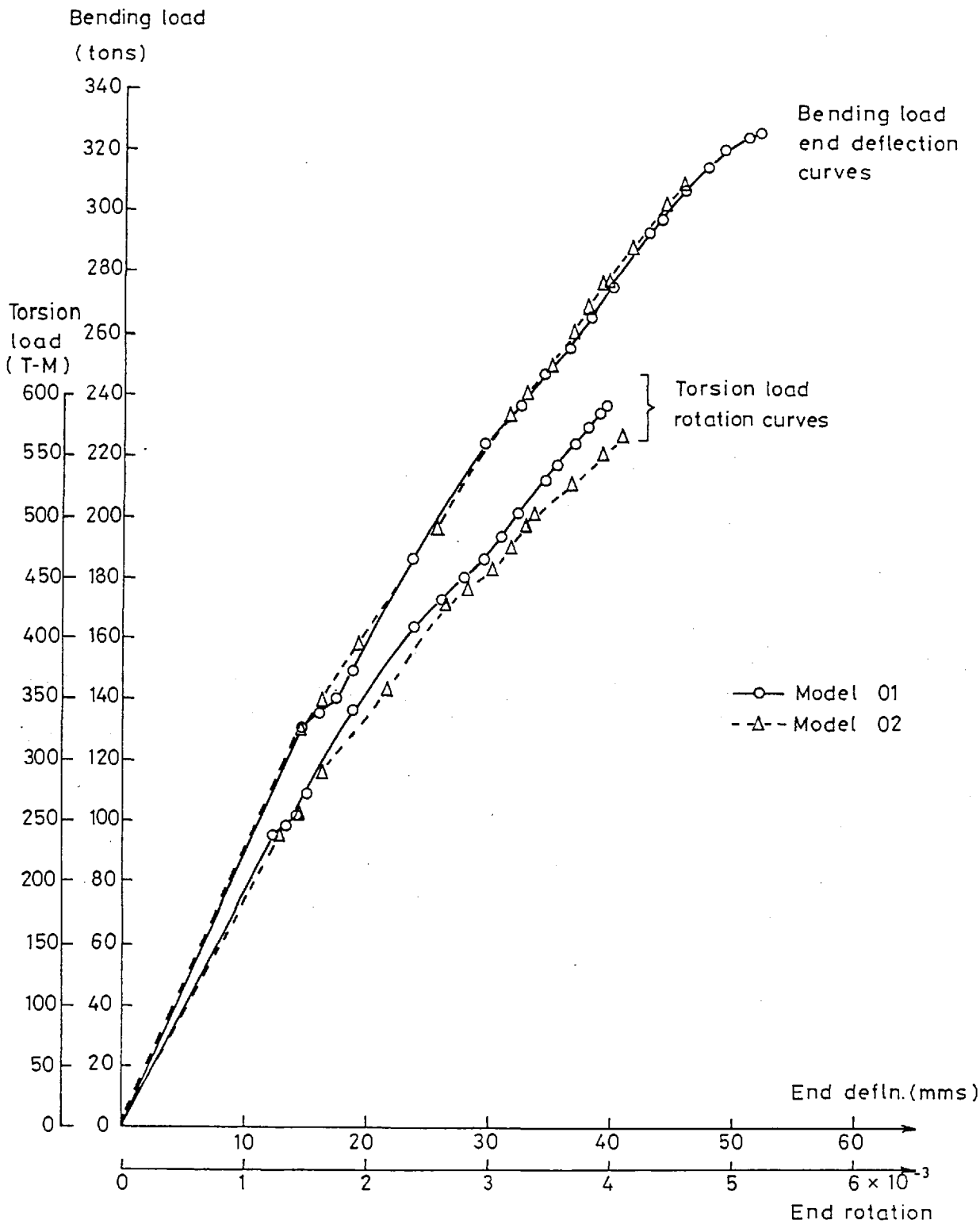

Fig 6·16 Load-deflection curves for models 01 & 02, Load case 2

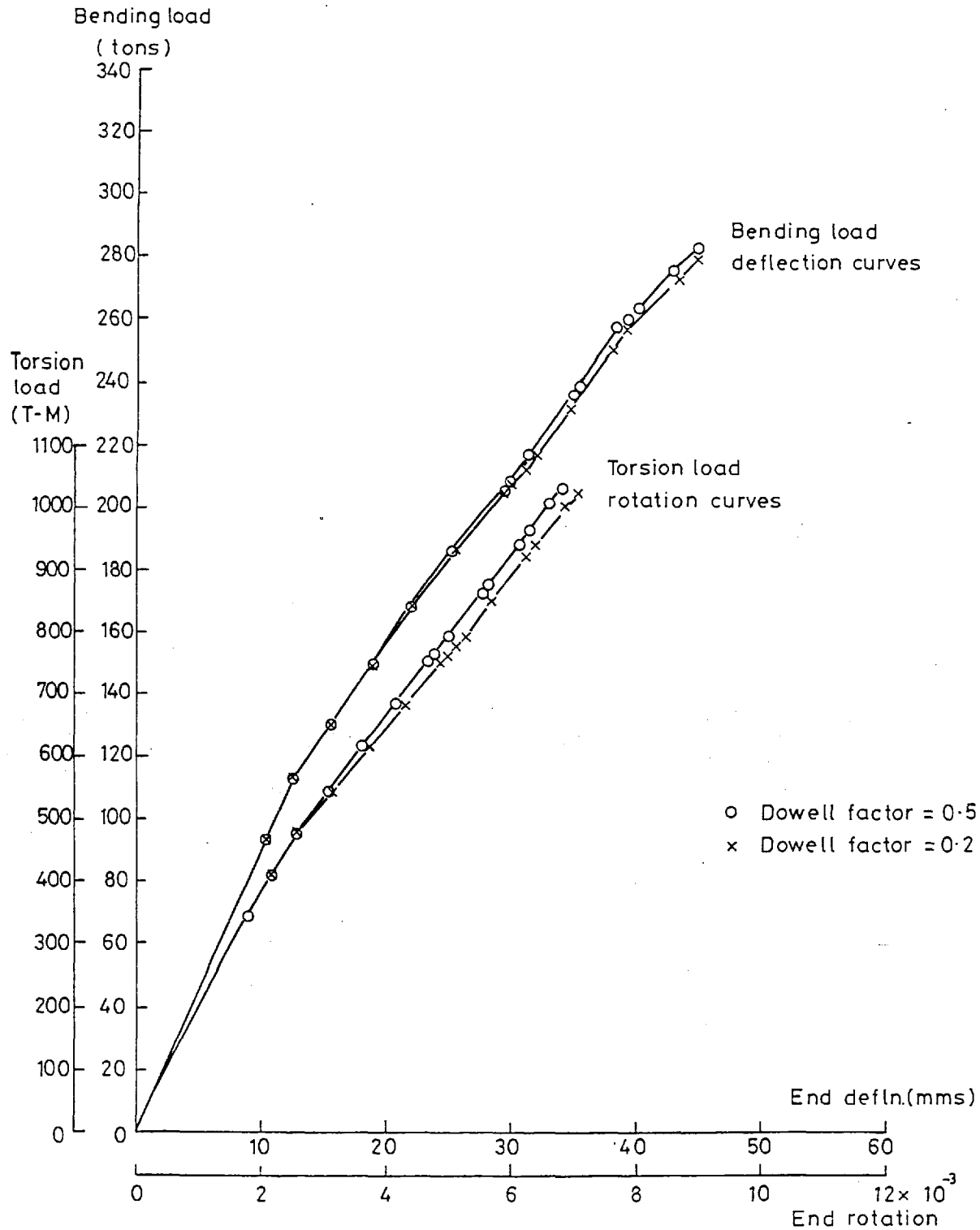

Fig 6·17 Effect of variation of Dowell factor on behaviour of model 01 (load case 3)

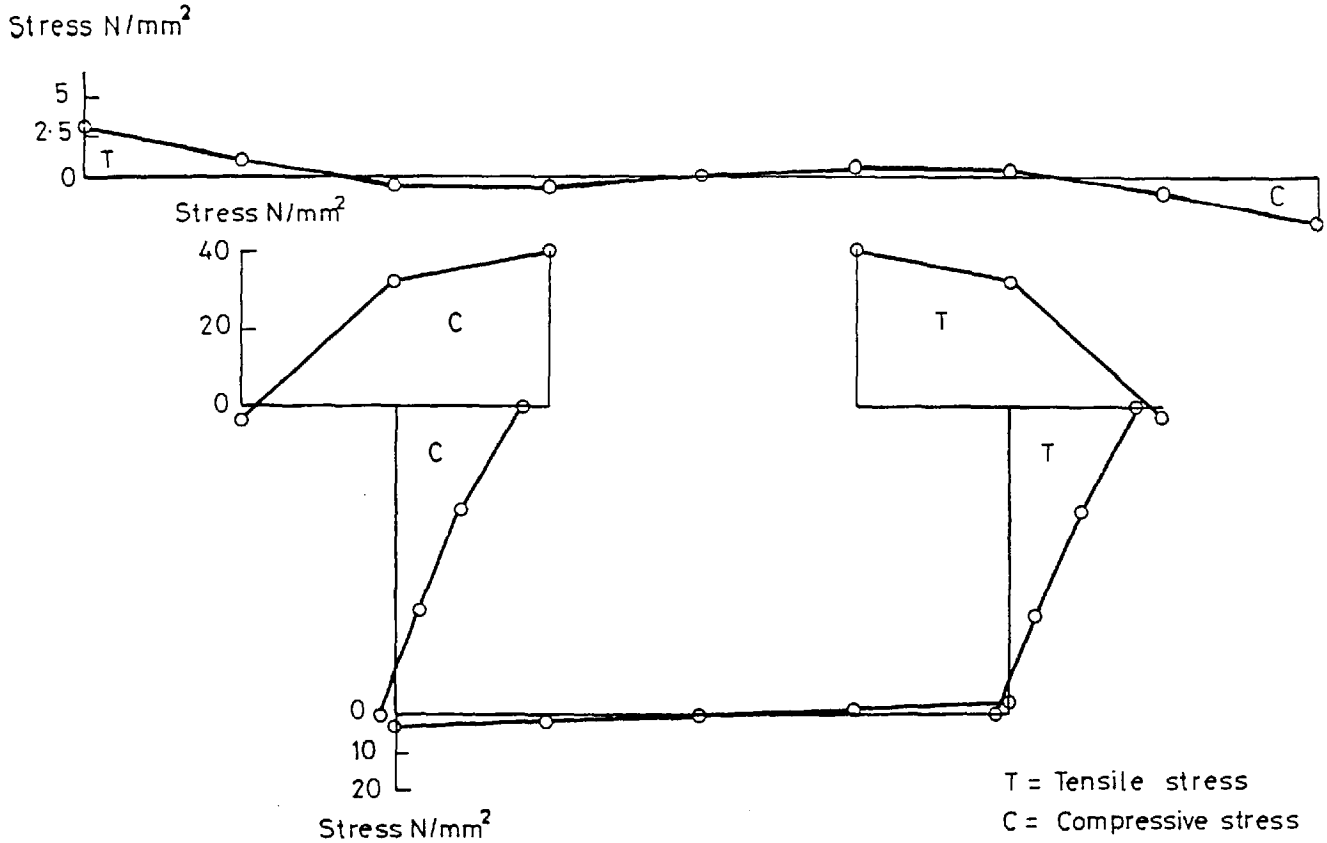

Fig 6·18 Model 01, Stress distribution at cantilever support, load case 4

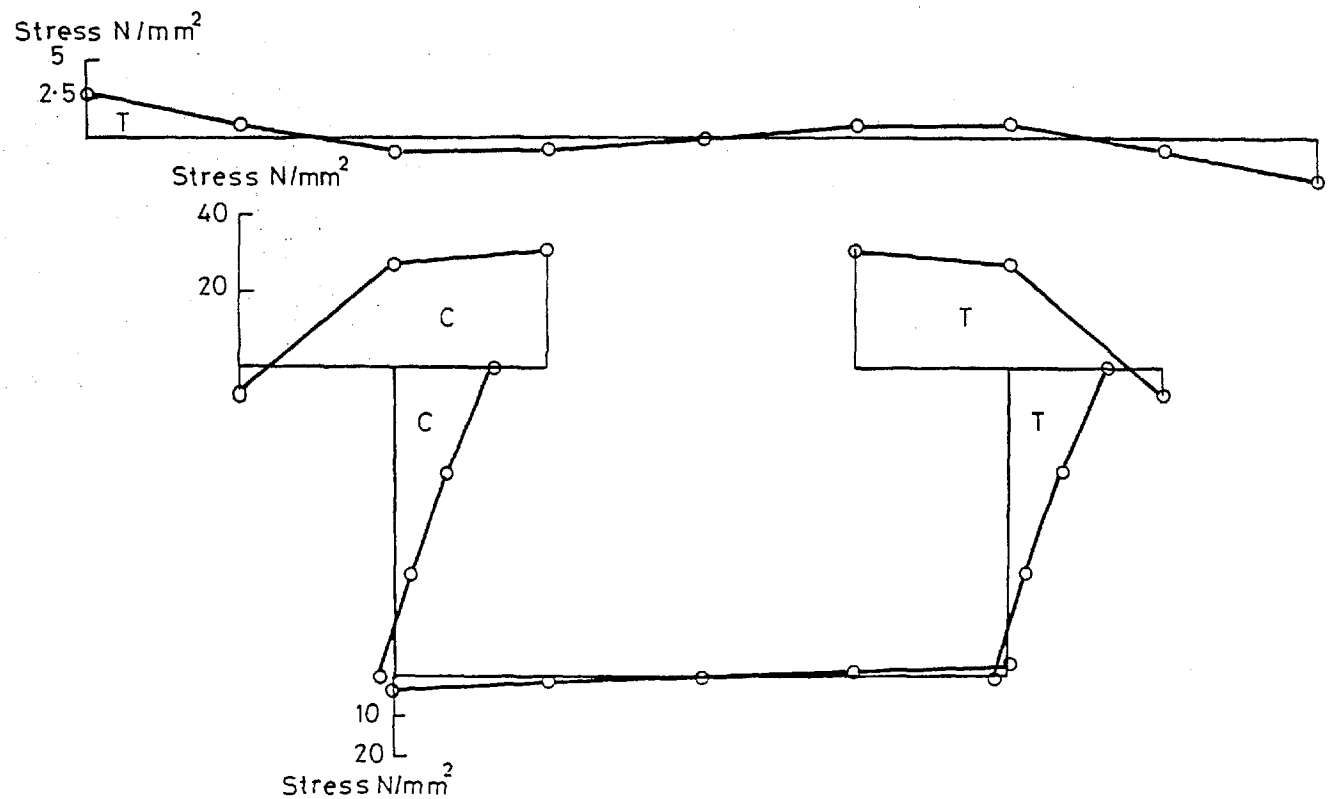

Fig 6·19 Model 01, Stiff. shear connection, direct stress distribution at cantilever support, load case 4

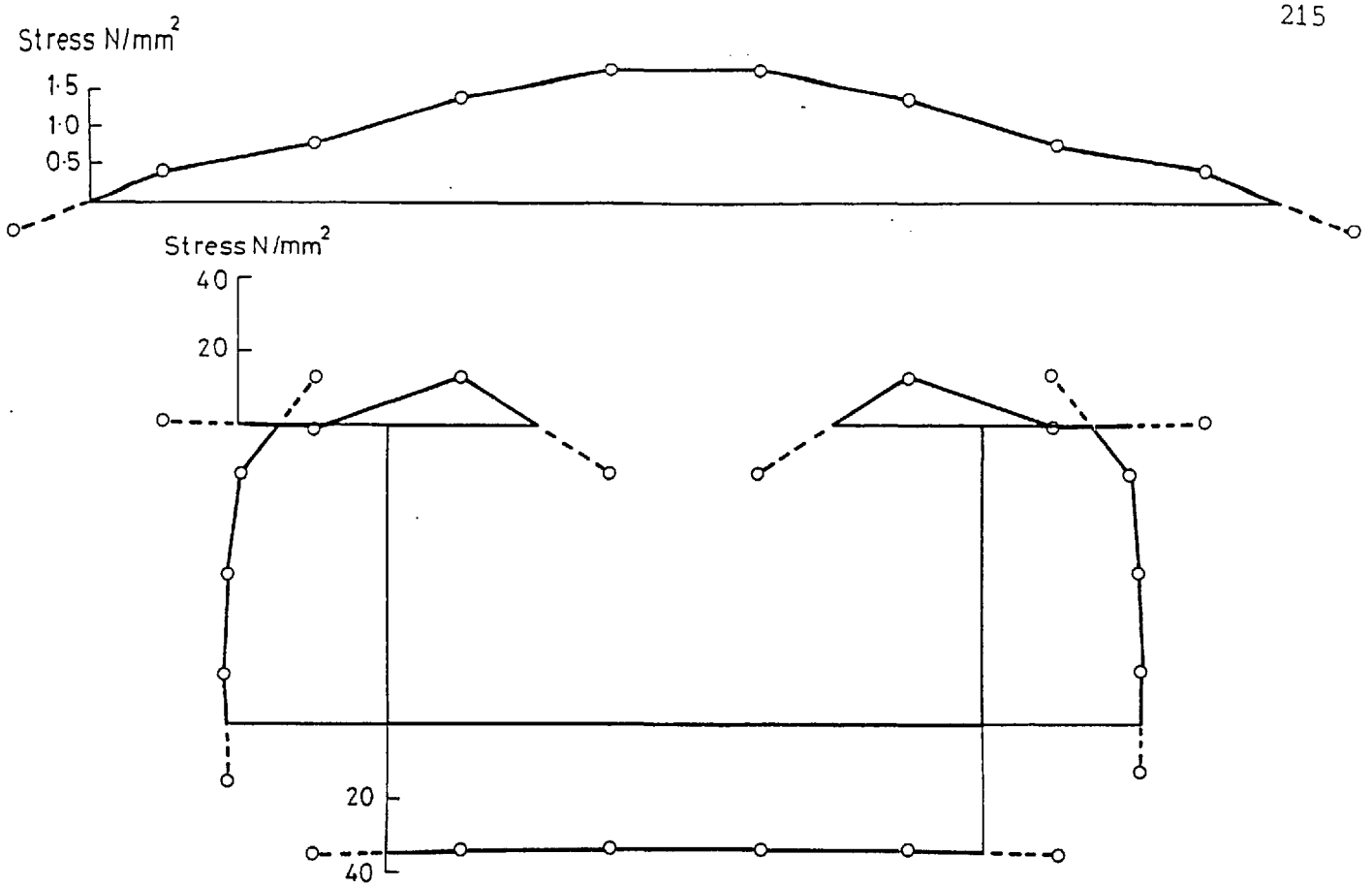

Fig 6·20 Model 01, Shear stress distribution at cantilever support, load case 4

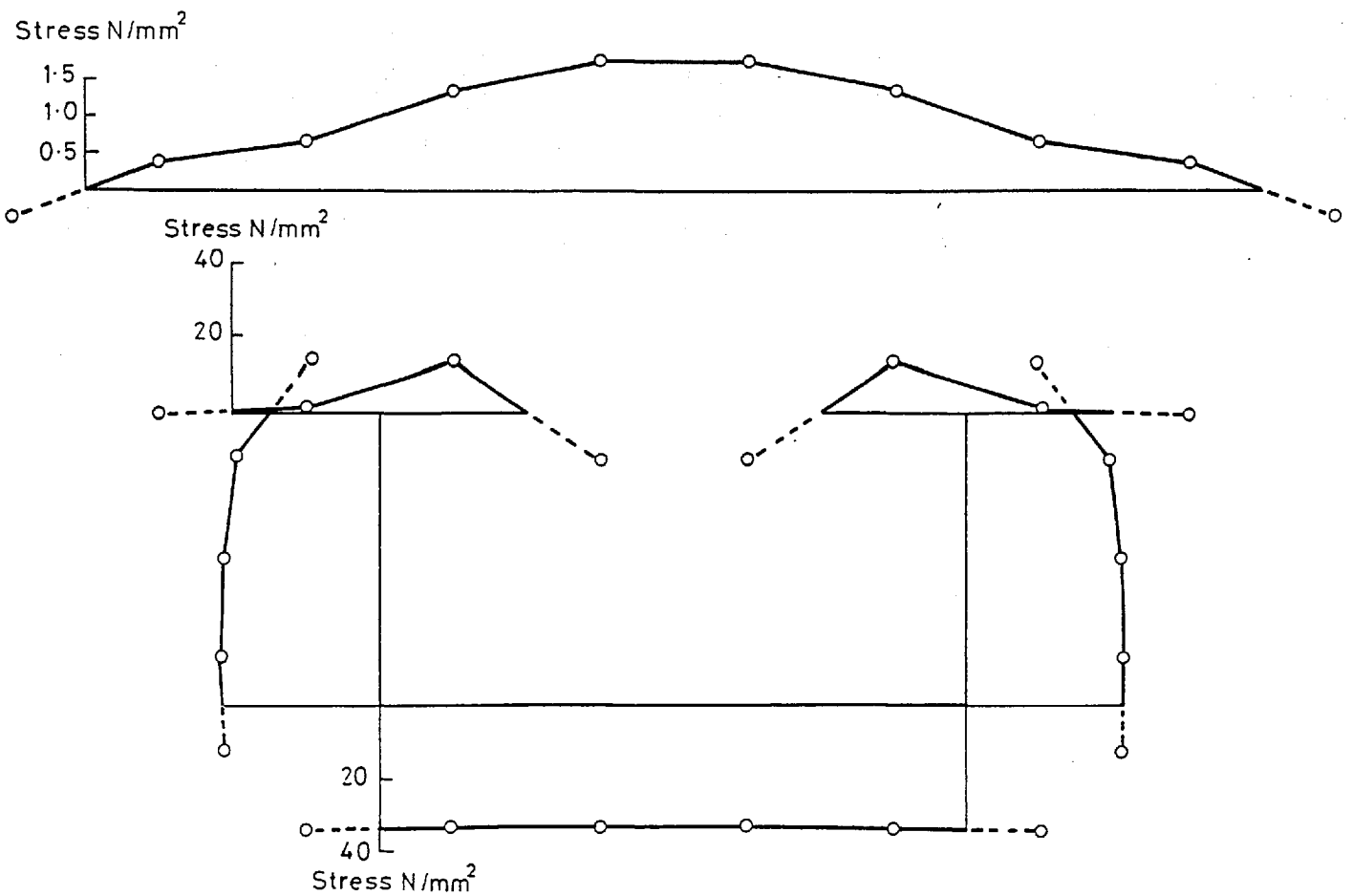

Fig 6·21 Model 01 Stiff. shear connection shear stress distribution at cantilever support load case 4

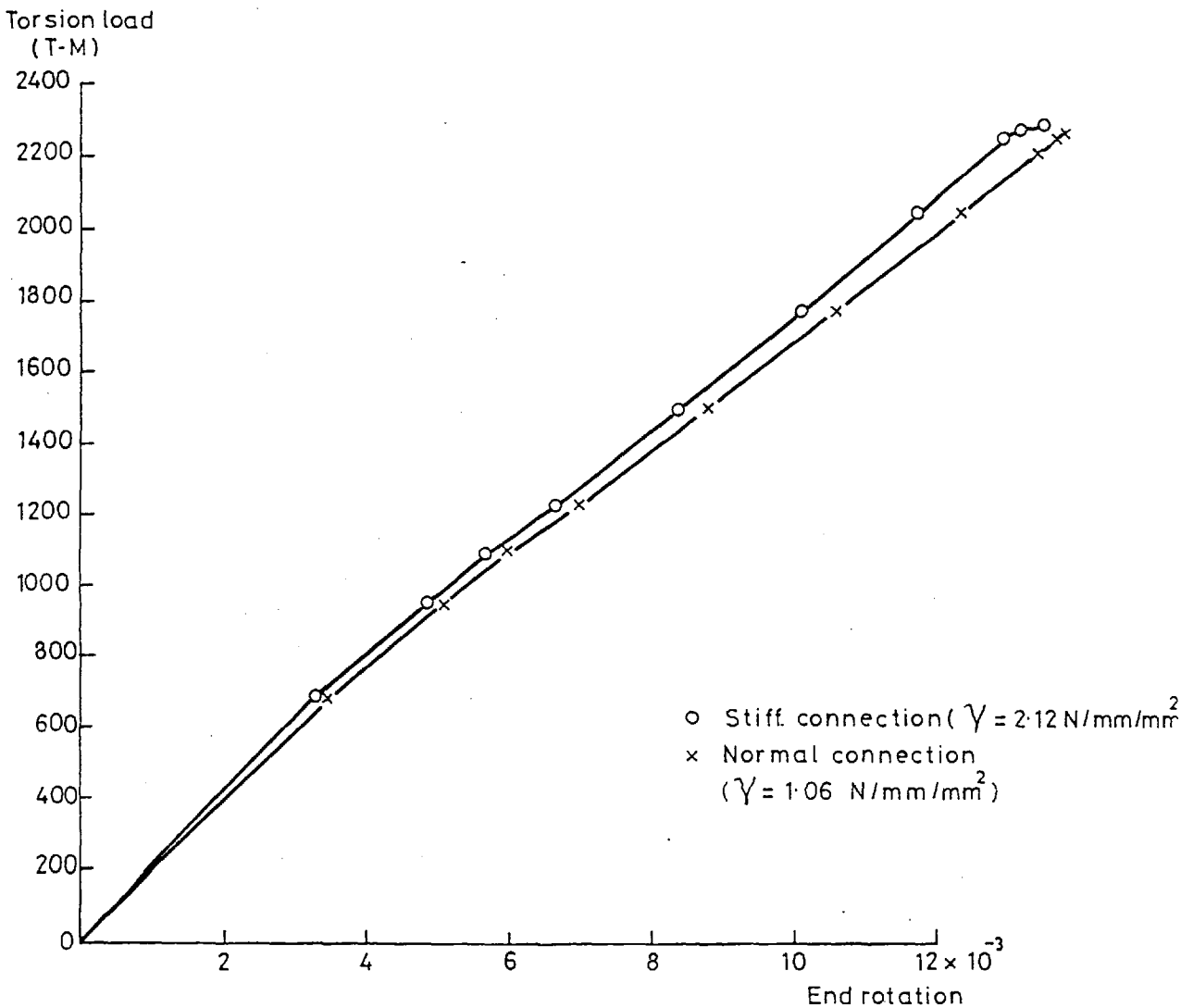

Fig 6·22 Effect of variation of shear connection stiffness on behaviour of model 01 (load case 4)